Modification and patterning of planar graphitic surfaces with molecular films

---

A thesis submitted in partial fulfilment of the requirements for the

Degree of Doctor of Philosophy in Chemistry

at the University of Canterbury

Andrew J. Gross

University of Canterbury

2012

Table of contents

Abstract

Modification and patterning of planar graphitic surfaces with molecular films

Andrew J. Gross, University of Canterbury, PhD Thesis, 2012

Chapter 1 provides an overview of the current literature regarding molecular level modification of conducting surfaces. The modification of carbon surfaces are discussed, with particular attention being given to the use of aryldiazonium salt compounds. Patterning of molecular layers using aryldiazonium salts and arylazides is detailed. The objectives of the project are outlined.

Chapter 2 contains the general experimental methods, instrumentation, chemicals, and materials used throughout this thesis.

Chapter 3 details the development of two technical methods: a heat treatment method for regenerating diazonium-modified or deactivated pyrolysed photoresist film electrodes, and a method for preparing evaporated carbon film electrodes. Although regeneration of the evaporated carbon surfaces was unsuccessful, the surfaces exhibited good electrochemical properties and are useful substrates for studying diazonium-derived films.

Chapter 4 reports the covalent modification of carbon, gold, and indium tin oxide surfaces with thin porphyrin films via the electrochemical reduction of porphyrin aryldiazonium salts. Surface characterisation studies revealed that the films are stably-attached and exhibit well-defined redox and optical properties.

Chapter 5 describes the preparation and patterning of organic films on carbon and silicon surfaces using arylazides combined with photolithography. Strategies were investigated to generate continuous mixed films and surfaces presenting patterns of one or two components. For all grafted surfaces, the reactivity of tether species was confirmed by coupling electroactive targets or gold nanoparticles to the tethers, followed by electrochemical analysis or surface microscopy.

Chapter 6 details the modification of carbon surfaces with diazonium-derived films via aryltriazenes. Also described in this chapter is the development of microfluidics, for use with aryltriazene and aryldiazonium salt solutions, for generating parallel surface patterns.

Chapter 7 concludes and answers to the challenges reported in this study. Future directions are briefly discussed.

Acknowledgements

It is a great pleasure for me to thank the many people who made this thesis possible. I am very grateful for the special and rewarding years spent as a PhD student at the University of Canterbury, New Zealand, and the months spent at the Université Joseph Fourier, Grenoble.

I would like to show my greatest appreciation to my Ph.D. supervisor, Prof. Alison J. Downard. Since Alison accepted me into her research group she has been a constant source of knowledge, inspiration, and optimism, and I am very thankful for her continued and spirited guidance throughout this endeavour. I would also like to express, with pleasure, great appreciation to Prof. Jean-Claude Moutet, Dr Christophe Bucher, Dr. Liliane Coche-Guerente and Prof. Pierre Labbé, for providing me with excellent guidance and supervision in the Département de Chimie Moléculaire at the Université Joseph Fourier. Both Liliane and Christophe worked with me in the lab and provided excellent hands-on lessons in synthesis and electrochemistry. I also wish to further acknowledge Prof. Moutet for enthusiastically accepting me into his lab for a second round of experiments in 2011, at a time when the University of Canterbury was closed due to earthquake damage.

During this thesis I have been fortunate enough to receive technical support from various excellent chemists and engineers. I am thankful to all of them. I express many thanks to Dr Bucher for providing me with aminoporphyrin compounds, and Dr Volker Nock for providing me with PDMS microchannels and introducing me to microfabrication. I thank Dr B. James and Dr C. Doyle from the University of Auckland for processing the XPS data. Many thanks to Helen Devereux and Gary Turner for technical support in the Nanolab in the Electrical Engineering Department. From the Chemistry Department I would like to thank, in particular, Drs Marie Squire and Matt Polson for processing NMRs

and mass-specs, and assisting in any way possible. Fortunately for them, there were only a few spells of organic synthesis as part of this thesis.

I also wish to extend my thanks to many non-permanent past and present members of the Chemistry Department, the MacDiarmid Institute, the Nanolab, and the Département de Chimie Moléculaire with whom I have shared time with. In particular, I thank those who provided me with constant friendship and a fantastic time here in New Zealand, far away from my home in the South-East of England. I would especially like to thank past and present members of the Downard (Brad, Clem, Dave, Frankie, Lita, Paula, Josh, and Sam) and Golovko groups (David and Dr Golovko himself), and the MacDiarmid Emerging Scientists Association (MESA) team. In addition, I thank the MacDiarmid Institute for a PhD scholarship and the University of Canterbury for generous access to resources and financial support.

Despite being mentioned after everybody else, and even institutes, I thank my family for always being there. I thank a few very close friends; namely, the Edwards, the Smarts, Oliver, Simon, Jimmy, Juan, Florian, Fabien, Marc, and Nikita. Last but not least, I thank ma chérie Johanna, for her affection and friendship, for romance, and for always being supportive.

I dedicate this thesis in loving memory of my father, Dr Leon P. Gross (May 16, 1954 – October 21, 2012).

List of publications

Book Chapter

1. A. J. Downard, **A. J. Gross**, and B. M. Simons, "Patterned Molecular Layers on Surfaces", pp. 53-68, published in Aryl Diazonium Salts: New Coupling Agents in Polymer and Surface Science, Wiley-VCH, 2012.

Journal Publications

5. F. J. Rawson, **A. J. Gross**, D. J. Garrett, A. J. Downard, and K. H. R. Baronian, "Mediated Electrochemical Detection of Electron Transfer from the Outer Surface of the Cell Wall of Saccharomyces Cerevisiae", *Electrochemistry Communications*, **15** (1), pp. 85-87, 2012.

4. A. J. Gross, C. Bucher, L. Coche-Guerente, P. Labbé, A. J. Downard, and J-C. Moutet, "Nickel (II) Tetraphenylporphyrin Modified Surfaces via Electrografting of an Aryldiazonium Salt", *Electrochemistry Communications*, **13** (11), pp. 1236-1239, 2011.

3. A. J. Gross and A. J. Downard, "Regeneration of Pyrolyzed Photoresist Film by Heat Treatment", *Analytical Chemistry*, **83** (6), pp. 2397-2402, 2011.

2. A. J. Gross, S. C. Yu, and A. J. Downard, "Two Component Mixed and Patterned Films on Carbon Surfaces through the Photografting of Arylazides", *Langmuir*, **26** (10), pp. 7285-7292, 2010.

1. B. S. Flavel, **A. J. Gross**, D. J. Garrett, V. M. Nock, and A. J. Downard, "A Simple Approach to Patterned Protein Immobilization on Silicon via Electrografting from Diazonium Salt Solutions", *ACS Applied Materials and Interfaces*, **2** (4), pp. 1184-1190, 2010. **(Cover Article)**

Copyright

Abbreviations

The following abbreviations have been used in this thesis:

2D	Two-dimensional
3D	Three-dimensional
Å	Ångstroms
a-C	Amorphous carbon film
ACN	Acetonitrile
AFM	Atomic force microscopy
AMP	*p*-(Aminomethyl)phenyl
AMP_D	*p*-(Aminomethyl)phenyl diazonium salt
AMP_{DMT}	[*p*-(dimethyltriaz-1-en-1-yl)phenyl]methylamine
AP	Aminophenyl
AP_A	*p*-Azidoaniline hydrochloride
AP^{AZ}	AP films prepared from AP_A
Au-QC(s)	Gold-coated piezoelectric quartz crystal(s)
BrP	Bromophenyl
BrP_D	*p*-Bromophenyldiazonium salt
BSA	Bovine serum albumin
C	Coulomb
cm	Centimetre
CNTs	Carbon nanotubes
C-OTEs	Carbon optically transparent electrodes
CP	Carboxyphenyl
CP_D	*p*-Carboxyphenyldiazonium salt
CP_{DMT}	*p*-(Dimethyltriaz-1-en-1-yl)benzoic acid
C-QC(s)	Carbon-coated piezoelectric quartz crystal(s)
CV(s)	Cyclic voltammogram(s)
ºC	Degree Celsius
Ø	Diameter
ΔE_p	Peak-to-peak potential separation
δ_H	Hydrogen chemical shift
DCM	Dichloromethane
df	Degrees of freedom
DFT	Density functional theory
DIPEA	*N,N*-Diisopropyl ethylamine
DMF	*N*,*N*-Dimethylformamide
DNA	Deoxyribonucleic acid
DOS	Density of electronic states
DPV	Differential pulse voltammetry

$E_{1/2}$	Half-wave potential
e-beam	Electron-beam
ECR	Electron cyclotron resonance
E_{pa}	Anodic peak potential
E_{pc}	Cathodic peak potential
EPPG	Edge plane pyrolytic graphite
E-QCM	Electrochemical-quartz crystal microbalance
ESI-TOF	Electrospray ionisation time-of-flight
EtOAc	Ethyl acetate
eV	Electron volt
E_{λ}	Switching potential
Fc	Ferrocene
FCA	Ferrocenemonocarboxylic acid
g	Gram
GC	Glassy carbon
h	Hour(s)
H_2TPP	Free-base tetraphenylporphyrin
H_2TPP_A	5-(*p*-Aminophenyl)-10,15,20-triphenylporphyrin
H_2TPP_D	Tetraphenylporphyrin mono-aryldiazonium salt
HOPG	Highly ordered pyrolytic graphite
HRMS	High-resolution mass spectroscopy
Hz	Hertz
I_p	Peak current
I_p^0, I_p^{BSA}, I_p^{mod}, I_p^{GC}	Peak current of ferrocenemonocarboxylic acid
I_{pa}	Anodic peak current
IPA	Isopropyl alcohol
I_{pc}	Cathodic peak current
IR	Infrared
iR	Potential drop
ITC	Phenyl isothiocyanate
ITC_A	*p*-Azidophenyl isothiocyanate
ITC^{AZ}	ITC films prepared from ITC_A
ITO	Indium tin oxide
J	Coupling constant
K	Kelvin
keV	Kiloelectron volt
kHz	Kilohertz
kJ	Kilojoule
k^o	Electron-transfer rate constant
λ_{max}	Maximum absorption wavelength
L	Litre
M	Molar

m.p.	Melting point
mA	Milliampere
MEMS	Microelectromechanical systems
MHz	Megahertz
min	Minute(s)
mL	Millilitre
mm	Millimetre
mM	Millimolar
mol	Moles
mV	Millivolt
mW	Milliwatt
MΩ	Megaohm
NiTPP	Nickel (II) tetraphenylporphyrin
$NiTPP_A$	5-(*p*-Aminophenyl)-10,15,20-triphenylporphyrinatonickel (II)
$NiTPP^A$	NiTPP films prepared from $NiTPP_A$
$NiTPP_D$	Nickel (II) tetraphenylporphyrin mono-aryldiazonium salt
nm	Nanometre
NMR	Nuclear magnetic resonance
	br. Broad
	d Doublet
	m Multiplet
	s Singlet
NP	Nitrophenyl
NP_A	*p*-Azidonitrobenzene
NP^{AZ}	NP films prepared from NP_A
NP_D	*p*-Nitrophenyl diazonium salt
Ω/sq	Ohm per square
O/C	Oxygen-to-carbon ratio
p	*Para*
P	Probability value
PB	Phosphate buffer
PBS	Phosphate buffer saline
PDMS	Poly(dimethylsiloxane)
PEG	Methoxy-poly(ethylene glycol)
PEG_a	Methoxy-poly(ethylene glycol)-amine
PFPA	Perfluorophenylazide
PPF	Pyrolysed photoresist film
ppm	Parts per million
QCM	Quartz crystal microbalance
r^2	Coefficient of determination
R_a	Arithmetic average roughness
RDE	Rotating disk electrode

rms	Root mean square roughness
rt	Room temperature
rpm	Rotations per minute
R_q	Geometric average roughness
s	Second(s)
SAMs	Self-assembled monolayers
sat.	Saturated
SCE	Saturated calomel electrode
SECM	Scanning electrochemical microscopy
SEM	Scanning electron microscopy
SPL	Scanning probe lithography
STM	Scanning tunnelling microscopy
t	Student's t-distribution
T	Temperature
TBAB	Tetrabutylammonium bromide
$TBABF_4$	Tetrabutylammonium tetrafluoroborate
TEG	Triethylene glycol
TEG_a	Triethylene glycolamine
TEM	Transmission electron microscopy
THF	Tetrahydrofuran
TMCS	Trimethylchlorosilane
ToF-SIMS	Time-of-flight secondary ion mass spectroscopy
TPP	Tetraphenylporphyrin
TsOH	*p*-Toluenesulfonic acid
TSTU	*O*-(*N*-succinimidyl)-*N*,*N*,*N*′,*N*′-tetramethyluronium tetrafluoroborate
µA	Microampere
µCP	Microcontact printing
µFNs	Microfluidic networks
µm	Micrometer
UV	Ultraviolet
V	Volt
W	Watt
XPS	X-ray photoelectron spectroscopy

Introduction

1.1 Introduction to surface modification

The chemical manipulation of a surface, also known as surface modification, is a powerful and versatile route to new advanced materials. The goal is to impart new functional properties to a surface whilst maintaining the bulk properties of the material. Both industrial coatings and nanocoatings represent popular forms of surface modification when applied to materials such as glass to impart self-cleaning properties, or to metals to introduce anti-fouling or anti-corrosion properties[1-3]. The attachment of thin nanoscale films, or "nanocoatings", to surfaces is becoming increasingly important in the modern world. According to market research analysts, global revenue for nanocoatings is estimated to increase from US $1559 million to between US $4371-7821 million over the next 10 years[4]. This is in contrast to the general coatings industry which has declined[4]. Nanocoatings comprising only a few molecular layers have the potential to provide significant improvements in material properties such as anti-bacterial, self-cleaning, anti-fouling, anti-scratch, wear and corrosion resistance, and flame retardant properties.

Surface modification of electrodes with molecular layers "by design" has remained a hot topic in materials chemistry for a number of decades[5-9]. The main attraction is the ability to obtain precise control over the chemical nature of the surface by deliberately reacting chemical reagents to it. Through careful consideration of the chemical reagents, the desired functionalities such as organic compounds, metal complexes, and biomolecules can be attached at the surface to give "chemically modified" surfaces.

The concept of *chemically modified electrodes* was first reported in the early 1970s by Lane and Hubbard[10-11] and subsequently established by Murray and co-workers[6-7, 12]. In the

pioneering experiments, Lane and Hubbard reacted alkene and alkyne modifiers at Pt surfaces to yield various organic monolayers with tailored functional groups. Surfaces were derivatised with groups such as alkylamine, quinone, and carboxylic acid groups. The concept of surface coupling reactions was also demonstrated in this work. Surface coupling is an important strategy where functional groups at the surface are used for performing chemical reactions. Surface coupling can be used, for example, for selective attachment of biomolecules to surfaces for preparation of biochips[13-14]. Popular methods of surface coupling include Sharpless "click chemistry"[15], amide-bond formation[13], and Diels-Alder chemistry[16].

Many types of surface modification have been explored with the goal of forming robust and well-defined molecular layers on surfaces. These methods are categorised by three main types of chemical attachment: (i) reversible chemisorption, (ii) covalent attachment, and (iii) polymer film coating. The various methods, including the most prominent types of surface chemistry, are briefly summarised below:

i. *Reversible chemisorption*[17] methods require that the chemical modifier has a strong but not irreversible affinity for the surface. The nature of the bonding varies substantially between that of completely ionic to covalent character. The most prominent examples of chemisorption used today are the self-assembly of thiols on gold[18]. The chemisorbed methods were the first to be described and are the most widely studied. Self-assembly has the advantage that modification is achieved simply by immersing the appropriate substrate into a solution of the chemical modifier. Chemisorption requires direct contact between the modifier and the surface hence monolayers or sub-monolayers form.

ii. *Covalent attachment* methods give the most physically robust layers due to the formation of covalent bonds between the surface and the modifier. The most popular method is the reaction of alkylsilanes on silicon dioxide and other hydroxylated

surfaces such as glass[19-20]. A second method, which has gained significant and increasing attention over the last two decades, is the reaction of aryldiazonium ions at carbon and various other surfaces[21]. Methods based on silanes and aryldiazonium salts give monolayer or multilayer films, depending on the conditions used. If the surface modification conditions are precisely controlled and film polymerisation suppressed, well-ordered self-assembled monolayers (SAMs) can be formed using silanes[22]. In contrast, molecular layers with a disordered film structure are formed using aryldiazonium salt chemistry.

iii. *Polymer film coating:* The formation of polymer films at electrode surfaces has received considerable attention since the initial reports by Bard and co-workers[23], and the Miller group[24]. These studies showed that electrodes could be modified with thick multilayer polymer films. Polymer film coatings have since been developed and are classified as redox polymers, ion-exchange polymers, electronically-conductive polymers, or non-conducting polymers[25]. The resulting polymer layer usually deposits at the surface due to its low solubility in the contacting solution. This approach gives stably-attached films, with the stability being largely solvent-dependent[12]. Polymer films are considered more stable than chemisorbed monolayer films and can be prepared with significantly higher concentrations of surface functionalities (redox active or chelating groups, for example)[12]. Polymer films are not suited to monolayer formation and comprise a disordered cross-linked structure. Polymer films coatings typically range between 5 nm and 10 μm in thickness[25]. Important examples of polymer film coatings include Nafion (ion-exchange polymer), polypyrrole (electronically-conducting polymer), and poly(vinylferrocene) (redox polymer).

1.2 Molecular level design

Since the discovery by Nuzzo and Allara that long-chain alkylthiols chemisorb on gold to form ordered SAMs[26] there has been considerable interest in the modification of electrodes with "molecular level control"[27]. *Molecular level control* refers to the careful construction of molecular assemblies with well-defined properties. The goal is to obtain the highest level of control over structural and chemical parameters such as film density and packing, film growth and thickness, chemical functionality, surface concentration, spatial distribution, and the stability of the attachment.

Alkanethiols are the best-established route to achieving molecular level control. Alkanethiols form a dense and highly-oriented layer of alkane chains that attach to the surface via a gold-thiolate bond. The molecules align in a trans conformation, tilted ≈ 20-30° to the direction of the surface normal[20]. The modification method is simple and reproducible, and can be controlled to give sub-monolayer or monolayer coverage. Modification using silane chemistry and aryldiazonium salt chemistry also permit a high degree of molecular level control. However, the resulting interfaces are less well-defined (in terms of structure) due to the tendency for multilayer formation.

Figure 1.1 shows a simplified representation of a molecular layer attached on a surface, illustrating the anatomy and characteristics of a typical assembly. There are four general design considerations: (i) the substrate (such as gold); (ii) the head group that attaches to the substrate (a thiolate); (iii) a spacer group (alkyl and/or aryl groups); and (iv) a terminal functional group (such as $-NH_2$ or –COOH).

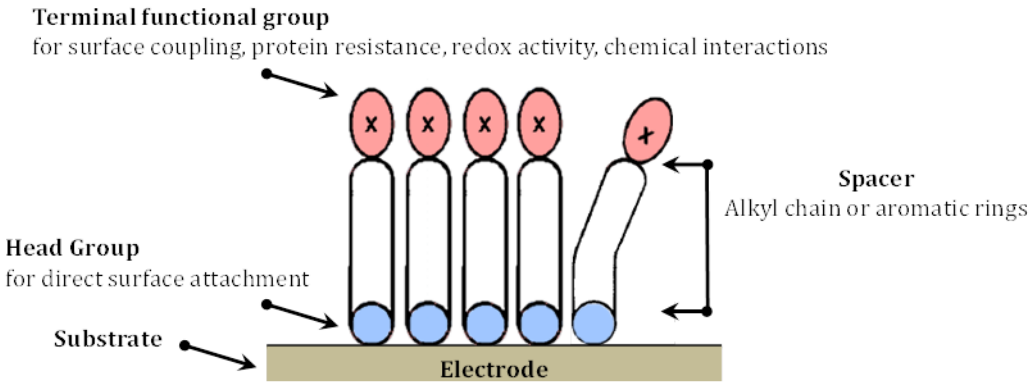

Figure 1.1 Molecular layer on an electrode surface. Molecules are designed with a head group, for direct surface attachment, the aryl or alkyl chain, which provides a well-defined thickness, and the terminal group. Image adapted from Swalen and co-workers[7].

1.3 Properties of carbon electrodes

Carbon materials containing sp^2-hybridised carbon atoms – fullerenes, carbon nanotubes, graphene, graphitic carbons, and amorphous carbons – are of significant technological importance[28] and are widely used in electrochemistry[29-30]. In general, these carbon materials share many desirable properties that have attracted their use as electrode materials such as their chemical and thermal stability, high thermal conductivity, and good electrochemical properties[30].

Of particular interest in this thesis are planar graphitic electrodes; namely, glassy carbon (GC) and pyrolysed photoresist film (PPF). While it is not practical to describe all aspects of these materials, it is important to consider the main aspects that dictate their use and electrochemical reactivity.

1.3.1 Glassy carbon

GC is one of the most widely used electrode materials in electrochemistry. Its popularity stems from its low cost, robustness, and excellent electrochemical properties: good

electrical conductivity, wide potential window, gas and solution impermeability, compatibility with surface modification, and the ease with which it can be reused[30].

Compared to noble metal electrodes, GC has a wider electrochemical stability window, wider compatibility with strong acids, alkali, and non-aqueous solutions, and is much lower in cost[30-31]. The wide potential window is important as it provides access to a greater range of electroactive species. GC can also be fabricated into microstructured carbon materials using moulding and heat-treatment methods, as demonstrated by Whitesides and co-workers[32-33]. Conducting carbon microstructures have potential applications as components in microelectromechanical systems (MEMS). It is proposed that GC microstructures could be used as sensors or actuators for operation under extreme conditions such as elevated temperatures and corrosive environments, therefore having benefits compared to silicon[32].

GC is fabricated by pyrolysing polymeric precursors in a non-oxidising atmosphere to temperatures in excess of 1000 °C and as high as 3000 °C[29]. GC is often produced using polymeric precursors such as phenol-formaldehyde resin, furfuryl alcohol-phenol copolymers, and polyacrylonitrile[29, 33-35]. Whitesides and co-workers prepared GC electrodes by pyrolysis of furfuryl alcohol-phenol copolymers at temperatures between 600-1100 °C in vacuum or in an argon atmosphere[33].

Pyrolysis is performed slowly through a series of potential ramps which are characterised by three main stages: pre-carbonisation, carbonisation, and annealing[36]. During pre-carbonisation (T < 300 °C) solvent and unreacted monomer are eliminated from the polymer precursor. Between 300-500 °C heteroatoms such as oxygen and halogens are eliminated and a network of conjugated carbon is formed. In the later stages of carbonisation (500-1200 °C), hydrogen, oxygen, and nitrogen atoms are completely eliminated, resulting in the formation of an interconnected aromatic network. Annealing is performed at higher temperatures (T > 1300 °C) to improve structural homogeneity and to

remove further impurities[29]. The resulting GC is a disordered form of non-graphitising carbon containing predominantly sp^2-hybridised carbon atoms[31, 37]. The term non-graphitising originates from the inability of the carbon structure to completely graphitise (Figure 1.2a)[31].

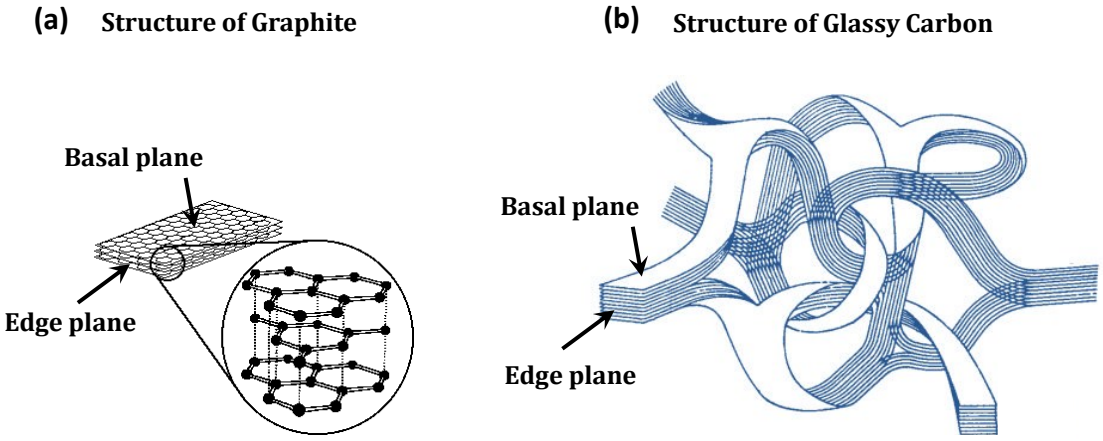

Figure 1.2 Models of carbon structures for (a) crystalline graphite and (b) glassy carbon according to the model proposed by Jenkins and Kawamura. Images adapted from website: http://www.chem.wisc.edu; and Jenkins and Kawanura[38].

The most widely known and accepted structural model for GC is that proposed by Jenkins and Kawamura, which considers the structure to be a complex network of interwoven aromatic ribbons (or fibrils) cross-linked by covalent carbon-carbon bonds (Figure 1.2b)[38]. The model explains well most properties but the porosity present within the structure inadequately accounts for the impermeability of GC towards gases and solutions[31]. The fullerene-related model proposed by Harris provides a better explanation for the inertness and impermeability of GC[39]. However, the model suffers from a lack of direct evidence that GC contains the pentagonal rings of fullerene structures. According to various models, GC has a randomly oriented structure containing both graphite edge plane and basal plane sites[38-40]. Both sites differ greatly in chemical and electrochemical reactivity[41]. In the case of GC, both of these sites are exposed to the electrolyte solution during electrochemical

experiments. This is in contrast to other carbon electrodes such as edge plane pyrolytic graphite (EPPG) and highly ordered pyrolytic graphite (HOPG), where only edge or basal plane sites are exposed to solution during experiments, excluding the presence of defects.

Several reports have identified the importance of basal plane and edge plane sites on the electrochemical reactivity of carbon electrodes[42-43]. In the early 1990s, a number of studies by McCreery and co-workers demonstrated that HOPG basal plane exhibits heterogeneous electron transfer-rate constant (k^o) values for ≈ 20 redox systems which are 1−5 orders of magnitude slower than those on GC[41, 43-45]. These studies draw the general conclusion that edge sites are considerably more reactive than basal plane sites towards electron transfer and adsorption. Adsorption to basal planes is considered relatively weak since there are no permanent dipoles, electrostatic charges, or unsatisfied valences[30]. The slower electron transfer rates at HOPG, particularly for "outer sphere" redox systems, have been attributed to a lower density of electronic states (DOS) compared to GC [41, 44-45]. In contrast, a very recent study by Unwin and co-workers has shown that freshly-exposed basal plane graphite does exhibit fast electron transfer activity[46]. The results obtained by Unwin and co-workers are interesting and contest a large body of literature.

Under ambient conditions, the surface of GC is terminated with a significant amount of oxygenated functionalities[47]. X-ray photoelectron spectroscopy (XPS) studies of GC show that polished GC has an oxygen-to-carbon ratio (O/C) typically between 7-20%, depending on surface treatment and history[47-48]. A general model of the chemical surface of GC (Figure 1.3) considers that various oxygen-containing functional groups are heterogeneously distributed at edge-plane sites[47]. XPS, Raman spectroscopy, and electrochemical analyses have identified oxygenated functionalities such as phenol, ketone, carboxylic acid, lactone, and quinone at the surface of polished GC [47, 49-50].

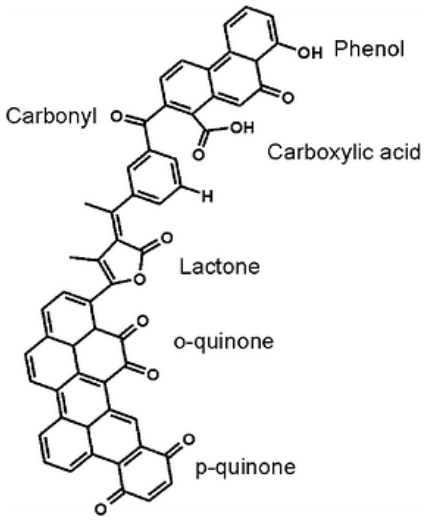

Figure 1.3 A schematic representation of typical functionalities present on the surface of GC under ambient conditions. Image adapted from McDermott and McCreery[51].

The surface of GC becomes deactivated over time with repeated use and with exposure to air[52-53]. Periodic pre-treatment is required to obtain reproducible electrochemical behaviour. The standard method for regenerating GC surfaces is mechanical polishing[30, 52, 54-55]. Another important aspect that dictates the electrochemical response of GC is the surface roughness. For polished GC sourced from Tokai Carbon Co Ltd., typical average surface roughness values range between ≈ 2-4 nm[51, 56-60]. The performance and reproducibility of GC electrodes is largely dependent on the history and pre-treatment method, hence careful handling of GC electrodes is required to obtain reproducible results.

1.3.2 Pyrolysed photoresist film

PPF electrodes are thin films of predominantly sp^2-hybridised carbon on a silicon wafer[61-63]. PPF exhibits similar properties to GC, but unlike GC, has a very low surface roughness (rms ≤ 0.5 nm)[61, 64-66]. The low surface roughness makes PPF an ideal surface for high-resolution imaging using atomic force microscopy (AFM) and scanning electron microscopy (SEM)[65, 67-68]. In particular, PPF can be used as a substrate for determining the film thickness of molecular layers with sub-nanometre accuracy[65-66, 68]. Another attraction

of PPF is that it is amenable to photolithographic processing, hence can be fabricated into microelectrodes for sensing applications[69-70], or complex 3D architectures for carbon-MEMS[62, 71]. To fabricate 3D carbon microstructures the precursor of choice is negative photoresist (SU-8) as this type of photoresist enables high aspect ratio processing[71].

Lyons and co-workers pioneered the fabrication of pyrolysed conducting carbon films[72-73]. Kinoshita and co-workers were the first to report the development and optimisation of PPF as an electrode material[63]. McCreery and co-workers developed the use of PPF further by exploiting the low surface roughness property of PPF to characterise molecular layers[64, 68]. PPF has since been developed for applications ranging from detectors in capillary electrophoresis[70] to molecular electronics devices[74-75]. With the increasing interest in PPF electrodes, both the Gooding and Compton groups have addressed methods of improving its fabrication[76-77]. Gooding and co-workers identified important variables but did not improve the performance or reproducibility of existing methods. Compton's method improves processing times but significantly increases the surface roughness (rms = 1.44 nm), which is undesirable for thin film characterisation studies[77].

PPF materials are fabricated by pyrolysis of positive or negative photoresist precursors to temperatures between 600-1100 °C[63]. Surfaces prepared at higher temperatures have considerably lower resistivities and show better electrochemical properties, hence PPF is generally pyrolysed to temperatures between 1000-1100 °C[62-63]. Pyrolysis is conducted in a reducing atmosphere[62, 64, 66], in an inert gas[61-63], or under vacuum[62]; these conditions prevent O_2 reacting at the surface. Initially, the spin-coated photoresist is hard-baked at a mild temperature (≤ 115 °C) to facilitate evaporation of the solvent, which helps to minimise cracking[63]. The carbonisation stage involves a slow increase in temperature (< 50 °C/min) up to the maximum pyrolysis temperature[61]. A final heat treatment is performed at the maximum processing temperature for 1 h. PPF surfaces prepared in this way are reduced in thickness from a 6-8 μm photoresist layer to an ≈ 2 μm carbon layer[61-62].

High-resolution transmission electron microscopy measurements of PPF pyrolysed at 1100 °C have shown that PPF has graphitic crystallites like those observed at GC but with smaller dimensions[62-63]. Raman spectroscopy shows that both sp^2 and sp^3-hybridised carbon atoms are present within the structure of PPF pyrolysed to 1100 °C, and that PPF is more disordered than GC[30, 61]. More quantitative conclusions such as the relative amounts of sp^2 to sp^3 carbon atoms in these materials remain elusive, however. Concerning surface chemistry, PPF has a lower surface oxygen content (O/C ≈ 2%) and is more stable towards air oxidation compared to GC[64]. The lower oxygen content at PPF relative to GC has been attributed to a greater presence of H-terminated carbon[64].

The electrochemical properties of PPF are similar to GC but not identical[64]. The surface resistivity of PPF is similar to that of GC[64]. Capacitance is significantly smaller at PPF by approximately a factor of four[62, 64]. Electron transfer rates for some redox systems ($Ru(NH_3)_6^{3+/2+}$ and $K_3Fe(CN)_6^{3-/4-}$) are similar for GC and PPF, whereas slower electron transfer rates are observed at PPF for Fe^{3+}/Fe^{2+}, ascorbic acid, and dopamine[64]. In terms of chemical modification, both PPF and GC generally exhibit similar reactivity towards electrochemical modification via aryldiazonium salt solutions[64].

1.4 Covalent modification of carbon surfaces

Covalent chemical modification of sp^2-hybridised carbon electrodes is an active area of research due to the potential to form very stable molecular coatings with different functionalities on an important class of conducting substrates. Current surface modification methods rely on the formation of highly reactive species such as aryl radicals[78-79] and aminyl radicals[80], nitrenes[81], and carbenes[82], which react with high-efficiency at the surface. Derivatised GC and PPF surfaces are attracting interest for applications in molecular electronics[83-84], energy storage and conversion[85-86], and for chemical[87-89] and biosensors[90-91].

Electrografting is a widely used strategy for covalent modification of carbon and other conducting surfaces. In addition, a number of non-electrochemical methods have also been explored. Both of these strategies have been reviewed recently by Pinson and Bélanger in 2011[92], and by Downard and Barrière in 2008[93].

Electrografting is performed using either reduction or oxidation reactions. Oxidative grafting methods have been developed using the following modifiers: amines[94-96], thiols[97], alcohols[98], arylacetates[99], and arylhydrazines[79, 100]. Reductive methods have been developed using aryldiazonium salts[78], sulfonium salts[101], iodonium salts[102-103], and alkylhalides[104-105]. Non-electrochemical methods include the spontaneous reaction of aryldiazonium salts[106], and the photochemical reactions of alkenes[107], alkynes[107], azides[81], and diazirines[82].

Of particular interest in this thesis are the following electrografting methods: the electrochemical reduction of aryldiazonium salts, the electrochemical oxidation of aliphatic amines, and the photochemical reaction of arylazides. These modification strategies are discussed in more detail in Sections 1.4.1, 1.4.2, and 1.4.3, respectively.

1.4.1 Electrochemical oxidation of amines

The electrochemical oxidation of amines at carbon fiber and GC surfaces to give covalently-attached thin films was first reported in 1990[94]. The method was established by Pinson and co-workers and was the first example of electrochemically-assisted covalent modification. Aliphatic amines containing alkyl groups such as butylamine[95] or ethylenediamine[94, 108-109], and aromatic amines such as *p*-nitrobenzylamine[110], have been grafted at different carbon surfaces including GC[94-95, 108, 110], carbon fiber[94], PPF[96], HOPG[81], and carbon nanotubes (CNTs)[109]. In addition to carbon, the grafting method is also applicable for the modification of gold and platinum substrates[110].

The electrochemical reaction is most commonly performed in aprotic medium (DMF[110] and ACN[94]), but has also been reported in aqueous media[96] and ionic liquids[111]. Aliphatic amines are oxidised at high potentials (typically ≥ 1 V vs. saturated calomel electrode (SCE) in ACN or DMF)[94, 110]. Adenier and co-workers have investigated the reaction in detail and established that the surface attachment proceeds via a radical-based reaction[110]. The proposed and generally accepted reaction path is shown in Scheme 1.1.

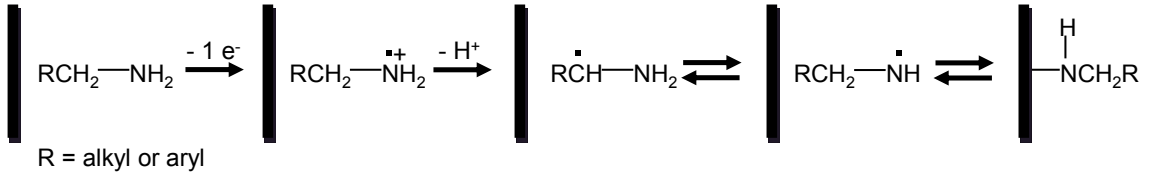

Scheme 1.1 Surface modification by electrochemical oxidation of amines at carbon, gold, and platinum.

The reaction proceeds via an irreversible one-electron oxidation of the amine to form a radical cation. The radical cation deprotonates to give a carbon radical and then an aminyl radical which subsequently binds to the surface. Indirect evidence that the attachment occurs via the aminyl radical has been obtained using cyclic voltammetry, XPS, and infrared reflection-absorption spectroscopy[110]. The attachment is resistant to sonication in different solvents, which is consistent with the formation of a covalent bond between the layer and the surface[95, 110]. Although no direct evidence for the covalent bond has been elucidated on carbon, evidence for the covalent bond has been observed on gold and Pt[110]. XPS data showed the appearance of a nitride signal after modification, confirming the formation of Au-N and Pt-N bonds between the layer and the surface.

The successful modification of carbon electrodes is most widely studied using cyclic voltammetry. The presence of a molecular layer can be tested be recording the voltammetry of solution redox species at the surface before and after modification. A change in response is consistent with modification. Different redox probes can be

examined which can reveal information about the "dynamic" behaviour of the films, including pH or charge-dependant properties. A powerful technique to test for the presence of a film is to graft modifiers that contain electroactive groups such as ferrocene[111-112] catechol[95], and nitrophenyl[111] (NP) groups. These groups can be identified at the surface after modification. If the electroactive groups are chemically reversible then it is possible to test the stability of the groups to conditions such as repeat cycling or sonication treatment[95]. The redox peaks can be integrated to yield an estimate of the surface concentration of functional groups. From this information, it is possible to estimate the efficiency of the grafting reaction and whether monolayer or multilayer films are formed.

AFM is also a powerful technique for directly measuring the physical properties of films such as thickness, topography, and film density. For example, Geneste and co-workers have studied amine-derived films on PPF by AFM and showed that monolayers or multilayers can be prepared depending on the electrolysis time and the solvent used[96]. AFM measurements performed by Cruickshank and co-workers also showed that the film thickness of amine-derived films on PPF can be carefully controlled using different electrolysis times, to give films ranging from sub-monolayer to multilayers[113].

Amine-derived films have been used widely as "tether layers" for coupling molecules and nanostructures. In one example, an ethylenediamine-derived film attached to PPF was used as a tether layer for coupling single-walled CNTs to the surface via amide bond formation using *N*,*N*'dicyclohexylcarbodiimide[114]. In another example, osmium bipyridine complexes were electrografted directly to the surface via an amine-containing derivative[115]. In the same report, osmium complexes were attached to the surface indirectly via chelation to a surface-bound ligand. The surface-bound ligand had been grafted by electrochemical oxidation of *p*-aminopyridine. Both CNT-modified and osmium bipyridine-modified surfaces are desirable for electrocatalytic sensing applications [116-117].

1.4.2 Electrochemical reduction of aryldiazonium salts

Surface modification using aryldiazonium salt compounds has been widely studied since the electrochemically-assisted reduction of aryldiazonium ions at GC was first described by Pinson, Savéant and co-workers in 1992[78]. Since then there have been numerous publications, reviews, patents, and a book published on the topic[118-120]. The key attractions of aryldiazonium salt chemistry are the ability to form a covalent surface-film attachment and the high versatility for forming reactive and functional layers[118]. With aryldiazonium salt chemistry it is possible to graft films at almost any material (carbon, metals, semi-conductor, and non-conducting) with a wide range of molecules (organic, metal complexes, and biomolecules)[121]. The electrochemical reaction is the best-established method of grafting at carbon surfaces[92, 122]. The spontaneous grafting reaction is the main alternative method for modifying carbon surfaces. Spontaneous grafting is experimentally very simple; providing the substrate has reducing capabilities, grafting is achieved by immersion of the substrate in diazonium solution.

The electrochemical reduction of aryldiazonium salts was first explored as a method of modifying carbon surfaces such as GC, HOPG, carbon black, and carbon fiber, with stable organic layers[78, 122]. The electrochemical reduction of *p*-nitrophenyl diazonium salt (NP_D) in ACN (with 0.1 M $TBABF_4$ as supporting electrolyte) was the first modifier explored. In the follow up work in 1997, Pinson, Savéant and co-workers expanded the electrografting method to a wide range of chemical modifiers; namely, *p*-nitrophenyl, anthraquinone, naphthalene, *p*-acetamido, and *p*-bromophenyl diazonium salt derivatives[122]. Further consideration of the reaction mechanism led to the conclusion that the reduction of aryldiazonium salts in aprotic medium generates reactive aryl radicals which subsequently bind at the surface to form a covalent bond[122]. The proposed mechanism for electrochemical modification of carbon and other surfaces is shown in Scheme 1.2. Andrieux and Pinson have shown that the aryldiazonium cation undergoes a homolytic

dediazoniation with a concerted cleavage of nitrogen (without the formation of a diazenyl intermediate), to give a phenyl radical and a dinitrogen molecule[123]. The homolytic pathway was demonstrated for simple *para*-substituted diazonium derivatives and is considered generally applicable for other diazonium derivatives of anthraquinone and porphyrins, ruthenium and osmium complexes, and modified proteins, to name a few. The reaction is usually performed in ACN but can also be performed in aqueous acid. Aryldiazonium salt solutions used for grafting are prepared either from the isolated salt or *in situ* via arylamine or aryltriazene precursors.

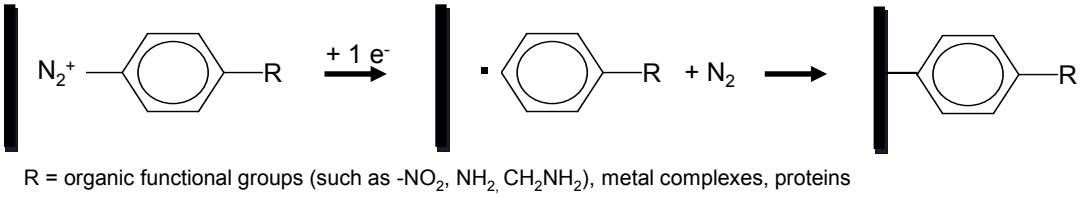

Scheme 1.2 Surface modification by electrochemical reduction of aryldiazonium salts at carbon.

An important aspect of aryldiazonium salt chemistry is the ability to form a covalent attachment between the surface and the layer. Evidence for the presence of a covalent bond is obtained by testing the stability of the layer and examining the modified surface using spectroscopy and computational methods. The stability of diazonium-derived films has been tested against a number of different conditions: exposure to ambient conditions, sonication in various solutions, heat treatment, applied potential, and mechanical testing[21].

A large number of reports show that electrografted diazonium-derived films are persistent towards sonication treatment in various solvents. For example, an electroactive nitrophenyl layer on GC remained essentially unchanged after 15 min sonication in non-aqueous organic solvents such as ACN and DCM[122]. The films are also very stable under ambient conditions; no difference in the XPS spectrum was observed after exposure to air for six months[122]. The thermal stability of modified surfaces under inert gas atmosphere has not

been studied on GC and PPF; however, on carbon powder the films were stable up to 200 °C[124]. All of these examples of high stability show strong evidence for the existence of a strong C-C bond between the surface and the organic layer.

The presence of a covalent bond between the surface and the organic layer has been investigated using surface spectroscopy and density functional theory (DFT) methods. Time-of-flight secondary ion mass spectroscopy (ToF-SIMS) analysis of modified GC surfaces clearly reveals the formation of covalently attached films[125-126]. The ToF-SIMS data shows direct evidence for the presence of C-aryl fragments corresponding to the bond between GC and the aryl film[125]. O-aryl fragments were also found, confirming that the modifier also attaches at surface sites containing oxygenated functionalities such as those shown in Figure 1.3. Surface characterisation studies using attenuated total reflectance infrared and Raman spectroscopy have shown evidence consistent with a covalent attachment[127]. These studies revealed that the molecules are oriented approximately perpendicular to the plane of the surface, as would be expected for molecules attached via a single head group (Figure 1.1)[127]. The IR spectra showed no evidence for a nitrogen-nitrogen triple bond stretching vibration, which would be present if the diazonium moieties remained unreacted. On graphene, which can be used as a structural model for GC and PPF, Raman spectroscopy shows the appearance of sp^3-hybridised carbon atoms on the surface after modification, consistent with newly formed covalent bonds[128]. In general, spectroscopic techniques are rarely sufficiently sensitive to obtain direct evidence of the surface-aryl bond, due to interference from the high density of C-C bonds on the carbon surface. Nevertheless, the few examples mentioned here clearly support the presence of a covalent bond. DFT calculations are also in good agreement with the formation a covalent bond between an sp^2-hybridised carbon surface (graphene) and the organic layer, as shown by the models in Figure 1.4[129]. Computational calculations by Jiang and co-workers have shown that favourable bonding attachment occurs at the edge plane sites of a graphene

sheet, converting the sp^2-hybridised carbons to sp^3 carbons. Bonding strengths consistent with covalent attachment (107 and 265 kJ/mol) were observed on armchair and zigzag sites, respectively. The additional bond strength observed at zigzag sites is explained by the concept of a "partial radical", where localised π-electrons at the edge site act collectively when binding with another radical. The formation of a sp^3-hybridised carbon-carbon bond was also observed at the basal plane, although the attachment was weakly bonded (24 kJ/mol).

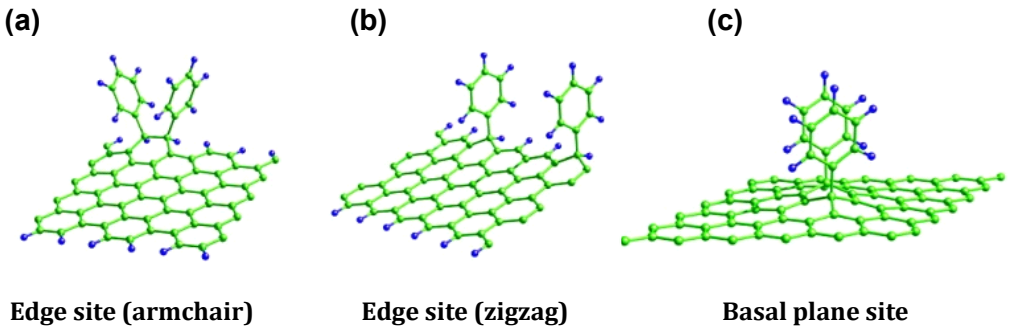

Figure 1.4 Optimised structural models for diazonium-derived phenyl groups on a pristine graphene sheet at different sites: (a) armchair edge sites, (b) zigzag sites, and (c) basal plane sites. Image adapted from Jiang and co-workers[129].

Electrochemical reduction of aryldiazonium salts at carbon surfaces typically leads to the formation of multilayers, as determined by AFM, cyclic voltammetry, XPS, and other spectroscopic techniques[21]. The mechanism for multilayer formation is discussed in the next paragraph. In general, the thickness of the films can be controlled from monolayer to many multilayers by controlling factors such as the modifier concentration, reaction time, solvent, charge passed, applied potential, and the bulkiness of the substituents on the modifier[65-66, 130-133]. Reliable approaches to forming monolayers have been developed such as the "formation-degradation" approach, first reported by Daasbjerg and co-workers[134-135]. In one example, a multilayer film containing cleavable disulphide bonds is electrografted to the carbon surface in the first step. In the second step, the disulphide bond is cleaved

electrochemically to yield a thiol phenolate monolayer. A similar strategy for forming monolayer films on GC and PPF surfaces, developed by Hapiot and co-workers, involves grafted a silyl-protected ethnyl aryl multilayer in the first step[136]. In the second step, the bulky silyl groups are deprotected in tetrabutylammoium fluoride solution, yielding a close-packed monolayer on GC and PPF. Confirmation for the attachment of monolayers in these studies was obtained using both electrochemical and AFM measurements.

Unless the electrografting conditions are precisely controlled or specially designed modifiers with cleavable or sterically-hindered substituents are used, multilayer films will form with thicknesses ranging from a few nanometres to microns[131, 133]. A general mechanism has been proposed by Combellas, Pinson and co-workers which accounts for multilayer film growth, as shown in Figure 1.5[125].

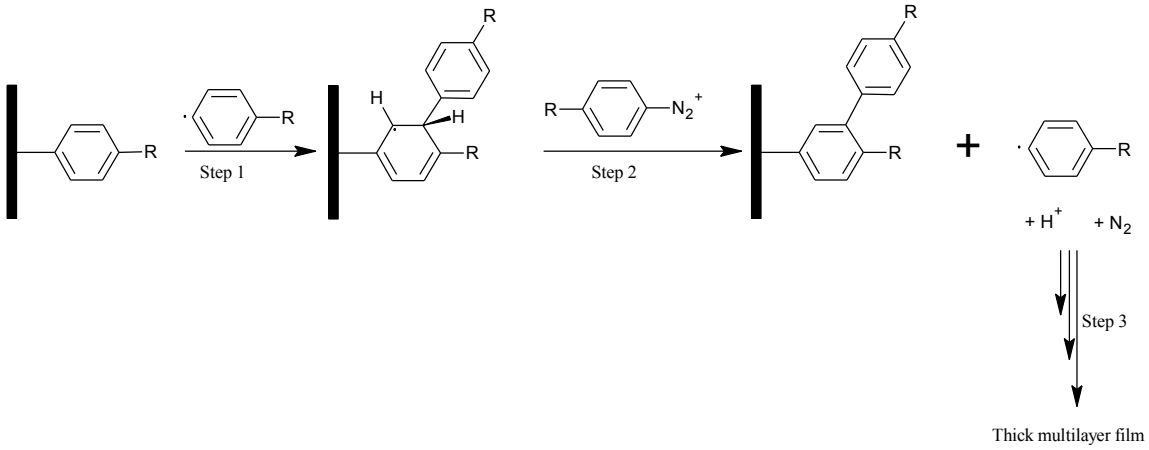

Figure 1.5 Multilayer film formation by reduction of aryldiazonium salts at carbon using electrochemical or spontaneous methods. Adapted from Combellas, Pinson and coworkers[125].

After formation of the first layer, multilayer growth proceeds via aromatic homolytic substitution. In the first step of multilayer formation an aryl radical attacks the already grafted phenyl group, yielding a surface-bound cyclohexadienyl radical. The radical attaches at the *ortho* position (*meta* to the surface) of the surface-bound *para*-substituted

aryl groups, due to steric effects[118]. The cyclohexadienyl is then oxidised by electron transfer from another diazonium cation. The diazonium cation itself is reduced (Step 2), yielding another aryl radical which can continue the growth process (Step 3). Aryl radicals are also generated electrochemically by electron transfer through the film, depending on the applied potential and the passivating nature of the layer. It is important to note that this mechanism does not account for the incorporation of azo linkages into the films, which have been observed using XPS and ToF-SIMS[126, 137-138]. Mechanisms have been proposed which account for the incorporation of azo bonds in the films[139]. According to Pinson and co-workers, azo bonds form via a coupling reaction between a diazonium cation and surface-bound cyclohexadienyl radicals[126].

Carbon surfaces modified via aryldiazonium salt electrografting have been investigated in a number of different studies for applications such as biosensing[91, 116, 140-142], chemical sensing[140, 143], surface patterning[144], and molecular electronics[84, 145].

1.4.3 Reaction of azides

Azide compounds are widely used as photoaffinity labelling agents[146], in organic synthesis[147], for surface "click chemistry"[15, 148], as cross-linkers in photoresists[149], and for covalent surface modification[150]. In surface chemistry, arylazides and alkylazide derivatives are used as precursors for the formation of nitrene species, which react at surfaces of materials such as carbons[151, 152 , 153-154], polymers[155-156], and metals[150], to give film-modified surfaces. Surface modification is achieved by drop-coating or spin-coating an arylazide solution on the surface, or immersing the substrate in the solution, followed by exposure of the surface to UV irradiation or heating. Grafting conditions are mild and typically performed by UV exposure at ≈ 365 nm or by thermal decomposition at ≤ 160 °C in a single step. In the case of *para*-substituted arylazides, the substituent in the *para* position can be tailored to provide surfaces with different functionalities such as

poly(ethyleneglycol)[157], hydroxylalkyl[151] and fluoroalkyl groups[151, 157], bromo[151, 158] and amino groups[154, 158].

The reactions of arylnitrenes include insertion into C-H, O-H, and N-H bonds, addition reactions with C=C bonds, rearrangement reactions leading to ring expansion, hydrogen abstraction, and dimerisation (Scheme 1.3)[159].

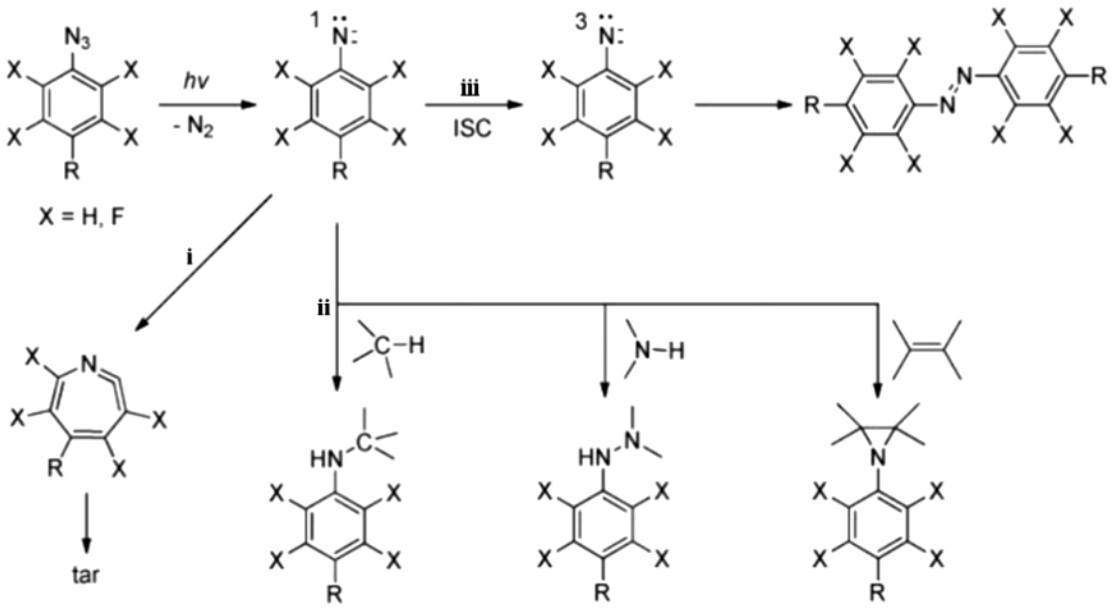

Scheme 1.3 Reaction scheme for arylazide photochemistry illustrating (i) ring expansion, (ii) insertion and addition reactions, and (iii) intersystem crossing. Adapted from Liu and Yan[150].

In terms of surface modification, any of these reactions may occur during grafting, depending on factors such as the substituents on the ring, the solvent, and the surface structure of the substrate. For GC and PPF, the surface reaction most likely proceeds via insertion or addition reactions with the sp^2-hybridised network, various oxygenated functionalities, and sp^3 carbon atoms. The general reaction pathway for surface modification using arylazides is represented in Scheme 1.4[150].

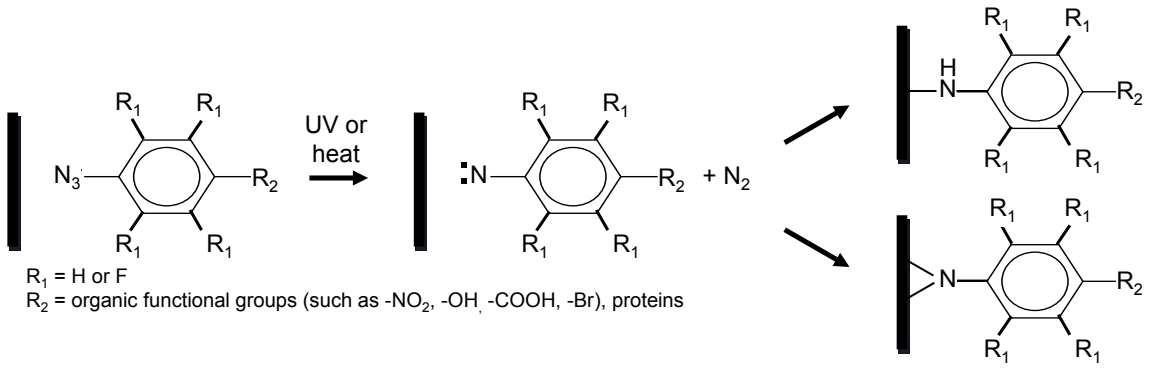

Scheme 1.4 Surface modification by photochemical and thermal reaction of arylazides at surfaces via arylnitrenes which undergo insertion and addition reactions.

The first demonstration of the use of arylazides for covalent modification of carbon surfaces was reported in 1994 by Yan and co-workers[160]. In this work, the surface of C60 was modified using *N*-hydroxysuccinimide perfluorophenyl azide by either a photochemical or thermal reaction. Arylazides, most notably perfluorophenylazide (PFPA) derivatives, have since been used for modifying other carbon materials such as GC[154, 161], PPF[154], HOPG[81, 156], CNTs[151, 162], and graphene[157-158, 163]. On the basis of results obtained on graphene, CNTs, and C60, modification of graphitic carbon surfaces occurs via addition of nitrenes across C=C bonds to form C-N (aziridine) bonds. Evidence for covalent bond formation has been demonstrated by XPS and sonication treatment after reaction of PFPA at graphene[158]. Spectroscopic analysis of CNTs after modification via nitrenes is also consistent with covalent bond formation[162]. No spectroscopic data has been obtained on GC and PPF to confirm the nature of the bonding.

In contrast to graphene and CNTs, modification of GC and PPF using azides is relatively unexplored. Kuhr and co-workers developed the reaction at GC using photobiotin, an azide derivative of biotin[161, 164-167]. More recently, Niwa and co-workers demonstrated the efficient grafting of electroactive ferrocene groups on the surface of GC and HOPG[153]. Depending on the modifier concentration drop-coated onto the surface, monolayer or

multilayer films were obtained at GC and HOPG surfaces. The similar surface concentrations observed at both GC and HOPG suggests that the reaction of nitrenes proceeds at both the edge and basal planes. In work reported by Yu, a simple spin-coating procedure was developed which permitted the formation of loosely-packed monolayers on GC and PPF surfaces[154]. Yu also demonstrated that the azide-derived films resisted sonication for 5 min in DCM, confirming that the films are stably-attached. Evidence for covalent bond formation is based on the stability of the attachment and spectroscopic studies performed on other types of sp^2-hybridised carbon.

Overall, arylazides provide a simple, efficient, and versatile route to covalent modification of graphitic surfaces. Nitrenes are generated in a single step using either light or heat under mild conditions, and can be reacted at a wide range of graphitic surfaces. Although not discussed here (see section 1.5.1) the ease at which patterning can be achieved is a useful characteristic of the photochemical grafting reaction.

1.5 Patterning surfaces using aryldiazonium salts and arylazides

Patterning surfaces with functional materials such as molecular layers, polymers, and metals is important in many fields of modern science and technology[131, 168-169]. Applications range from the production of patterned integrated circuits on silicon substrates, data storage and MEMS devices, to the fabrication of electrode arrays for chemical and biological sensor applications. For a large number of applications both in industry and in research, patterned surfaces are fabricated using photolithographic techniques such as projection photolithography. Non-photolithographic patterning techniques such as dip pen nanolithography and soft lithography are of interest for many device-based applications due to potential advantages such as lower capital and processing costs, higher speed, higher resolution, and better compatibility with biological and chemical solutions.

The main goal of patterning is to precisely control the spatial distribution of chemical and physical properties on the surface. The combination of molecular level modification with patterning enables the preparation of sophisticated molecular assemblies. For some applications, a surface presenting multiple regions of different chemical functionalities is desired, for example, on multi-receptor arrays for analyte detection. For other applications, the goal is not to define multiple functionalities but to prepare geometric patterns of the same chemical functionality. In this case, the patterned functionality might be used to control the growth or death of cells on a surface, or as a platform for preparing highly-ordered arrays of quantum dots or metallic nanoparticles. At this stage, the most promising applications of patterned diazonium and azide layers are as platforms for biological sensor devices. The main attraction of aryldiazonium salt and arylazide chemistry for the fabrication of sensing interfaces is the greater stability compared with using alkanethiol chemistry.

1.5.1 Patterning using aryldiazonium salts

There are four main categories of methods which have been developed for patterning using aryldiazonium salts[144]: (i) scanning probe lithography (SPL); (ii) soft lithography; (iii) lithography; and (iv) surface-directed patterning. The reported methods for patterning from aryldiazonium salts are summarised in Table 1.1.

It is important to note the two general types of patterning: serial and parallel patterning[170]. Serial patterning refers to those methods where regions of the surface are defined with chemical functionalities by drawing or scribing on the surface. Serial methods are inherently slow and require significant investment in equipment. However, these methods enable the production of high-resolution (sub-100 nm) surface patterns. In contrast, parallel methods such as photolithography allow the rapid generation of repeat patterns at the micro or nanoscale, but at lower resolution than serial methods. Parallel methods are suited

for rapid patterning of high-density feature over large areas (> cm^2), and are lower in cost compared to serial methods.

Table 1.1 Patterning techniques using aryldiazonium salts, and their processing type, demonstrated critical feature size, and demonstrated substrate compatibility.

Technique	Process type	Minimum feature size	Substrate
(i) Nanoshaving using AFM	Serial	140 nm[171]	PPF
(i) SECM	Serial	20 μm[172]	GC
(i) SECM-AFM	Serial	200 nm[173]	Au
(i) Pin spotting	Serial	150 μm[174]	Au
(ii) Microcontact printing	Parallel	20 μm[175]	PPF, Au, Si, Cu
(ii) Electroprinting	Parallel	130 μm[176]	Au
(ii) Micromolding	Parallel	18 μm[177]	PPF
(ii) Nanosphere lithography	Parallel	200 nm[178]	GC[178], Au[178]
(iii) Photolithography	Parallel	2 μm[142]	Polymer substrates
(iii) SAMs as a sacrificial resist	Parallel	5 μm[179]	Au
(iii) Photo-deactivation using a mask	Parallel	500 μm[142]	Au, polyaminophenylene
(iii) Localised doping and electrografting	Parallel	2 μm[180]	Si(100)
(iv) Electrode arrays via photolithography	Parallel	3 μm[181]	Mo

SPL methods are high-resolution serial patterning techniques that feature a sharp tip in close proximity to the surface to pattern low micro and nanoscale features on the surface. These strategies are based on AFM, scanning tunnelling microscopy (STM), and scanning electrochemical microscopy (SECM)[182-183]. The smallest repeated feature size of a diazonium-derived surface pattern was obtained using nanoshaving[171]. In nanoshaving, a well-defined region of a film is mechanically removed with an AFM tip, leaving a region of the underlying substrate exposed. In addition to the single component patterns, two-component patterns have also been prepared by grafting a second film to the freshly exposed region.

Soft lithography, pioneered by Whitesides and co-workers, is a suite of patterning techniques that can be used to pattern micro and nanoscale features on surfaces, in an

ordinary laboratory, using very simple and low-cost techniques[184-185]. The key to soft lithography is the use of a patterned elastomer, typically poly(dimethylsiloxane) (PDMS), for printing, moulding, embossing, or a combination thereof. Aryldiazonium salts have been patterned using printing and moulding methods[67, 176-177]. Microcontact printing (μCP) is one of the most promising aryldiazonium salt patterning methods due to its experimental simplicity and versatility[67, 175]. The method is based on the spontaneous reaction hence no potentiostat or complicated equipment is required for routine patterning. Low micrometre-scale patterns, relatively short processing times (< 1 h) and wide substrate compatibility are important features. In addition, patterned μCP films have been used for tethering carbon nanotubes, gold nanoparticles, and simple organic molecules[175]. Despite significant promise, no sensor or electronics applications have been developed using μCP at this stage.

A number of lithographic methods have been developed for use with aryldiazonium salts. Surprisingly, prior to this thesis, conventional photolithography using standard photoresists has not been explored. Furthermore, none of the lithographic patterning methods had been developed for use with carbon surfaces. During the course of this thesis work a patterning method for modifying gold surfaces was reported by Palacin and coworkers[142]. A grafted diazonium-terminated film was irradiated through a photomask, decomposing the diazonium groups in the exposed regions. The non-exposed regions of the film were then used as reactive tethers to couple glucose oxidase, demonstrating how the method could be used for fabricating biosensors.

Use of electrode arrays is the best-established method of patterning aryldiazonium salts and has been exploited for preparing biosensors[141, 186-187]. These methods are conceptually and experimentally simple. First, individually-addressable metal or semiconductor microelectrode arrays are fabricated, followed by electrografting (or coupling) different modifiers onto selected electrodes. In one example, two different modifiers were grafted sequentially on a screen-printed carbon electrode microarray with 8 individually

addressable electrodes[188]. The modifiers were diazonium derivatives of antibodies which enabled the preparation of a multifunctional biosensor array.

1.5.2 Patterning using arylazides

Patterning surfaces using arylazides has been restricted to methods based on lithography. For carbon surfaces, patterning has been achieved by photochemical decomposition of arylazides either through a photomask or using maskless photolithography. The latter strategy was initially explored by the Kuhr group who developed two methods: interference patterning and dynamic confocal patterning. The first technique, interference patterning, featured a laser interference pattern that was illuminated on an azide-covered GC surface for between 20-300 s[161, 164, 166-167]. The method is typically used to generate micrometre-sized line patterns with line widths and spacings between 2 and 10 μm. In one example, the resolution of the method was optimised and surface patterns were generated with sub-micron feature sizes (line widths = 0.85 ± 0.1 μm)[166]. The second technique, a type of serial patterning, required the use of a laser scanning confocal microscope[165, 167] to "write" onto the azide-coated surface. The substrate is placed on an x-y-z piezoelectric stage which can be programmed to move underneath the laser. Surface patterns with widths of 5-20 μm have been produced using this technique. The patterning rate ranges from 30 to 100 μm/s, which is fast compared to other serial patterning methods. Both types of maskless photolithography permitted the attachment of biomolecules on micron or sub-micron patterned regions which could be used for biosensing technologies such as enzyme immunoassays.

Photopatterning of azides on graphitic surfaces using a photomask was first investigated on HOPG[156] and has since been used for patterning GC and PPF[154], and CNTs [151]. Use of a photomask is an experimentally simple and fast route to micron-sized patterns on carbon surfaces. The general procedure requires a photomask to be placed in contact or in close proximity with an azide-coated surface. The coated surfaces are prepared by drop-coating,

spin-coating, or immersion in modifier solution, then dried before contacting with the photomask. After the photomask is placed on the surface, the samples are irradiated for periods up to 30 min. The dimensions of the resulting surface patterns range from features as small as 5 μm to features with sizes of 450 μm. Applications of the azide-derived surface patterns on carbon include preparation of platforms for biosensing[156] and a stable hydrophobic-hydrophilic surface which effectively mimics the back of a Stenocara beetle of the Namib desert[151].

1.6 Aims

The overall aim of this thesis is to develop new strategies for covalent attachment and patterning of molecular layers on carbon surfaces, and to investigate the properties of the films using electrochemical and other surface characterisation techniques. The specific aims are given below:

- To develop new methods for preparing low-cost and high performance graphitic carbon electrodes for thin film characterisation studies and electroanalysis.
- To prepare new functional molecular layers on surfaces, particularly planar graphitic carbon, using aryldiazonium salts, arylazides, and alkylamine modifiers.
- To expand the scope of methods available for patterning molecular layers by combining covalent surface modification with microfabrication techniques such as photolithography and soft lithography.
- To gain insight into the structural and chemical properties of molecular layers such as surface concentration, film growth and thicknesses, film stability, and chemical functionality.
- To investigate the utility of film-modified surfaces as tether layers for surface coupling and immobilisation reactions.

General experimental

2.1 Introduction

This chapter describes the chemicals, materials, instrumentation, and general experimental procedures used throughout this thesis. Chapter-specific experimental methods not described here are found in the experimental section of the relevant results chapter.

2.2 Chemicals and preparative methods

2.2.1 Solutions and solvents

All aqueous solutions were prepared using Milli-Q water (Millipore, USA) with resistivity ≥ 18 MΩ/cm. Phosphate buffer saline (PBS) solutions, pH 7.4 and pH 11.4, were prepared from 0.04 M phosphate buffer (PB) with added 0.1 M NaCl. $K_3Fe(CN)_6$ solutions were prepared in PBS (pH 7.4) unless stated otherwise.

The following solvents were used as received: *N*,*N*-dimethylformamide (DMF, Sigma-Aldrich, 99.8% anhydrous) (DMF, Scharlau Chemie, 99.9%), dichloromethane (DCM, Acros Organics, 99.5% stabilised with molecular sieves, extra dry), isopropyl alcohol (IPA, Sigma Aldrich), acetone (99.5%, Mallinckrodt Baker), ethanol (EtOH, 99.9%, Merck), ethyl acetate (EtOAc, Emsure® ACS, ISO, Reag), methanol (MeOH, Sigma Aldrich, ≥ 99.8%).

Acetonitrile (ACN, 99.9%, BDH), tetrahydrofuran (THF, Sigma Aldrich, 99.9%) and diethyl ether (Sigma Aldrich, ≥ 99.5%) were refluxed under N_2 for at least 2 h prior to distilling in a N_2 atmosphere. All solvents were distilled under a N_2 atmosphere.

2.2.2 Reagents

The following reagents were used as received: potassium ferricyanide ($K_3Fe(CN)_6$, Riedel-de Haen), potassium phosphate monobasic (KH_2PO_4, Sigma Aldrich, ≥ 99.0%), disodium hydrogen orthophosphate phosphate (Na_2HPO_4, Analar, 99.5%), sodium nitrite ($NaNO_2$, 98%, Panreal), sodium hydroxide (NaOH, Fisher Scientific, 98.6%), potassium chloride and sodium chloride (NaCl and KCl, J. T. Baker, 100%), sodium citrate (BDH, > 99.0%), ferrocene (Fc, Sigma-Aldrich, 98.0%), fluoroboric acid (HBF_4, 50 wt. % in water, Acros Organics), tetrabutylammonium hydroxide (TBAOH, 40 wt. % in water, Acros Organics), hydrogen tetrachloroaurate(III) hydrate ($HAuCl_4$, Strem Chemicals, 99.9%), *p*-nitrobenzoyl chloride (> 98.0%) and ethylenediamine (> 99.0%) (both Merck-Schuchardt), methoxy-poly(ethylene glycol)-amine (PEG_a) (> 99.0%, Laysan Bio), triethylene glycolamine (TEG_a) (> 97.0%, Prime Organics), and *p*-nitrobenzoic acid (BDH, > 99.0%), benzylchloroformate (Acros Organics, 97 wt. % stabilised), glacial acetic acid (May & Baker, 99.7%), dimethylamine (40 wt. % in water, Merck), sodium azide (99.0%, Fisons), palladium/charcoal activated (BDH, 10% Pd), nitrosonium tetrafluoroborate ($NOBF_4$, 97.0%), bovine serum albumin (BSA, lyophilised powder, ≥ 96.0%), *p*-toluenesulfonic acid monohydrate (TsOH, 98.5%), *p*-nitroaniline (≥ 99.0%), *p*-bromoaniline (97.0%), *p*-aminobenzoic acid (97.0%), *p*-(aminomethyl)aniline (99.0%), tetramethylammonium tetrafluoroborate ($TMABF_4$, ≥ 98.0%), copper (II) acetate monohydrate ($Cu(OAc)_2$, 98.0%), *p*-azidophenyl isothiocyanate (ITC_A), *p*-azidoaniline hydrochloride (AP_A), *p*-nitrobenzoic hydrazide, ferrocenemonocarboxylic acid (FCA), hydroxymethylferrocene (FcOH), *O*-(*N*-succinimidyl)-*N*,*N*,*N*′,*N*′-tetramethyluronium tetrafluoroborate (TSTU), and *N,N*-diisopropyl ethylamine (DIPEA) (all Sigma-Aldrich, purity ≥ 97.0%).

Common laboratory grade reagents and materials used as received: sulphuric acid (H_2SO_4), hydrochloric acid (HCl), hydrogen peroxide (H_2O_2), sodium sulphate (Na_2SO_4), Celite®, thin layer chromatography silica gel plates.

2.2.3 Preparation of tetrabutylammonium tetrafluoroborate electrolyte

Tetrabutylammonium tetrafluoroborate ($TBABF_4$) was prepared and isolated by reaction of TBAOH with HBF_4. 5 mL of 50% HBF_4 was diluted to 25 mL with Milli-Q water. 20 mL of TBAOH was diluted to 100 mL with Milli-Q water. The diluted HBF_4 solution was added to the diluted TBAOH solution, with stirring, to yield a white precipitate. The precipitate was washed with Milli-Q water and filtered under vacuum overnight. The electrolyte was subsequently dried under vacuum at 80 °C for a minimum of one day. The dry electrolyte was stored under vacuum and in the dark.

2.2.4 Synthesis of para-substituted aryldiazonium tetrafluoroborate salts

p-Nitrophenyldiazonium salt (NP_D), *p*-carboxyphenyldiazonium salt (CP_D), and *p*-bromophenyldiazonium salt (BrP_D) were synthesised and isolated from their arylamine precursors under aqueous conditions using literature methods[59, 189]. The synthesis was performed in a yellow room to minimise UV exposure.

5 mmol of the arylamine precursor was dissolved in a HBF_4 solution prepared by dilution of 2 mL 50% HBF_4 to 4 mL with Milli-Q water. The mixture was subsequently cooled in an ice/acetone bath. 5 mmol of $NaNO_2$ dissolved in 1 mL of Milli-Q water was added dropwise to the mixture and the solution stirred for a further 15 min in an ice/acetone bath. The precipitated product was collected by vacuum filtration and washed with ice cold Milli-Q water and diethyl ether. The product was dissolved in a minimum volume of room temperature ACN then re-precipitated slowly with the addition of ice cold ether over an ice/acetone bath. The final product was filtered and dried under vacuum for 15 min. The *para*-substituted aryldiazonium salts were stored in the dark under vacuum. ***Caution: diazonium salts are potentially explosive and synthesis should be limited to small amounts.***

2.2.5 Synthesis of tetraphenylporphyrin mono-aryldiazonium salts

Free-base and nickel (II) tetraphenylporphyrin mono-aryldiazonium salts were synthesised and isolated from their arylamine precursors under non-aqueous conditions using $NOBF_4$. The arylamine precursors, 5-(*p*-aminophenyl)-10,15,20-triphenylporphyrin (H_2TPP_A)[190] and 5-(*p*-aminophenyl)-10,15,20-triphenylporphyrinatonickel (II) ($NiTPP_A$)[191] were synthesised by Dr Christophe Bucher (Université Joseph Fourier, Grenoble, France) according to reported methods[192-193].

The corresponding mono-aryldiazonium tetrafluoroborate salts, H_2TPP_D and $NiTPP_D$, were synthesised in the dark under an Ar atmosphere using $NOBF_4$ as the diazotising agent. $NOBF_4$ was freshly purified by washing in a mixture of acetic anhydride (10%) in acetic acid, followed by filtration under Ar, washing with dry DCM, and drying under vacuum to yield a white crystalline powder[192]. H_2TPP_A (6.36×10^{-5} mol) or $NiTPP_A$ (5.82×10^{-5} mol) was dissolved in a minimum volume of dry THF and added dropwise to a solution of $NOBF_4$ (1.2 eq) in dry ACN (≈ 1 mL), with stirring, and maintained at -30 °C using a liquid N_2/acetone ice bath. The solution was stirred for 30 min and H_2TPP_D or $NiTPP_D$ was precipitated using dry diethyl ether, collected by filtration, washed with diethyl ether, and dried under vacuum.

2.2.6 Synthesis of 3, 3-dimethylaryltriazenes

The 3,3-dimethylaryltriazenes, [*p*-(dimethyltriaz-1-en-1-yl)phenyl]methylamine (AMP_{DMT}) and [*p*-(dimethyltriaz-1-en-1-yl)]benzoic acid (CP_{DMT}), were synthesised and used as precursors for the *in situ* preparation of *p*-(aminomethyl)phenyldiazonium (AMP_D) and *p*-carboxyphenyldiazonium tetrafluoroborate salt solutions. The carboxyphenyl aryltriazene derivative, CP_{DMT}, was prepared according to the method of Audette and co-workers[194]. The *p*-(aminomethyl)phenyl aryltriazene derivative, AMP_{DMT}, was prepared using a similar synthetic procedure to the method of Hansen and co-workers[195].

2.2.7 Synthesis of [p-(dimethyltriaz-1-en-1-yl)]benzoic acid

0.1 mol of *p*-aminobenzoic acid was suspended in 50 mL of Milli-Q water then cooled in an ice/acetone bath to 0 °C. 25 mL of concentrated HCl was added to the solution, with stirring. 0.1 mol $NaNO_2$ was dissolved in a minimum volume of Milli-Q water then added dropwise, with stirring, and the solution stirred for a further 15 min in an ice/acetone bath. $CaCO_3$ was added followed by the addition of 0.11 mol dimethylamine. After stirring for a further 30 min, the pH of the solution was adjusted to pH 4 by the addition of HCl, to yield a light yellow precipitate. The precipitated product was collected by filtration, redissolved in ACN, then reprecipitated slowly with the addition of ice cold ether over an ice/acetone bath. The final product was filtered, dried under vacuum for 15 min, and stored under vacuum. ***Caution: dimethylaryltriazenes are known mutagens and carcinogens.***

2.2.8 Synthesis of [p-(dimethyltriaz-1-en-1-yl)phenyl]methylamine

^{1}H-NMR spectra for compound **2, 3,** and **4** are reported in Appendix S-1, Appendix S-2 and Appendix S-3 respectively.

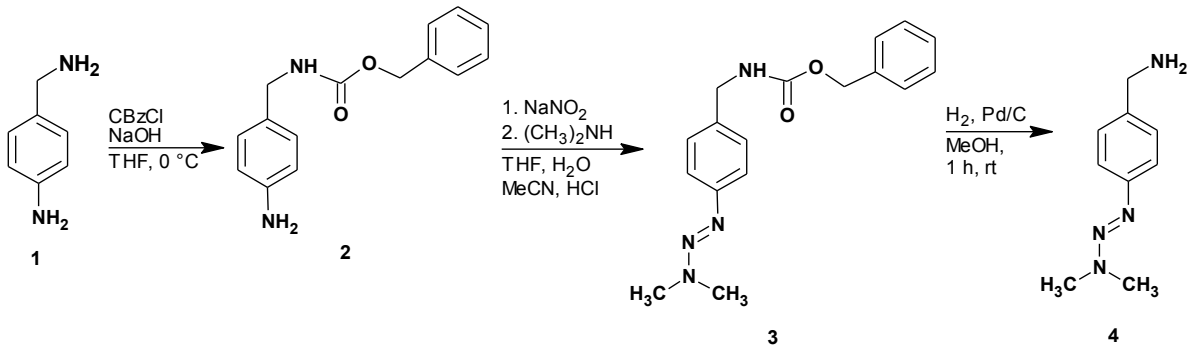

Figure 2.1 Synthesis of [p-(dimethyltriaz-1-en-1-yl)phenyl]methylamine.

p-(Aminomethyl)aniline **1** (1.00 g, 8.22 mmol) was dissolved in THF (30 mL) and NaOH (1 M, 7.3 mL). The mixture was stirred and then cooled in an ice/acetone bath. Benzyl chloroformate (1.29 mL, 9.20 mmol) in THF (10 mL) was then added dropwise over a

period of 10 min at 0 °C. The reaction mixture was stirred for 17.5 h at room temperature. The aqueous phase was extracted with EtOAc (3 × 15 mL), and the organics were combined to be washed with brine. The solvent was evaporated and the residue was purified by a silica gel column chromatography (DCM/EtOAc 2:1) to afford benzyl (4-aminobenzyl)carbamate **2** as a yellow powder (1.22 g, 4.76 mmol, 58%), m.p. 63-65 °C; δ_H (500 MHz, $CDCl_3$, ppm) 4.15 (2H, s, CH_2-NH), 5.08 (2H, s, CH_2-O), 6.67 (2H, d, ^3J 8.5 Hz, Ar-H), 7.02 (2H, d, ^3J 8.5 Hz, 2 × Ar-H), 7.28-7.34 (5H, m, 5 × Ar-H); HRMS (ESI-TOF) Calcd. for $C_{15}H_{16}N_2O_2Na^+$ 279.1104. Found 279.1101 (MNa^+).

Compound **2** (1.00 g, 3.91 mmol) was dissolved in a mixture of THF (8.5 mL), H_2O (8 mL), ACN (4.25 mL) and concentrated HCl (2 mL). The reaction mixture was cooled to 0 °C. A solution of sodium nitrite (350 mg, 5.09 mmol) dissolved in THF (1.25 mL) and H_2O (1.25 mL) was added slowly. Afterwards, the reaction mixture was added dropwise to 40% dimethylamine (11 mL) under vigorous stirring, then immediately extracted with DCM (3 × 8 mL). The organics were combined and washed with H_2O before being dried over Na_2SO_4, filtered, and concentrated to afford benzyl [4-((1E)-3,3-dimethyl-1-triazen-1-yl)benzyl]carbamate **3** as a pale yellow powder (910.6 mg, 2.92 mmol, 75%), m.p. 117-119 °C, δ_H (500 MHz, $CDCl_3$, ppm) 3.31 (6H, br. s, 2 × CH_3), 4.33 (2H, s, CH_2-NH), 5.11 (2H, s, CH_2-O), 7.20-7.23 (2H, m, 2 × Ar-H), 7.29-7.36 (7H, m, 7 × Ar-H); HRMS (ESI-TOF) Calcd. for $C_{17}H_{20}N_4O_2Na^+$ 335.1478. Found 335.1480 (MNa^+).

Compound **3** (800 mg, 2.56 mmol) was suspended in MeOH (10 mL) and 10% Pd/C (100 mg) was added. The reaction was stirred for 1 h at room temperature under a H_2 atmosphere. The solution was then filtered through Celite and the remaining catalyst washed with MeOH. The solution was evaporated under reduced pressure to afford [p-(dimethyltriaz-1-en-1-yl)phenyl]methylamine **4** as a yellow solid (446.15 mg, 2.50 mmol, 98%), m.p. 112-114 °C; δ_H (500 MHz, $CDCl_3$, ppm) 3.31 (6H, br. s, 2 × CH_3), 3.82 (2H, s,

$C\underline{H_2}$-NH_2), 7.24 (2H, d, ^3J 8.5 Hz, 2 × Ar-H), 7.37 (2H, d, ^3J 8.5 Hz, 2 × Ar-H); HRMS (ESI-TOF) Calcd. for $C_9H_{14}N_4Na^+$ 201.2240. Found 201.2241 (MNa^+).

2.2.9 Synthesis of p-nitrophenylazide

p-Nitrophenylazide (NP_A) was synthesised and isolated from *p*-nitrophenyldiazonium salt (NP_D) under aqueous conditions using literature methods[154, 196]. The synthesis was performed in a yellow room. One equivalent of NaN_3 was added slowly to an ice-cold aqueous solution of freshly prepared NP_D, with stirring. The reaction mixture was allowed to react for 30 min in an ice/acetone bath. The precipitated product was washed with ice cold water and ACN, then collected by filtration and filtered under vacuum for 15 min. The product was stored in the dark under vacuum. ***Caution: arylazides are potentially explosive and care should be taken.***

2.2.10 Synthesis of citrate-capped gold nanoparticles

Citrate-capped gold nanoparticles were synthesised using literature methods[197-198]. To prepare gold nanoparticles with an average diameter of ≈ 13 nm[197], 500 mL of a 1 mM solution of $HAuCl_4$ in Milli-Q water was boiled. 50 mL of 38.8 mM sodium citrate in Milli-Q water was added to the solution; the solution changed from a pale yellow to a burgundy colour. Boiling of the solution, with stirring, was maintained for 10 min and then allowed to react for a further 30 min. Once cooled to room temperature, the solution was filtered through a membrane filter (Millipore, 0.22 μm).

To prepare gold nanoparticles with an average diameter of ≈ 25 nm[198], 0.75 mL of $HAuCl_4$ (0.1 wt. %) in Milli-Q water was heated to boiling then 0.5 mL of sodium citrate (1 wt. %) was added. Boiling of the solution, with stirring, was maintained for 10 min then allowed to react for a further 30 min after the boiling was stopped. After cooling, the solution was filtered through a membrane filter as above.

2.3 Surface preparation

2.3.1 Glassy carbon

GC plate (≈ 15 × 15 × 3 mm) or rod electrodes (Ø = 3 mm) (both Tokai Carbon Co. Ltd) and GC rotating disk electrodes (RDE) (Ø = 3 mm, CH-Instruments Inc.) were used in this work. Examples of GC plate and rod electrodes are shown in Figure 2.2. The GC rod electrodes were fabricated in-house by sealing a pristine plug of GC inside a tight fitting Teflon tube in a manner that ensured that only the flat surface of GC is exposed to the surface.

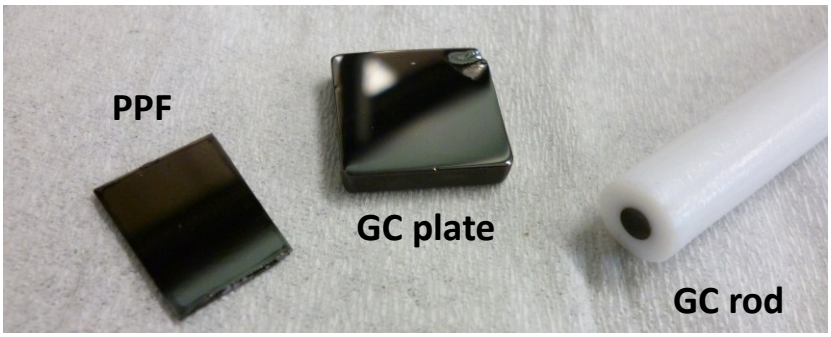

Figure 2.2 Planar graphitic electrodes used: PPF, GC plate, and GC rod electrodes.

GC surfaces were polished using successively smaller alumina-Milli-Q slurries (1 μm then 0.05 μm particle size) on a polishing cloth (all Leco materials), sonicated in Milli-Q water for 5 min after each polishing step, and dried under a stream of N_2. Immediately prior to use, electrodes were rinsed according to procedures described in the experimental section of the relevant chapter.

2.3.2 Pyrolysed photoresist film

The procedure for fabricating PPF electrodes (Figure 2.2) in this work is based on the method of Brooksby and co-workers[66]. Initially, a sacrificial protective layer of AZ1518 photoresist (Microchemicals) was spin-coated onto a pristine silicon (100) wafer (Silicon

Quest) at 2000 rpm, then baked onto the silicon wafer at 90 °C for 2 min. The wafer was typically cut into ≈ 14 × 14 mm pieces using a diamond scribe, and the sacrificial coating removed from the substrates by successive sonication in acetone and IPA for 5 min each. After drying with a stream of N_2, AZ4620 photoresist (Clariant) was spin-coated onto the pre-cut pieces of silicon for 30 s at 3000 rpm. The surfaces were soft-baked in an oven at 60 °C. The photoresist-coated layers were loaded into a quartz boat and placed in the centre of a furnace tube (Radatherm Model 2216e) and sealed. A forming gas atmosphere (95% N_2 + 5% H_2, BOC Gases NZ Ltd) with a flow rate of 2 L/min was maintained during the pyrolysis programme. Pyrolysis was performed at 500 °C for 30 min, 750 °C for 30 min, then 1100 °C for 1 h. The furnace was left to cool to ≤ 60 °C under gas flow before samples were removed from the furnace. PPF surfaces were sonicated in IPA for 10 s then dried with a stream of N_2 prior to use, unless stated otherwise.

The sheet resistance of each sample was tested prior to use as a form of quality control. Typical values ranged from 7 to 30 Ω/sq. Surfaces with sheet resistances > 30 Ω/sq were discarded due to poor electrochemical performance. Sheet resistances were determined using gold conductive wires set in a square arrangement[66]. The pressure exerted is spring-loaded but neither the contact pressure nor the resistance of the set-up is known. Measurements were recorded using a Digitech QM1320 multimeter.

2.4 Electrochemistry

2.4.1 Instrumentation

Electrochemical measurements were typically performed at room temperature using an Eco Chemie Autolab PGSTAT 302 or 302N potentiostat running GPES 4.9 software. Experiments undertaken in Chapter 4 were also performed using a Biologic SP-300 potentiostat running EC-lab software V10.10 and a CHI 440 (CH-Instruments Inc.) potentiostat running CHI 440 software. All experiments were performed under N_2 using

degassed solutions. Cyclic voltammograms (CVs) were recorded at a scan rate of 100 mV/s unless stated otherwise.

2.4.2 Electrochemical cells and electrodes

Custom-made glass electrochemical cells were stored in a 10% HNO_3 acid bath. Prior to use, the cells were rinsed thoroughly with Milli-Q water then acetone. An additional rinse in Milli-Q water was performed prior to aqueous electrochemistry. A three-electrode cell set-up was used for all electrochemical experiments comprising a working electrode (carbon, gold, or indium tin oxide (ITO)), a reference electrode (SCE, Ag wire, $Ag/AgNO_3$, or Ag/AgCl), and a Pt mesh auxiliary electrode. Radiometer Scientific SCE electrodes were used: REF 401 and REF 921 for aqueous and non-aqueous experiments, respectively. Additional details concerning the working and reference electrodes are stated in the relevant chapter. Two types of glass cell were used: a spring-loaded cell (Figure 2.3a) and a pear-shaped cell (Figure 2.3b).

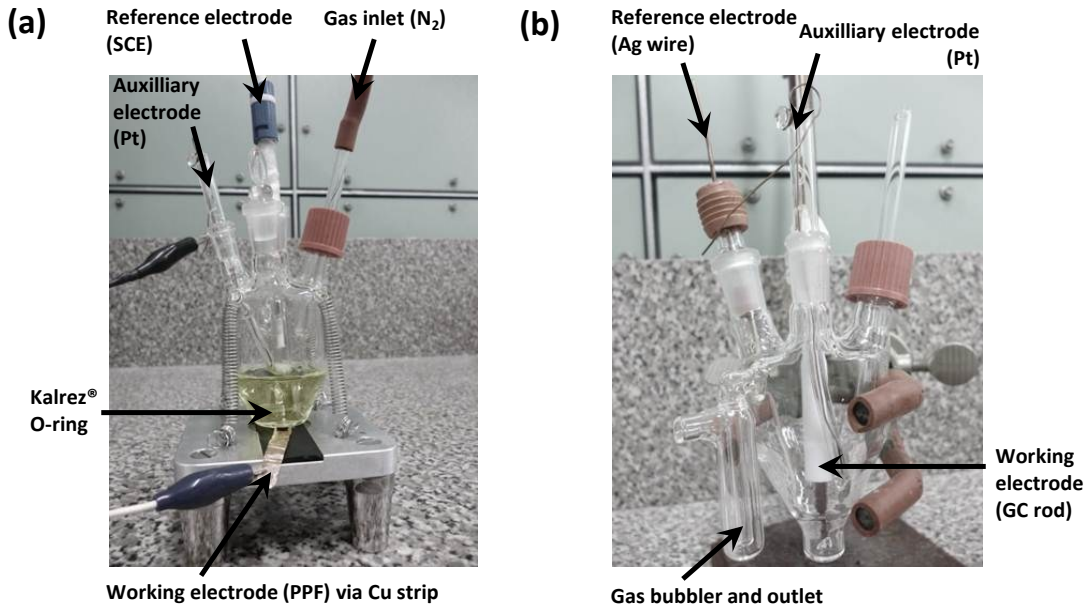

Figure 2.3 Three-electrode electrochemical cells used: (a) spring-loaded cell and (b) pear-shaped cell.

The spring-loaded cell set-up was used for electrochemical experiments involving plate working electrodes such as GC plate and PPF. The working electrode is placed on an insulated region of a metal stage. An o-ring was placed onto the sample to define the geometric area of the working electrode. A copper strip is then placed on the electrode surface to achieve electrical contact. The copper strip is held in place using a second o-ring which ensures good contact is made between the copper and the surface. A customised glass cell with a hole (Ø ≈ 2.5 mm) in the bottom is pressed onto the central o-ring and secured under spring-loaded pressure by attaching four springs to four positions on the cell. A tight and leak-free seal is maintained on the plate working electrode, with the area exposed to solution being defined by the inner diameter of the central o-ring. Unless otherwise stated, a 008 Kalrez o-ring (formulation 4079, Ø = 6.07 mm) was used for surface modification experiments and a 007 Kalrez o-ring (Ø = 3.68 mm) for surface characterisation. The inner diameter of the o-rings defined geometric areas of 0.29 cm^2 and 0.11 cm^2, respectively.

2.4.3 Analysis of electrochemical data

Determination of voltammetric peak areas and heights was performed using Linkfit 4.1 curve fitting software (Chapter 3 and Chapter 5) or EC-lab software V10.10. Using Linkfit, curves were fitted to the peaks, after baseline subtraction, using a mixed Lorentzian / Gaussian algorithm[199]. Using EC-lab software, peak areas were integrated manually using a linear fit without baseline subtraction. Peak current measurements were obtained by extrapolation of baselines. All voltammograms were redrawn in Sigmaplot 9.0 software for presentation of the data.

From the calculated peak areas the surface concentration of electroactive groups was estimated using the following equation (Equation 1):

$$\Gamma = \frac{Q}{nFA} \tag{1}$$

Where Γ is the surface concentration (mol/cm^2), Q is the charge associated with the observed redox process (in C), n is the number of electrons in the redox process, F is the Faraday constant (96485 C/mol), and A is the area of the working electrode (cm^2). The value of Q for each process was obtained by dividing the voltammetric peak area value by the scan rate used (0.1 V/s unless otherwise stated).

2.5 Atomic force microscopy

2.5.1 Instrumentation

AFM measurements were recorded in air on dry films or surfaces using a Nanoscope Dimension 3100 and Nanoscope IIIa controller (both Digital Instruments).

2.5.2 Imaging and surface roughness analysis

Topographical imaging was performed in tapping-mode using a silicon cantilever with a fundamental frequency of 200-400 kHz (TAP300Al-G series, Budget Sensors, Innovative Solutions Bulgaria Ltd). Images were recorded at a scan rate of either 1 Hz or 0.5 Hz with a resolution of 512 samples per line. The amplitude set point and gains were optimised for each sample. Measurements were obtained from 1 × 1 μm regions of height images unless otherwise stated. Surface roughness values are reported as the geometric average roughness (R_q, commonly referred to as rms), except for Chapter 5, where roughness average (arithmetic) (R_a) values are also reported. Standard image processing and roughness measurements were performed using Nanoscope Analysis v1.2 software.

2.5.3 Film thickness measurements by depth-profiling

AFM film thickness measurements were performed at PPF surfaces following procedures reported by Brooksby and co-workers[66]. The method involves using an AFM tip to mechanically remove a section of the film from a modified surface, then subsequently recording a depth profile over the trench using a clean AFM tip. The technique of depth-

profiling features a three cantilever AFM probe (CSC 12, Ultrasharp). To remove a section of the film ("scratching"), the AFM laser is focussed on the shortest tip in tapping-mode. When the tip engages with the surface the longer tip is embedded into the film. As a tapping-mode image is recorded, a section of the film is removed which corresponds to the scan size (1 × 10 μm). After "scratching", the probe was disengaged and the AFM laser re-focussed onto the short tip. The short tip was positioned over the AFM scratch and imaged in tapping-mode by scanning orthogonally across the trench. The same procedure was applied to regions of unmodified PPF and, in some cases, a faint indentation of ≤ 0.2 nm was observed. In those cases the measured depths of the films were corrected for. The depth of each trench was calculated from topographical height images using the Nanoscope Analysis step height calculation tool.

Two scratches were made on each modified surface and at least one image obtained per scratch. Three sections from each imaged were analysed, giving two measurements per section: one from the left scratch-film boundary and one from the right. Between 12 and 18 film thickness measurements were recorded per sample in order to determine the final average film thickness.

2.6 Water contact angle measurements

Static water contact angle measurements were obtained at room temperature by delivering a 2 μL droplet of Milli-Q water onto the surface of a sample placed on a horizontal stage. The droplet was delivered manually using a 1-5 μL microsyringe. An image of the droplet on the surface was recorded immediately using an Edmund Scientific video camera and Matrox Intellicam software. Contact angles were analysed using the Drop Analysis plugin with ImageJ v1.37 software.

2.7 X-ray photoelectron spectroscopy

XPS analysis was performed by Dr Bryony James and Dr Colin Doyle (Department of Chemical and Materials Engineering, University of Auckland, New Zealand). XPS spectra were recorded using a Kratos Axis Ultra DLD spectrometer equipped with a monochromatic Al Kα X-ray source (1486.6 eV), operated at 150 W. Elemental survey spectra were recorded with a pass energy of 160 eV and a step size of 1 eV. Narrow scans were recorded with a pass energy of 20 eV and a step size of 0.1 eV. The analysis area was ≈ 300 × 700 μm. Peaks were fitted and quantified using CasaXPS version 2.3.15. Binding energies were referenced to the hydrocarbon (C) signal at 285 eV.

2.8 UV-visible absorption spectroscopy

UV absorption spectra of film-modified ITO substrates were recorded in the dark in a glovebox using a Zeiss MCS 501 UV-VIS-NIR spectrophotometer with Aspect Plus software. Images were background subtracted.

2.9 Optical microscopy

Optical microscopy images were recorded using an Olympus BX60 microscope equipped with a Leica DFC320 camera unit. Optical images were recorded with 5×, 10×, 20× and 50× objectives. Condensation figures were obtained by delivering a small amount of water vapour to the carbon surface and immediately recording an image. Image processing was performed using Leica Application Suite v2.3.1 R1 software.

2.10 Stylus profilometry

Film thickness measurements on metal and carbon layers (> 15 nm) were recorded using a Veeco Dektak 150 profilometer with Vision v9.1.1.6 software. A standard stylus with a radius of 12.5 μm was used.

2.11 Scanning electron microscopy

SEM micrographs were recorded in secondary electron imaging mode using a 7000 SEM (JEOL) or Raith 150 electron-beam lithography system operating with accelerating voltages between 10-15 keV.

2.12 Standard photolithography

Photomask files were prepared using L-edit v13 (Tanner EDA) and written into a chrome-on-glass mask using a Heidelburg TPG101 mask writer by Dr Volker Nock (Department of Chemistry, University of Canterbury, New Zealand). Photolithographic pattern transfer was performed using an MA-6 mask aligner (Suess Microtec). The procedures for standard photolithographic patterning are described later in this thesis.

All solutions and materials were used as received: AZ1518, SU-8 2100 (Microchem), SU-8 developer (Merck), poly(dimethylsiloxane) pre-polymer kit (PDMS, Sylgard® 184, Dow Corning), trimethylchlorosilane (TMCS, Sigma Aldrich), AZ MIF326 developer (Microchemicals).

2.13 Thermal and electron-beam evaporation

Thermal evaporation of metals was performed using a 510 thermal evaporator (Balzers). E-beam evaporation of metals and carbon was performed using an Auto 500 e-beam evaporator (BOC Edwards). Molybdenum boats or graphite crucibles were used (Kurt J. Lesker Vacuum Technology).

Methods for fabrication and regeneration of planar carbon surfaces for diazonium-derived film studies

3.1 Introduction

This chapter describes simple and cost-effective methods for preparing and regenerating planar carbon surfaces. This research is motivated by an increasing demand for low-cost and robust carbon electrodes for thin film characterisation studies and electroanalytical applications.

Graphitic carbons such as GC, PPF, and evaporated amorphous carbon film (a-C) are versatile materials that have a wide range of applications in electrochemistry. The preparation and various physical and chemical properties of GC and PPF electrodes have been reviewed in Chapter 1. a-C surfaces prepared by vacuum deposition of carbon using e-beam or sputtering methods vary in their sp^2 and sp^3 carbon content depending on their preparation[200-203]. A number of reports have shown that a-C can be prepared with predominantly sp^2-hybridised carbon atoms and hence these substrates can be used as alternatives to GC and PPF electrodes[201, 203, 204].

A common application of graphitic surfaces is their use as substrates for thin film characterisation studies[66, 68, 205]. The development of PPF and a-C enables investigations of surface species that would otherwise not be possible using GC. As mentioned in Chapter 1, the low surface roughness of PPF (rms $\leq$ 0.5 nm) permits the characterisation of molecular layers with high-resolution using AFM. Evaporated a-C surfaces have also been prepared with low surface roughness (rms $\approx$ 0.1 nm[204] or 0.8 nm[202]). Both materials have been used as optically transparent electrodes (C-OTEs) for the characterisation of surface layers using techniques such as UV-visible spectroelectrochemistry[206-209]. a-C is also promising for the preparation of carbon-coated piezoelectric quartz crystals (C-QCs)[210]. In contrast,

pyrolysed photoresist materials, which are fabricated at temperatures in excess of 800 ºC, are not suitable as coatings for quartz crystals; single crystal quartz undergoes an irreversible change in crystallographic structure at $T = 573$ ºC (the Curie point)[211]. C-QCs provide new opportunities for investigating molecular species at carbon surfaces using quartz crystal microbalance (QCM) or electrochemical QCM (E-QCM) techniques.

C-QCs are not currently mass-produced and are only available commercially "on request" by manufacturers and suppliers of QCM equipment (Q-Sense and Gamble Technologies[212-213], for example). C-QCs are provided with limited guarantees of quality and are significantly more expensive than Au-QCs. There is also no reported standard method for preparation of glassy carbon-like C-QC materials. A small number of methods for preparation of C-QCs with either graphite- or diamond-like properties have been reported; however, further improvements in the electrochemical performance and physical stability of these materials are necessary[205, 210, 214-215]. In addition to improving their performance as electrodes, it is also necessary to develop a method for regenerating these materials, without significantly oxidising the surface. C-QCs are currently used as high-cost and disposable carbon electrodes. The regeneration methods used for Au-QCs, namely, ozonation and strong acidic treatment, involve strongly oxidising conditions, and are not ideally suited to carbon surfaces.

PPF is a well-established electrode material that is prepared in small batches of samples using a time-consuming procedure[63]. A limitation to greater use of PPF is that it is treated as a single-use material; there are no reported regeneration methods that restore both the electrochemical characteristics and the low surface roughness of deactivated PPF. To expand the use of PPF, it is necessary to develop a simple approach that allows its regeneration and reuse for electrochemical applications. Numerous regeneration methods for carbon surfaces have been reported, including mechanical polishing[216], ultrasonication[217], heat treatment[53, 218], electrochemical[219], and solvent treatments[54]. Of

these methods, only mechanical polishing, heat treatment, and electrochemical treatments are suitable for removing both covalently bound diazonium-derived films and physisorbed species from carbon surfaces. However, neither mechanical polishing nor electrochemical treatments allow the very low surface roughness of PPF to be maintained. Heat treatment under reduced pressure or high vacuum has been shown to improve the electrochemical activity of GC, but there are no reports on the efficacy of these methods for regenerating film-modified GC surfaces[53, 218]. Recently, Wightman and co-workers proposed an oxidative electrochemical treatment to renew PPF surfaces following physisorption[219]. The method resulted in a significant increase in both surface oxide content and roughness of surfaces, which is not a desirable outcome for many applications of PPF.

The aim of this chapter is to develop new methods that will expand the use of PPF and evaporated a-C for electrochemical applications and for diazonium-derived film studies. Section 3.3 addresses the development of a method that allows PPF surfaces to be regenerated and reused following electroanalysis and film modification. This research was undertaken with the view that the regeneration method could be applied in later work for regenerating C-QCs. In Section 3.4, the feasibility of preparing evaporated a-C electrodes on gold was investigated as a possible alternative to PPF for studying molecular films. In Section 3.4, the regeneration method developed in Section 3.3 is tested on a-C electrodes. The latter work was motivated by the goal of fabricating reusable C-QCs for E-QCM studies of thin films at graphitic carbons.

3.2 Experimental

3.2.1 Surface preparation

GC and PPF electrodes were prepared as described in Chapter 2. Prior to use, all carbon surfaces were rinsed for 10 s in IPA then dried with a stream of N_2.

3.2.2 Fabrication of evaporated carbon and metal surfaces

a-C electrodes were prepared by e-beam evaporation from a graphite source (Chapter 2) located 20 cm from the sample holder. Before deposition, the vacuum chamber was evacuated to a base pressure of 7.5×10^{-6} Torr. Film growth rates were between 0.1-0.5 nm/s. After evaporation, the substrates were kept under vacuum for at least 1 h before the chamber was vented. The temperature of the substrate holder typically reached ≤ 120 ºC during deposition. The thickness of carbon layers (100 nm) was determined using a quartz crystal monitor. Pt and Al layers were prepared by e-beam evaporation using similar experimental conditions.

Gold substrates (Au/NiCr/Si) were prepared by thermal evaporation of 20 nm NiCr, followed by 100 nm Au, onto pre-cut (10 × 10 mm) silicon wafer. Ni and Ti layers (20 nm) were deposited by evaporation onto gold substrates that had been exposed to air for periods ≤ 24 h. The thickness of metal layers was determined using a quartz crystal monitor. All carbon and metals were prepared by evaporation through a metallic mask, giving a geometric area of 0.79 cm^2 on each sample[220].

3.2.3 Electrochemistry

The geometric working area of electrodes was 0.29 cm^2 for electrografting and 0.11 cm^2 for electrochemical characterisation. SCE (sat. KCl) and Ag wire pseudo-reference electrodes were used for aqueous and non-aqueous electrochemistry, respectively. The

hydroxymethyl ferrocene/ferrocenium couple ($FcOH/FcOH^+$ in 0.1M $TBABF_4$-ACN) appeared at $E_{1/2}$ = 0.21 V vs. Ag wire.

3.2.4 Surface modification

Non-aqueous electrografting was performed in 0.1 M $TBABF_4$-ACN solutions containing 1 mM NP_D or 1 mM BrP_D. NP_D was grafted using two CV scans from 0.3 to -0.6 V, followed by electrolysis at E_{pc} -150 mV for 300 s. BrP_D was grafted using two CV scans from 0.3 to -0.9 V, followed by electrolysis at E_{pc} -150 mV for 60 s. (E_{pc} is the diazonium cation reduction peak potential obtained during the first scan). Aminophenyl (AP) films were generated by electroreducing NP films in 0.1 M H_2SO_4 for 120 s at a potential 150 mV negative of the NP reduction peak.

Aqueous electrografting was performed in 0.1 M H_2SO_4 containing 1 mM NP_D. NP_D was grafted using two CV scans from 0.5 to -0.4 V.

Unless stated otherwise, all surfaces were sonicated in ACN for 60 s after film modification, rinsed with IPA, then dried with a stream of N_2.

3.2.5 Carbon surface regeneration by heat treatment

Heat treatment experiments were performed in a tube furnace (Radatherm Model 2216e) under Ar (99.99%, Southern Gas Services Ltd.) or forming gas at a 1 L/min flow rate. The furnace temperature was measured using a digital thermometer (Omron ESC15) inserted into the quartz working tube, with Ar flow. All reported temperatures have an uncertainty of ± 25 °C. Unless stated otherwise, heat treatment conditions were 545 °C for 30 min under Ar (1 L/min). Heat treated samples were allowed to cool to ≤ 60 °C under gas flow before removal from the furnace. "As-prepared" PPF refers to pristine samples that were fabricated and stored for periods of up to 1 month.

3.3 Method for regeneration of pyrolysed photoresist film by heat treatment

Regeneration of film-modified and as-prepared PPF electrodes was investigated in this work using heat treatment in an Ar atmosphere. PPF electrodes were modified with thin organic films via electrochemical reduction of the aryldiazonium salt compounds shown in Figure 3.1.

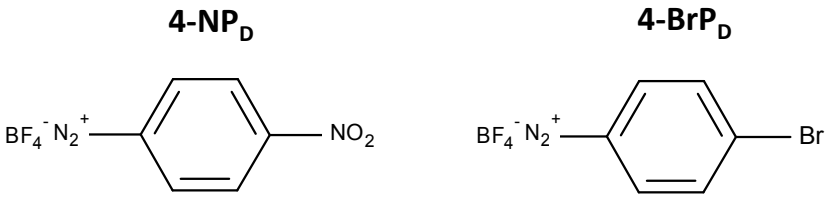

Figure 3.1 *Para*-substituted aryldiazonium salts, NP_D and BrP_D, used to graft NP and bromophenyl (BrP) films at PPF surfaces.

3.3.1 Electroreduction of NP_D and BrP_D at PPF in ACN

Film-modified surfaces were prepared by the electrochemical reduction of aryldiazonium tetrafluoroborate salts, NP_D or BrP_D, in ACN containing 0.1 M $TBABF_4$ as supporting electrolyte, as described in Section 3.2.4. The deposition conditions were chosen in order to prepare a grafted film that would inhibit the redox reaction of the $Fe(CN)_6^{3-/4-}$ couple. CVs obtained in diazonium grafting solutions (Figure 3.2) show a broad and irreversible reduction peak on the first scan, which is assigned to the one-electron reduction of NP_D (Figure 3.2a) and BrP_D (Figure 3.2b) at PPF.

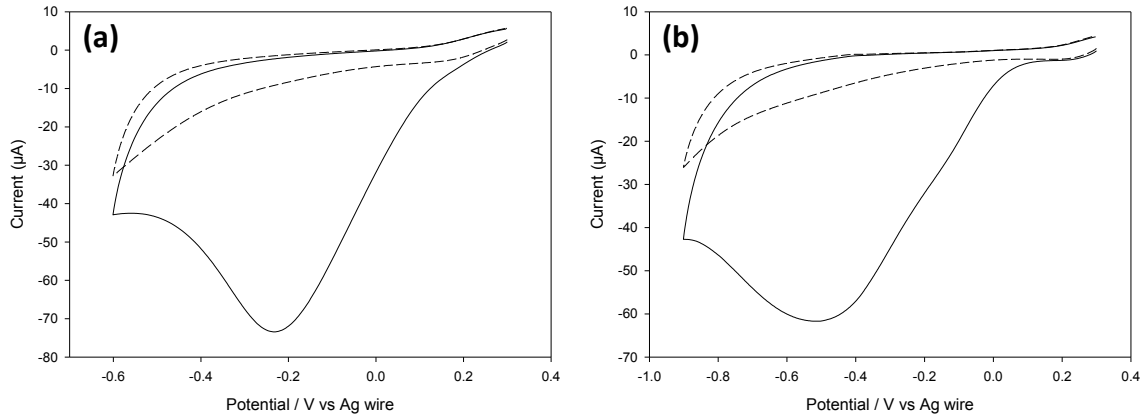

Figure 3.2 First and second scan CVs of (a) 1 mM NP_D and (b) 1 mM BrP_D in ACN-$TBABF_4$ at PPF.

The one-electron irreversible reduction of simple *para*-substituted aryldiazonium salts leads to the formation of aryl radicals at the electrode surface, which subsequently react to form a monolayer or multilayer film[65, 68, 121]. The accepted general mechanism for film formation is shown in Scheme 1.2 in Chapter 1. The complete loss of the reduction peak on the second scan is consistent with the formation of a strongly passivating film, which impedes electron transfer from the surface to aryldiazonium ions in solution. The blocking behaviour of diazonium-derived films has been reported by other workers[65-66, 78].

3.3.2 Electrochemical investigations at as-prepared, modified, and heat-treated PPF

The electrochemical response of 5 mM $Fe(CN)_6^{3-}$ was used to examine the behaviour of as-prepared, modified, and heat-treated PPF surfaces. This redox probe is well-known to have surface-sensitive electrochemistry. At as-prepared PPF, the CV of $Fe(CN)_6^{3-}$ (Figure 3.3a, ---) is well-defined and chemically reversible with a peak-to-peak potential separation (ΔE_p) of 176 mV. After modifying PPF by electrografting of NP_D, the CV obtained in $Fe(CN)_6^{3-}$ solution (···) shows only very low currents, with no features attributed to $Fe(CN)_6^{3-}$. This behaviour is consistent with the presence of a blocking NP film on the PPF surface[221]. After recording the CV, the sample was rinsed with Milli-Q water and heated at 545 °C for 30 min under an Ar atmosphere, and then cooled to room temperature.

The CV of $Fe(CN)_6^{3-}$ obtained at the heat-treated sample (–) is well-defined with peak currents slightly larger, and ΔE_p slightly smaller (152 mV), than the CV scan prior to modification and heat treatment. These changes indicate that the electron transfer rate for the redox couple is at least as fast as before modification, suggesting that the NP film has been completely removed by heating to give a PPF surface with similar electrochemical activity to the as-prepared sample. At the same time there is no change in the background current, indicating that there is no change in capacitance. Similar effects on electrode kinetics were observed when samples were analysed several days after heat treatment.

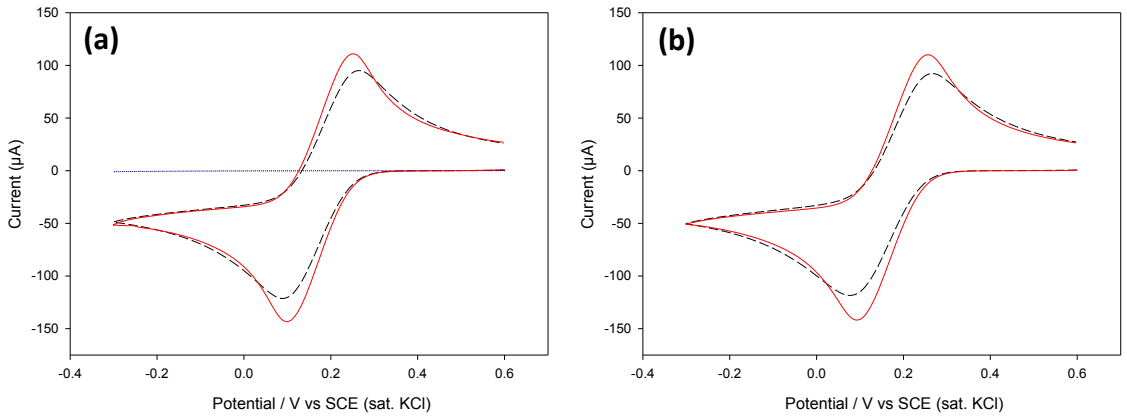

Figure 3.3 First scan CVs of 5 mM $Fe(CN)_6^{3-}$ at as-prepared PPF (---); (a) PPF modified with NP groups before (···) and after (–) heat treatment; (b) PPF modified with NP groups after heat treatment (–).

The effect of heat treatment on as-prepared PPF (i.e. without a grafted film) was also monitored by recording CVs of $Fe(CN)_6^{3-}$. Figure 3.3b shows that after heating PPF at 545 °C in Ar for 30 min, ΔE_p decreases from 188 to 164 mV and there is a small increase in peak currents. These changes are consistent with an improvement in the electron transfer kinetics of $Fe(CN)_6^{3-}$, an effect that is attributed to removal of adventitious adsorbates from the "pristine" PPF surface. This result also confirms that the activation of the surface after heat treatment of film-modified surfaces is not related to the film.

To further investigate the effect of heat treatment, the presence of NP groups on the surface was directly monitored by cyclic voltammetry. Figure 3.4 shows the characteristic CV, recorded in 0.1 M H_2SO_4, of a freshly-grafted NP film on PPF (–)[138]. The large peak at E_{pc} = -0.7 V, corresponds to reduction of NP groups to aminophenyl (Equation 1) and hydroxyaminophenyl groups (Equation 2). On the return sweep, the oxidation of hydroxyaminophenyl to nitrosophenyl goups (Equation 3) is observed at $E_{pa} \approx 0.4$ V. The hydroxyaminophenyl/nitrosophenyl redox couple is chemically reversible and was observed on the second and subsequent CV scans (data not shown).

$$\text{Surface---Ph-NO}_2 + 6\,H^+ + 6\,e^- \rightarrow \text{Surface---Ph-NH}_2 + 2\,H_2O \quad (1)$$

$$\text{Surface---Ph-NO}_2 + 4\,H^+ + 4\,e^- \rightarrow \text{Surface---Ph-NHOH} + H_2O \quad (2)$$

$$\text{Surface---Ph-NHOH} \rightleftharpoons \text{Surface---Ph-NO} + 2\,H^+ + 2\,e^- \quad (3)$$

From the integrated area of the reduction and oxidation peaks of 4 samples, the average surface concentration of electroactive NP groups was estimated to be $18 \pm 2 \times 10^{-10}$ mol/cm^2. Based on the known relationship between surface concentration and thickness of NP films on PPF, the film has an estimated thickness of 6 nm and hence is multilayered[66]. A second region of the same PPF-NP sample, that had not been electrochemically analysed, was heated at 545 °C for 30 min in Ar. After cooling, a CV of the sample was recorded in 0.1 M H_2SO_4 (Figure 3.4, ---) and shows no evidence of electroactive NP groups, consistent with loss of the NP film. However, the CV does show a broad peak at $E_{pc} \approx$ -0.4 V. This peak is always observed at PPF samples used in this thesis (both as-prepared and after heat treatment) during the first scan (only) in aqueous acid solution and has also been observed by other workers[63]. The nature of the species giving this response is unknown.

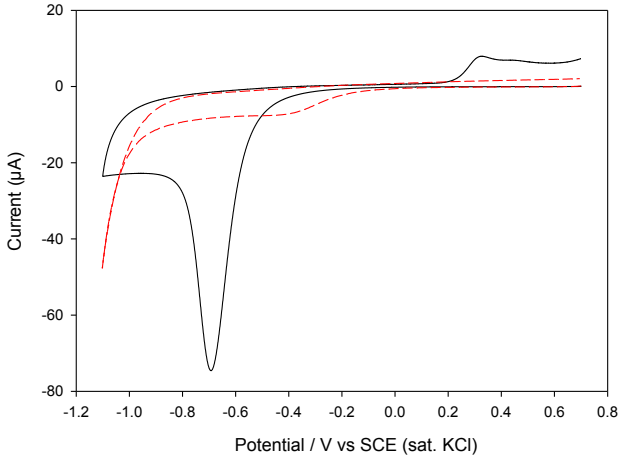

Figure 3.4 First scan CVs in 0.1 M H_2SO_4 at PPF modified with NP groups before (–) and after (---) heat treatment.

The influence of temperature, gas type, and heating time on PPF and PPF-NP samples was investigated by undertaking experiments similar to those described above, but heating at 385, 445, and 495 °C in Ar for 30 min, and also at 545 °C in forming gas for 30 min. Figure 3.5a shows the ΔE_p values of CVs of $Fe(CN)_6^{3-}$ recorded at each PPF surface: as-prepared (left bar lines), after NP modification (middle bar lines, where three bar lines are shown), and after heat treatment (right bar lines). Heat treatment of PPF-NP surfaces at 385 °C appears to partially regenerate the PPF surface, whereas at 445, 495 and 545 °C (with the exception of one experiment at 445 °C) heat treatment yields more active surfaces than before modification. Similarly, the kinetics of the $Fe(CN)_6^{3-/4-}$ redox couple are enhanced after as-prepared PPF is treated at all temperatures from 385-545 °C. Use of forming gas while heating at 545 °C for 30 min (Figure 3.5a), and heating at 545 °C for 120 min under Ar (three samples, data not shown) gave similar activation to heating in Ar for 30 min. For subsequent experiments, the standard procedure was heating at 545 °C for 30 min under an Ar atmosphere.

The thermal stability of grafted films is known to depend, to some extent, on the aryl substituent and layer thickness,[222] and hence the effect of heat treatment on PPF modified

with different films was monitored using the method described above. Figure 3.5b shows the results obtained at PPF modified with NP (blue bar lines), AP (red/orange/yellow bar lines), and BrP (green bar lines) films. Based on changes in ΔE_p values for CVs of $Fe(CN)_6^{3-}$, all modified surfaces were effectively re-activated by heating at 545 °C for 30 min under Ar.

It is noted that Figure 3.5 reveals a significant variability in ΔE_p values for CVs of $Fe(CN)_6^{3-}$ recorded at as-prepared PPF. This is typical of our PPF material and is presumably due to differences in temperature along the furnace working tube during pyrolysis[76], and also to the length of storage of samples prior to use.

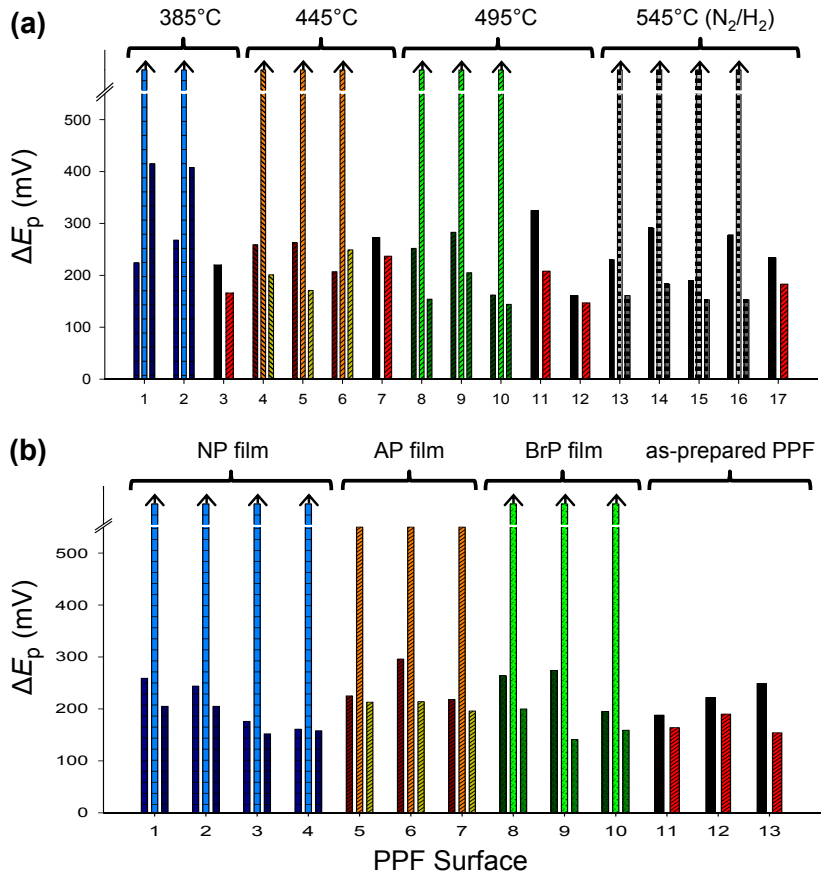

Figure 3.5 Bar charts showing ΔE_p values for CVs of $Fe(CN)_6^{3-}$ obtained at PPF: as-prepared (left bar lines), modified (middle bar lines, where three bar lines are shown), and after heat treatment (right bar lines). (a) Modifier is NP film; surfaces heated to the temperatures shown under Ar, or to 545 ºC under N_2/H_2. (b) Modifier as shown on the chart; surfaces heated to 545 ºC under Ar.

3.3.3 Electroreduction of NP_D at regenerated PPF and electrochemical film characterisation

The use of regenerated PPF electrodes for electrografting reactions was examined by comparing CVs obtained in 1 mM NP_D solution at as-prepared PPF, and at the same sample of PPF after heat treating to remove the grafted NP film. No significant differences were observed in the grafting scans (Figure 3.6a compared to 3.2a) indicating that the two surfaces have very similar activity for electrografting. Reduction of the NP-film grafted on regenerated PPF gives a very similar CV in 0.1 M H_2SO_4 solution (Figure 3.6b) to that obtained for NP on an as-prepared PPF surface (Figure 3.4), confirming that regenerated PPF is a suitable material for electrografting experiments. The calculated surface concentration for regenerated PPF modified with NP groups was $18 \pm 1 \times 10^{-10}$ mol/cm^2 (average of 2 samples), the same as that found at as-prepared PPF.

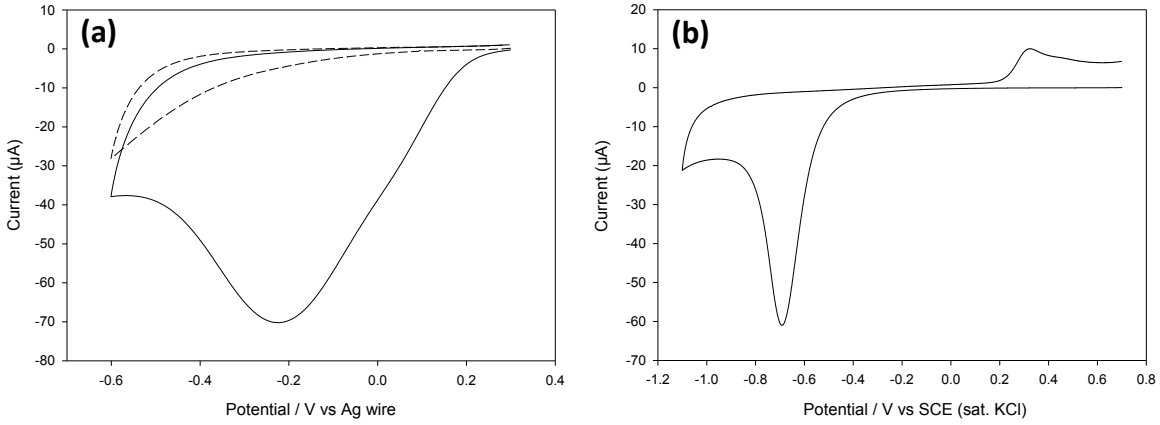

Figure 3.6 (a) First and second scan CVs of 1 mM NP_D in ACN-$TBABF_4$ at heat-treated PPF-NP. (b) First scan CV in 0.1 M H_2SO_4 at heat-treated PPF-NP subsequently re-modified with NP groups.

3.3.4 X-ray photoelectron spectroscopy at as-prepared, modified, and heat-treated PPF

XPS spectra were obtained at as-prepared PPF, PPF-NP and PPF modified with bromophenyl groups (PPF-BrP), and at a separate set of corresponding samples after the

standard heat treatment. Data from the survey scans of the six samples (Appendix S-4) are listed in Table 3.1. Figure 3.7 shows the N 1s core level spectra for NP and BrP modified PPF before and after heat treatment.

Table 3.1 XPS data for as-prepared and modified PPF surfaces before and after heat-treatment.

Sample Type	Atomic %				
	C	N	O	Br	Si
PPF[a]	93.9	0.5	4.8	-	0.5
PPF[a] (heat-treated)	95.3	0.3	3.6	-	0.6
PPF-BrP	88.3	3.1	4.5	3.8	0.0
PPF-BrP (heat-treated)	86.6	0.3	9.0	0.0	3.8
PPF-NP	82.0	7.0	10.4	-	0.3
PPF-NP (heat-treated)	92.2	1.9	5.0	-	0.2

[a] As-prepared PPF.

The two as-prepared (unmodified) samples show no significant differences in elemental composition, indicating that adventitious adsorbates removed by heat treatment have an insignificant effect on the chemical composition of the surface. (Although the heat-treated, as-prepared sample has a lower % O than the as-prepared PPF sample, this difference is likely to be within the variability of the measurements and samples). The PPF-BrP sample has a significant Br signal (3.8 atomic %) and a similar amount of N. The N 1s core level spectrum of the PPF-BrP sample shows a single N signal at a binding energy of ≈ 399 eV (Figure 3.7b) confirming that the N signal originates from azo groups in the BrP film. Incorporation of azo linkages during grafting is well known for films derived from diazonium salts[126, 138, 220]. No Br is detected in the heat-treated PPF-BrP sample and the N content (Figure 3.7c) is the same as that of as-prepared PPF, confirming the complete loss of the film during heat treatment. However, after heat treatment, the PPF-BrP sample has a high O and Si content which is attributed to contamination of the sample by SiO_2 from the underlying silicon wafer.

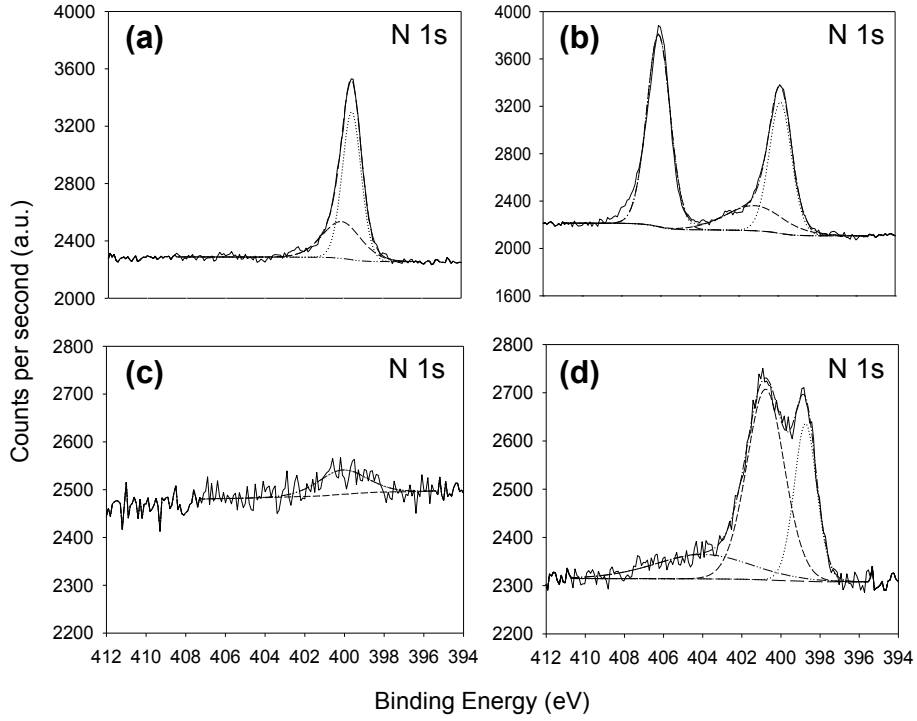

Figure 3.7 Nitrogen 1s core level spectra of PPF surfaces modified with (a) BrP groups, (b) NP groups, (c) BrP groups and subsequently heat-treated, and (d) NP groups and subsequently heated.

As expected, grafting an NP film to PPF gives a surface with an increased N and O content. The narrow scan of Figure 3.7b shows a N signal at 406 eV, confirming the presence of $–NO_2$ groups, and a signal at ≈ 399 eV, which is attributed to azo groups[126, 138]. The origin of the small signal at ≈ 402 eV is not known but has been reported in earlier studies[220]. The heat-treated PPF-NP sample (Figure 3.7d) has a significantly lower N and O content than the non-heat treated PPF-NP sample, indicating loss of the NP film. The O content observed following heat treatment (5%) is similar to that of as-prepared PPF in this work, and values reported by others (typically between ≈ 1-6%)[64, 219]. On the other hand, the N content (1.9%) is significantly higher than expected for unmodified PPF (≤ 0.5%). The narrow scan spectrum of Figure 3.7d shows a broad peak centred at 404 eV, and sharp peaks at 401 eV and 399 eV. Similar signals have been reported by Toupin and Bélanger for NP-modified carbon black, heated to similar temperatures in air and N_2[124]. The authors

suggest that NO, generated during thermal decomposition of NP groups, reacts with the surface resulting in incorporation of N in the form of pyrrolic (binding energy of 400.9 eV), nitrile (399.8 eV), graphitic (403.6 eV) and pyridinic (398.6 eV) species. Similarly, Tomita and co-workers have shown that these nitrogen-containing species are present after reaction of NO with a carbon substrate[223]. Hence it appears that although the NP film is completely removed from the surface by heat treatment, the chemical composition of the PPF surface undergoes small changes.

3.3.5 Atomic force microscopy at as-prepared, modified, and heat-treated PPF

The effect of heat treatment on the surface roughness of PPF was examined by tapping-mode AFM measurements of a PPF sample before and after modification with NP groups, and after heat treatment. The average surface roughness, R_q, calculated from 1 × 1 µm topographical height images (Figure 3.8) was 0.37 nm (as-prepared PPF), 0.49 nm (PPF-NP), and 0.44 nm (PPF-NP after heat treatment). Clearly, heat treatment does not affect the surface roughness, and regenerated surfaces are suitable for AFM imaging of nanoscale film features.

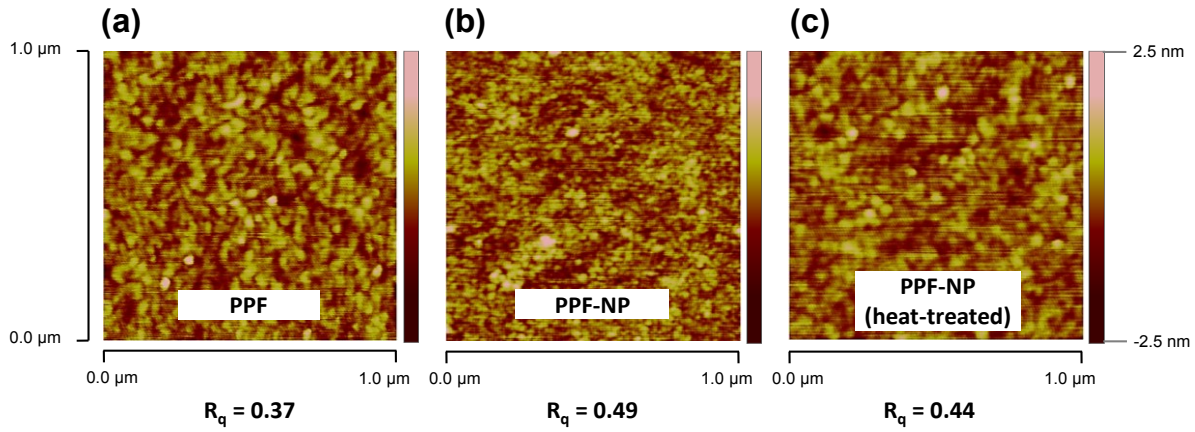

Figure 3.8 Tapping-mode AFM images of as-prepared PPF, PPF modified with NP groups, and PPF modified with NP groups after heat treatment. Images were recorded at a scan rate of 1 Hz.

3.3.6 Water contact angle measurements at as-prepared, modified, and heat-treated PPF

Water contact angle measurements were performed to determine the effect of heat treatment on the surface chemistry and/or morphology of PPF. No significant differences between as-prepared PPF, PPF-NP, and heat- treated PPF and PPF-NP were observed (Table 3.2), indicating no major changes in hydrophilicity/hydrophobicity or micro- or nanostructure after heat treatment.

Table 3.2 Water contact angle measurements at as-prepared PPF, as-prepared PPF after heat treatment, PPF modified with NP groups, and PPF modified with NP groups after heat treatment.

PPF[a]	PPF[a] (heat-treated)	PPF-NP	PPF-NP (heat-treated)
75 ± 4%[b] (n = 13)[c, d]	77 ± 2% (n = 4)	74 ± 4% (n = 9)[e]	76 ± 2% (n = 6)[e]

[a] As-prepared PPF.
[b] Values reported as mean ± relative standard deviation.
[c] Number of individual droplets measured (2 μL volume).
[d] Using three replicate electrodes.
[e] Using two replicate electrodes.

On the basis of these surface characterisation studies, heat treatment of film-modified PPF surfaces removes the grafted film and regenerates the surface, which, with the exception of a small amount of incorporation of nitrogen into the surface, exhibits identical surface properties to that before modification.

3.4 Method for fabrication of evaporated a-C electrodes on gold

This section describes the preparation and electrochemical characterisation of evaporated a-C on gold via a metal adhesion layer. The application of these surfaces for studying molecular surface modification by electrochemical reduction of aryldiazonium salt solutions is demonstrated. Preliminary studies investigating the feasibility of regenerating a-C electrodes by heat treatment are also described.

A critical issue when preparing a-C substrates is the adhesion between the carbon film and the underlying substrate; the films must bond strongly to the substrate and show good adhesion during use. In general, thin film adhesion can be divided into the following categories[224]: (i) interfacial adhesion, where the adhesion forces are centred around a well-defined interface and minimal mixing occurs; (ii) interdiffusion adhesion, where the film and substrate diffuse into one another; (iii) intermediate layer adhesion, where a layer (a surface oxide layer of a few nanometres, for example) enables chemical bonding; and, (iv) mechanical interlocking, which occurs when the film penetrates into irregularities at the surface (pores or holes, for example) and locks mechanically to the substrate.

In cases where poor adhesion is observed between two substrates, the most widely-accepted solution is to use a thin intermediate layer, known as an "adhesion layer". Commonly used adhesion layers in microfabrication are metals such as Ti and Cr[225]. Adhesion layers are typically prepared with thicknesses of 5-20 nm using evaporation or sputtering methods. Materials such as Ti and Cr are widely used due to their ability to easily form oxides layers, which can promote chemical bonding e.g. through metal-oxygen bonds. Deposition of carbon films by deposition in vacuum is most frequently performed on glass[200, 203, 226] or silicon-based materials[204, 214, 227-228], but has also been deposited on a wide range of metals such as Ti[205, 229], TiC[229-230], Pt[209-210], Al[231], Cr[232], Au[210], and stainless steel[227]. In general, carbon and noble metals are termed "non-reactive" due to their greater chemical stability, and hence difficulties with adhesion stability are often encountered when working with carbon and gold films[225]. The issue of adhesion stability must be addressed on a case-by-case basis, particularly when the goal is to achieve strong adhesion between carbon and a noble-metal substrate.

Evaporated gold films were chosen as a model substrate to demonstrate the feasibility of preparing C-QCs (via deposition of carbon onto the surface of Au-QCs). After addressing the issue of adhesion stability, the electrochemical and physical properties of a-C

electrodes were explored using cyclic voltammetry, AFM, stylus profilometry, sheet resistance measurements, and optical microscopy. Surface modification by electrografting NP_D in 0.1 M H_2SO_4 at a-C electrodes was also demonstrated. The purpose of electrografting was to test the suitability of a-C as an alternative to PPF for studying molecular films. The heat treatment method developed in Section 3.3 was briefly explored both as a possible annealing method and also to test the feasibility of regenerating the surface.

3.4.1 Interfacial adhesion of evaporated a-C electrodes prepared at metal substrates

The formation of stable a-C on gold was initially investigated by surveying a series of metal adhesion layers. NiCr, Ti, Al, Ni, and Pt adhesion layers (20 nm) were deposited on gold by thermal or e-beam evaporation (Section 3.2.2). Control samples were prepared by deposition of carbon directly on gold substrates.

The strategy used for fabrication of evaporated a-C electrodes is shown in Figure 3.9. Gold substrates (i) were fabricated by thermal evaporation of Au (100 nm) onto Si(100) surfaces, using NiCr (20 nm) as an adhesion layer. A second metal layer (ii, for example, Ni) was then deposited, followed by e-beam evaporation of graphite to give a 100 nm thick a-C film (iii).

An a-C thickness of 100 nm was chosen because previous studies have shown that the onset of conductivity for e-beam deposited carbon films is ≈ 4 nm[203]. Other workers have established that 7 nm and 200 nm thick carbon films deposited by e-beam onto highly-doped silicon exhibit good electrochemical properties [204]. In the study by Blackstock and co-workers it was found that 200 nm films exhibited faster electron transfer rates ($k°$) than 7 nm films for three of the four redox systems studied, hence thicker films ≈ 200 nm were desired in this work. A final thickness of 100 nm was chosen due to slow evaporation rates

and high temperatures in excess of 120 °C being reached after ≈ 100 nm of carbon film was deposited.

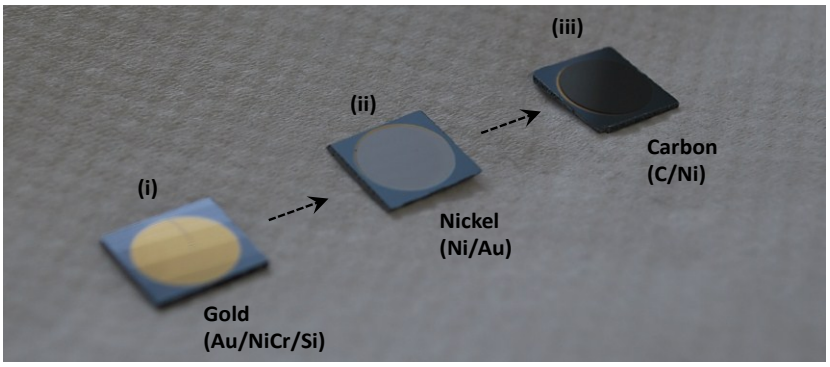

Figure 3.9 Preparation of a-C electrodes by e-beam evaporation of graphite onto thermally evaporated metal surfaces on silicon: (i) 100 nm layer of gold on 20 nm nichrome; (ii) 20 nm metal binding layer (nickel is shown); and (iii) 100 nm carbon layer. Surface area of silicon substrates = 10 mm^2.

The changes in surface colour are consistent with those observed for the materials in their bulk form. It is important to note that metal adhesion layers (ii) were exposed to air for short periods prior to deposition of the carbon layer (except when Al or Pt layers were deposited using e-beam evaporation). Consequently, any oxide layer formed on the metal surfaces on exposure to air was not removed prior to carbon deposition.

The adhesion stability of a-C electrodes was initially evaluated by monitoring film delamination after immersion of samples in solutions of Milli-Q water and 1 mM $Fe(CN)_6^{3-}$ for periods up to 120 min. The adhesion test used in this work was qualitative (like the commonly used Scotch tape test) and simple, yet directly tested the stability of the surfaces for applications in aqueous electrochemistry. For these experiments, a-C was deposited simultaneously on a number of different metal films to avoid any variation in the a-C layer.

Table 3.3 shows that for the five metal adhesion layers investigated, four metals (Ti, Al, Ni, and Pt) were stable in both Milli-Q water and $Fe(CN)_6^{3-}$ solution for periods of at least 2 min. Ni and Pt gave a-C substrates with the greatest adhesion stability; C/Ni/Au and

C/Pt/Au interfaces showed no signs of delamination after exposure to Milli-Q water for 30 min and exposure to $Fe(CN)_6^{3-}$ solution for 120 min. When an adhesion layer was not used, the stability of a-C substrates was very poor. Partial delamination was observed immediately after immersion of C/Au interfaces in Milli-Q water, consistent with the inertness of these materials. The excellent stability of samples with a Pt adhesion layer is surprising, given that Pt, like gold, is a noble metal. The adhesion mechanism for these surfaces is clearly complex and was not studied further. The poor stability observed for the interfaces prepared by deposition of carbon on gold contrasts with that reported by Pinto and co-workers, who found good physical stability for an electrode prepared by RF magnetron sputtering of graphitic carbon onto a Au-QC[210]. Such inconsistencies in adhesion stability between studies are common due to factors such as different carbon sources and processing techniques. It is noted that the greater instability of surfaces in $K_3Fe(CN)_6$ in PBS (pH 7.4) solution could be related to the presence of chloride ions which are known to be aggressive towards corrosion of metal interfaces[233].

Table 3.3 Observations of interface failure for a-C substrates prepared via metal adhesion layers after immersion in Milli-Q water and $K_3Fe(CN)_6$ solutions[a]

Adhesion Layer	Immersion in Milli-Q H_2O		Immersion in aqueous $K_3Fe(CN)_6$			
	2 min	30 min	2 min	10 min	120 min	48 h
NiCr	Partial delamination at C/NiCr	Delaminated at C/NiCr	Delaminated at C/NiCr	-	-	-
Ti	Stable	Stable	Stable	Partial delamination at Ti/C	Delaminated at Ti/C	-
Al	Stable	Stable	Stable	Partial delamination at Au/Al and C/Al	Delaminated at Au/Al	-
Ni	Stable	Stable	Stable	Stable	Stable	Stable
Pt	Stable	Stable	Stable	Stable	Stable	Stable
Au[b]	Partial delamination at C/Au	Delaminated at C/Au	Delaminated at C/Au	-	-	-

[a] Substrates were completely immersed in solution. Interface failure was monitored visually or by microscopy.
[b] No adhesion layer present.

3.4.2 Sheet resistance and surface resistivity of a-C (Ni) electrodes

Prior to electrochemical characterisation studies, sheet resistance measurements were performed. The sheet resistance of a-C (Ni) surfaces was calculated as an average of 9 repeat measurements obtained using two separate samples, giving 2.0 ± 0.4 Ω/sq. For comparison, PPF surfaces typically exhibit a sheet resistance of between 7-30 Ω/sq.

For an average film thickness of 118 nm, as measured by 5 individual step height measurements using a Dektak, the resistivity of the a-C surface was estimated as 2.4×10^{-5} Ω/cm. In contrast, the resistivity of PPF, with a film thickness of ≈ 1.5 μm, is typically in the range ≈ 1.5 - 4.5×10^{-3} Ω cm[66]. Clearly, the a-C (Ni) surface is significantly more conductive than the surface of PPF, suggesting that the flow of electrical current at the a-C surface is governed by paths through the underlying metal substrate. It is noted that e-beam deposited carbon surfaces on highly-doped silicon yield lower sheet resistances than those observed here (0.04 Ω/sq compared to 2.0 ± 0.4 Ω/sq), suggesting that the underlying substrate largely dictates the conductivity of thin layer carbon films of $\leq$ 200 nm.

The electrochemical characteristics of a-C electrodes with Ni and Pt adhesion layers were initially investigated by studying the voltammetry of $Fe(CN)_6^{3-}$. The $Fe(CN)_6^{3-/4-}$ redox probe allows comparison of a-C surfaces with the PPF surfaces used in Section 3.3, and other carbon electrodes used in this thesis and in the literature[30].

Figure 3.10 shows that CVs of 5 mM $Fe(CN)_6^{3-}$ at a-C (Ni) and a-C (Pt) are well-defined and chemically reversible. At a scan rate of 0.1 V/s, the average ΔE_p values are 326 ± 30 mV (n = 5 samples) and 368 ± 16 mV (n = 2 samples) at a-C (Ni) and a-C (Pt), respectively. At low scan rates (0.01 V/s), the average ΔE_p value at a-C (Ni) surfaces was 192 mV ± 5 mV (n = 2 samples). The observed ΔE_p values are larger than that typically obtained at PPF (Section 3.3.2) and GC surfaces, consistent with amorphous carbon surfaces having slower electron transfer kinetics than PPF and GC.

The stability of a-C (Ni) and a-C (Pt) surfaces to repeat cycling was tested, as shown in Figure 3.10. a-C (Ni) surfaces were more stable than a-C (Pt) surfaces (and are much cheaper) and hence were used for further electrochemical studies. In addition, the stability of a-C (Ni) surfaces toward sonication treatment was also assessed. Essentially no changes in the voltammetry of $Fe(CN)_6^{3-/4-}$ were observed after sonication for 5 min in Milli-Q water (data not shown).

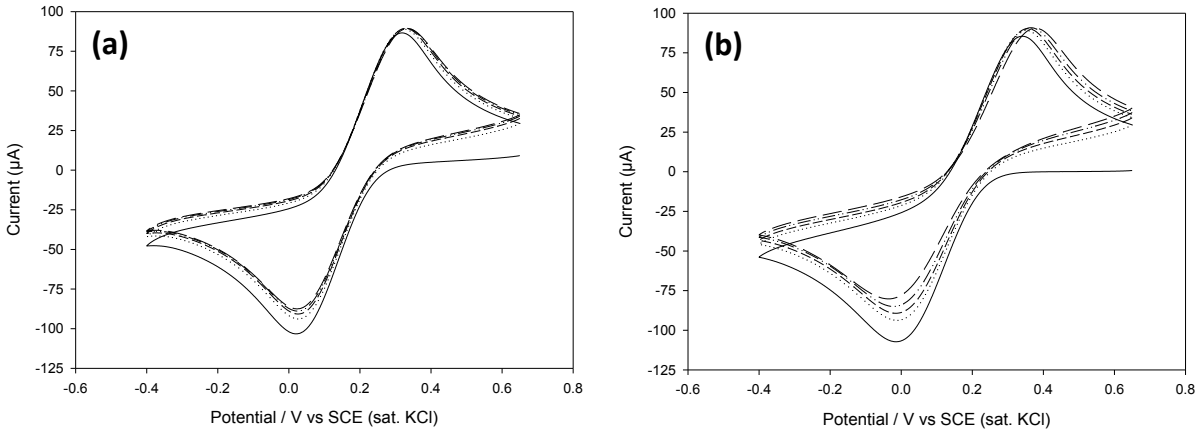

Figure 3.10 First five consecutive scan CVs of 5 mM $Fe(CN)_6^{3-}$ at a-C (100 nm): (a) a-C (Ni) prepared with a nickel adhesion layer and (b) a-C (Pt) prepared with a platinum adhesion layer.

3.4.3 Electrochemical studies of evaporated a-C (Ni) in $Fe(CN)_6^{3-}$ solution

The electrochemical performance of a-C (Ni) for $Fe(CN)_6^{3-}$ voltammetry was examined in more detail. Figure 3.11a shows CVs recorded at scan rates of 10–200 mV/s in $Fe(CN)_6^{3-}$ solution. The line of best fit on the plot of anodic peak current versus the square root of the scan rate does not pass through the origin (Figure 3.11b). Furthermore, the ΔE_p values for the CVs of $Fe(CN)_6^{3-}$ increase with scan rate from 189 mV (10 mV/s) to 420 mV (200 mV/s). These observations indicate that the electron transfer kinetics of $Fe(CN)_6^{3-}$ at a-C electrodes are quasi-reversible[234], which is consistent with the electrochemical behaviour

commonly observed for many carbon electrodes, including evaporated carbon film electrodes[204].

Compared with e-beam evaporated carbon films on highly-doped silicon, significantly larger ΔE_p values were observed on a-C (Ni) surfaces for $Fe(CN)_6^{3-}$ for the same scan rates. For example, ΔE_p = 420 mV at a-C (Ni) compared to 88 mV at previously reported e-beam evaporated carbon films, at 200 mV/s[204].

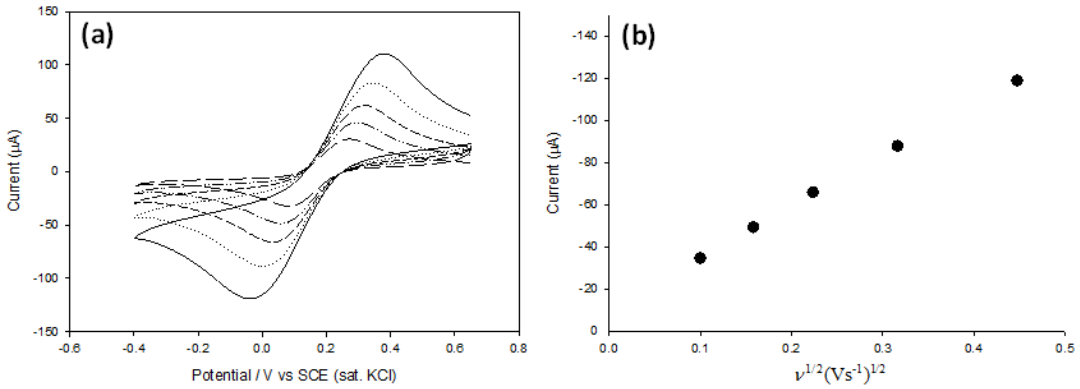

Figure 3.11 (a) First scan CVs of 5 mM $Fe(CN)_6^{3-}$ at a-C (Ni) recorded at scan rates of 0.01 to 0.2 V/s. (b) Corresponding Randles-Sevcik plot of I_p against $\nu^{1/2}$.

The standard heterogeneous electron transfer rate constant, k^o, for the $Fe(CN)_6^{3-/4-}$ redox reaction was calculated by the method of Nicholson[235]. The diffusion coefficients were estimated using the Randles-Sevcik equation (Equation 4) and the CV obtained at 10 mV/s (this scan rate gives the smallest deviation from electrochemically reversible behaviour).

$$I_p = (2.69 \times 10^5) n^{3/2} A D^{1/2} \nu^{1/2} C_0 \qquad (4)$$

where I_p is the peak current, n is the number of electrons, A the electrode area, C the concentration, D the diffusion coefficient, and ν the scan rate. The experimentally determined diffusion coefficients (at room temperature) were $D_a = 5.88 \times 10^{-6}$ cm^2/s and

D_c = 5.43 × 10^{-6} cm^2/s. These values are in the approximate range, but slightly lower, of previously reported values[236].

To determine k^o the working curve published by Nicholson was used[235]. Only the CV obtained at 10 mV/s had a ΔE_p value (189 mV) in the range of the working curve (61 mV/s to 212 mV/s) and hence this data was used, giving k^o = 1.8 × 10^{-3} cm/s.

Estimated k^o values for $Fe(CN)_6^{3-/4-}$ in aqueous electrolyte solution are the most commonly used benchmark for assessing the electron transfer kinetics of carbon electrodes[237]. The estimated k^o value for $Fe(CN)_6^{3-/4-}$ at a-C (Ni) surfaces are shown in Table 3.4, along with a range of reported k^o values for other planar carbon electrodes. As-prepared a-C (Ni) surfaces exhibit a k^o for $Fe(CN)_6^{3-/4-}$ of 1.8 × 10^{-3} cm/s. This value is closely similar to those obtained on other evaporated or sputtered carbon surfaces (1.2 × 10^{-3} cm/s [208, 210], 2.4 × 10^{-3} cm/s [228], and 5.7 × 10^{-3} cm/s [204]). The k^o value for sputtered a-C surfaces (1.2 × 10^{-3} cm/s) is of particular relevance to this work as this electron transfer rate was recorded at a C-QC. The rate constant observed for sputtered a-C surfaces prepared by Pinto and co-workers is notably smaller than that reported for a-C (Ni) surfaces in this work. Thus it might be expected that a-C (Ni) coated Au-QCs (using the e-beam evaporation method developed in this chapter) would exhibit faster electron transfer kinetics than previously reported amorphous carbon-coated quartz crystals[210].

Table 3.4 shows that various disordered carbon electrode materials exhibit rate constants in the range of 10^{-3} to 10^{-2} cm/s. Due to the high sensitivity of $Fe(CN)_6^{3-/4-}$ to the surface chemistry of carbon electrodes, observed k^o values vary widely between studies. This is particularly evident for GC electrodes, where differences in pre-treatment and surface history account for the large variation in k^o values[54, 237-238]. Compared to the estimated k^o values for PPF (6.3 × 10^{-3} cm/s) and heat-treated PPF surfaces (8.8 × 10^{-3} cm/s) prepared in

this chapter, the a-C (Ni) surfaces exhibit slower electron transfer kinetics by a factor of 3-5 times.

Table 3.4 Heterogeneous electron transfer kinetics for $Fe(CN)_6^{3-}$ at various planar carbon electrode materials. All of the presented k^o values were estimated using cyclic voltammetry.

Electrode material	Pre-treatment	Scan rate (V/s)	k^o ($Fe(CN)_6^{3-/4-}$) (× 10^{-3} cm/s)	Reference
E-beam carbon (100 nm) on Ni	IPA	0.01	1.8	This work
E-beam carbon (200 nm) on H-Si[a,b]	IPA/AC[c]	0.10-0.50	5.7 ± 0.9[d]	[204]
E-beam carbon (28 nm) on glass	-	-	1.2	[208]
ECR[e] carbon (40 nm) on Si[b]	-	0.01	2.4 and 12[f]	[228]
Sputtered carbon[g] (500 nm) on Au	-	0.01	1.2	[210]
GC	IPA/AC[c]	-	90	[54]
GC	Polished	-	5 ± 3	[238]
GC	Sonicated	-	80	[47]
PPF (1-2 µm)	IPA	0.10	6.3	This work
PPF (1-2 µm)	Heat-treated	0.10	8.8	This work
PPF (1-2 µm)	-	-	12[d], 15	[64, 62]
HOPG (basal plane)	-	0.20	10^{-3}	[45]

[a] Highly doped silicon (100).
[b] Hydrogen-terminated silicon.
[c] Isopropyl alcohol, activated carbon, sonication.
[d] k^o values corrected for uncompensated cell resistance.
[e] Electron Cyclotron resonance (ECR) sputtering.
[f] For surfaces prepared by 20 V and 70 V ion accelerating voltages, respectively.
[g] RF magnetron sputtering (energy 1 keV).

The lower electron transfer rate at a-C compared to other types of carbon could be due to a number of factors as the $Fe(CN)_6^{3-/4-}$ couple is sensitive to both the surface reactivity and the electronic structure of carbon surfaces. The lower reactivity is most likely due to the a-C surfaces prepared in this work having a higher sp^3/sp^2 carbon ratio and a lower density of graphite edge plane sites. The lower reactivity of the a-C surfaces compared to other carbon surfaces may also be due to differences in the functional groups on the surface, for example [41, 45, 47, 237-238].

3.4.4 Electrochemical studies of evaporated a-C (Ni) in KOH solution

To test whether a-C (Ni) surfaces are pinhole free and uncontaminated by Ni, cyclic voltammetry was used to monitor for the presence of nickel hydroxides in 1 M KOH. Figure 3.12 shows the typical CV behaviour of an evaporated Ni adhesion layer before (a) and after (b) deposition of a carbon layer. For each type of surface, two consecutive CVs were recorded in 1 M KOH, after applying a fixed potential of -1.1 V for 60 s.

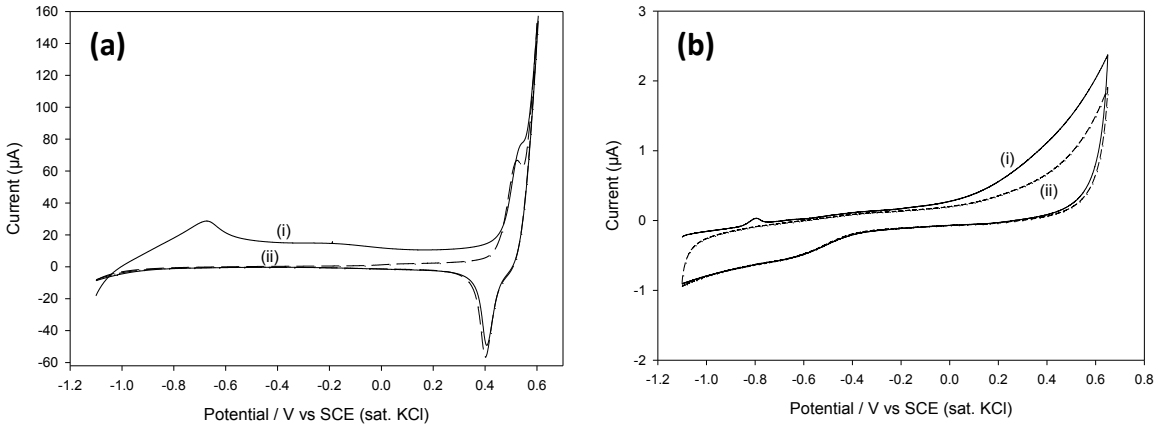

Figure 3.12 First (i) and second (ii) scan CVs in 1 M KOH at (a) a nickel adhesion layer surface and (b) a-C (Ni) surface. Scan rate = 50 mV/s.

On a freshly prepared Ni adhesion layer (Figure 3.12a), a CV starting at -1.1 V shows anodic current peaks at $E_{pa} \approx$ -0.7 V and 0.5 V. On the reverse scan a cathodic peak is observed at $E_{pc} \approx$ 0.4 V. The peak at -0.7 V is due to the formation of a nickel hydroxide layer at the surface (Equation 5) and the redox couple at $E_{1/2}$ = 0.46 V is due to the chemically reversible redox reaction shown in Equation 6[239].

$$\text{Surface---Ni} + 2\ OH^- \rightarrow \text{Surface---Ni-(OH)}_2 + 2e^- \quad (5)$$

$$\text{Surface--- Ni-(OH)}_2 + OH^- \rightleftarrows \text{Surface---Ni-OOH} + 1e^- + H_2O \quad (6)$$

For the a-C (Ni) surface (Figure 3.12b), only very low background currents are observed for the two consecutive CVs recorded in 1 M KOH, with the exception of a small irreversible anodic peak at $E_{pa} \approx$ -0.8 V on the first scan. This is consistent with the presence of a small amount of Ni at the surface, attributed to the formation of pinholes in the carbon film. Although the amount of Ni has not been quantified, the absence of the nickel hydroxide/nickel oxyhydroxide system at $E_{1/2}$ = 0.46 V suggests that the trace level Ni contamination will not be a problem in use of these surfaces.

3.4.5 Electrochemical studies of evaporated a-C (Ni) in 1 M KCl and in PBS (pH 7.4) solutions

One of the most important and useful attributes of planar graphitic electrodes is their wide electrochemical potential window in aqueous conditions, particularly when compared to other electrode materials such as the noble metals, for example[29-30].

Cyclic voltammetry was used to investigate the potential window of evaporated a-C (Ni) in PBS (pH 7.4) (Figure 3.13, –). In the same medium, the potential window for a freshly polished GC plate was also recorded for comparison (Figure 3.13, ---). The potential window has previously been defined as the potential range between the current limits that do not exceed ± 500 μA/cm^2 [240-241]. However, a potential range with current limits that do not exceed ± 180 μA/cm^2 is more appropriate here because the potential applications for these surfaces include mono and multilayer film deposition and detection, which typically requires low background currents.

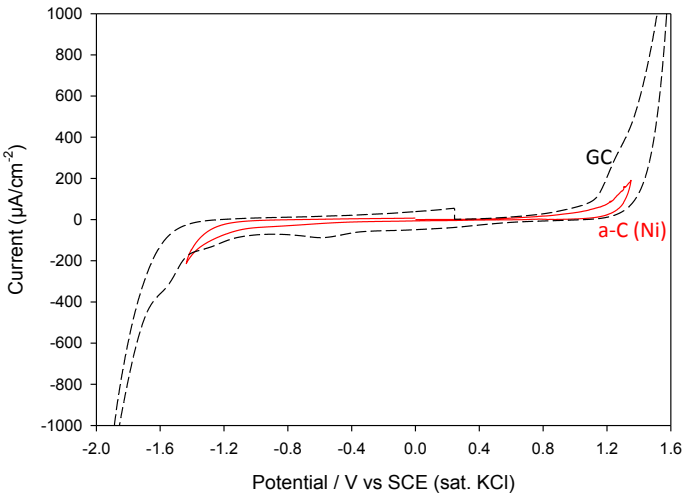

Figure 3.13 First scan CVs in PBS (pH = 7.4) at a-C (Ni) surface (–) and polished GC (---). Scan was initiated at 0 V towards positive potentials.

Considering the potential over which the current is ≤ ± 180 µA, the potential window for a-C (Ni) is 2.7 V (-1.4 V to 1.3 V vs. SCE) and for GC is 2.6 V (-1.4 V to 1.2 V vs. SCE). Featureless background currents are observed over these potential ranges, except for a broad reduction process at E_{pc} ≈ -0.6 V at both surfaces. A similar process (a broad wave at E_{pc} ≈ -0.4 V) is also observed at as-prepared and heat-treated PPF samples in aqueous acid solution (Figure 3.4); the nature of these peaks is unknown but they appear to be related.

At both a-C (Ni) and GC surfaces the negative potential limit is the same. For oxidation, however, the a-C surface has a slightly wider potential window. The potential window values observed in aqueous solution are generally between 2.5-3.0 V for GC surfaces[30,242]. In PBS solution (pH 6.8), a potential window value of 2.5 V has been reported at GC (current range = ± 200 µA/cm^2)[242].

Figure 3.13 shows clearly that there are significant differences in the background current between a-C (Ni) and GC electrodes, hence further studies investigating electrode capacitance were performed. The electrode capacitance was estimated by recording CVs

between -0.2 V and 0.55 V (vs. SCE) on freshly prepared a-C and GC at 1 V/s in Milli-Q water with 1 M KCl. Average capacitance values were determined from at least two separate samples and three separate CV scans using Equation 7:

$$i = Cv \tag{7}$$

where i is the charging current (A), C is the capacitance (F), and v is the scan rate (V/s). In this work the charging current, i, was obtained by averaging the sum of the anodic and cathodic currents measured at 0.4 V from a single CV scan. The average capacitance value for a-C at 1 V/s was 8.3 ± 1.3 μF cm^2 (n = 3 samples) which compares to an average capacitance of 23.1 ± 2.9 μF cm^2 at polished GC. The data shows quantitatively that the voltammetric background currents are significantly lower at a-C surfaces, consistent with the previous observation in PBS shown in Figure 3.13. Compared to e-beam evaporated carbon surfaces analysed in 1 M KCl, the capacitance values obtained here are slightly lower. In fact, the values obtained for a-C in this work are very similar to capacitance values previously observed for PPF surfaces (9.2 μF cm^2)[64].

Large differences in background and capacitance, like that observed here, have also been observed between GC and other types of carbon electrodes such as PPF, ECR sputtered carbon, doped diamond, and the basal plane of HOPG[64, 240, 243]. Low voltammetric background currents and capacitances at particular carbon materials have been attributed to factors such as low surface roughness, a low content of ionisable carbon-oxygen functionalities at the surface (carboxyl and hydroxyl groups, for example), a high proportion of sp^3-hybridised carbon, and a low DOS[30, 44, 64, 240]. All of these factors might be relevant for the evaporated a-C surfaces.

3.4.6 Atomic force microscopy at a-C (Ni) surfaces

Tapping-mode AFM images were recorded to determine the surface roughness of a-C surfaces, and to examine to what extent the roughness of the nickel substrate changes after deposition of the carbon film.

Figure 3.14 shows 1 × 1 µm AFM images recorded in tapping-mode at a Ni/Au surface before and after deposition of a 100 nm carbon layer. Average surface roughness values were obtained for a-C and Ni surfaces by examining multiple images recorded at different scan sizes (1 × 1 and 5 × 5 µm). The average surface roughness value obtained for a-C was R_q = 0.85 ± 0.15 (n = 12). For Ni surfaces, R_q = 0.98 ± 0.10 (n = 9). The data shows that the deposition of a carbon layer does not significantly change the roughness of nickel surfaces. More importantly, the a-C surfaces have a very low surface roughness, with $R_q \leq$ 1 nm up to surface areas of 1 × 1 µm. The surface roughness is greater than is observed for PPF, similar to e-beam evaporated carbons on silicon surfaces, and significantly less rough than the smoothest reported values for polished GC.

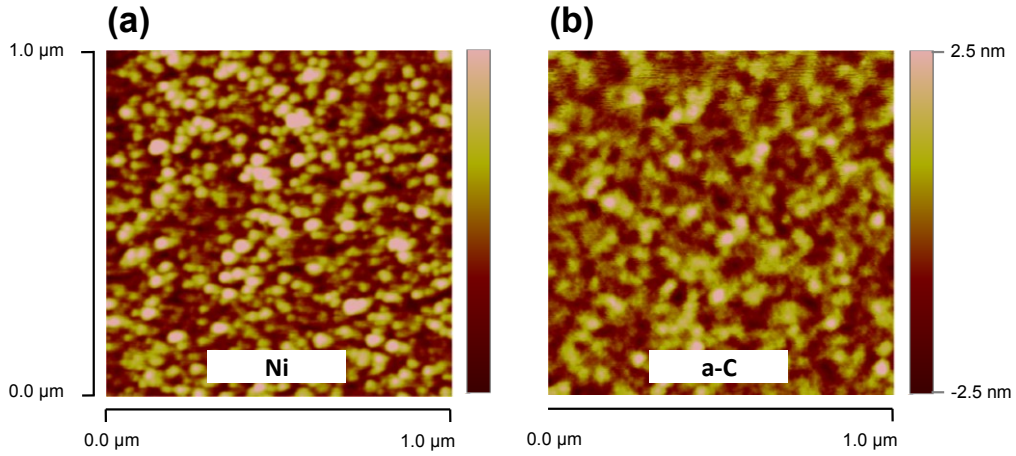

Figure 3.14 Tapping-mode AFM images recorded at (a) a nickel adhesion layer surface and (b) a-C (Ni) prepared by deposition of carbon on the nickel adhesion layer shown in (a).

3.4.7 Electroreduction of NP_D at a-C (Ni) in 0.1 M H_2SO_4 and subsequent NP film characterisation

The use of a-C surfaces as substrates for spontaneously grafting diazonium-derived films has recently been reported by Colavita and co-workers[227]. However, there have been no reports of studies of electrografted diazonium-derived films. In this work, electrografting and subsequent film characterisation were undertaken in aqueous acid. This medium is a common alternative to acetonitrile for grafting via aryldiazonium ions[66, 244].

Diazonium-derived films were grafted from 1 mM NP_D in 0.1 M H_2SO_4. Surface modification was achieved by recording two CVs in 1 mM solution between 0.5 V and -0.4 V vs. SCE. Figure 3.15a shows the broad, irreversible reduction peak on the first CV scan, assigned to the one-electron reduction of NP_D. No peak is seen on the second CV scan, consistent with grafting a blocking film. The CVs are closely similar to those observed at PPF (Figure 3.2), despite the difference in substrate and solvent-electrolyte. The diazonium reduction potential of $E_{pc} \approx 0$ V is the same as that observed at PPF by Brooksby and co-workers under identical grafting conditions (1 mM NP_D in 0.1 M H_2SO_4, vs. SCE)[66].

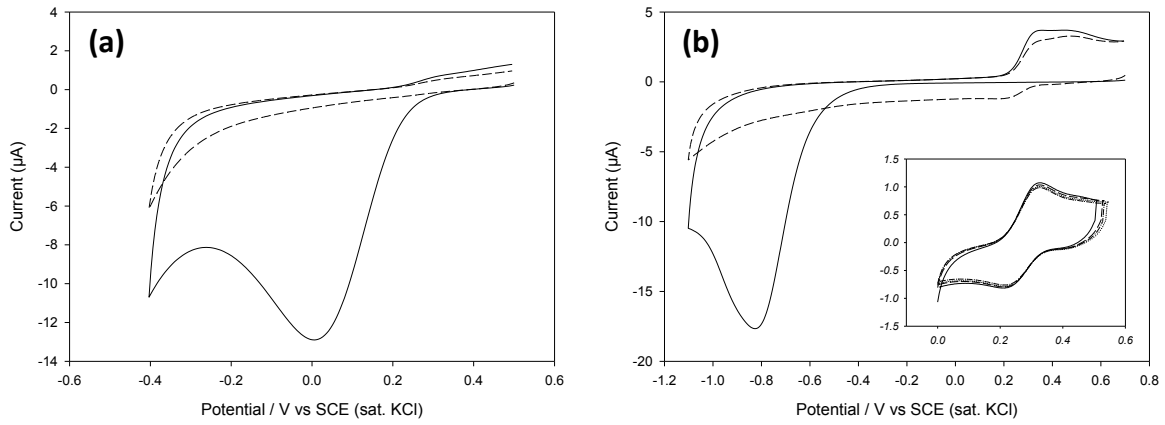

Figure 3.15 (a) First (–) and second (---) scan CVs of 1 mM NP_D in 0.1 M H_2SO_4 at a-C (Ni). (b) First (–) and second (---) scan CVs in 0.1 M H_2SO_4 at a-C (Ni) modified with NP groups; Inset: third, fourth, and fifth scan CVs recorded in oxidation of the reduced NP film on a-C (Ni).

The electroactivity of the NP modified a-C (Ni) surface was investigated in 0.1 M H_2SO_4 by cyclic voltammetry. Figure 3.15b shows the characteristic first (–) and second (---) CV scans for a freshly grafted NP film on an a-C (Ni) surface. The large peak at E_{pc} = -0.8 V corresponds to reduction of NP groups to aminophenyl and hydroxyaminophenyl groups (Equation 1 and 2, Section 3.3.2). The NP reduction peak is significantly broader and has shifted ≈ -100 mV relative to that at PPF (Figure 3.4). The observed changes may be due to differences in the interfacial characteristics of the a-C and PPF surfaces, or alternatively, due to differences in the films themselves, possibly arising from the use of different grafting media. For example, Brooksby and co-workers have tentatively proposed that shifts in the electrode potential for $–NO_2$ group reduction in similar films, prepared at PPF, occur due to differences in proton diffusion through the films[65].

On the return scan (Figure 3.15b, ---), a relatively small and broad oxidation wave is observed (E_{pa} ≈ 0.4 V), corresponding to the oxidation of hydroxyaminophenyl to nitrosophenyl groups (Equation 3, Section 3.3.2). The hydroxyaminophenyl/nitrosophenyl redox couple was characterised further by recording consecutive CVs in oxidation between 0 V and 0.5 V (Figure 3.15b, inset). The half wave potential, $E_{1/2}$, of this couple was $E_{1/2}$ = 0.27 V vs. SCE, which compares closely with that observed for the same couple after NP film reduction at GC and PPF electrodes (values for $E_{1/2}$ of ≈ 0.3 vs. Ag/AgCl or SCE are typically observed)[138, 175].

From the integrated area of the reduction and oxidation peaks for the example shown in Figure 3.15b, the surface concentration of electroactive NP groups was estimated to be 7.4 × 10^{-10} mol/cm^2. Based on the known relationship between surface concentration and thickness of NP films on PPF, the NP film at a-C (Ni) has an estimated thickness of 2.5 nm and hence is multilayered[66]. The lower surface concentration of NP groups at a-C (Ni) compared to PPF or heat-treated PPF (18 ± 1 × 10^{-10} mol/cm^2) was anticipated, as the films

grafted at PPF were prepared using an additional potential electrolysis step (300 s at E_{pc} - 150 mV), which increases NP film growth[65, 68].

3.4.8 Electrochemical investigations at heat-treated a-C (Ni)

Regeneration of a-C (Ni) and a-C (Al) surfaces was explored using the heat treatment method developed in Section 3.3, but with lower temperatures (445 or 495 °C). It was also of interest to establish whether the electrochemical performance and physical stability of a-C could be enhanced by thermal annealing. Azarko and co-workers have shown that heating of evaporated carbon structures to ≈ 225 °C under vacuum (during deposition) causes a decrease in the level of stresses in coatings, and an increase in the sizes of crystallites of sp^2 carbon[245]. Heat treatment of evaporated carbon surfaces at higher temperatures (1000 ºC) is also known to improve electron transfer kinetics[204]. Further, Besold and co-workers have shown that heat-treatment of evaporated carbon at 700 °C in Ar for 15 min increases the electrical conductivity of the carbon surfaces by a factor of 2 relative to the non-pyrolysed sample[203]. In the present work, the maximum temperature used was below the Curie point for quartz so that the method could be applied to a-C coated QCM crystals.

Prior to heat treatment, a-C surfaces were black in colour, as shown in Figure 3.9 (iii) and Figure 3.16. After heat treatment at either 445 or 495 °C, significant changes in the surface colour were observed. Figure 3.16 shows that the heat-treated a-C (Ni) surface is red and "cloudy", whereas the heat treated a-C (Al) surface is silver and "speckled". These changes suggest that the heat-treated surfaces are carbon-metal composites. Wiltner and co-workers showed that significant carbon diffusion occurs at 400 °C in vacuum for a thin carbon layer evaporated on Ni (100)[246]. At 450-550 °C, complete diffusion of the carbon into the nickel substrate occurred. Hence it is assumed that diffusion of carbon into the metal layers accounts for the changes in these surfaces.

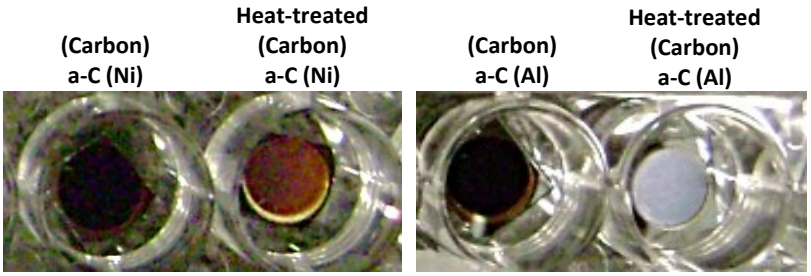

Figure 3.16 Digital camera images recorded at a-C (Ni) and a-C (Al) surfaces before and after heat treatment at 495 ± 25 °C.

To further investigate the surface properties, a heat-treated a-C (Ni) sample was examined by recording the electrochemical response of 1 mM $Fe(CN)_6^{3-}$. The CVs (Figure 3.17a) are well-defined and chemically reversible, with ΔE_p = 98 mV. The heat treated surface exhibits diffusion-controlled behaviour for the $Fe(CN)_6^{3-/4-}$ couple for scan rates between 5-200 mV/s (Figure 3.17b) and hence appears to be a suitable electrode material. The finding that heat-treated a-C (Ni) surfaces exhibit faster electron transfer electron kinetics than heat-treated PPF (heat-treated under identical conditions) is surprising. The electrochemical experiments therefore would support the formation of a carbon-based metal composite electrode, or a metallic electrode, following heat treatment of a-C (Ni) at 495 °C in Ar.

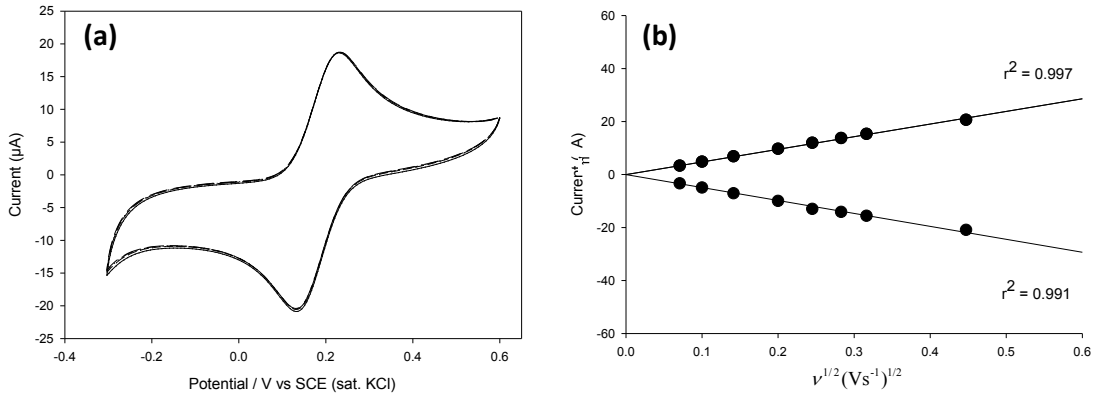

Figure 3.17 First five consecutive scan CVs of 1 mM $Fe(CN)_6^{3-}$ at (a) a-C (Ni) after heat treatment at 445 ± 25 ºC for 30 min in Ar at 1 L/min. (b) Corresponding Randles-Sevcik plot of I_p against $\nu^{1/2}$ for scan rates of 0.005 to 0.2 V/s.

3.5 Conclusion

Two technical methods have been developed which expand the use of planar carbon electrodes for performing thin-film studies: a heat-treatment method for regenerating PPF surfaces, and a method for fabricating amorphous carbon film electrodes on gold. The latter could be applied to gold-coated QCM crystals to give carbon-coated quartz crystal surfaces for QCM and E-QCM measurements.

Heat treatment at 545 ± 25 °C for 30 min in Ar is a simple method for regenerating film-modified surfaces for re-use. After heat treatment, the electrochemical activity of PPF surfaces showed small improvements compared to PPF prior to modification. The same procedure yielded small improvements in the electrode kinetics of $Fe(CN)_6^{3-}$ at unmodified PPF, presumably by removing traces of impurities which adsorb on the PPF surface during storage. A lower temperature (495 ± 25 °C) effectively regenerated PPF modified with NP groups but should be tested before use with other grafted films.

Surface characterisation techniques revealed that the surface roughness and hydrophobicity of PPF surfaces remained unchanged compared with the PPF prior to modification. XPS analysis of PPF modified with a BrP film and subsequently heat-treated confirmed complete removal of the film. For NP film-modified PPF, the heat-treated sample showed higher N content than as-prepared PPF. The incorporation of N into the PPF surface is attributed to a previously reported reaction between PPF and NO liberated during decomposition of NP groups.

E-beam deposition from a graphite source onto gold via a Ni or Pt metal adhesion layer gave carbon films with useful electrochemical properties and good physical stability. a-C (Ni) showed excellent stability on exposure to aqueous solutions for periods of many hours or days. The surfaces are highly conductive with estimated sheet resistance and resistivity values of 2.0 ± 0.4 Ω/sq and 2.4 × 10^{-5} Ω/cm, respectively. The high conductivity values

reflect that conduction is influenced by the underlying metal, as has been observed in previous reports for evaporated carbon thin films ≤ 200 nm thick.

Voltammetric studies show that a-C (Ni) surfaces exhibit well-defined and chemically reversible behaviour towards the $Fe(CN)_6^{3-/4-}$ redox couple, a wide potential window (2.7 V), and low background currents in aqueous PBS (pH 7.4). Capacitance values of 8.3 ± 1.3 μF cm^2 obtained in aqueous 1 M KCl are much lower than those obtained at GC (23.1 ± 2.9 μF cm^2). Such low capacitance values are desirable for possible electroanalytical applications. For the $Fe(CN)_6^{3-/4-}$ redox couple, a-C (Ni) surfaces exhibited an average ΔE_p value of 326 ± 30 mV (scan rate = 100 mV/s), and an electron transfer rate constant, k^o, of 1.8 × 10^{-3} cm/s. The k^o values are smaller than those observed at PPF surfaces in this work (6.6 × 10^{-3} cm/s), and values of k^o reported in other studies for GC and PPF surfaces. Compared to previously reported values for evaporated or sputtered thin-film carbon electrodes, the values found in this work at a-C (Ni) are amongst the highest reported.

AFM analysis of a-C (Ni) surfaces revealed that the films have a lower surface roughness than GC but a higher surface roughness than PPF. The low surface roughness (R_q = 0.85 ± 0.15) should be sufficient to enable depth-profiling experiments to be performed on grafted multilayer films although this was not tested.

The electrografting behaviour of NP_D in 0.1 M H_2SO_4 was the same as has previously been observed under the same conditions at PPF. The resulting NP films were examined in 0.1 M H_2SO_4 and showed the characteristic response of a multilayered NP film at GC and PPF electrodes.

Heat treatment of a-C (Ni) and a-C (Al) surfaces at 495 ± 25 °C for 30 min in Ar resulted in the formation of a composite metal-carbon or metallic surface, as revealed by a significant change in colour of the electrode (black to red/silver) and faster electron-transfer kinetics towards $Fe(CN)_6^{3-/4-}$ at the heat-treated surface. These changes are

attributed to diffusion of carbon atoms into the bulk metal structure. Heat-treatment (≥ 495 ± 25 °C in Ar) of evaporated carbons deposited at metal substrates is therefore not a suitable surface "activation" or regeneration method.

The most significant advancement in this work is the development of a simple, time- and cost-effective method that allows re-use of PPF surfaces. The method should substantially expand the applications of PPF as an electrode material. The heat treatment method used for PPF should be applicable to other pyrolysed photoresist film and graphitic materials, depending on the composition of the underlying substrate. The method developed for preparing evaporated a-C (Ni) is also a significant advancement as it has gone some way towards developing a standard method for preparing carbon-coated gold substrates, for example, gold-coated quartz crystals. However, regeneration of the surfaces remains to be achieved and single-use QCM crystals are unlikely to find wide use due to the time and cost involved in their fabrication.

Modification of surfaces by electrochemical reduction of free-base and nickel (II) tetraphenylporphyrin diazonium salts

4.1 Introduction

This chapter describes the preparation and characterisation of thin diazonium-derived porphyrin films on planar electrode surfaces. This research is motivated by the importance of designing well-defined electroactive and photoactive layers which are thinner than electropolymerised polymers and more stable than monolayers generated via self-assembly such as alkanethiol SAMs.

Free-base porphyrin and metalloporphyrin films have excellent optical, photoluminescent, electrical, and catalytic properties, which have led to their application as components of solar photovoltaic cells[247-250], charge-based memory devices[251-252], and electrochemical sensors[253-256]. The importance of nickel porphyrin films on carbon electrodes for sensing applications has been demonstrated by Malinski and Taha who developed a microsensor for detection of nitric oxide release from single-cells[257]. More recently, nickel porphyrin films have been used for the electrocatalytic oxidation of analytes including methanol[258-260], ethanol[258-259], phenols[261], and hydrazine[259]. Free-base porphyrins have received comparatively little interest for electrocatalytic applications due to the absence of a catalytic metal centre. Nevertheless, free-base porphyrin films have been used widely for optical and voltammetric sensing of volatile organic compounds[262], metal ions such as Cu^{2+}, Zn^{2+}, Hg^{2+}, Pb^{2+}, and Ni^{2+} [263-265], and for pH monitoring[143]. For fabrication of metal ion sensors, free-base porphyrin films are ideal due to the porphyrin ring providing a vacant site at its centre which can bind many different metal cations.

Several methods exist for the direct attachment of porphyrin films to conducting and semiconducting surfaces, including anodic electropolymerisation[258, 266-269], alkanethiol self-

assembly on gold[250, 253, 255, 270-271], thermal reactions of thiols[199], selenols[199], alcohols[199], alkenes[272-273], and alkynes[272-273], and diazonium salt chemistry[274-278]. Surprisingly, only a few examples of porphyrinic substrates prepared via aryldiazonium salt chemistry have been reported. Notably, none of these examples demonstrate electrografting from non-aqueous diazonium salt solutions prepared from isolated salt precursors. Guo and co-workers modified single-walled carbon nanotubes via a thermal reaction with *in situ* generated free-base tetraphenylporphyrin diazonium salts and characterised the materials using spectroscopy and microscopy[277-278]. Similarly, Lu and co-workers exploited the spontaneous reaction of *in situ* generated tetraphenylporphyrin diazonium salts at hydrogen-terminated silicon to graft porphyrin films[275]. Very recently, Barrière and co-workers reported electrografting of *in situ* generated free-base tetraphenylporphyrins (H_2TPP) at GC and PPF, which gave thick (80 nm) polymer films with poorly defined electroactivity[276]. Interestingly, the authors reported that stable surface attachment was only achieved using the tetra-substituted diazonium salt and not the mono-substituted porphyrin derivative.

The aim of this research is to explore the formation of free-base and metalloporphyrin films on different planar surfaces using mono-substituted aryldiazonium salt derivatives. The strategy should establish electrografting from non-aqueous solutions as a generally applicable method for forming a wide range of porphyrin film-modified surfaces. Section 4.3.1 addresses the electrografting behaviour of free-base and nickel (II) tetraphenylporphyrin aryldiazonium salts. The oxidative grafting behaviour of an amine-containing nickel (II) tetraphenylporphyrin derivative is reported in Section 4.3.2. Sections 4.3.3 to 4.3.12 describe the characterisation of porphyrin-modified surfaces using electrochemistry, spectroscopy, and AFM.

4.2 Experimental

4.2.1 Surface preparation

GC rod and PPF were prepared as described in Chapter 2. Gold electrodes (Ø = 2 mm, CH-Instruments Inc.) were prepared using the same procedures as those used for GC. ITO coated glass slides (Sigma Aldrich, ≤ 15 Ω/sq resistivity) were cleaned prior to use for 30 s in H_2SO_4/H_2O_2 3:1, then rinsed in Milli-Q water. Prior to use, carbon and gold surfaces were rinsed with ACN then dried with a stream of N_2. ITO surfaces were rinsed successively with ACN and IPA then dried with N_2.

4.2.2 Electrochemistry

The geometric working area of rod electrodes was 0.07 cm^2 (GC) and 0.03 cm^2 (gold) for electrografting and electrochemical characterisation. The geometric area of PPF and ITO for electrografting was not defined, and was 0.11 cm^2 for electrochemical characterisation. All potentials are reported versus the Ag/AgCl (sat. KCl) (BAS Inc.) reference electrode. Rotating disk electrode (RDE, Radiometer Analytical) experiments were carried out at a rotation rate of 500 rpm. All non-aqueous electrochemistry was performed under strictly dry conditions using degassed solutions. All reported surface concentrations and $E_{1/2}$ values were estimated from the second scan.

4.2.3 Electrochemical modification of surfaces

Unless stated otherwise, H_2TPP films were electrografted by cycling (30 cycles) between 0.4 V and -0.7 V in ACN containing 0.5 mM H_2TPP_D with 0.1 M $TBABF_4$. Nickel (II) tetraphenylporphyrin (NiTPP) films were electrografted by cycling (30 cycles) between 0.5 V and -0.35 V in ACN:DMF (4:1) containing 0.5 mM $NiTPP_D$ with 0.1 M $TBABF_4$. $NiTPP^A$ films were electrografted by cycling (30 cycles) between 0.5 V and 1.3 V or 1.45 V in DCM containing 0.5 mM $NiTPP_A$ with 0.1 M $TBABF_4$. After modification, samples

were sonicated for 60 s in DMF (or DCM when samples were prepared for analysis in DCM), and dried using a stream of N_2. Note for clarity: the naming of the grafted films, NiTPP and H_2TPP, refers to the diazonium-derived films. NiTPP^A refers to the amine-derived films.

4.2.4 Post-assembly metallation of H_2TPP-modified surfaces

The insertion of metal ions was achieved by immersion of freshly prepared H_2TPP film-modified GC electrodes in DMF solution containing 10 mM of copper (II) acetate monohydrate for 48 h. Surfaces were subsequently sonicated for 5 min in DMF, and dried under a stream of N_2 before characterisation.

4.3 Electrochemical modification of surfaces with H_2TPP, NiTPP, and $NiTPP^A$ films

Modification of electrode surfaces with free-base tetraphenylporphyrin (H_2TPP) and nickel (II) tetraphenylporphyrin (NiTPP) films was investigated by electrochemical reduction of the corresponding aryldiazonium ions and by electrochemical oxidation of $NiTPP_A$. The free-base and metallated tetraphenylporphyrin derivatives used for surface modification contain a mono-diazonium or mono-amine moiety for direct surface attachment (Figure 4.1).

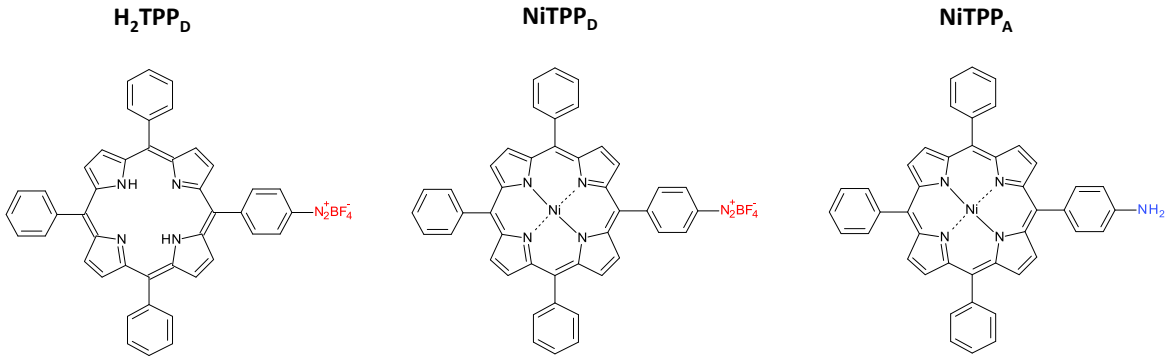

Figure 4.1 Modifiers used to graft H_2TPP, NiTPP and $NiTPP^A$ films at electrode surfaces.

Electrografting was investigated using non-aqueous aryldiazonium salt solutions prepared from isolated tetrafluoroborate salts. This is in contrast to the recent work of Barrière and co-workers who investigated grafting of free-base porphyrins using aqueous *in situ* generated tetraphenylporphyrin aryldiazonium salt solutions[276].

4.3.1 Electroreduction of H_2TPP_D and $NiTPP_D$ in non-aqueous solution

Electrochemical reduction of aryldiazonium salts, H_2TPP_D and $NiTPP_D$, was investigated by potential cycling at GC, PPF, gold, and ITO surfaces under strictly anhydrous

conditions. Film-modified surfaces were obtained using freshly prepared aryldiazonium salt solutions as described in Section 4.2.3.

Figure 4.2 shows successive CVs of H_2TPP_D in ACN-$TBABF_4$ (Figure 4.2a) and $NiTPP_D$ in DMF:ACN-$TBABF_4$ (Figure 4.2b) at GC. On the first scan in the cathodic direction, a broad and irreversible peak is observed at $E_{pc} \approx 0.2$ V (H_2TPP_D) and $E_{pc} \approx 0.1$ V ($NiTPP_D$), corresponding to the reduction of aryldiazonium ions and subsequent film formation. Similar grafting CVs were also observed at PPF, gold, and ITO surfaces (data now shown).

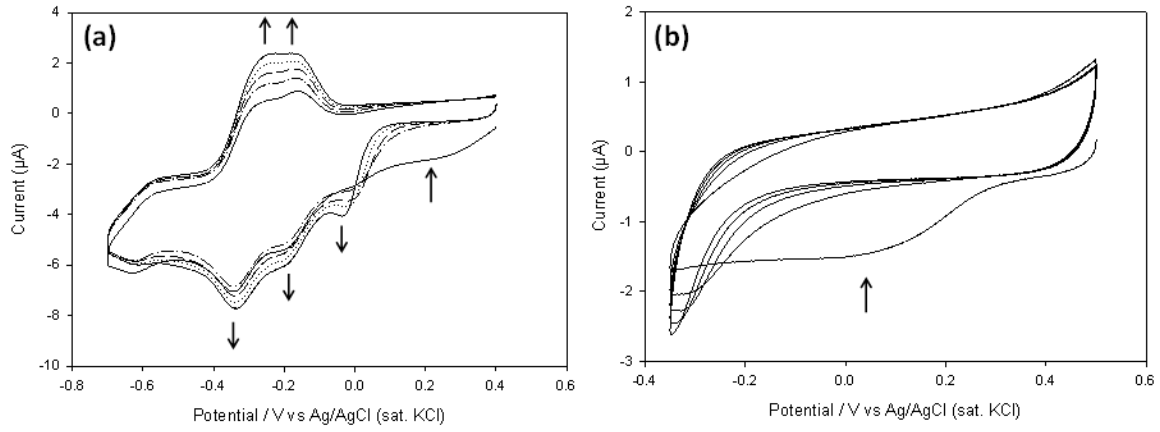

Figure 4.2 Consecutive CV scans of (a) H_2TPP_D in ACN-$TBABF_4$ and (b) $NiTPP_D$ in DMF/ACN (4:1)-$TBABF_4$ at GC. Arrows indicate changes in current with consecutive scans.

In addition to the general features of aryldiazonium ion electrografting, the CVs obtained for H_2TPP_D at GC reveal additional voltammetric features between 0.1 V and -0.6 V. The same features were also observed at PPF and gold surfaces. A cathodic pre-peak appears at around 0 V on the second and subsequent scans. Similar pre-peaks have been observed during grafting of diazotated ruthenium complexes[279], and are commonly observed during electropolymerisation of redox polymers[280-281]. Similar to these studies, the pre-peak observed here on repeat scanning is attributed to redox transformations of trapped charges. The redox processes which occur between -0.1 V and -0.5 V are tentatively attributed to

reduction and subsequent re-oxidation of protonated porphyrin species present with different degrees of protonation[282]. Protonated porphyrin species are indicated by the green grafting solution (not shown). In a separate set of experiments, evidence that these redox processes are due to protonated porphyrin groups was obtained by comparing the electroactivity of H_2TPP_A in DMF before and after addition of acid (TsOH). Before addition of the acid, no redox processes were observed. After the addition of 1 equivalent of acid, a broad reduction peak and corresponding oxidation peaks between -0.25 V and -0.55 V appeared, consistent with electroactive protonated porphyrin groups (data not shown)[282].

Interestingly, Figure 4.2a shows that the peak currents for the redox processes between -0.10 and -0.50 increase steadily with each CV scan. This behaviour was observed for repeat cycling up to 60 cycles and points to a steady increase in film growth. A concomitant increase in peak current on repeat CV cycling, with little evidence for passivation, is characteristic of a diazonium salt grafting process recently termed "redox grafting" by Daasbjerg and co-workers[133, 283-284]. For this growth mechanism, electroactive groups at the surface mediate charge transport through the film and catalyse electrochemical reduction of aryldiazonium ions, which leads to faster film growth and thick-film formation.

At the end of the grafting process, the electrodes were seen to be covered with a purple deposit, which remained after rinsing and sonication cleaning (5 min in DMF). Film-modified electrodes were characterised as described in later sections.

4.3.2 Electrooxidation of $NiTPP_A$ in DCM solution

Murray and co-workers were the first to report the electrochemical oxidation of amino-substituted tetraphenylporphyrins, for attachment of adherent polymeric porphyrin films on electrodes[285-286]. Electropolymerisation is typically achieved using meso-substituted

tetraaminophenylporphyrins by oxidative cycling in DCM or ACN solution. Film deposition proceeds in a manner analogous to aniline polymerisation[267, 286].

In this work, electrochemical oxidation of a monoamine-substituted tetraphenylporphyrin derivative, $NiTPP_A$, in DCM solution was investigated at GC as an alternative grafting method. According to Walter and co-workers, polymer films are generated by electropolymerisation in DCM using tetra-, tri-, and di-substituted derivatives with *p*-aminophenyl groups, but not mono-substituted derivatives[267]. Despite the report of Walter and co-workers, the feasibility of using electrochemical oxidation as a route to surface modification of GC was explored here on the basis of work of Pinson and others[94-95]. It was anticipated that grafting of H_2TPP^A would proceed via reaction of radical cations at the surface, leading to covalent attachment of a porphyrin film. This is in contrast to electropolymerisation, where porphyrin radical cations couple with one another via phenazine linkages to form an insoluble polymeric structure on the surface[267].

Figure 4.3 shows the first (–) and thirtieth (---) scan CVs of $NiTPP_A$ in DCM-$TBABF_4$ at GC recorded by cycling from 0.5 V to 1.3 V (Figure 4.3a) and 0.5 V to 1.45 V (Figure 4.3b).

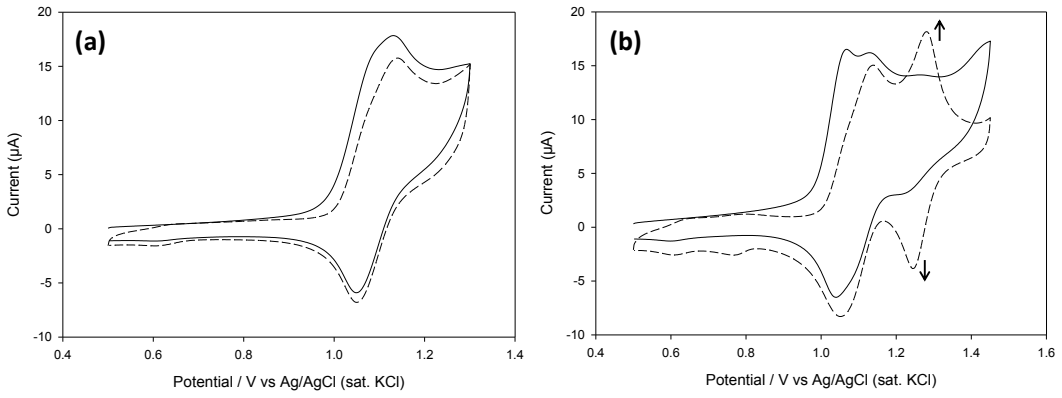

Figure 4.3. First (–) and thirtieth (---) scan CVs of $NiTPP_A$ in DCM-$TBABF_4$ at GC prepared using different switching potentials: (a) E_λ = 1.3 V and (b) E_λ = 1.45 V. Arrows indicate increasing current with consecutive scans.

For the two potential ranges investigated, two closely-overlapping oxidation couples are observed between 1.05 and 1.15 V for all CV scans; these are assigned to two one-electron oxidations which occur at the porphyrin macrocycle. Evidence for irreversible oxidation of the AP group is shown in Figure 4.3b (broad peak at ≈ 1.4 V). When the switching potential (E_λ) was set at 1.3 V (Figure 4.3a), only small changes in the peak currents were observed over 30 cycles. In contrast, when the switching potential was E_λ = 1.45 V (Figure 4.3b), a new voltammetric feature appeared at $E_{1/2}$ = 1.26 V, which increased in intensity with successive scans. This redox couple is consistent with the growth of a porphyrin film on the surface; the reversible behaviour is attributed to surface-bound porphyrin groups (ΔE_p = 37 mV). The electrochemistry of surface-bound porphyrin groups is described in more detail in Section 4.3.5.

4.3.3 Electrochemical characterisation of H_2TPP films on GC and gold

The electroactivity of H_2TPP films on GC and gold surfaces was examined using cyclic voltammetry. The objective of these studies was to confirm the successful attachment of free-base tetraphenylporphyrin groups via H_2TPP_D grafting, and to identity the presence and electrochemical characteristics of reversible redox couples at the surface.

After modification, rinsing, and sonication in DMF, modified electrodes were studied in dry and oxygen-free non-aqueous solutions containing 0.1 M $TBABF_4$. H_2TPP-modified surfaces were investigated in DMF and ACN solutions by recording consecutive CVs at 100 mV/s in either reduction or oxidation. Similar redox processes were observed using both solvents. For simplicity, only the electrochemical behaviour in ACN is reported below.

Figure 4.4a shows the first (···), second (–), and thirtieth (---) CV scans to negative potentials in ACN-$TBABF_4$ for a H_2TPP-modified GC surface. The CVs show two well-defined and chemically reversible reductions at $E_{1/2}$ ≈ -1.1 V and -1.5 V, corresponding to

two successive one-electron reductions at the conjugated porphyrin ring, yielding the π-anion radical (Equation 1) and dianion (Equation 2), respectively[287-288].

$$\text{Surface---Ph-TPP} + 1e^- \rightleftharpoons \text{Surface---Ph-TPP}^{-\cdot} \quad (1)$$

$$\text{Surface---Ph-TPP}^{-\cdot} + 1e^- \rightleftharpoons \text{Surface---Ph-TPP}^{2-} \quad (2)$$

Both reduction processes are commonly exhibited for free-base porphyrins in non-aqueous solution[287-288], and have been observed in porphyrin films[276, 286]. Compared to other reports where TPP films show broad and ill-defined or overlapping waves at negative potentials [269, 289], the films examined here show two well-resolved and narrower pairs of peaks.

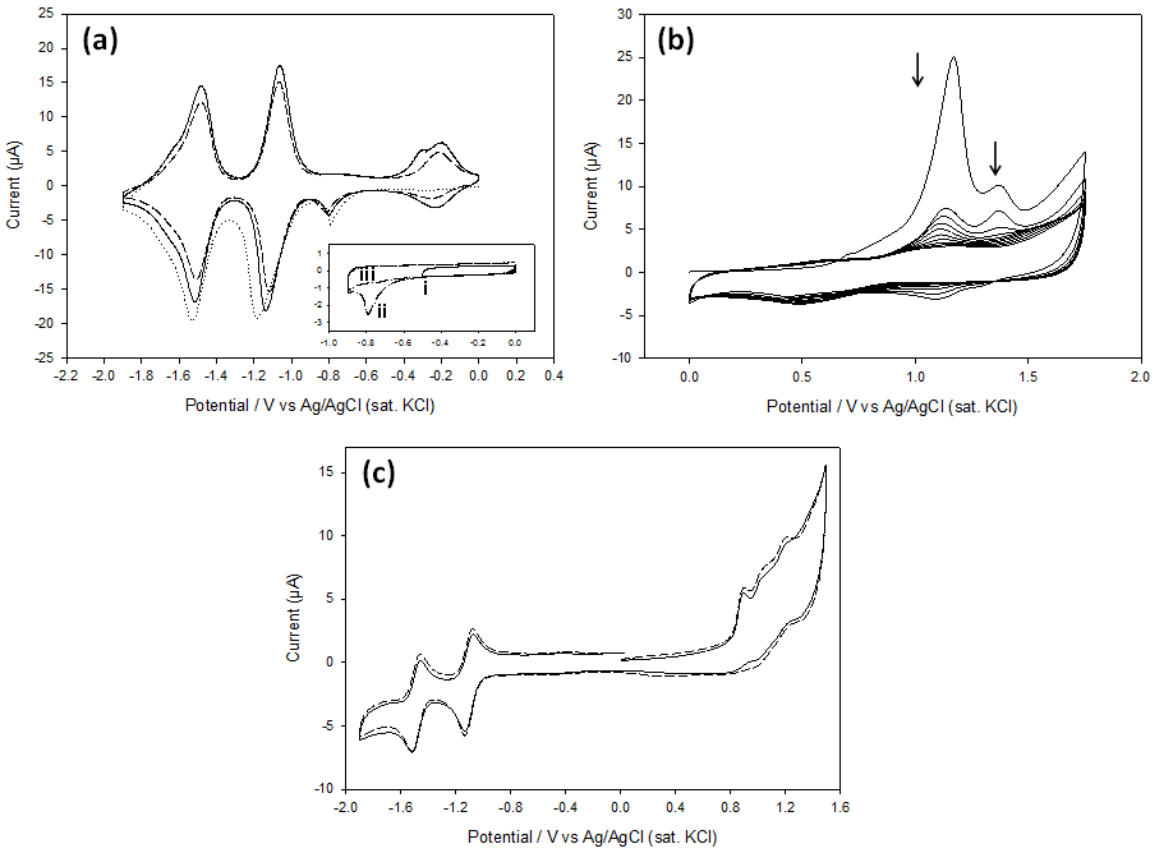

Figure 4.4 CV scans of (a, b) H_2TPP-modified GC and (c) 0.5 mM H_2TPP_A in ACN-$TBABF_4$ at unmodified GC. (a) first (⋯), second (–), and thirtieth (---) CVs are shown. The inset shows three consecutive CVs recorded at switching potentials of E_λ = -0.5 V (scan 1, i) or E_λ = -0.9 V (scan 2 and 3, ii and iii). (b) First ten CVs are shown. (c) First (–) and second (---) CVs shown. Arrows indicate decreasing current with consecutive scans.

In addition to the pairs of peaks described above, the CVs of H_2TPP-modified GC in ACN-$TBABF_4$ show two small pre-peaks at $E_{pc} \approx$ -0.80 and $E_{pa} \approx$ -0.31 V and a redox couple at $E_{1/2} \approx$ -0.22 V. The latter couple does not appear on the first scan and appears on the second and subsequent scans when the switching potential is more negative than the first reversible reduction at $E_{1/2} \approx$ -1.1 V (Figure 4.4a, inset). This behaviour confirms that a by-product of the formation of π-cation radicals is responsible for the redox couple at $E_{1/2} \approx$ -0.22 V. The behaviour of the pre-peaks at $E_{pc} \approx$ -0.80 and $E_{pa} \approx$ -0.31 V is not well understood. These peaks are tentatively attributed to a charge-trapping phenomenon[279-280].

Figure 4.4b shows consecutive CVs recorded to positive potentials for H_2TPP-modified GC. The films are electroactive but poor reversibility is observed. Similarly irreversible behaviour was also observed in DMF-$TBABF_4$ (data not shown). The poorly reversible oxidation behaviour is consistent with previous reports for H_2TPP in DMF-$TBABF_4$ at a Pt electrode[290] and H_2TPP films in DCM-$TBABF_4$[276].

Figure 4.4c shows two consecutive CVs of solution-based H_2TPP_A. As previously reported for *para*-substituted tetraphenylporphyrin derivatives, two reversible one-electron reduction processes are observed at negative potentials[291]. The half-wave potentials of these couples match the potentials observed for the surface-bound species ($E_{1/2} \approx$ -1.1 V and $E_{1/2} \approx$ -1.5 V) on H_2TPP-modified GC. In contrast, irreversible oxidations are observed when scanning in the positive potential range. The irreversible oxidation of the aminophenyl moiety of H_2TPP_A groups is expected to occur at similar potentials to those of the porphyrin macrocycle, leading to complex behaviour at positive potentials.

Further experiments were undertaken to confirm that the redox behaviour of H_2TPP-modified electrodes is due to surface-bound species. Figure 4.5a shows a series of CVs recorded in ACN-$TBABF_4$ in the potential region of the $TPP/TPP^{-\cdot}$ redox couple at scan rates in the range 40-200 mV/s. The variation of peak current with scan rate follows a linear relationship (Figure 4.5b), confirming that H_2TPP groups are attached to the

surface[234]. Linear plots were also obtained for the $TPP/TPP^{-\cdot}$ redox couple at gold surfaces ($r^2 \geq 0.99$, data not shown).

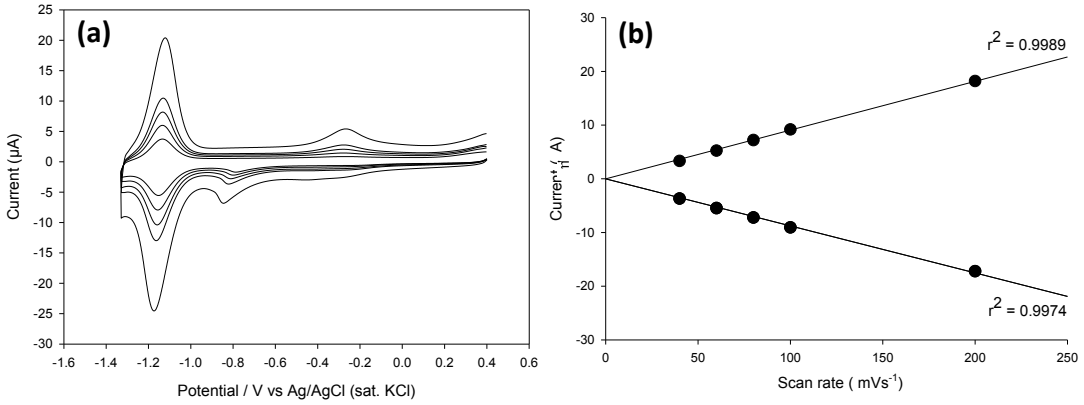

Figure 4.5 (a) CV scans of H_2TPP-modified GC in ACN-$TBABF_4$ recorded at different scan rates. (b) Corresponding plot of anodic and cathodic peak current vs. scan rate.

The ability to modify a wide range of conducting substrates is an important advantage of diazonium salt grafting methods compared to other methods such as the self-assembly of alkanethiols on noble metals. To demonstrate the versatility of the porphyrin grafting strategy, electrochemical reduction of H_2TPP_D at gold surfaces was also investigated. Figure 4.6a shows the first (–) and fifteenth (---) scan CVs of H_2TPP-modified gold in DMF-$TMABF_4$, after rinsing and sonication in ACN for 2 min. For comparison, a H_2TPP-modified GC surface (Figure 4.6b) was prepared and characterised using identical conditions.

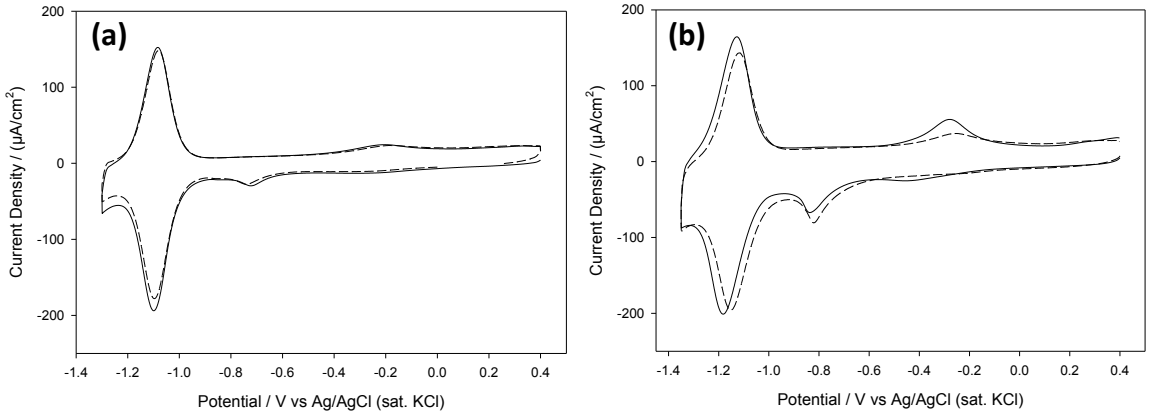

Figure 4.6 Second (–) and fifteenth (---) scan CVs of H_2TPP-modified (a) Au and (b) GC in DMF-$TMABF_4$.

Similarly well-defined and reversible TPP/$TPP^{-\cdot}$ couples are observed ($E_{1/2} \approx 1.09$ V and $E_{1/2} \approx 1.15$ V at gold and GC, respectively) confirming that electrografting of H_2TPP_D enables successful attachment of free-base porphyrin films on gold. The films obtained on GC and gold are generally similar; nevertheless, some differences are observed. The half-wave potential for the TPP/$TPP^{-\cdot}$ redox couple occurs 60 mV more negative at GC compared to gold electrodes. The electrode-dependant potentials are assumed to be due to differences in electronic effects created by the substrates.

ΔE_p values corresponding to the TPP/$TPP^{-\cdot}$ redox couple in DMF-$TMABF_4$ were obtained at various scan rates on GC and gold surfaces in order to further investigate differences between the substrates. ΔE_p values varied from 20 mV to 55 mV for H_2TPP-modified GC compared to values ranging from 10 mV to 37 mV for H_2TPP-modified gold. The data in Table 4.1 shows that H_2TPP films exhibit faster electron transfer characteristics on gold than on GC[292]. Faster electron transfer through diazonium-derived films at gold compared to GC has also been observed by the Gooding group[292]. It is also noted here that significantly higher capacitance currents are apparently observed at GC compared to gold as evidenced by the higher background currents at GC (Figure 4.6)[293].

Table 4.1 ΔE_p values obtained at different scan rates for the first reversible reduction in DMF-$TMABF_4$ at H_2TPP-modified Au and GC.

	H_2TPP on Au	**H_2TPP on GC**
Scan rate (mV/s)	**ΔE_p (mV), $TPP/TPP^{-\cdot}$**	**ΔE_p (mV), $TPP/TPP^{-\cdot}$**
200	37	55
100	18	35
80	16	30
60	11	24
40	10	20

Further film characterisation studies were performed on H_2TPP-modified electrodes and are detailed below in Sections 4.3.10 and 4.3.12.

4.3.4 Metallation of H_2TPP films on GC by incorporation of copper ions

Post-assembly metallation of free-base porphyrin films provides easy access to a wide range of metalloporphyrins[294-296]. Compared to the formation of metallated films, post-assembly insertion of metal ions has the advantage that coordination and other side reactions of the metal centre during grafting are minimised. Such side reactions could lead to loss of the metal or poorly defined films, depending on the coordinating properties of the metal. The insertion of metal ions into surface films has previously been achieved by applying a cathodic potential[296] or by refluxing metal salt solutions [294-295].

Metallation of GC surfaces presenting H_2TPP groups was investigated by immersion of H_2TPP-modified electrodes in 10 mM copper (II) acetate in DMF for 48 h. After rinsing and sonicating in DMF for 5 min, the electrodes were transferred to a DMF-$TBABF_4$ solution free of copper ions. The electrochemical response (Figure 4.7) of H_2TPP films before and after the metallation procedure was monitored to establish the extent of complexation of metal ions into the film.

At H_2TPP-modified GC, the CV obtained at negative potentials (Figure 4.7a, ---) shows reversible couples at $E_{1/2} \approx$ -1.13 V and $E_{1/2} \approx$ -1.53 V, consistent with two successive one-electron reductions of the porphyrin macrocycle assigned to Equation 1 and 2, respectively.

After immersion of the surface in copper (II) acetate solution, rinsing and sonication cleaning, the CV obtained at negative potentials (Figure 4.7, –) shows the appearance of two additional redox couples at $E_{1/2} \approx$ -1.19 V and $E_{1/2} \approx$ -1.70 V. The two new redox couples are assigned to successive one-electron reductions of surface-bound CuTPP groups according to Equation 3 and 4[297-298]:

$$\text{Surface--Ph-Cu}^{II}\text{TPP} + 1e^- \rightleftharpoons \text{Surface--Ph-Cu}^{II}\text{TPP}^{-\cdot} \quad (3)$$

$$\text{Surface--Ph-Cu}^{II}\text{TPP}^{-\cdot} + 1e^- \rightleftharpoons \text{Surface--Ph-Cu}^{II}\text{TPP}^{2-} \quad (4)$$

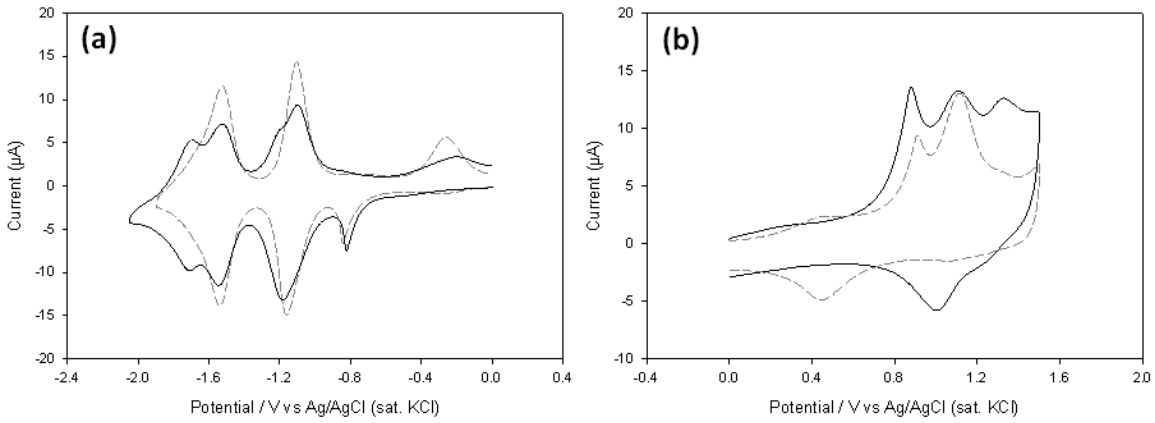

Figure 4.7 First scan CVs recorded at (a) negative potentials and (b) positive potentials of H_2TPP-modified GC in ACN-$TBABF_4$ before (---) and after (–) immersion in 10 mM copper acetate monohydrate.

The observation of redox couples assigned to both non-metallated and metallated TPP is consistent with partial metallation of the H_2TPP film. The observed shift towards negative potentials after insertion of copper ions is attributed to an increased electron density on the porphyrin ring which makes reduction thermodynamically more difficult[299-300].

In a separate set of experiments, the behaviour of H_2TPP-modified GC electrodes at positive potentials was examined in DMF-$TBABF_4$ before and after immersion in copper (II) acetate solution (Figure 4.7b). Before metallation, only irreversible oxidations are observed (Figure 4.7b, ---). After metallation, the CV (Figure 4.7b, –) shows evidence for a reversible oxidation process at $E_{1/2} \approx 1.06$ V and evidence of a poorly reversible oxidation process at $E_{1/2} \approx 1.29$ V. The change in redox behaviour following exposure to Cu^{2+} ions provides further confirmation that metalloporphyrin molecules are attached at the surface following the simple post-assembly metallation treatment.

4.3.5 Electrochemical characterisation of NiTPP films on GC and gold

The electroactivity of NiTPP films prepared by electrografting $NiTPP_D$ on GC and gold was examined. After modification, the electrodes were transferred to blank electrolyte solution (0.1 M $TBABF_4$) and the CVs shown in Figure 4.8a and Figure 4.8b were obtained. Well-defined and chemically reversible reduction and oxidation redox couples are observed at $E_{1/2} \approx -1.15$ V and $E_{1/2} \approx 1.23$ V in DMF and DCM solutions, respectively. This redox behaviour is consistent with that of NiTPP complexes in non-aqueous solution[301-304] and is assigned to a one-electron reduction and a two-electron oxidation as shown in Equation 5 and 6[305-306]:

$$\text{Surface---Ph-Ni}^{\text{II}}\text{TPP} + 1e^- \rightleftharpoons \text{Surface---Ph-Ni}^{\text{II}}\text{TPP}^{-\cdot} \quad (5)$$

$$\text{Surface--Ph-Ni}^{\text{II}}\text{TPP} - 2e^- \rightleftharpoons \text{Surface--Ph-Ni}^{\text{II}}\text{TPP}^{2+} \quad (6)$$

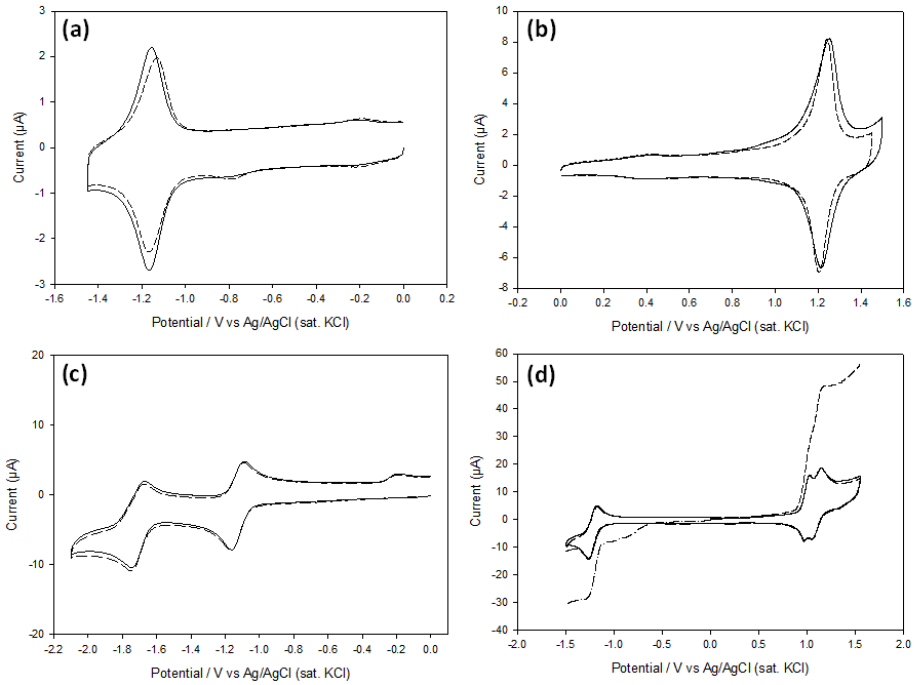

Figure 4.8 (a, b) First (–) and fifteenth (---) scan CVs of NiTPP-modified GC at (a) negative potentials in DMF-TBABF$_4$ and (b) positive potentials in DCM-TBABF$_4$. (c, d) First (–) and second (---) scan CVs in 0.5 mM NiTPP$_A$ in (c) DMF-TBABF$_4$ and (d) DCM-TBABF$_4$. RDE voltammograms were recorded in DCM-TBABF4 as shown in (d).

The one-electron reduction of surface bound NiTPP groups leads to the formation of a π-anion radical (Equation 5)[302, 306-307]. No evidence for a second reversible reduction process was found when the switching potential was extended to a more negative potential (E_λ = -2.2 V). The oxidation behaviour is consistent with a reversible, macrocycle-based two-electron oxidation of surface bound NiTPP groups, giving a Ni (II) π-dication as the final oxidised product (Equation 6)[301, 305-306]. The occurrence of a single two-electron transfer in oxidation, as opposed to two separated one-electron oxidations, is attributed to anion binding (BF_4^-) which stabilises the formation of the dication[306]. The binding constant for coordination of the anion to the dication is much larger than that for anion binding to the monocation; hence formation of the dication becomes more favourable than formation of the π-cation radical. The same oxidation behaviour has been observed in solution by

Kadish and co-workers, who reported the anion-binding effect in the presence of ClO_4^- ions.

Further inspection of the CVs in Figure 4.8a and Figure 4.8b reveals that NiTPP-modified GC exhibits voltammetry consistent with surface-bound species[234]. For the second scan CVs, ΔE_p = 7 mV (Figure 4.8a) and ΔE_p = 39 mV (Figure 4.8b) for the reduction and oxidation redox couples, respectively. Compared to the porphyrin groups in free-base films at GC, the porphyrin groups in metallated films show lower ΔE_p values and therefore faster apparent electron transfer rates. Figure 4.9a shows CVs recorded in DCM-$TBABF_4$ in the potential range of the NiTPP/ $NiTPP^{2+}$ couple at scan rates from 20-300 mV/s. Linear relationships ($r^2 \geq 0.95$) between peak current and scan rate were observed for the oxidation couple (Figure 4.9b) and the reduction couple (data not shown), confirming that the NiTPP groups are surface-bound.

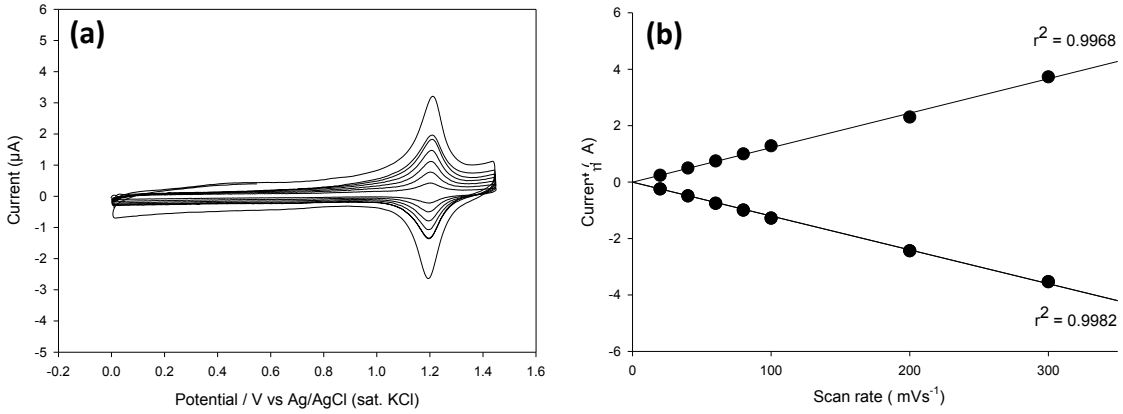

Figure 4.9 (a) CV scans of NiTPP-modified GC in DCM-$TBABF_4$ recorded at different scan rates. (b) Corresponding plot of anodic and cathodic peak current vs. scan rate.

The presence of reversible redox couples at NiTPP-modified surfaces was found to be strongly dependant on the non-aqueous solvent used for analysis. Poor irreversibility was

observed for the reduction processes in ACN-$TBABF_4$ and for the oxidation processes in DMF and ACN-$TBABF_4$ solutions (data not shown).

The behaviour of the NiTPP film was compared with that of the solution-based NiTPP species, $NiTPP_A$. Figure 4.8c and Figure 4.8d show two consecutive CVs of $NiTPP_A$ at GC in DMF-$TMABF_4$ and DCM-$TBABF_4$, respectively. As is commonly reported in the literature for *para*-substituted nickel tetraphenylporphyrin derivatives, two one-electron reductions and two-closely overlapping one-electron oxidations are observed[302, 304]. The first reduction couple at $E_{1/2} \approx$ -1.22 V occurs at a comparable potential to that of the surface-bound species ($E_{1/2} \approx$ -1.1 V). The deviation of ≈ 120 mV is largely attributed to the solution species not being the identical structural analogue of the surface-bound species.

The two closely-overlapping oxidation couples at $E_{1/2} \approx$ 1.0 V and $E_{1/2} \approx$ 1.1 V correspond to the formation of the monocation and dication, respectively[302]. The observation of two redox couples suggests that the dication of the solution species is not stabilised to the same extent as observed for the surface-attached species.

RDE voltammograms were recorded in order to confirm the ratio of steady-state limiting currents for the oxidation and reduction redox couples. The RDE voltammograms show a current ratio of ≈ 2:1, supporting the transfer of two electrons for oxidation and a single electron for reduction.

Electrochemical characterisation of NiTPP-modified GC was also performed in aqueous alkaline solution. Figure 4.10 shows the first five consecutive CVs in 0.1 M NaOH of a freshly prepared NiTPP film on GC. As has previously been observed for an electropolymerised nickel porphyrin film[259], a large and irreversible anodic current (> 0.8 V) is observed on the first scan, followed by the appearance of a new redox couple ($E_{1/2} \approx$ 0.57 V) on the second and subsequent scans. This couple has been assigned to the NiTPP

Ni^{II}/Ni^{III} couple. On successive cycling, the current for the process grows, reaching a near steady-state after 5 cycles. The shape of the final CV is demonstrated clearly in Figure 4.10 and shows a well-defined and very similar response to that reported in the literature for nickel macrocycle-based films[259, 308]. However, the redox response is also very similar to that of $Ni(OH)_2$ surfaces[309], raising some doubt as to the nature of the nickel species at the surface.

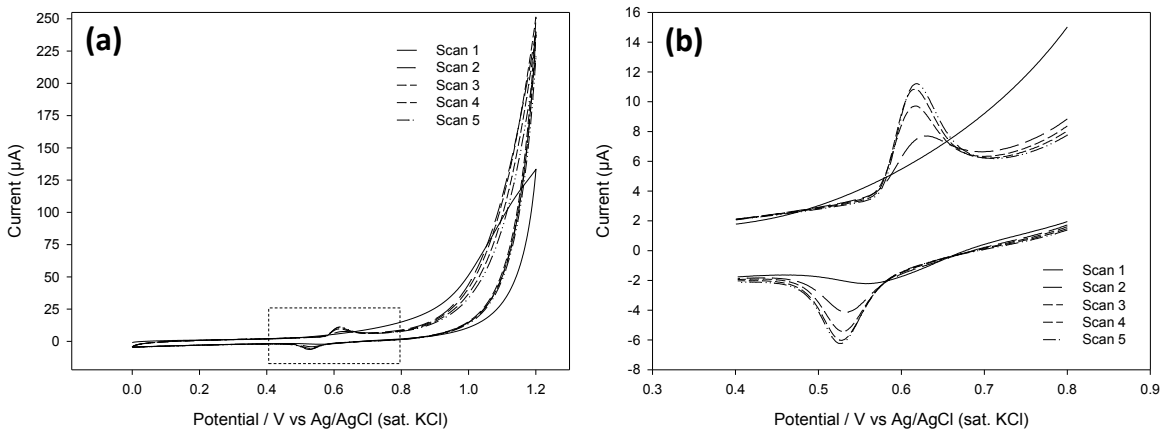

Figure 4.10 (a, b) Consecutive CVs recorded of NiTPP-modified GC in 0.1 M NaOH: (a) complete CV cycles shown and (b) Close-up corresponding to the dashed box shown in (a).

4.3.6 Electrochemical characterisation of $NiTPP^A$ films on GC and gold

GC surfaces prepared by electrochemical oxidation of $NiTPP_A$ in DCM by potential cycling from 0.5 V to 1.3 V (Figure 4.3a) and 0.5 V to 1.45 V (Figure 4.3b) were transferred to DCM-$TBABF_4$ solution and examined over the potential range of NiTPP oxidation. Figure 4.11 shows the second scan CV of $NiTPP^A$-modified GC surfaces prepared using two different switching potentials, E_λ = 1.3 V (---) and E_λ = 1.45 V (–).

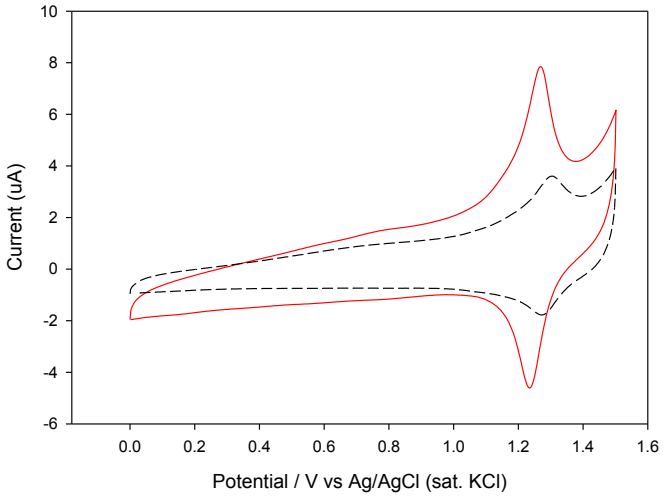

Figure 4.11 Second scan CVs of NiTPP-modified GC in DCM-$TBABF_4$ prepared using different switching potentials: (a) E_λ = 1.3 V and (b) E_λ = 1.45 V.

The CVs show that both grafting methods lead to modified surfaces presenting electroactive NiTPP groups. In particular, the $NiTPP^A$ films prepared using the more positive switching potential exhibit a well-defined and reversible oxidation process ($E_{1/2} \approx$ 1.25 V), closely similar to that obtained for diazonium-derived NiTPP films ($E_{1/2} \approx$ 1.23 V). Whilst modification using E_λ = 1.3 V gives a film with a reversible oxidation couple, a lower grafting efficiency and less-well defined peaks are observed compared with films grafted using E_λ = 1.45 V or using the diazonium grafting method.

4.3.7 Surface concentration of electroactive groups in H_2TPP and NiTPP films on GC, gold and PPF

The average surface concentration of electroactive porphyrin groups was estimated for H_2TPP and NiTPP films prepared using standard grafting conditions (Section 4.2.3) on GC, gold, and PPF substrates. Surface concentrations were calculated based on the first reversible reduction couple (H_2TPP and NiTPP films) and the reversible oxidation couple (NiTPP films), according to Equation 1 as described in Section 2.4.3. The results are given in Table 4.2.

Table 4.2 Average surface concentrations of electroactive H_2TPP and NiTPP groups on modified electrodes. Films prepared using standard grafting procedures (30 grafting cycles and 0.5 mM modifier).

Substrate	Film	Redox system	Analysis medium	Surface concentration ($\times 10^{-10}$ mol/cm^2)[a]	Sample size (n)
GC	H_2TPP	Reduction[b]	DMF	16 ± 3.6	(n = 6)
GC	NiTPP	Oxidation	DCM	4.4 ± 1.7	(n = 13)
GC	NiTPP	Reduction[b]	DMF	4.8 ± 1.3	(n = 3)
GC	$NiTPP^{A}$[c]	Oxidation	DCM	3.0 ± 0.7	(n = 3)
PPF	NiTPP	Oxidation	DCM	2.6 ± 0.5	(n = 2)
Au	NiTPP	Oxidation	DCM	3.3 ± 1.3	(n = 12)

[a] surface concentrations calculated based on the first wave of the redox couple.
[b] surface concentrations calculated from the first reduction couple.
[c] NiTPP film prepared by oxidative grafting of $NiTPP_A$ using E_λ = 1.45 V.

Estimated surface concentrations for porphyrin monolayers reported in the literature range from 0.4 to 3.3 × 10^{-10} mol/cm^2 [273, 310-313]. The wide variation in surface concentration depends, to a large extent, on whether the porphyrin molecules are orientated in parallel, perpendicular, or tilted arrangements with respect to the surface. In this study, a monolayer equivalent is assumed to be ≈ 3.0 × 10^{-10} mol/cm^2 for both H_2TPP and NiTPP films, on the basis of experimental determinations by McCreery and co-workers for a tilted, covalently-attached zinc tetraphenylporphyrin monolayer on PPF[273]. Higher values of surface concentration are expected on GC and gold electrodes due to the higher surface roughness of polished surfaces. Surface roughness factors were not calculated in this work (actual/geometric area) but are expected to be negligible for PPF and ≈ 2 on polished GC and Au[60, 314].

The average surface concentration of electroactive groups obtained for H_2TPP modified GC of 16 ± 3.6 × 10^{-10} mol/cm^2 reveals the formation of multilayer films (≈ 5 monolayer equivalents). Assuming a monolayer film thickness of 1.42 nm[273], the H_2TPP films have an estimated thickness of ≈ 8 nm. This value is in contrast to the thick multilayer free-base

tetraphenylporphyrin films (80 nm) obtained on PPF reported by Barrière and co-workers using the tetra-substituted tetraphenylaryldiazonium salt[276].

The average surface concentration obtained for NiTPP groups on GC, PPF, and gold substrates range from ≈ 2.6 to 4.8 × 10^{-10} mol/cm^2. These values are equivalent to monolayer or near-monolayer films. Table 4.2 also shows that the same values of surface concentration (within experimental error) are calculated using the one-electron reduction and the two-electron oxidation of NiTPP films. This finding provides additional confirmation that one- and two-electron processes are the correct assignments for reduction and oxidation of surface-attached NiTPP groups, respectively.

The significantly higher surface concentrations observed for H_2TPP films compared to NiTPP and $NiTPP^A$ films on GC is consistent with catalytic growth of the H_2TPP films due to mediated electron transfer through the film during grafting (redox grafting)[284].

4.3.8 Electrochemical cycling stability of NiTPP films on GC, gold, and ITO

The reversible redox activity of surface-bound molecules provides a convenient means to monitor the stability of porphyrin films attached to electrode surfaces. The cycling stability of porphyrin film redox processes was found to be strongly dependent on both the medium (as described in previous sections) and the scan rate used for analysis. In this work it was observed that NiTPP-modified surfaces show significantly greater cycling stability when successive cycles were recorded at 1 V/s as opposed to 100 mV/s (Table 4.3). Figure 4.12 shows a representative example of 100 successive CV cycles recorded on a NiTPP-modified gold electrode in DCM-$TBABF_4$ at 1 V/s. The CVs clearly show that the electroactive NiTPP groups present on the gold surface are stable to repeat cycling at 1 V/s.

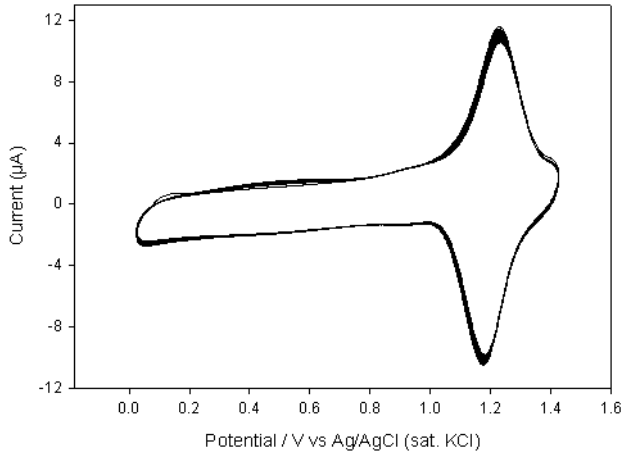

Figure 4.12 First 100 consecutive CVs of NiTPP-modified GC in DCM-$TBABF_4$ at scan rate = 1 V/s.

The stability of electroactive NiTPP groups at different substrates (GC, gold, and ITO) was surveyed by continuously cycling over the $Ni(TPP)/Ni(TPP)^{2+}$ couple and monitoring the change in response using different scan rates. Table 4.3 shows the percentage of electroactive NiTPP groups remaining at GC, gold, and ITO surfaces after repeat cycling through the oxidation couple in DCM-$TBABF_4$ at 100 mV/s and 1 V/s.

Table 4.3 Percentage of electroactive NiTPP groups on GC, Au, and ITO after electrochemical cycling in DCM-$TBABF_4$ through the $NiTPP/NiTPP^{2+}$ couple at 100 mV/s or 1 V/s. Films prepared using standard grafting procedures (30 grafting cycles and 0.5 mM modifier).

Number of CV cycles	Scan rate (mV/s)	NiTPP groups on GC		NiTPP groups on Au		NiTPP groups on ITO	
		oxidation wave	reduction wave	oxidation wave	reduction wave	oxidation wave	reduction wave
50	1000	100%[a]	100%	93%	95%	86%	91%
100	1000	100%	95%	88%	93%	-	-
150	1000	96%	91%	-	-	-	-
15	100	88%	86%	58%	67%	72%	70%

[a] Percentage surface concentration of electroactive groups remaining after cycling relative to the surface concentration of electroactive groups observed on the second CV scan prior to cycling.

No change in electrochemical response is observed for NiTPP-modified GC after 50 cycles at scan rate = 1 V/s. After 150 cycles at scan rate = 1 V/s, 91% to 96% of the initial film

electroactivity remained. In contrast, only 86% to 88% of the initial film electroactivity remained after 15 cycles at 100 mV/s. The same general trend was observed for NiTPP films on gold and ITO surfaces: the films are significantly more stable to repeat cycling at higher scan rates. The loss of electroactivity at lower scan rate (100 mV/s) is consistent with reaction of the π-dication, a strong electrophile, with nucleophiles such as water which may be present in solution at low-levels. At higher scan rates, the time that the film is in the dication state is sufficiently short that reaction of the dication is minimised. For the high scan rate experiments, all NiTPP-modified surfaces showed good stability to repeat cycling. At low scan rates, 58% to 72% of electroactive groups were present at gold and ITO electrodes after 15 cycles, whereas 86% to 88% of electroactive groups remained at GC. The increased stability at GC surfaces is attributed, at least in part, to the stronger C-C bond relative to a Au-C[129] bond.

4.3.9 Mechanical stability of NiTPP films on GC and gold

One of the main attractions of films grafted from aryldiazonium salts is the high stability of the surface attachment (a covalent bond between the surface and the modifier). The stability of NiTPP films on GC and gold surfaces was investigated further by subjecting these substrates to sonication in DMF for periods of up to 45 min. Changes in the film were monitored by comparing the surface concentration of electroactive groups on the surface before and after sonication treatments for 2 min, 5 min, 15 min, and 45 min. Surface concentrations were estimated based on both the anodic and cathodic waves of the NiTPP/NiTPP^{2+} redox couple in DCM-TBABF$_4$ at 100 mV/s. Figure 4.13 shows plots of the surface concentration of electroactive NiTPP groups at GC(▲ and Δ) and Au (● and ○) as a function of sonication time.

The plots (Figure 4.13) show that sonication treatment for periods of ≥ 2 min results in a significant loss of electroactive porphyrin groups from GC and gold surfaces. Qualitatively similar trends in film loss are observed at both GC and gold surfaces. Initially, very rapid

rates of film loss are observed as a function of sonication time for periods of up to 5 min. Electroactive groups are continually lost up to 45 min, although the rate of film loss is substantially slower after the first 5 min of sonication.

During sonication physisorbed material will be lost from the surface. However, sonication is a very rigorous and energetic treatment and hence the possibility of chemical transformation or covalent bond rupturing within the film, and between the film and the surface, may also be possible and may account for some film loss. Despite the loss of porphyrin groups from the surface, a significant amount of NiTPP groups remain stably-attached to both GC and gold following extensive periods of sonication (45 min).

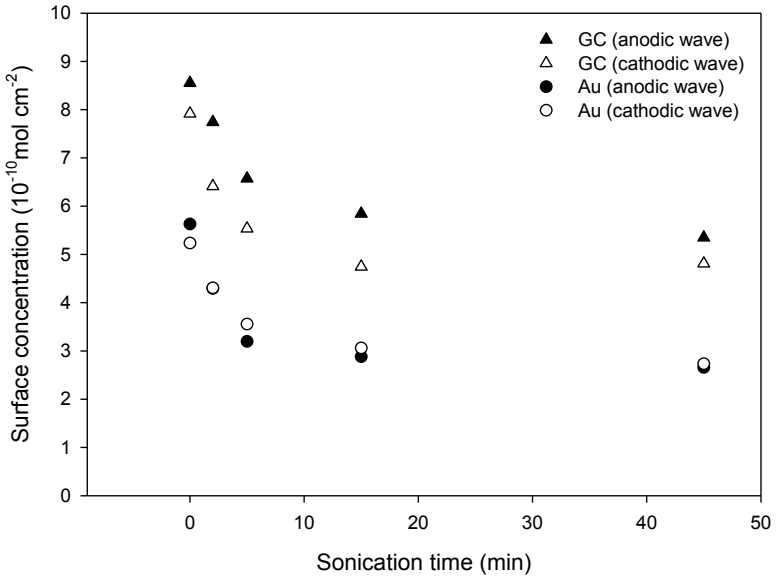

Figure 4.13 Plots of surface concentration of electroactive NiTPP groups on GC (▲, Δ) and Au (●, ○) versus sonication time in DMF. Surface concentrations were estimated based on the anodic and cathodic wave observed in oxidation in DCM-$TBABF_4$.

Table 4.4 lists the data plotted in Figure 4.13 and shows the quantitative changes in surface concentration of NiTPP groups as a function of sonication time for NiTPP-modified GC and gold surfaces. As expected, for all sonication times studied, the percentage of electroactive film loss at gold electrodes was greater than that observed at GC, consistent

with the superior stability of the C-C attachment compared to Au-C. Figure 4.13 and Table 4.4 show that 45 min sonication in DMF results in ≈ 50% of the initial electroactive NiTPP groups being lost from the gold surface, which compares to a value of ≈ 40% at GC. The estimated film losses observed in this work for GC and gold surfaces are higher than those previously reported by Shewchuck and McDermott for electrografted diazonium-derived NP layers on gold[315]. Reported film losses of 35% were obtained for NP-modified Au after 30 min sonication in ACN[315]. The greater extent of film loss observed for NiTPP films compared to NP films indicates that the porphyrin films have a comparatively higher proportion of physisorbed monomers and dimers at the surface.

Table 4.4 Surface concentration and percentage surface concentration of electroactive NiTPP groups on GC and Au after sonication treatment in DMF for increasing periods of time between 2 and 45 min.

Sonication time (min)	Surface concentration of electroactive NiTPP groups (× 10^{-10} mol/cm^2)							
	anodic wave	% film on GC	cathodic wave	% film on GC	anodic wave	% film on Au	cathodic wave	% film on Au
0	8.6	100%	7.9	100%	5.6	100%	5.2	100%
2	7.7	91%	6.4	81%	4.3	76%	4.3	81%
5	6.6	77%	5.5	70%	3.2	57%	3.6	68%
15	5.8	68%	4.7	60%	2.9	51%	3.1	58%
45	5.4	63%	4.8	61%	2.7	47%	2.7	52%

4.3.10 Effect of grafting cycles on surface concentration of electroactive H_2TPP and NiTPP groups

To investigate the effect of potential cycling on the surface concentration of electroactive porphyrin groups, different substrates (GC, PPF, and gold) were electrografted using between 2 and 60 grafting cycles. After modification, rinsing, and sonication, as described in Section 4.2.3., the first reversible oxidation couple (NiTPP) or reduction couple (H_2TPP) was examined at each surface in DCM-$TBABF_4$ or ACN-$TBABF_4$, respectively.

Figure 4.14a shows a plot of the surface concentration of electroactive NiTPP groups on GC (●), PPF (■), and Au (×) as a function of the number of potential cycles used to modify

the surface. Each of the data points corresponds to an individual measurement on a freshly prepared electrode.

The plots show that film growth is initially rapid for the first 5 cycles (time scale ≈ 300 s). For all substrates, the surface concentration of NiTPP groups increases up to ≈ 20 cycles, where it reaches a near-limiting value of ≈ 4×10^{-10} mol/cm^2 (at GC) or 2.5×10^{-10} mol/cm^2 (at gold and PPF). The same general trend was observed for all substrates and demonstrates that the NiTPP films are grafted via a self-limiting growth mechanism. As the NiTPP film grows, electron transfer through the film becomes slower and finally stops due to the layer becoming passivating (≈ 20 cycles). Similar observations have been made by previous workers who have shown that films prepared by electrografting NP_D (0.6 mM) at PPF reach a limiting surface concentration after ≈ 300 s of electrolysis at a potential more negative than the NP_D reduction peak[66].

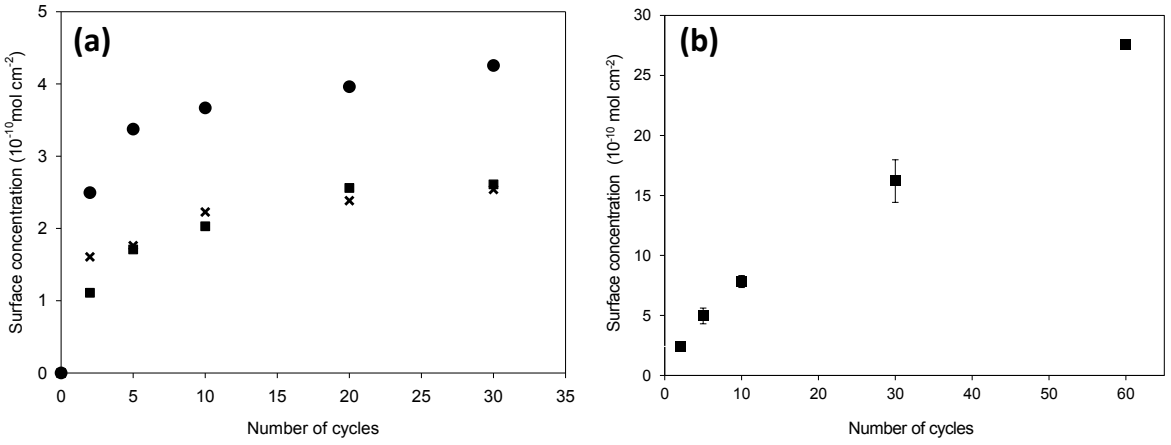

Figure 4.14 Plots of surface concentration of electroactive (a) NiTPP and (b) H_2TPP groups vs. number of grafting cycles on GC (●), PPF (■), and Au (×). Each data point in (a) represents a single measurement only. Error bars shown in (b) represent one standard deviation from the mean. Mean values were determined from between two and seven individual samples.

Figure 4.14b shows a plot of the surface concentration of electroactive H_2TPP groups on GC surfaces as a function of the number of grafting cycles. The plot shows that the rate of film growth decreases only slightly with scan number (up to 60 cycles). As mentioned

earlier, redox units in the growing film can mediate electron transfer from the underlying surface to aryldiazonium ions diffusing from solution.

The highest surface concentration obtained in this work, 28×10^{-10} mol/cm^2, is equivalent to a multilayer film containing ≈ 6-7 monolayer equivalents, assuming a monolayer surface concentration of ≈ 4-5 $\times 10^{-10}$ mol/cm^2 on GC. Assuming a monolayer thickness of 1.4 nm and a tilt angle of 37° to the surface normal[273], the porphyrin films prepared by 60 grafting cycles have an estimated thickness of 8-10 nm.

4.3.11 Atomic force microscopy investigations of NiTPP films on PPF

AFM depth-profiling experiments of porphyrin films were undertaken to investigate film growth and to establish whether or not monolayer films are formed on PPF after grafting $NiTPP_D$ by potential cycling.

NiTPP films were prepared on PPF surfaces using different numbers of grafting cycles and analysed by AFM in tapping-mode. For all samples, a 1 × 10 μm section of the film was completely removed by scratching with an AFM tip and subsequently analysed as described in Section 2.5.3. Figure 4.15 shows a topographical height image (right) of a NiTPP film on PPF after a section of the film was removed. Average section profiles (left) were obtained from regions of the surface free from debris and analysed to determine average film thickness values.

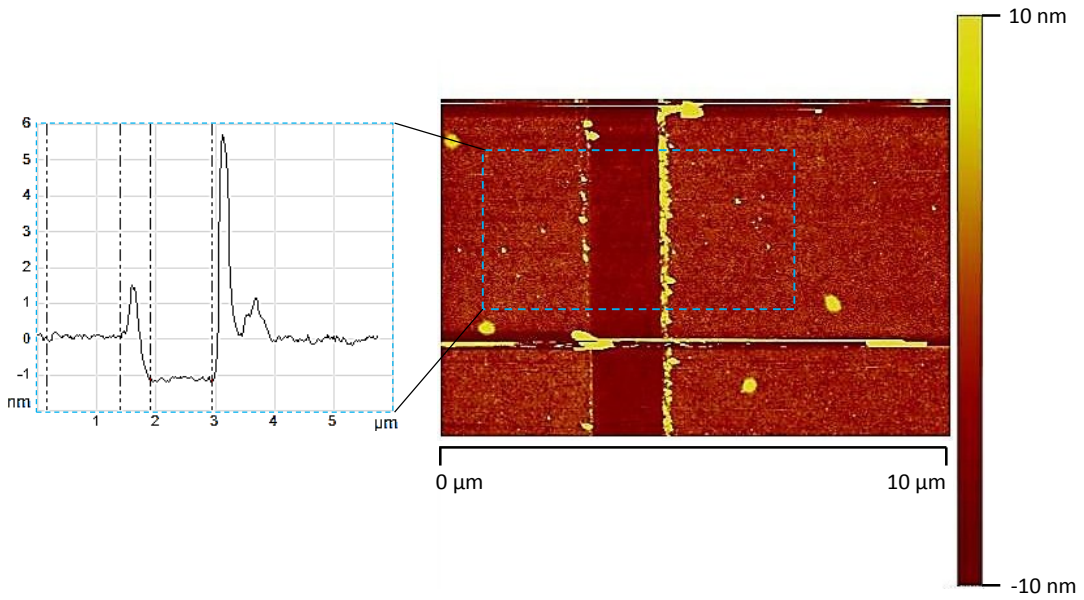

Figure 4.15 Tapping-mode AFM image and corresponding line profile of scratched NiTPP film on GC.

Figure 4.16 shows a plot of average film thickness as a function of the number grafting cycles for films prepared by electrografting $NiTPP_D$. The plot reveals that the average thickness for NiTPP films increases with the number of grafting cycles, reaching a near-limiting value of 1.4 ± 0.2 nm after 20 grafting cycles. The plot shows the same trend as the plots of surface concentration vs. the number of grafting cycles (Figure 4.14a), hence both the electrochemical data and film thickness data support the formation of self-limiting films after ≈ 20 cycles.

Average film thicknesses for NiTPP films at PPF ranged from 0.7 to 1.4 ± 0.2 nm. Based on the theoretical length of a NiTPP molecule (1.9 nm maximum diameter[316]), the observed thicknesses are consistent with sub-monolayer films. Detailed surface studies of a zinc TPP film thermally grafted to PPF from an alkyne-substituted derivative, revealed that the porphyrin molecules had an average tilt angle of 37°, and a disordered monolayer structure[273]. Tilt angles ranging from 31° to 44° have also been determined for organic molecules grafted to PPF from aryldiazonium salts[127]. Assuming a small tilt angle to the

surface normal, the maximum NiTPP film thickness estimated by AFM measurements (1.4 ± 0.2 nm) is thus consistent with a monolayer of NiTPP molecules (a theoretical monolayer height ≈ 1.5 nm for molecules with a tilt angle of 44°). It is noted that the NiTPP films prepared using 20 grafting cycles have very similar film parameters (surface concentration and film thickness) to those reported for zinc tetraphenylporphyrin monolayers on PPF[273], hence the tilted arrangement of molecules is assumed to accurately describe the films prepared in this work.

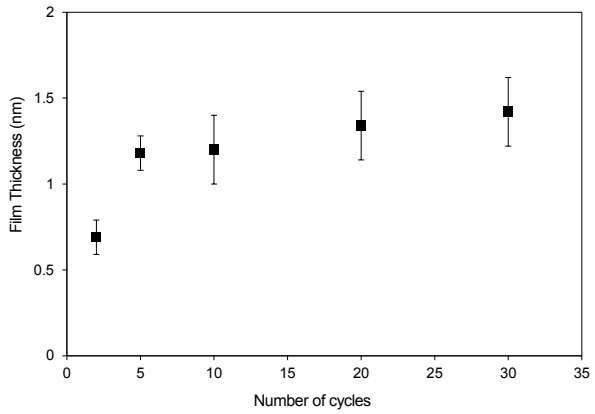

Figure 4.16 Plot of average film thickness vs. number of grafting cycles for NiTPP films on PPF. Error bars represent one standard deviation from the mean.

A plot of the surface concentration of electroactive NiTPP groups versus the corresponding film thickness reveals information about the uniformity of film growth and also packing density. Figure 4.17 shows that there is an approximately linear relationship between average surface concentration and film thickness, consistent with the film structure remaining uniform during film growth on PPF. The same approximately linear relationship has previously been observed on PPF for other electrografted diazonium-derived films[66].

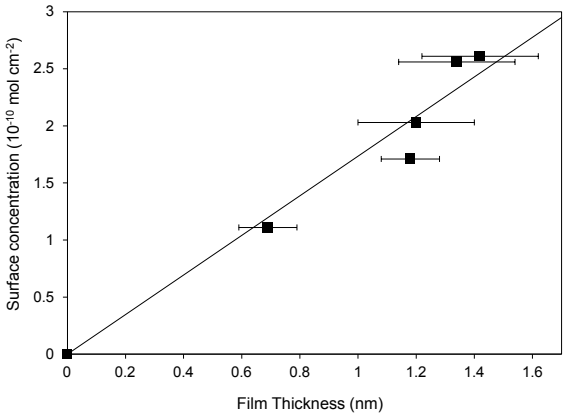

Figure 4.17 Plot of surface concentration of electroactive NiTPP groups vs. film thickness on PPF. Regression line forced through zero with slope = 1.7×10^{-10} mol/cm^2/nm; $r^2 = 0.96$. Error bars shown represent one standard deviation from the mean for film thickness measurements. Each surface concentration data point represents a single measurement only.

From the slope of the regression line, the density of electroactive NiTPP films on PPF is estimated as 1.7×10^{-10} mol/cm^2/nm. This corresponds to an estimated packing density of 2.6×10^{-10} mol/cm^2 per monolayer thickness, assuming that an ideal diazonium-derived NiTPP monolayer has a tilt angle of 44° and a film thickness of 1.5 nm.

4.3.12 UV-visible absorption spectroscopy of H_2TPP and NiTPP films on ITO

Figure 4.18 shows the UV-visible absorption spectra of H_2TPP-modified (---), NiTPP-modified (–), and unmodified ITO (––) electrodes. The films were prepared by 30 grafting cycles using standard modification conditions as described in Section 4.2.3. The film-modified surfaces were rinsed and sonicated for 2 min in DMF prior to analysis in order to obtain spectra corresponding to surface-attached species.

The absorption spectrum of NiTPP presents a broad Soret band at λ_{max} = 427 nm and a strong Q-band at 530 nm, which are the characteristic absorption peaks of NiTPP in solution[317-319]. The absorption spectrum of H_2TPP also presents a broad, strong Soret band (λ_{max} = 426 nm), as well as Q-bands between 500 and 700 nm (519 nm, 552 nm, 597 nm, and 633 nm). This absorption behaviour closely matches that observed for free-base

tetraphenylporphyrin porphyrin films and in solution[276, 317]. Hence the absorption spectra provide clear evidence for the successful attachment of nickel- and free-base tetraphenylporphyrin molecular films by electrografting from the corresponding mono-aryldiazonium salt precursors.

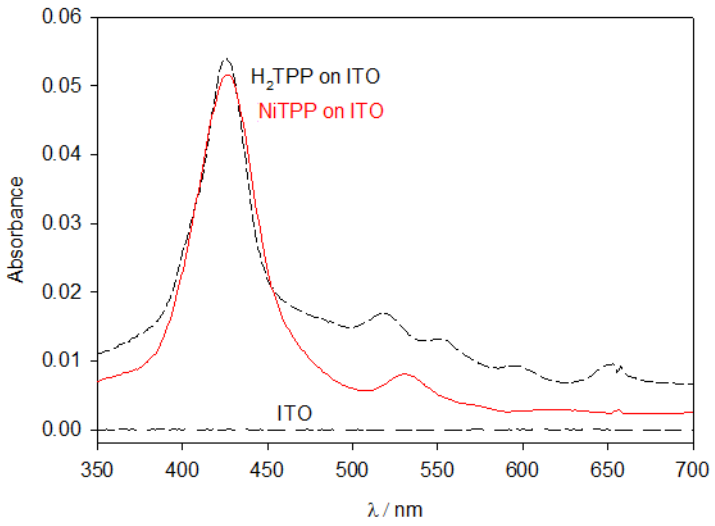

Figure 4.18 UV-visible absorption spectrum of (---) H_2TPP-modified ITO, (–) NiTPP-modified ITO, and (– –) unmodified ITO.

4.4 Conclusion

Thin H_2TPP and NiTPP films can be readily electrografted to GC, PPF, gold, and ITO from the corresponding mono-aryldiazonium salt derivatives in non-aqueous electrolyte solutions. Oxidation of mono-amine tetraphenylporphyrin derivatives in DCM-electrolyte solution also led to film formation, giving films similar to those prepared by the aryldiazonium salt method but with lower concentrations of electroactive porphyrin groups.

H_2TPP and NiTPP films exhibit the expected UV-visible absorption spectra and have well-defined and reversible redox chemistry, characteristic of free-base and metallated tetraphenylporphyrin complexes. The redox behaviour observed in reduction is noteworthy as previous studies of porphyrin films in the literature commonly focus on the oxidative behaviour of the films and seldom report well-defined and reversible systems in reduction.

H_2TPP films give two consecutive chemically reversible one-electron reductions but no reversible oxidations in ACN and DMF solutions. For NiTPP films, a single one-electron reduction and a two-electron oxidation are observed in DMF and DCM, respectively. The chemically reversible processes observed in non-aqueous solvents for both H_2TPP and NiTPP films are assigned to electron transfer reactions occurring on the porphyrin macrocycle (and not the metal centre, as could be the case for NiTPP films). Metal-centred oxidation was observed for NiTPP films at GC in aqueous alkaline solution under anodic conditions, supporting that the complexed metal remains intact during grafting. The nickel centre of the porphyrin has the potential to be used as an electrocatalytic site for sensing although this was not studied.

NiTPP films on GC are more stable to repeat cycling at low and high scan rates compared to NiTPP films on gold and ITO. Similarly, NiTPP-modified GC exhibits greater stability towards extended sonication treatment in DMF than modified gold. The cycling stability

studies show that porphyrin films are susceptible to film losses (up to 40% of electroactive groups, depending on the substrate) at low scan rate (100 mV/s) after 15 scans. In general, these films are not ideally suited to multiple electrochemical experiments at commonly employed scan rate. However, results obtained for NiTPP-modified GC and gold subjected to potential cycling at higher scan rate (1 V/s) show that the films are stable under these conditions. NiTPP films on GC are particularly robust, exhibiting no loss of electroactive groups after 50 cycles at higher scan rate.

Although significant film losses are observed following sonication treatment (up to 50%, depending on the substrate), presumably due to the removal of strongly physisorbed monomers and dimers, significant concentrations of electroactive groups remain bound to the surface. The ability for these groups to withstand extensive periods of sonication supports, indirectly, the formation of covalent bonds between the film and the substrate. The stability studies highlight an advantage in stability for diazonium-derived films grafted to GC surfaces compared to those grafted on gold and ITO. These findings are consistent with the greater bonder strength of C-C compared to Au-C.

Both the electrochemical data and film thickness data support the formation of close-packed NiTPP films via a self-limiting growth mechanism typical of diazonium surface chemistry. After a rapid rate of film growth during the first 5 cycles, self-limiting behaviour is observed after ≈ 20 grafting cycles. The surface concentration and film thickness data reveal that close to a monolayer of NiTPP groups are grafted at GC, PPF, and gold surfaces. The films obtained after 20 grafting cycles at PPF show very similar film parameters compared with literature values obtained for a zinc tetraphenylporphyrin monolayer on PPF, further supporting the conclusion that monolayer NiTPP films are obtained in this work.

Under the conditions explored, grafting of H_2TPP films proceeds via a growth mechanism referred to as “redox grafting”. As a result of mediated electron transfer through the film

during grafting, H_2TPP film growth increases linearly as a function of the number of grafting cycles. The redox grafting method is versatile as both monolayer (using 2 grafting cycles) and multilayer films (≈ 6-7 monolayer equivalents, using 60 grafting cycles) can be easily prepared simply by varying the number of grafting cycles. No evidence of film passivation or self-limiting behaviour was observed for up to 60 grafting cycles; hence the grafting method could easily be extended to the formation of thicker multilayer films or thick films reminiscent of electropolymerised polymers.

Modification and patterning of surfaces using arylazides, aryldiazonium salts, and alkylamines, with photolithography

5.1 Introduction

This chapter describes surface modification and microscale patterning strategies for preparing single and two-component patterned films on carbon and silicon substrates. This research is motivated by an increasing interest in multifunctional surfaces containing spatially-addressable chemical functionalities for sensor applications.

In recent years there has been considerable interest in the fabrication of micro and nanoscale patterned arrays of biomolecules such as proteins[320-323], peptides[141, 324-326], and DNA[187, 327] on surfaces. Microarrays have become valuable tools for biological research for applications in biosensing, molecular diagnostics, functional protein studies, and drug discovery[328-329]. The enabling technology of biosensors and biochips is the chemical preparation method which must allow site-selective immobilisation of chemical and biological species to the surface[13, 330]. Preparation of patterned surfaces for these devices typically involves the use of a self-assembled monolayer and surface patterning strategies such as microcontact printing[331-332], dip-pen nanolithography[321, 327], conventional photolithography[333-335], e-beam lithography[336-337], and photochemical activation[323, 326, 338]. Special attention is given to patterning techniques which enable rapid derivatisation of surfaces with molecular species of well-defined feature size, shape, and spacing[321, 339].

As highlighted in Chapter 1, there are several methods for covalent attachment of molecular layers on surfaces, including the photochemical and thermal reactions of azides[150, 340]. To briefly recap, arylazides are attractive modifiers for surface modification which can be used to attach a wide range of molecules to many different substrates, in a simple, efficient, and reproducible manner[150]. Generation of nitrenes via UV photolysis or

thermal decomposition of arylazides is simple and enables the modification of materials such as polymers[155-156], semiconductors[341], carbon[151-153, 156, 161, 167, 342], quartz[167], and film-modified surfaces. For substrates with an organic surface layer, highly reactive nitrenes can insert into O-H, N-H, and C-H bonds, and also undergo C=C addition reactions with neighbouring molecules[159]. Arylazides also benefit from being very well suited to chemical patterning[156, 161, 340].

The formation of mixed layer surfaces presenting two or more components is attractive for sensing applications as these surfaces present regions of different chemical functionalities. The formation of two-component films at gold using alkanethiols has been widely reported for over two decades[343-345]. In contrast, the formation of two-component films at carbon using aryldiazonium salts or arylazides is relatively unexplored. Since the first examples of two-component surfaces were reported by the Downard and Gooding groups[346-347], a number of sophisticated mixed layer surfaces have emerged using aryldiazonium salts[88, 175, 186, 293, 348-349].

The simplest approach for preparing two-component surfaces involves grafting from a binary solution in a single step[293, 345-346]. More sophisticated strategies are based on step-wise grafting[175, 186, 331, 343, 348]. If combined with a suitable surface patterning technique such as AFM scratching[171], photolithography[350], spotting[351] or printing[175], it is possible to precisely control the positioning of multiple chemical functionalities at the surface. Desirable two-component surfaces include those containing surface functionalities for tethering and a second "non-reactive" component to minimise non-specific adsorption of biomolecules[331, 346, 350, 352]. Surfaces containing two or more different reactive surface tethers are also highly desirable[175, 186, 350].

The formation of two-component films using a step-wise approach involving both aryldiazonium salts and arylazides was recently developed by Yu[154]. For this strategy, a diazonium-derived layer is first deposited across the whole surface. In the second step, an

azide-derived layer is photografted and patterned onto the film-modified surface. This step-wise method is very versatile as the first layer can be grafted by any convenient means, giving a wide range of possibilities for forming patterned two-component surfaces with different chemical functionalities.

The aim of this research is to expand the use of *para*-substituted arylazide compounds as versatile and efficient modifiers for functionalising surfaces. The goal is to build on the work of Yu and establish the use of arylazides for developing surfaces with patterned tether layers. Such surfaces could be used in future studies for positioning biomolecules on the surface at well-defined locations. There are three main objectives of this study: (i) to prepare and characterise new two-component films with tether layers and non-reactive layers; (ii) to explore tethering reactions at single and two-component films; and (iii) to develop new modification and patterning approaches using arylazides.

Section 5.3 describes the preparation of single-component films at GC surfaces using electrografting and photografting methods. In Section 5.4, novel two-component films were prepared and the activity of the components demonstrated. Section 5.5 describes the formation of patterned surfaces comprising a patterned tether species on a non-reactive background layer. Section 5.6 reports the development of a new modification and patterning procedure using arylazides with conventional photolithography for modification of silicon substrates.

5.2 Experimental

5.2.1 Surface preparation

GC rod and plate electrodes were prepared as described in Chapter 2. Prior to use, surfaces were sonicated in ACN for 5 min. An additional rinse in DCM or DMF was performed prior to photochemical modification.

5.2.2 Electrochemistry

The geometric working area of GC rod electrodes was 0.07 cm^2 for electrografting and electrochemical characterisation. The geometric area of GC plate electrodes for electrografting was not defined, and was 0.11 cm^2 for electrochemical characterisation. The geometric area of PPF and ITO for electrografting was not defined, and was 0.11 cm^2 for electrochemical characterisation. SCE (sat. KCl) and Ag/AgCl reference electrodes were used for aqueous electrochemistry. Ag/Ag^+ (10^{-2} M $AgNO_3$ in 0.1 M $TBABF_4$-ACN) was used for non-aqueous electrochemistry. The hydroxymethylferrocene/ferrocenium couple ($FcOH/FcOH^+$ in $TBABF_4$-ACN) appeared at $E_{1/2} = 0.022$ V vs. $Ag/AgNO_3$.

5.2.3 Surface modification

Non-aqueous electrografting was performed in 0.1 M $TBABF_4$-ACN solutions containing 1 mM NP_D or 5 mM CP_D, or 3 mM solutions of TEG_a or PEG_a. The general procedure for electrografting diazonium salts involved two initial CV cycles from 0.30 to -0.8 V (NP_D) or from 0.30 to -0.65 V (CP_D), followed by electrolysis at E_{pc} -150 mV for 30 s (CP_D) or 300 s (NP_D). (E_{pc} is the diazonium cation reduction peak potential obtained during the first scan). TEG_a and PEG_a were electrografted using two initial CV cycles from 0 to 1.35 V, followed by electrolysis at 1.35 V for 300 s.

AP films generated by electrochemical conversion of NP films were prepared in 0.1 M H_2SO_4 by electrolysis at E_{pc} -150 mV for 120 s.

Unless stated otherwise, all electrografted surfaces were sonicated in ACN for 5 min after film modification, rinsed with IPA, and dried with a stream of N_2.

5.2.4 Photochemical modification and patterning of GC substrates

For the standard photografting procedure, polished or film-modified GC plate surfaces were spin-coated with two coats of arylazide solution at 1000 rpm for 30 s. Solutions of NP_A (200 mM) and ITC_A (20 mM) were prepared in DCM, and AP_A (20 mM) was prepared in DMF. Non-patterned surfaces were irradiated at 365 nm inside a Rayonet Srinivasan-Griffin photochemical reactor (equipped with six 3650 Å reaction lamp tubes, ≈ 1 mW/cm^2) for 30 min. All photografted substrates were sonicated for 5 min in DCM or DMF then 5 min in acetone, rinsed with IPA, and dried with a stream of N_2.

To prepare film patterned surfaces at GC, spin-coated arylazide samples were irradiated through a chrome-on-glass mask in a home-made photoreactor fitted with a 365 nm UV lamp (Philips HPR 125 W, 0.8 mW/cm^2). Direct exposure was achieved with the mask directly in contact with the sample. The mask was thoroughly cleaned with acetone and IPA before and after use.

5.2.5 Post modification coupling reactions

GC samples derivatised with isothiocyanate groups were immersed in an aqueous solution of *p*-nitrobenzoic hydrazide (5 mM) for 30 min at room temperature with stirring. After reaction, the surfaces were sonicated for 2 min in DMF followed by 2 min in Milli-Q water. Acid chloride species were coupled to amine-terminated surfaces by immersion of modified GC samples in a saturated DCM solution of *p*-nitrobenzoyl chloride (≈ 200 mM) for 15 h with vigorous stirring. Post modification sonication for 20 min in, successively, DCM, DMF, and Milli-Q water, was necessary to remove unreacted species. Surfaces photografted with NP_A were electrochemically reduced prior to coupling with an activated

N-succinimidyl ester prepared by reacting 0.01 M *p*-nitrobenzoic acid with 1.2 molar equivalents of DIPEA and TSTU in dry DMF for 3 h under N_2. The resulting amine groups were reacted with the activated *N*-succinimidyl ester solution for at least 24 h under N_2. After coupling, the samples were sonicated in DMF for 5 min, and rinsed with a stream of N_2.

5.2.6 Standard photolithography on silicon

Photolithographically patterned photoresist templates on silicon (Figure 5.1) were prepared using standard photolithography. First, silicon wafers were cut into 2 × 2 cm sized wafers and cleaned by sonication for 5 min in acetone then 5 min in IPA, and dried under a stream of N_2. To ensure complete removal of any remaining residues, substrates were treated using an Emitech K1050X plasma asher (Emitech) operating at 100 W RF power in high purity oxygen (BOC Limited) for a period of 10 min. Immediately after cleaning, positive tone photoresist AZ1518 (Microchemicals) was spin-coated to a thickness of ≈ 2 μm at 3000 rpm for 30 s on a PWM32-PS-R790 spinner system (Headway Research Inc.) and soft baked for 60 s at 100 °C on a standard hot plate. A MA6 mask aligner (Suess Microtec) operating in vacuum-mode was used to generate patterns into the photoresist by a 24 s exposure to a 350 W UV lamp through a chrome on glass mask. After exposure, the photoresist was developed by immersion in AZ MIF326 developer (Microchemicals) for 25 s, rinsed with Milli-Q water, and dried with a stream of N_2.

Preparation of patterned films was achieved by immersing patterned photoresist templates in AP_A (20 mM), ensuring that the photoresist templates were filled with solution for the duration of grafting. For thermal grafting, substrates immersed in solution were heated at 80 °C on a hot plate for 30 min in the dark. For the photografting reaction, substrates immersed in solution were exposed inside a Rayonet Srinivasan-Griffin photochemical reactor for 30 min. The solution temperature (≤ 25 °C) was measured after the reaction was

completed to verify that the effect of heating on the substrates was minimal. Immediately after grafting, the silicon substrates were rinsed then sonicated in acetone for 2 min to remove the photoresist, then sonicated in Milli-Q water for 5 min, rinsed with IPA, and dried with a stream of N_2. It was noted that the grafting solutions turned brown/orange and a dark precipitate formed in all grafting solutions.

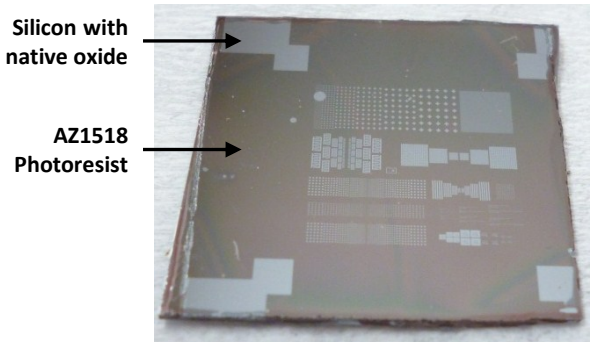

Figure 5.1 Photolithographically patterned photoresist (AZ1518) template on a piece of silicon wafer.

5.2.7 Immobilisation of gold nanoparticles

Gold nanoparticles were assembled on surfaces by immersion in as-prepared nanoparticle solution, with gentle stirring, for 20 min at room temperature in the dark. After preparation, surfaces were rinsed with Milli-Q water and gently dried with a stream of N_2. Unless stated otherwise, sonication cleaning in Milli-Q water was not performed.

5.3 Single-component modification of GC using arylazides, aryldiazonium salts, and alkylamines

Modification of GC surfaces with *para*-substituted NP, AP, carboxyphenyl (CP), and phenyl isothiocyanate (ITC) films was explored using the modifiers shown in Figure 5.2. These molecules contain an azide, diazonium salt, or primary amine functional group for direct surface attachment. Modifiers containing isothiocyanate, amine, and carboxylic acid *para*-substituents were employed because films containing these substituents incorporate reactive sites for tethering or coupling reactions. Compounds containing *p*-nitrophenyl groups were routinely used as the electroactivity of the NP groups enables electrochemical monitoring of its surface concentration, as demonstrated previously in Chapter 3. Furthermore, NP groups are reduced in protic media to (mainly) AP groups, giving a useful amine tether layer[138]. The alkylamines contained a short-chain poly(ethylene glycol) group and a suitable head group for the purpose of preparing films that are "non-reactive" and resist non-specific protein adsorption[353-354].

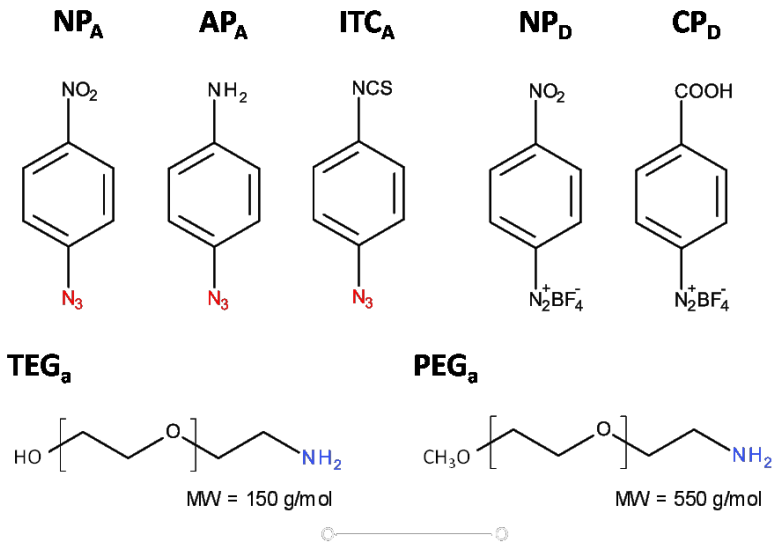

Figure 5.2 Modifiers used: arylazides, NP_A, AP_A, and ITC_A for photografting NP^{AZ}, AP^{AZ}, and ITC^{AZ} films; aryldiazonium salts, NP_D and CP_D, for electrografting NP and CP films; and mono-amine polyethylene glycols, TEG_a and PEG_a, for electrografting TEG and PEG films.

The modification strategies used for preparing single and two-component films on GC surfaces are shown in Scheme 5.1. Single-component films were prepared by photolysis of arylazides (a), or by electrochemical reduction of aryldiazonium salts and oxidation of primary alkyl amines (b). Two-component films were prepared by photolysis from a binary solution of arylazides (c) or by photolysis of arylazides onto GC surfaces modified with electrografted films (d).

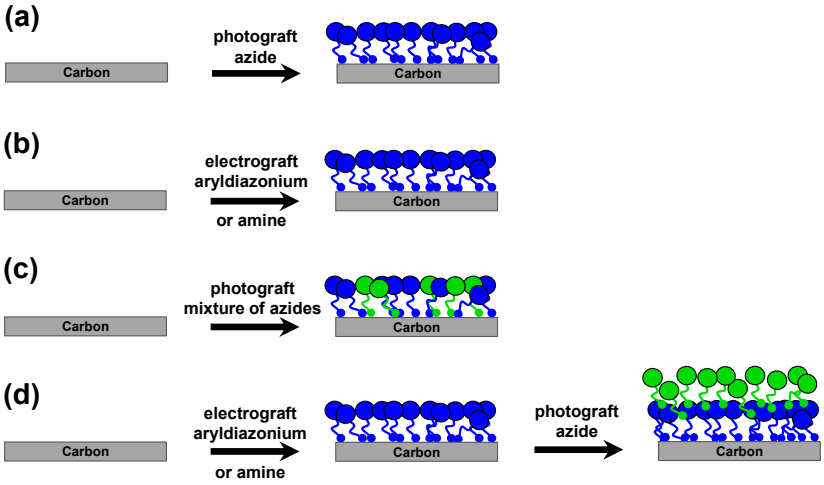

Scheme 5.1 Surface modification strategies used for preparing (a, b) single and (c, d) two-component films.

5.3.1 Photolysis of NP_A, ITC_A, and AP_A at GC

Three arylazide derivatives, shown in Figure 5.2, were used for photografting single-component films to GC surfaces. Herein, all films prepared by photografting of the arylazide derivatives, NP_A, ITC_A, and AP_A will be referred to as NP^{AZ}, ITC^{AZ}, and AP^{AZ} films. The electroactivity of NP groups attached either directly at the surface, or via tethering reactions, was used throughout this chapter to confirm the success of grafting reactions but also to explore the use of azide-derived films as tether layers.

After grafting NP groups, GC samples were mounted in an electrochemical cell for voltammetric analysis. Figure 5.3 shows the first and second consecutive CVs in 0.1 M

H_2SO_4 for a photografted NP^{AZ} film on GC. The first scan CV (–) shows the characteristic, irreversible reduction peak at $E_{pc} \approx$ -0.4 V (vs. Ag/AgCl) of surface-bound NP groups to AP and hydroxylaminophenyl groups (Equation 1 and 2, Section 3.3.2). The second scan CV (---) shows a small and broad oxidation wave at $E_{pa} \approx$ 0.3 V, corresponding to the oxidation of hydroxyaminophenyl to nitrosophenyl groups (Equation 3, Section 3.3.2). On the second scan the only significant feature is the reversible couple at $E_{1/2} \approx$ 0.3 V. These CVs demonstrate that the GC surface has been successfully modified with an NP^{AZ} film. In comparison to the voltammetric response of diazonium-derived NP films at PPF and a-C surfaces (Chapter 3), the NP peak potential for NP^{AZ} films at GC ($E_{pc} \approx$ -0.4 V) is shifted positive by ≥ 300 mV ($E_{pc} \approx$ -0.7 V for NP at PPF). This shift in peak potential most likely reflects differences in film structure, arising from the very different reactivity between aryldiazonium ions and nitrenes at carbon surfaces.

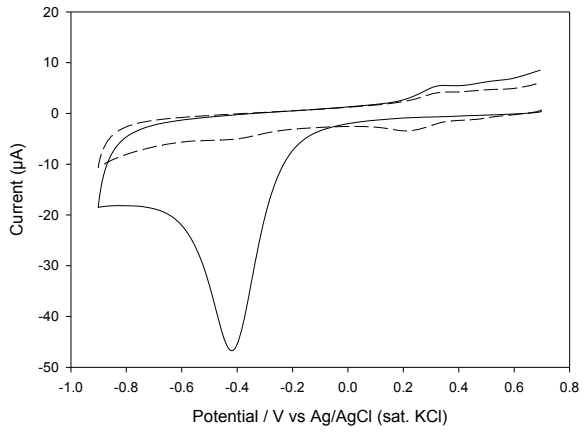

Figure 5.3 First (–) and second (---) scan CVs in 0.1 M H_2SO_4 of a GC surface spin-coated with two layers of 200 mM NP_A after photolysis for 30 min.

The average surface concentration of electroactive NP groups was estimated based on the integrated area of the reduction and oxidation peaks observed in the first scan CV, giving a surface concentration of NP^{AZ} groups of $\approx 18 \times 10^{-10}$ mol/cm^2 (Table 5.1). This value is the same as that found by Yu for NP^{AZ} films at GC ($\approx 18 \times 10^{-10}$ mol/cm^2) prepared under

identical conditions[154], and the same as that reported in Chapter 3 for diazonium-derived NP films at PPF surfaces ($18 \pm 2 \times 10^{-10}$ mol/cm^2). The surface concentration obtained for the NP^{AZ} film on GC is thus consistent with the formation of a multilayered film, given that an ideal close-packed monolayer of NP groups on a flat surface has a calculated surface concentration[355] of $\approx 12 \times 10^{-10}$ mol/cm^2. Furthermore, the NP^{AZ} film is not expected to be close-packed, but a rather disordered film structure, due to the high reactivity and non-specificity of nitrene reactions at the already inhomogeneous GC surface.

AFM investigations by Yu showed that NP^{AZ} films grafted at PPF under the same conditions as those reported here have average thicknesses of 0.6-1 ± 0.2 nm. The theoretical height of an ideal monolayer of NP is 0.8 nm[154], assuming that the molecules are oriented perpendicular to the plane of the surface via a C-N bond. The AFM line profile for an NP^{AZ} film at PPF, reported by Yu reveals peak-to-peak heights of 0.8-2.0 nm and hence it may be concluded that the NP^{AZ} films are loosely packed monolayers with multilayer domains.

Photografting reactions using spin-coated ITC$_A$ and AP$_A$ were also investigated. As expected, no oxidation or reduction in aqueous acidic conditions (0.1 M or 0.25 M H_2SO_4) was observed for photografted ITC^{AZ} or AP^{AZ} films. To confirm successful modification of GC surfaces with ITC^{AZ} and AP^{AZ} films, samples were reacted with appropriate NP-containing derivatives and then electrochemically characterised in aqueous acid. Providing that the tethering reaction is selective, and that the NP groups are accessible by proton diffusion through the film, it is possible to indirectly confirm film modification by monitoring the response of coupled NP groups. Table 5.1 lists concentrations of electroactive NP groups at the various surfaces.

Table 5.1 Surface concentration of NP groups in single and two-component films at GC prepared by photografting, electrografting, and tethering reactions[a].

Film	Coupling reagent	Surface concentration ($\times 10^{-10}$ mol/cm^2)[b]
NP^{AZ}	None	18 (n = 5)[c]
ITC^{AZ}	*p*-nitrobenzoic hydrazide	4.1 (n = 1)
AP^{AZ}	*p*-nitrobenzoyl chloride	2.7 (n = 3)
NP^{AZ}-AP^{AZ}	None	5.5 (n = 1)
TEG_a-NP^{AZ}	None	3.1 (n = 3)
TEG_a-NP^{AZ} [d]	*p*-nitrobenzoic acid	1.7 (n = 1)
CP-AP^{AZ}	*p*-nitrobenzoyl chloride	2.4 (n = 3)
NP	None	30 (n = 3)
NP-AP^{AZ}	None	27 (n = 3)

[a] Preparation conditions are described in Section 5.2.
[b] All surface concentrations have an estimated uncertainty of 20% based on the maximum observed relative standard deviation for repeated measurements. The error estimate includes sample-to-sample reproducibility and curve fitting.
[c] n is the number of separate samples analysed.
[d] The TEG_a-NP_A film was electrochemically reduced in 0.1 M H_2SO_4 prior to the coupling reaction.

The presence of ITC^{AZ} groups on GC was demonstrated by reaction with *p*-nitrobenzoic hydrazide and subsequent analysis by cyclic voltammetry. The surface coupling reaction is illustrated in Figure 5.4.

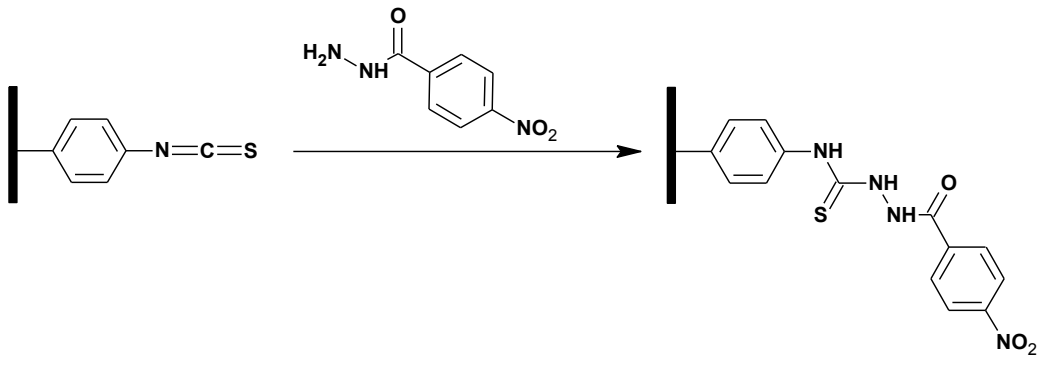

Figure 5.4 Surface coupling reaction between ITC^{AZ}-modified GC and 5 mM *p*-nitrobenzoic hydrazide under aqueous conditions for 30 min.

Figure 5.5a shows the first scan CVs obtained in 0.1 M H_2SO_4 at the grafted electrode (–) and at a polished GC electrode (---) that had been incubated in *p*-nitrobenzoic hydrazide under the same conditions. At both the grafted and polished GC electrodes, the irreversible reduction peak provides clear evidence of NP groups attached at the surface. Hydrazide reacts with surface carbonyl groups invariably present on polished GC[55]; however, after photografting with ITC_A, the amount of NP coupled to the surface is significantly greater, consistent with the successful reaction of hydrazide with grafted ITC^{AZ} groups.

The surface concentration of NP groups tethered at the ITC^{AZ}-modified surface was estimated from the first scan CV (–) in Figure 5.5a, giving a value of $\approx 4.1 \times 10^{-10}$ mol/cm^2. This value is significantly less than the concentration of NP^{AZ} groups directly photografted to GC, which may indicate that ITC_A has a lower photografting yield on GC than does NP_A. However, AFM analysis by Yu of ITC^{AZ} and NP^{AZ} films showed similar average thicknesses (0.6-1.0 ± 0.2 nm for both films) and surface topographies, suggesting that the surface concentration of ITC^{AZ} and NP^{AZ} groups should be similar. It is therefore assumed that the estimated surface concentrations of tethered NP groups do not accurately reflect the surface concentrations of reactive groups in the ITC^{AZ} layer. The significantly lower grafting yield observed for the tethered layer is presumably due to the coupling reaction only being successful at the outermost layer(s) of the ITC^{AZ} film, as a consequence of poor permeability and steric effects within the film[138, 356]. Nevertheless, the ability to detect and estimate the surface concentration of tethered molecules is useful for confirming the presence and reactivity of the first layer.

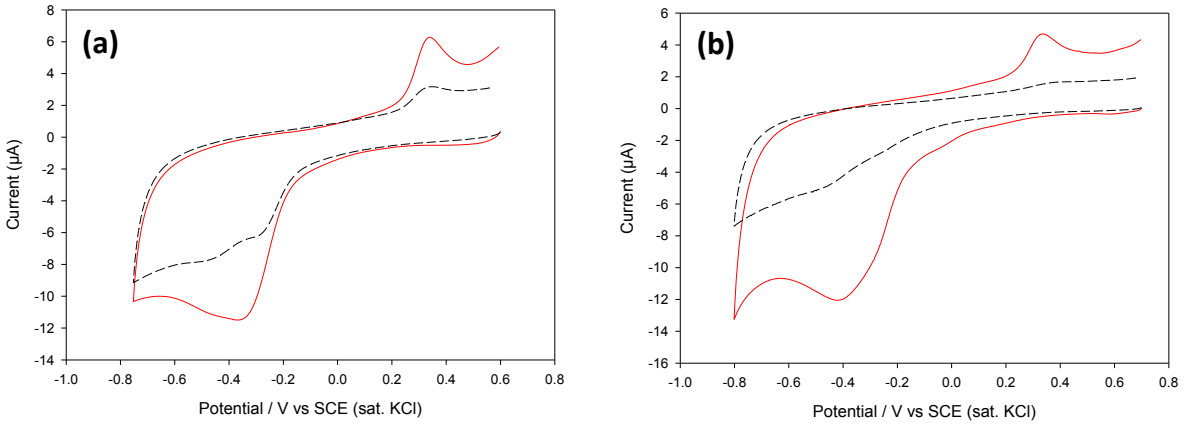

Figure 5.5 First scan CVs in (a) 0.1 M H_2SO_4 of GC photografted with ITC_A (–) and polished GC (---) after reaction with *p*-nitrobenzoic hydrazide, and (b) 0.25 M H_2SO_4 of GC photografted with AP_A (–) and polished GC (---) after reaction with *p*-nitrobenzoyl chloride.

The presence of AP^{AZ} groups at GC after grafting AP_A was demonstrated using a similar approach. Polished and AP^{AZ}-modified GC surfaces were reacted with *p*-nitrobenzoyl chloride and subsequently examined by cyclic voltammetry in aqueous acid (Figure 5.5b). The surface coupling reaction is illustrated in Figure 5.6.

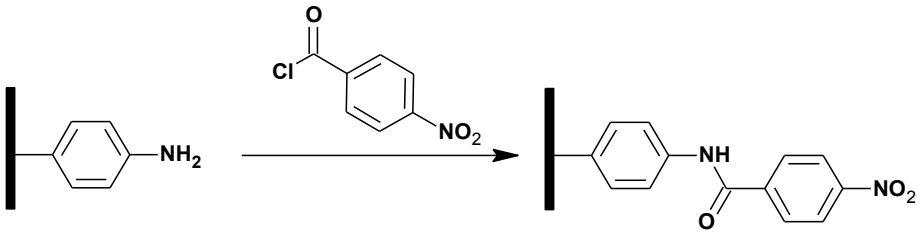

Figure 5.6 Surface coupling reaction between AP^{AZ}-modified GC and 0.2 M *p*-nitrobenzoic hydrazide in DCM for 15 h.

A higher concentration of acid was used here with the aim of improving the permeability of protons through the film and therefore the coupling yield; however, no differences in peak current were observed when different concentrations of acid were used. As was found for the tethered NP groups at ITC^{AZ}-modified GC, the NP reduction peak is broad and the

estimated surface concentration of NP groups is relatively low (≈ 2.7 × 10^{-10} mol/cm^2), presumably due to the reasons outlined above. Figure 5.5b also shows the first scan CV (---) of a polished GC electrode after reaction with *p*-nitrobenzoyl chloride under the same conditions as for the AP^{AZ}-modified surface. Trace amounts of NP groups are observed at the polished electrode as indicated by the very low reduction currents. This is attributed to a small amount of strongly adsorbed *p*-nitrobenzoyl chloride that persists despite extensive sonication cleaning (5 min in DMF).

5.3.2 Electrochemical reduction of NP_D and CP_D at GC

Figure 5.7 shows the electrografting behaviour of NP_D (Figure 5.7a) and CP_D (Figure 5.7b) at GC surfaces. The first scan CVs (–) are broad and irreversible and the current in the second and third scans are low, confirming the successful deposition of NP and CP films at GC via the one-electron reduction of aryldiazonium ions.

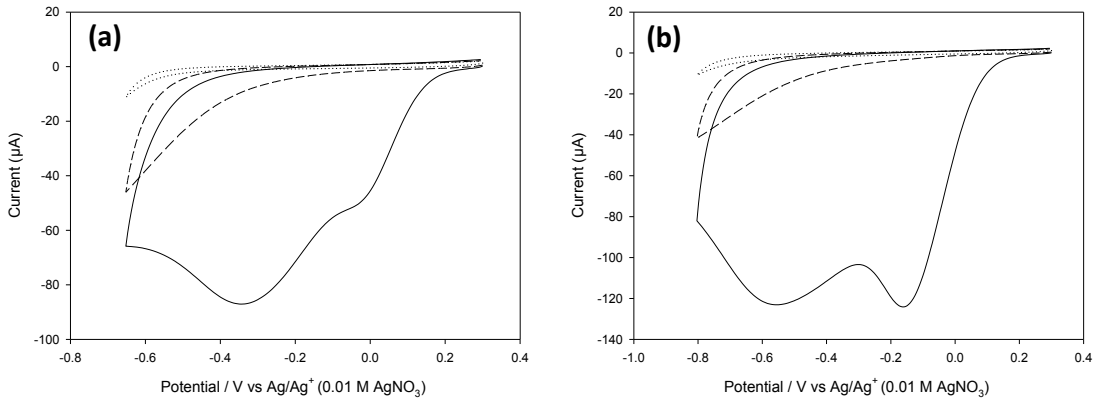

Figure 5.7 Consecutive CVs of (a) 1 mM NP_D and (b) 5 mM CP_D in ACN with 0.1 M $TBABF_4$ at GC.

The presence of two distinct reduction waves on the first cycle in NP_D and CP_D solutions at GC contrasts to the CV behaviour observed for NP_D reduction at PPF (Figure 3.2a), and reduction of in situ generated CP_D at PPF (Figure 6.3c). Multi-peaks such as those shown in Figure 5.7 have been observed previously for electrografting aryldiazonium salts at GC

and are attributed to the reduction of aryldiazonium ions at different active sites present at the surface[357-358]. After grafting, NP and CP-modified GC surfaces were rinsed and sonicated, then used as base layers for preparing two-component surfaces as described below in Section 5.4.

5.3.3 Electrochemical oxidation of TEG_a and PEG_a at GC

Electrografting of GC surfaces with poly(ethylene glycol) groups was investigated by electrochemical oxidation of primary aliphatic amines, TEG_a and PEG_a. The CV scan obtained at GC (Figure 5.8) show an irreversible oxidation peak on the first scans, which is assigned to the one-electron oxidation of the amine substituent. On the second scan, the oxidation wave decreases and shifts more positive, consistent with the surface becoming increasingly passivating due to grafting of a film. After electrolysis at E_{pa} +150 mV for 300 s, and recording a third CV scan, the surface is completely passivating towards the grafting solution. The strongly blocking behaviour observed at these electrodes is typical for films prepared by oxidation of primary amines at GC by electrolysis for 300 s at a potential more negative than the peak potential of the amine[95].

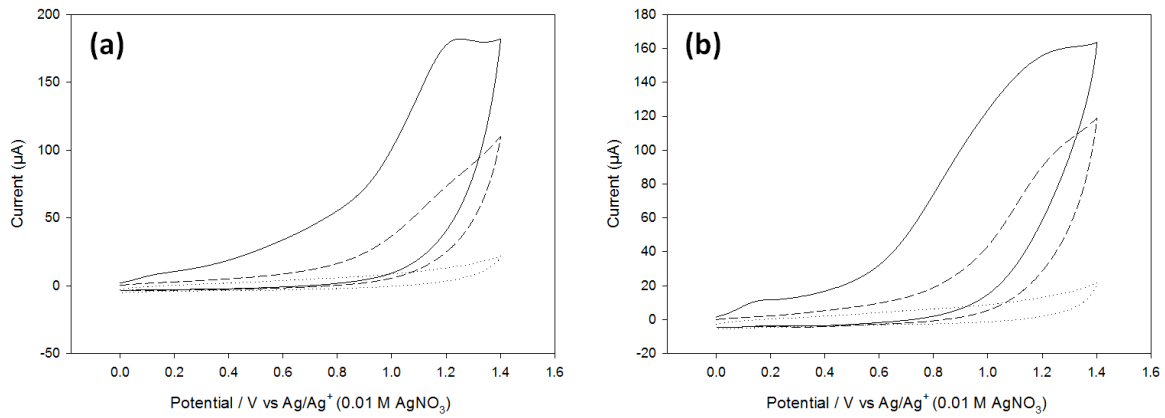

Figure 5.8 Consecutive CVs of (a) 3 mM TEG_a and (b) 3 mM PEG_a in ACN with 0.1 M $TBABF_4$ at GC.

The accepted mechanism leading to the attachment of an organic layer via electrochemical oxidation of primary amines in anhydrous conditions is based on the formation of a radical, obtained via a sequential pathway, which covalently attaches to the electrode surface[110] (Scheme 1.1).

The presence of PEG and TEG films at GC was investigated by comparing CVs of $Fe(CN)_6^{3-}$ before and after modification. At polished GC, the CV of $Fe(CN)_6^{3-}$ at pH 11.5 (Figure 5.9, –) is chemically reversible with ΔE_p = 256 mV (a) and 225 mV (b). After modifying GC with PEG_a or TEG_a, the CVs obtained in $Fe(CN)_6^{3-}$ solution (---) show only very low currents and ΔE_p values ≥ 800 mV. This behaviour is consistent with the presence of a strongly blocking film on the surface[113]. The blocking behaviour is slightly stronger at the TEG-modified surface (ΔE_p is larger), which may reflect that these films have a more compact and less permeable structure compared to PEG films.

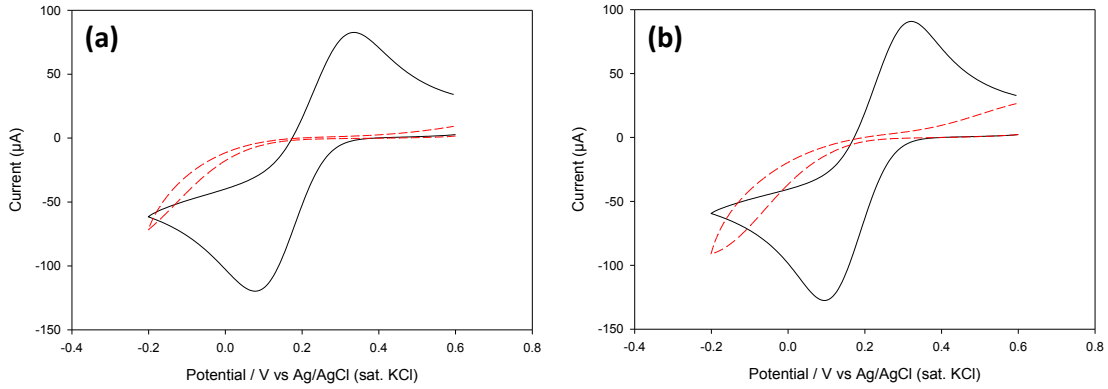

Figure 5.9 First scan CVs of 5 mM $Fe(CN)_6^{3-}$ (pH 11.5) at freshly polished GC before (–) and after (---) modification with (a) TEG and (b) PEG films.

5.3.4 Protein antifouling properties of GC electrodes modified with PEG films

The ability of TEG and PEG-modified GC surfaces to resist non-specific protein adsorption was investigated by monitoring the voltammetric response of ferrocenemonocarboxylic acid, FCA, at polished and modified GC electrodes in the

presence and absence of BSA. Investigations were undertaken using differential pulse voltammetry (DPV) according to the method of Downard and Mohammed[359]. The influence of BSA-FCA interactions in solution on the electrochemical response of FCA was shown to be insignificant under conditions similar to those used in the present study [359].

Adsorption of BSA at polished GC results in a decrease in the DPV peak current for oxidation of FCA (I_p^{BSA}) compared to that observed in the absence of BSA (I_p^0). At polished GC (Figure 5.10a), the DPV peak current for oxidation of 1 mM FCA decreases after immersion in 1 mM FCA with 4g/L BSA for 5 min, giving a peak current ratio of $I_p^{BSA} / I_p^0 = 0.81$. This behaviour is consistent with protein fouling at the electrode leading to suppression of the FCA signal.

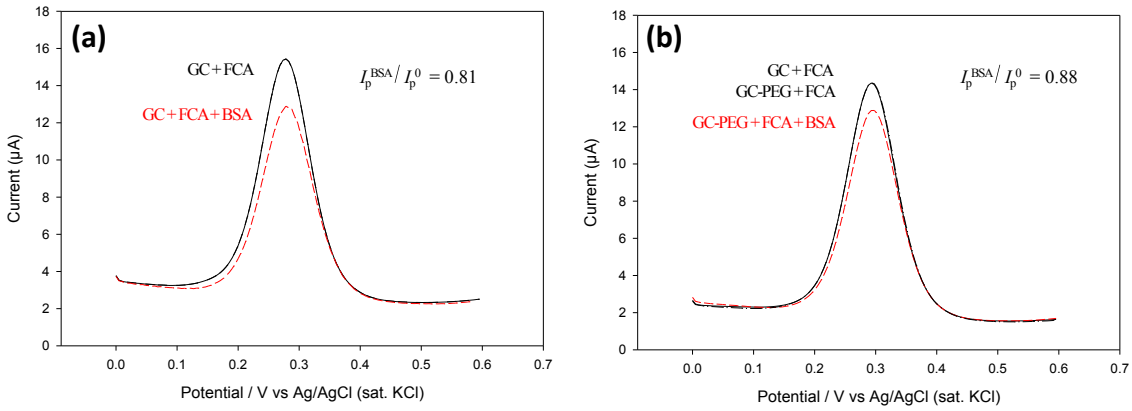

Figure 5.10 (a) DPV scans of 1mM FCA in PBS at GC in the absence (–) and presence (---) of 4g/L BSA. (b) DPV scans of 1 mM FCA in PBS at GC (–) and GC after modification with PEG (-.-), and DPV scans of 1 mM FCA in PBS at GC after modification with PEG in 4g/L BSA (---).

After modification of polished GC with a PEG or TEG film, a decrease in peak current for oxidation of FCA might be expected due to the deposition of a partially blocking film. For PEG-modified GC, the decrease in peak current (Figure 5.10b, --) is insignificant compared to the unmodified surface (Figure 5.10b, –) (the DPV scans for GC + FCA and

GC-PEG + FCA appear identical in Figure 5.10b). After immersion of PEG-modified GC in FCA and BSA solution, the DPV peak current for FCA (Figure 5.10b, ---) decreased, giving a ratio of $I_p^{BSA} / I_p^0 = 0.88$. Hence it appears that there is less BSA adsorption at GC after modification with PEG. For TEG-modified GC surfaces, a similar trend was observed (DPVs not shown) as shown by the data in Table 5.2.

Table 5.2 Ratios of DPV peak currents for oxidation of 1 mM FCA in PBS (pH 7.4) in the presence and absence of 4g/L BSA at polished, TEG-modified, or PEG-modified GC surfaces.

	BSA suppression	**Film permeability**
	(I_p^{BSA} / I_p^0)	**(I_p^{mod} / I^{GC})**
Polished GC	0.85 ± 0.03[a] (*n* = 7)[b]	1.00[c]
TEG[d]	0.94 ± 0.02 (*n* = 5)	0.75 ± 0.03 (*n* = 5)
PEG[d]	0.88 ± 0.01 (*n* = 4)	0.99 ± 0.04 (*n* = 5)

[a] Values reported as mean ± relative standard deviation.
[b] *n* is the number of separate samples analysed.
[c] Polished GC only with no film.
[d] Modified surfaces were prepared by grafting from a single CV between 0 to 1.3 V vs Ag/Ag^+.

The significance of differences in protein adsorption was validated by testing the null hypotheses that there is a difference in protein adsorption at GC compared to PEG and TEG-modified GC surfaces. At the 5% probability level, the difference between the sample means is significant for GC and GC-PEG (|t| = 5.26, 10 df), but is not significant for GC and GC-TEG (|t|= 1.89, 9 df). At the 10% probability level, the difference between the sample means for GC and GC-TEG (and GC and GC-PEG) surfaces is significant; hence the null hypothesis can be accepted when comparing GC to both types of modified surfaces. In other words, modification of GC with PEG or TEG films leads to a statistically significant decrease in BSA adsorption compared to polished GC at the 10% probability level. On the basis of these studies, both TEG and PEG show antifouling properties and could usefully be incorporated as a diluent or "background" modifier in mixed layers designed for use with biological samples[360].

5.4 Two-component modification of GC surfaces using arylazides, aryldiazonium salts, and alkylamines

Two strategies were explored for preparing two-component films at GC surfaces that could be useful for biosensor applications (Scheme 5.1c and Scheme 5.1d). Modifiers were selected so that at least one component could be used to tether biological molecules and the second component could either act as a tether or provide an interface that is resistant to non-specific adsorption of biological species.

In this work the chemical reactivity and accessibility of different components in mixed films were demonstrated by monitoring electroactive groups present within the film or tethered to the surface, or by immobilising gold nanoparticles that can be visualised by microscopy.

5.4.1 Two-component films by the photolysis of mixtures of arylazides

A mixed film comprising NP and AP groups was prepared by spin-coating a DCM/EtOH (50:50) solution of NP_A (100 mM) and AP_A (10 mM) onto GC surfaces and photolysing as described in Section 5.2.4. Figure 5.11 shows the first (–) and second CV scan (---) recorded in 0.1 M H_2SO_4 of a freshly grafted NP^{AZ}-AP^{AZ} mixed film. The presence of NP^{AZ} groups is confirmed by the presence of an irreversible reduction at $E_{pc} \approx 0.4$ V on the first scan, and a small hydroxyaminophenyl/nitrosophenyl redox couple on the second scan. The surface concentration of electroactive NP^{AZ} groups is $\approx 5.5 \times 10^{-10}$ mol/cm^2. As expected, this value is significantly lower than that for single-component NP^{AZ} films (Table 5.1), consistent with competition for surface sites during the photolysis of two-component mixtures, and also due to the lower concentration of NP_A used in the grafting solution.

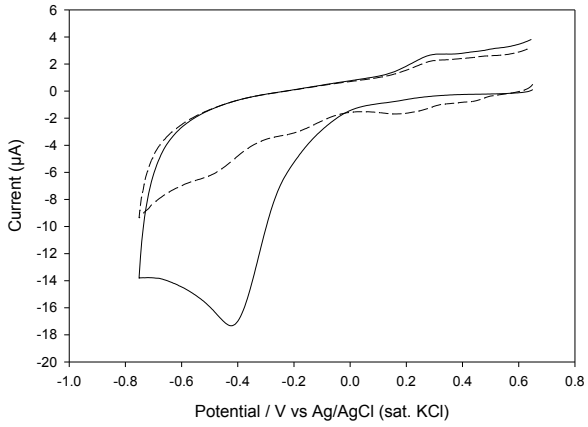

Figure 5.11 First (–) and second (---) scan CVs in 0.1 M H_2SO_4 of a GC surface spin-coated with a mixed layer from a DCM/EtOH (50:50) solution of NP_A (100 mM) and AP_A (10 mM), followed by photolysis for 30 min.

Successful grafting of AP^{AZ} groups in the mixed film was confirmed in a second set of experiments using the same modified GC surfaces. After photografting, then rinsing and sonication cleaning, the modified surfaces were immersed in a solution of citrate-capped gold nanoparticles for 20 min. Single component NP^{AZ} and AP^{AZ} films were also placed in gold nanoparticle solution for the same duration. After immersion, the surfaces were dried and imaged by SEM. Nanoparticle counts were calculated for each type of modified surface using ImageJ software and are listed in Table 5.3. Figure 5.12 shows clear evidence that gold nanoparticles are successfully immobilised at the AP^{AZ}-NP^{AZ} mixed film surfaces, through electrostatic interactions with AP groups. Unsurprisingly, the surface concentration of gold nanoparticles is less than (≈ 30%) that observed at single component films.

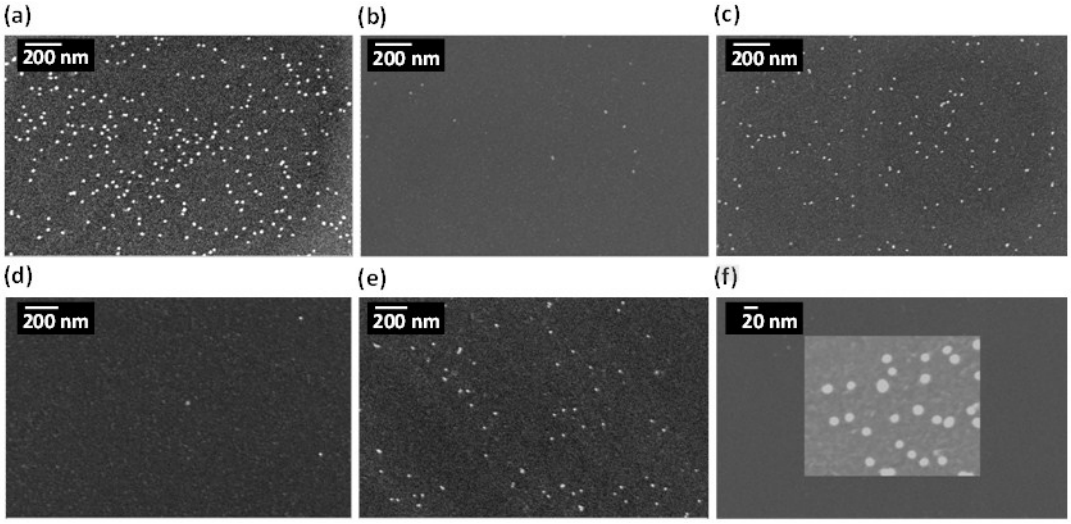

Figure 5.12 SEM micrographs of gold nanoparticles immobilised at GC surfaces modified with films using (a) AP_A, (b) NP_A, (c) NP_A/AP_A, (d) NP_D, and (e) NP_D/AP_A. (f) High magnification image of immobilised gold nanoparticles at the surface in panel a. All samples were immersed in gold nanoparticle solution for 20 min.

5.4.2 Two-component films by the photolysis of arylazides at film-modified surfaces

The photolysis of mixtures of arylazides, as described above, is the most straightforward approach to mixed films, but is limited by the requirement that all modifiers must be soluble in the same solvent or solvent mixture. The method is also not suitable for patterning the modifiers at different regions of the surface.

Using the step-wise strategy, immobilisation of the first modifier can be achieved using any of the electrografting and non-electrochemical grafting methods described in Section 1.4, for example. This versatility greatly expands the range of components that can be attached on the surface. Furthermore, another advantage of the step-wise approach is that it is easily adapted to surface patterning by photolysis using a photomask or maskless photolithography.

To demonstrate the formation of mixed films by the step-wise grafting approach (Scheme 5.1d), NP_A was photografted onto an electrografted TEG film, and AP_A was photografted onto electrografted CP or NP films.

For preparation of NP^{AZ}-TEG surfaces, the TEG layer was first electrografted to GC by the electrochemical oxidation of TEG_a using the standard procedure described in Section 5.2.3. NP_A was spin-coated onto the TEG-modified surface and subsequently exposed to UV light for 30 min. After cleaning by rinsing and sonication, the sample was analysed in 0.1 M H_2SO_4. Figure 5.13a (–) shows clearly that NP groups are accessible at the surface, but it is not clear where the groups are located within the film. The surface concentration of electroactive NP groups is $\approx 3.5 \times 10^{-10}$ mol/cm^2, which is lower than the concentration of NP groups estimated for NP^{AZ}-AP^{AZ} mixed films ($\approx 5.5 \times 10^{-10}$ mol/cm^2), presumably due to the NP groups being buried within the TEG layer; however, the film structure was not studied and this has not been confirmed. The photogenerated nitrene is expected to be able to react with the poly(ethylene glycol) chains of the TEG layer by insertion into C-H bonds, hence it seems likely that NP^{AZ} groups are attached to both the TEG film and the GC surface. The utility of TEG-NP^{AZ} surfaces was further explored by testing if AP groups, generated by electrochemical conversion of NP, are accessible for further tethering reactions. After electrochemical reduction of the TEG-NP^{AZ} surface in 0.1 M H_2SO_4 using the method described in Section 5.2.3, *p*-nitrobenzoic acid was reacted at the surface in DMF in the presence of DIPEA and TSTU, as described in Section 5.2.5.

Figure 5.13b shows the first and second scan CVs obtained in 0.1 M H_2SO_4 after the coupling reaction. Clear evidence for the presence of NP groups (surface concentration $\approx 1.7 \times 10^{-10}$ mol/cm^2) is observed, demonstrating the success of coupling at electrochemically-reduced NP films present within a mixed film environment.

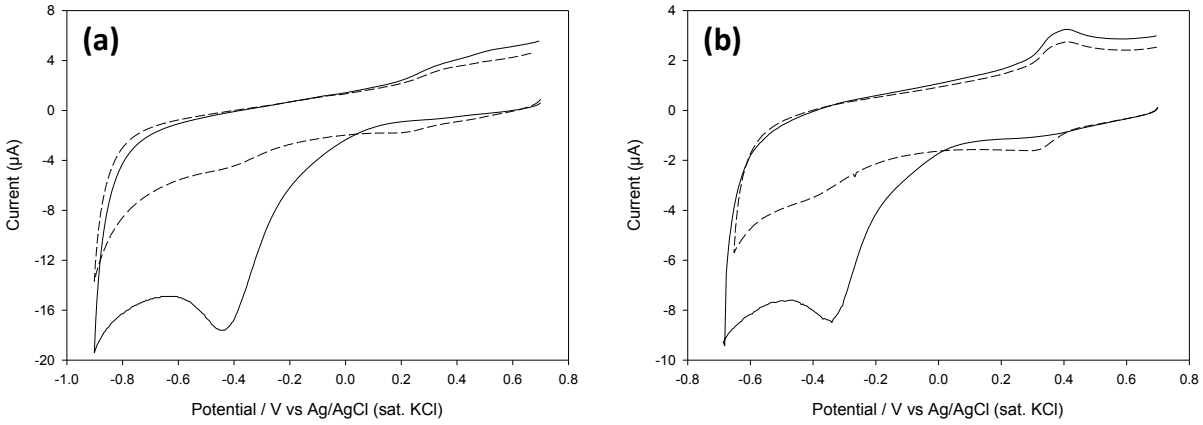

Figure 5.13 First (–) and second (---) scan CVs in 0.1 M H_2SO_4 of (a) TEG-modified GC after photografting NP_A and (b) the electrode in panel a after reduction and subsequent reaction with *p*-nitrobenzoic acid.

Using a similar approach, CP films were first grafted at GC by electrochemical reduction of the corresponding aryldiazonium salt precursor, CP_D. AP groups were attached to the surface by spin-coating a solution of AP_A onto the modified surface and photolysing the sample for 30 min. To test for the presence of reactive amine groups, the AP-CP surface was reacted with *p*-nitrobenzoyl chloride and the resulting surface examined by cyclic voltammetry. Subsequent voltammetric analysis in 0.25 M H_2SO_4 (data not shown) showed a response very similar to that obtained for NP groups tethered, by the same method, to an AP^{AZ} film directly attached to GC (Figure 5.5b, ---). For the two-component film, the estimated surface concentration of NP groups $\approx 2.4 \times 10^{-10}$ mol/cm^2, which compares with $\approx 2.7 \times 10^{-10}$ mol/cm^2 for NP groups coupled to the single-component AP film. This shows that AP groups have comparable reactivity for both single- and two-component films.

To investigate the chemical behaviour of two-component films further, AP_A was photografted to a GC surface modified with an NP layer, prepared by electrografting the corresponding aryldiazonium salt, NP_D. To confirm the activity of the AP component, NP-AP surfaces were immersed in a solution of gold nanoparticles, then rinsed in Milli-Q

water, dried with a stream of N_2, and characterised by SEM. The estimated surface coverage of gold nanoparticles at one set of two-component NP-AP films was compared with the assembly at single-component NP and AP films prepared using the same grafting conditions as those used for the two-component films.

The data in Table 5.3 shows that the surface coverage of nanoparticles at two-component NP-AP surfaces is markedly greater than at a single-component NP film, confirming that photografted AP groups are present at the surface of the mixed film. In a second set of experiments, the electroactivity of the NP component was assessed before and after grafting of AP groups.

Table 5.3 Average surface concentration of gold nanoparticles at single and two-component films on GC prepared from photografting and electrografting procedures.

	Single-component films			**Two-component films**	
	NP^{AZ}[a]	**AP^{AZ}[b]**	**NP**	**NP^{AZ}[a]/AP^{AZ}[b]**	**NP/AP^{AZ}**
Nanoparticle density ($np/\mu m^2$)	13 ± 16%[c]	297 ± 9%	3 ± 20%	87 ± 11%	48 ± 10%
n [d]	(n = 3)	(n = 3)	(n = 3)	(n = 4)	(n = 3)

[a] [NPA] = 10 mM.
[b] [APA] = 20 mM.
[c] values reported as mean ± relative standard deviation.
[d] number of individual SEM micrographs sampled.

Figure 5.14 shows CVs recorded in 0.1 M H_2SO_4 of a single component NP^{AZ}-modified surface (–) and a two-component NP-AP^{AZ} surface (---). In both cases, the typical CV behaviour corresponding to NP films is observed. The response for GC modified with NP groups is similar to that observed for GC modified with both NP and AP^{AZ} groups; however, the peak potential is shifted in the positive direction for the two-component NP-AP^{AZ} film. The shift is tentatively attributed to the addition of electron-withdrawing protonated AP substituents to the NP film. The average surface concentration estimated for electroactive NP groups for the two-component film $\approx 27 \times 10^{-10}$ mol/cm^2, which compares

with 18×10^{-10} mol/cm^2 for the single-component NP film. Importantly, the electroactivity of the NP film is not measurably decreased after photografting AP_A, confirming that the step-wise method affords two-component films in which each compound retains its usual activity.

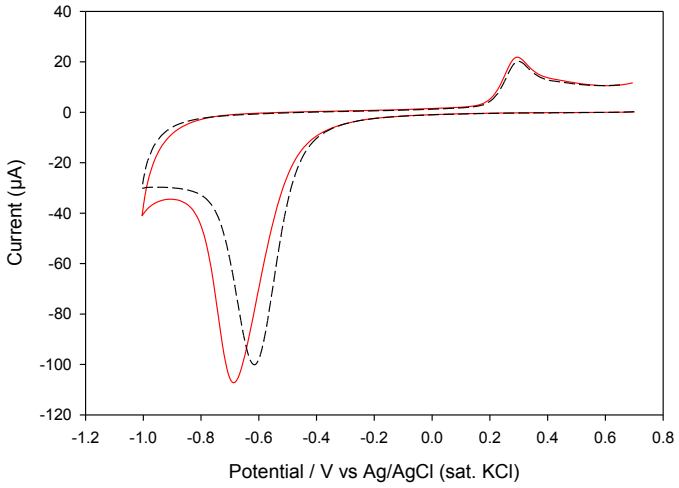

Figure 5.14 First scan CVs in 0.1 M H_2SO_4 of GC electrodes modified with an electrografted NP_D film (–) and an electrografted NP_D film followed by a photografted AP^A film (---).

The examples described in this chapter demonstrate that the step-wise "photografting-electrografting" approach gives two-component films with reactivities similar to that observed for single films. Further experiments were also undertaken using patterned AP^{AZ} and AP^{AZ}-TEG films to determine the feasibility of coupling carboxylic-acid containing biomolecules to the surface. Attempts were made to couple *D*-biotin to the surface via amide bond formation. These experiments proved unsuccessful and hence a completely new strategy based on standard photolithographic patterning of silicon surfaces was investigated, as described below.

5.5 Patterned two-component modification of GC surfaces using arylazides, aryldiazonium salts, and alkylamines

Having demonstrated the utility of the step-wise strategy for preparing two-component films, the method was applied for the preparation of patterned two component films using a photomask. The goal here is to use the previously established patterning method of Yu and Downard[154] to prepare new modified surfaces where different regions have different surface properties and reactivity. Two-component films incorporations TEG or PEG groups are of particular interest for preparation of surfaces that resist non-specific adsorption of biomolecules.

5.5.1 Patterned two-component surface modification

Photopatterning was achieved using the procedure shown in Scheme 5.2, as described in Section 5.2.6. In the first step, an electrografted film is deposited as a continuous layer on the surface. In the second step, a solution of arylazide is spin-coated onto the modified surface and the surface photolysed through a photomask which is in direct contact with the surface. Direct-contact imaging leads to ≈ 1:1 pattern transfer. The reaction of the arylazide occurs only in the areas exposed to the UV light and hence photografting of spin-coated arylazides occurs in these areas only. After removal of the mask, and subsequent rinsing and sonication cleaning, film-modified surfaces were dried and analysed using condensation figures or SEM.

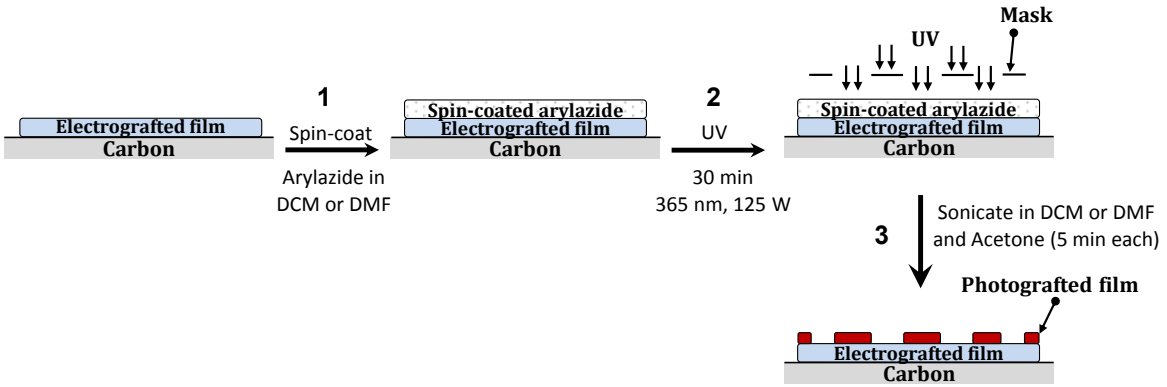

Scheme 5.2 Procedure for preparing patterned two-component films on carbon surfaces by combining electrografting and photografting methods.

SEM is a well-established tool for imaging patterned molecular layers on conducting and semiconducting surfaces[361-362]. Recent studies have shown that patterned thin films containing alkyl or aryl groups on carbon surfaces can be imaged with good contrast and microscale resolution[175, 177, 363]. Image contrast occurs due to differences in secondary electron emission between the organic film on the surface and the underlying substrate. Disordered molecular layers increase the amount of scattering at the surface; hence image contrast and resolution is typically better for self-assembled monolayers than disordered layers such as diazonium and azide-derived films[362]. Nevertheless, SEM is a powerful tool for imaging disordered mono- and multilayer systems and has been used in this thesis as the standard method for imaging patterned films.

Compared to SEM imaging, optical imaging of water condensation figures is a simpler and faster method for confirming the success of surface patterning[364]. Image contrast is dependent on different wettabilities, or surface free energies, between different regions of the surface pattern. The use of condensation figures is widely reported and has been applied previously for imaging films on carbon surfaces[175].

Figure 5.15a shows an optical micrograph of a condensation figure obtained for a two-component PEG-ITC^{AZ} film prepared by photopatterning ITC_A onto a PEG-modified GC surface. The contrast observed in the condensation figure is consistent with the deposition of surface functionalities in the region exposed to UV light. The high pattern contrast occurs due to differences in the water droplets formed between the photografted region and the background region. Control experiments were also performed to confirm that the observed image contrast occurs due to photografting. No evidence for any surface pattern was observed for the PEG-modified GC that had been photolysed under the same conditions, but in the absence of spin-coated arylazide. This confirms that surface patterning of two-component films was successful.

The SEM micrograph in Figure 5.15b shows a TEG film photopatterned with NP groups. The image contrast confirms the success of photopatterning at modified GC presenting an electrografted film. The SEM micrograph of the patterned two-component film has a similar appearance to the SEM micrographs reported for two-component films at PPF[154].

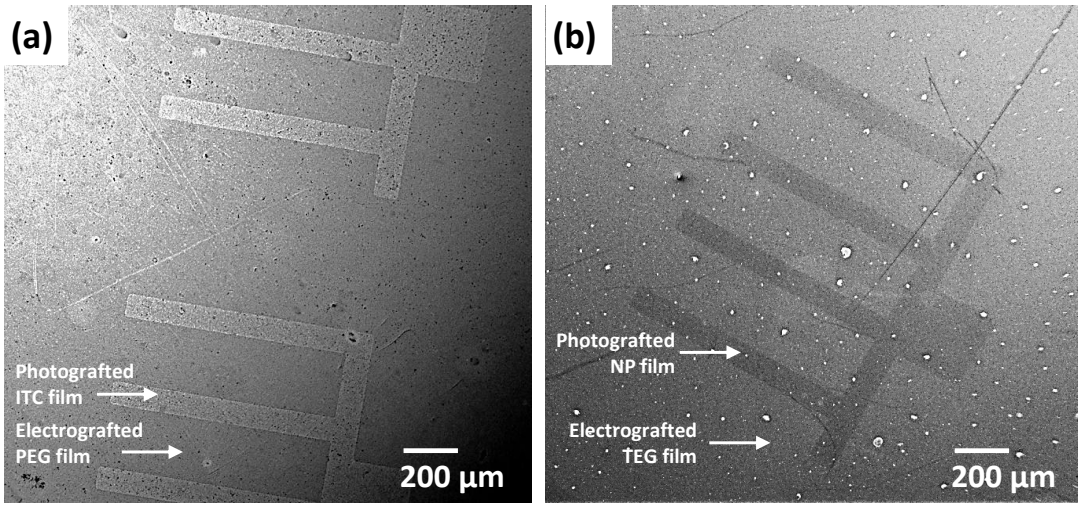

Figure 5.15 (a) Condensation figure of a GC surface presenting an ITC^{AZ} film photopatterned onto a PEG film. (b) SEM image of an NP^{AZ} film photopatterned onto a TEG film at GC.

All SEM and optical images obtained in this work are consistent with 1:1 image transfer from the photomask. Multiple isolated surface patterns were demonstrated (Figure 5.15) comprising line widths of ≈ 100 μm, with a maximum length of ≈ 1 cm. This method could be extended to pattern any number of arylazide derivatives to the surface, with the resolution dependant on the mask and/or optical patterning method used.

5.6 Patterned modification of silicon surfaces using arylazides with conventional photolithography

In this section of work, patterned photoresist was used as a template for thermal or photochemical grafting of AP_A to form patterns of AP films on silicon with its native oxide layer. Preliminary studies investigating the use of these films as tether layers are also reported.

Silicon is an attractive substrate for device-based applications because it can be combined with integrated circuit technology. The most straightforward strategies for modification of silicon surfaces are those that do not require removal of the native surface oxide layer or the use of rigorously dry and air-free conditions[350, 365]. Surface modification of silicon is most commonly performed using silane chemistry due to the formation of covalently-attached layers, and the availability of well-established patterning protocols[323, 366-367]. Aryldiazonium salts and arylazides chemistries have also been used successfully for covalent attachment of thin films at silicon surfaces[368-370]. Photolysis of spin-coated or drop-cast arylazide solutions at silanised surfaces has been reported[340, 371] and arylazide modifiers have also been reacted at hydrogen-terminated silicon[370] and silicon surfaces in ultrahigh vacuum[372]. Prior to this work, to the best of my knowledge, there were no reports demonstrating direct reaction of azides at silicon surfaces with the native oxide layer. Furthermore, for the few examples that demonstrate the modification of silicon surfaces, only the work of Wang and co-workers demonstrates the formation of surfaces derivatised with functional groups that can be used as tether layers[370].

A small number of reports detail the reaction of arylazides at oxide or hydroxylated surfaces; namely, TiO_2[341], ZnO[341], quartz[373], and glass[374]. These examples demonstrate the ability of photogenerated nitrenes to react at oxidised surfaces without the need to first remove the oxide or silanol layer. In the work of Ryan and Splitler, it was concluded that surface attachment occurred through the formation of an N-O bond between the nitrene nitrogen and an oxygen atom at the surface. For the photografting reaction at glass, Chin and Pantano proposed that reactive nitrenes inserted into the O-H bonds of the silanol layer. On the evidence of these two reports, it was hypothesised that the reaction of nitrenes at silicon surfaces in air, and without pre-treatment, would lead to surface attachment of a thin film.

5.6.1 Single-component patterning of AP^{AZ} films at silicon

Patterning of silicon substrates with arylazides using conventional photolithography was investigated by photochemical and thermal grafting reactions using aqueous solutions. Protocols for fabrication of photolithographically patterned templates and for grafting reactions are described in Section 5.2.6. The procedure for preparation of patterned AP films on silicon is illustrated in Scheme 5.3.

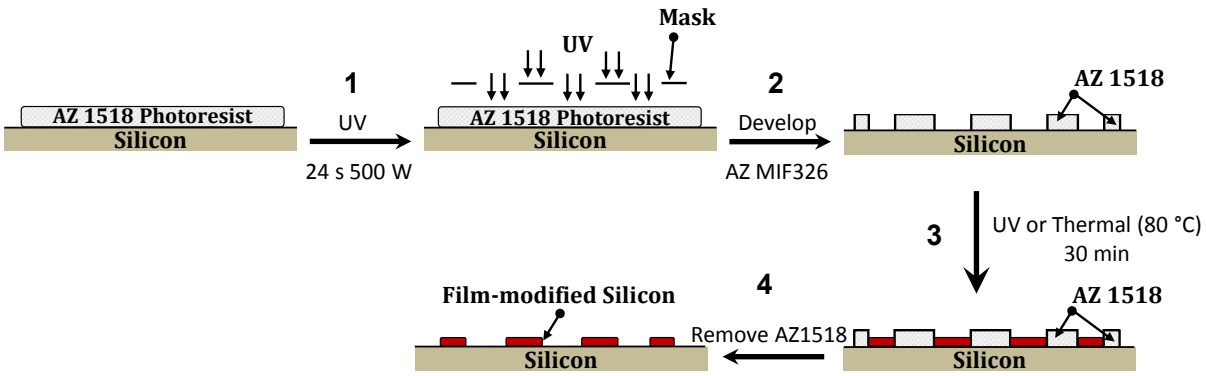

Scheme 5.3 Procedure for preparing patterned AP films on silicon surfaces by thermal or photochemical reaction of aqueous AP_A solution using photoresist patterned templates.

After patterning the highly-doped p-type silicon (100) wafer with micrometre-sized regions of photoresist, the template was immersed in AP_A solution (20 mM) and grafting was performed either on a hot-plate in the dark, or in a photochemical reactor (Section 5.2.6). After modification, the silicon substrates were immersed in acetone to rinse away the photoresist, followed by rinsing and sonication in Milli-Q water.

5.6.1.1 Scanning electron microscopy of patterned AP^{AZ} films at silicon

Figure 5.16 shows SEM micrographs of patterned AZ1518 photoresist on silicon after patterning by UV light exposure for 24 s through a photomask (Figure 5.16a), and after AP^{AZ} film deposition by UV photolysis and subsequent removal of the photoresist (Figure 5.16b).

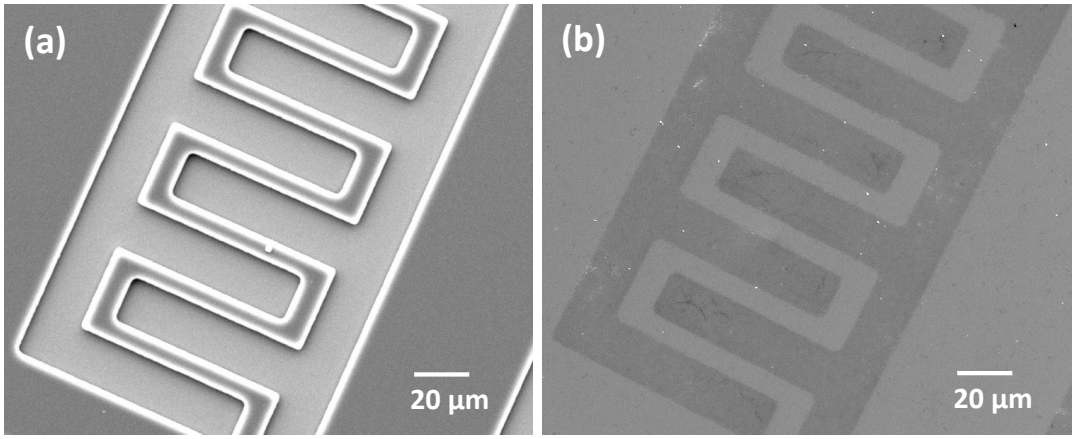

Figure 5.16 SEM micrographs of (a) patterned photoresist and (b) AP film after photochemical reaction of an aqueous solution of AP_A and subsequent removal of photoresist.

High pattern contrast is observed for the patterned photoresist on silicon, where the dark region corresponds to the insulating photoresist layer and the light grey region corresponds to the background silicon surface. The inverse pattern is observed after film deposition and photoresist removal, consistent with the deposition of a film in the region exposed to AP_A grafting solution. The high resolution of the surface pattern as shown in Figure 5.16b is consistent with the deposition of a homogeneous film and successful removal of the

photoresist. Qualitatively similar SEM micrographs were observed for patterned films prepared by thermal or photochemical grafting methods. The minimum line widths for the patterned film regions shown in Figure 5.16b are 20 μm, which compares closely with the minimum feature sizes obtained for films prepared by photografting arylazides directly using a photomask. A variety of geometric shapes with dimensions down to 1 μm were successfully patterned into the photoresist, hence patterned AP^{AZ} films with feature sizes of ≤ 20 μm were also successfully demonstrated in this work.

5.6.1.2 Atomic force microscopy of patterned AP^{AZ} films at silicon

AFM in tapping-mode was used to examine surface topography, pattern formation, and film thickness of patterned AP^{AZ} films grafted at silicon. Films were prepared using both photochemical and thermal grafting methods. AFM film thickness measurements were performed on surface patterns presenting 15 × 15 μm features. The "checkerboard" pattern (Figure 5.17) was designed specifically with these features to enable film thickness measurements using a single 50 × 50 μm scan. Roughness measurements, R_q, were obtained as averages of the modified and unmodified regions for the images shown.

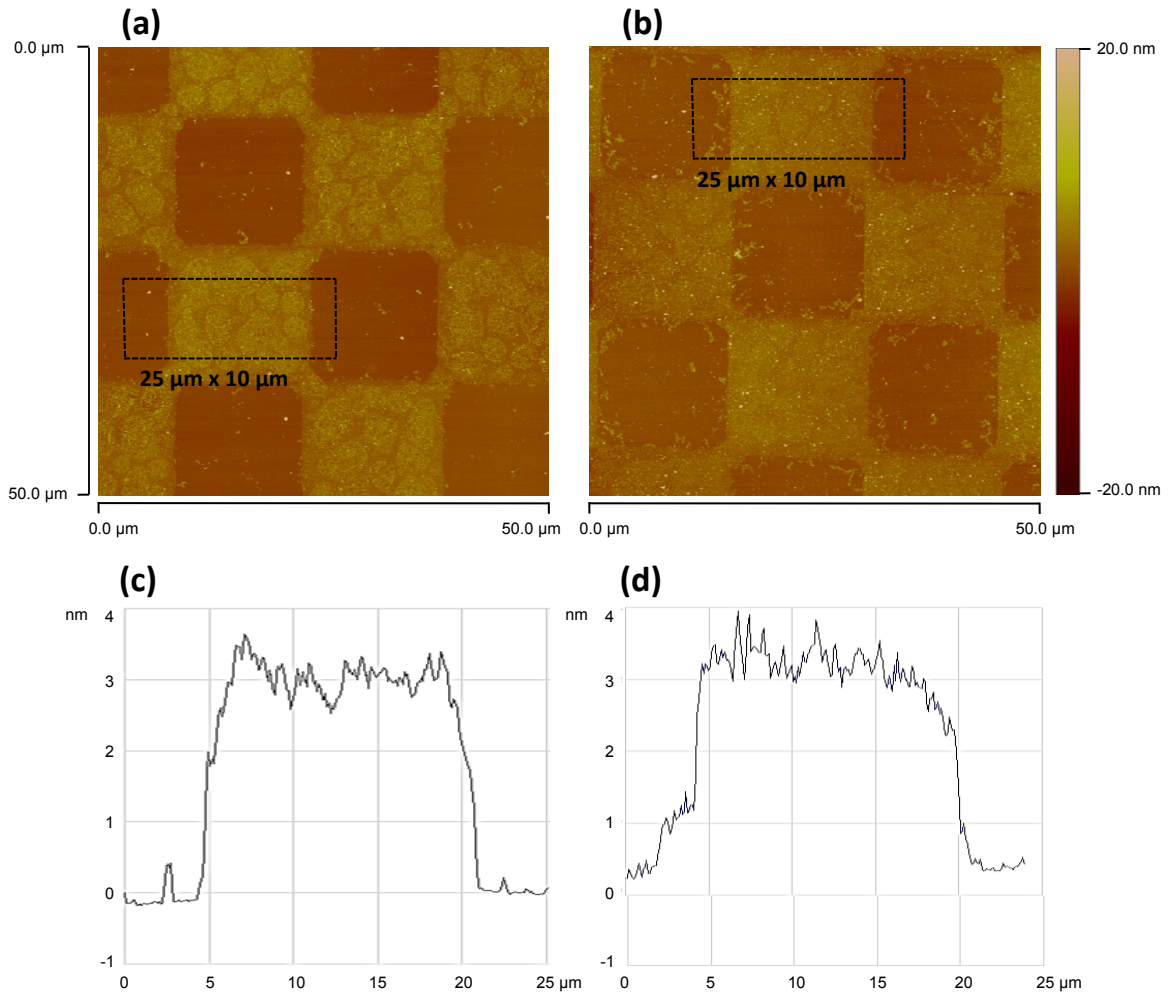

Figure 5.17 Tapping-mode AFM images of a 50 × 50 µm "checkerboard" pattern of AP films on silicon surfaces prepared by (a) thermal and (b) photochemical reaction of aqueous AP_A solution. (c, d). Average section profiles corresponding to the boxes (---) shown in (a) and (b).

The topographical images shown in Figure 5.17a and Figure 5.17b clearly show the formation of well-defined film patterns. The films are continuous across many patterned regions and are restricted only to those areas that were exposed to the grafting solution. As expected, the surface patterns correspond to the inverse of the photoresist pattern (image not shown) and are therefore accurate image transfers. With the exception of a small amount of surface contamination for the photografted AP^{AZ} film (Figure 5.17b), the unmodified silicon surface is clean, indicating effective removal of the photoresist material.

Figure 5.17 shows 50 × 50 μm AFM images and 25 × 10 μm average section profiles of patterned AP^{AZ} films prepared by thermal (a, c) and UV grafting (b, d). The topographical images reveal that the films are "grainy" with island-like structures present on the surface. The grainy appearance is consistent with the films having a loosely packed film structure similar to that observed for AP^{AZ} films photografted at PPF. The formation of islands is consistent with inhomogeneous film growth and a highly disordered film structure. The formation of islands may reflect differences in reactivity and surface wetting due to a non-uniform surface oxide layer. In particular, the reactivity will be greatly influenced by the oxide layer, given that the reaction of nitrenes occurs via insertion into O-H bonds of the surface oxide on semiconductor surfaces[341].

Measurements taken from average section profiles (Figure 5.17a and Figure 5.17b) gave average thickness values of 2.7 ± 0.3 nm and 2.5 ± 0.3 nm for films prepared by thermal and photochemical grafting reactions, respectively. The average line profiles (Figure 5.17c and Figure 5.17d) reveal that the films are relatively uniform in height over distances of ≈ 15 μm. The film thicknesses correspond to the formation of multilayers, and the close correspondence of the values indicate that the two grafting reactions must be very similar.

Surface roughness measurements were calculated from the AFM images in Figure 5.17 using Nanoscope Analysis software. For the unmodified silicon surface, in regions free of debris, average surface roughness values of R_q = 0.5 ± 0.1 nm and R_q = 0.4 ± 0.2 nm were obtained for the images shown in Figure 5.17a and Figure 5.17b, respectively. Surface roughness values of R_q = 1.5 ± 0.2 nm and 1.4 ± 0.1 nm were obtained for the grafted regions of the surface. As expected, the magnitude of the difference between unmodified and modified regions is large.

In combination with the qualitative image analysis and the film thickness measurements, the surface roughness measurements confirm changes upon modification and reveal the formation of highly disordered multilayer films.

5.6.1.3 Scanning electron microscopy of gold nanoparticles immobilised on patterned AP^{AZ} films at silicon

The presence of amine groups on the surface of patterned AP^{AZ} films at silicon was verified by reaction of AP^{AZ}-modified surfaces with a gold nanoparticle solution. After immersion of the patterned substrates in a solution of citrate-capped gold nanoparticles for 30 min, the samples were sonicated for 2 min in Milli-Q water and dried with a stream of N_2.

Figure 5.18 shows SEM micrographs of different regions of a silicon surface with patterned photoresist before (a, c) and after (b, d) surface modification with AP groups, removal of the photoresist, and immersion in gold nanoparticle solution. Figure 5.18b and Figure 5.18d show high densities of gold nanoparticles in the regions where AP^{AZ} films were grafted, consistent with the electrostatic assembly of the nanoparticles on surface-bound amine groups.

The maximum lateral resolution obtained for patterned AP^{AZ} films in this work was ≈ 5 μm (Figure 5.18b), which is very close to the maximum resolution obtained in the photolithographically patterned photoresist templates (Figure 5.18a). Figure 5.18b clearly shows that films with ≤ 10 μm features can be patterned with excellent image fidelity, and that AP^{AZ} films contain amine groups which can electrostatically assemble gold nanoparticles.

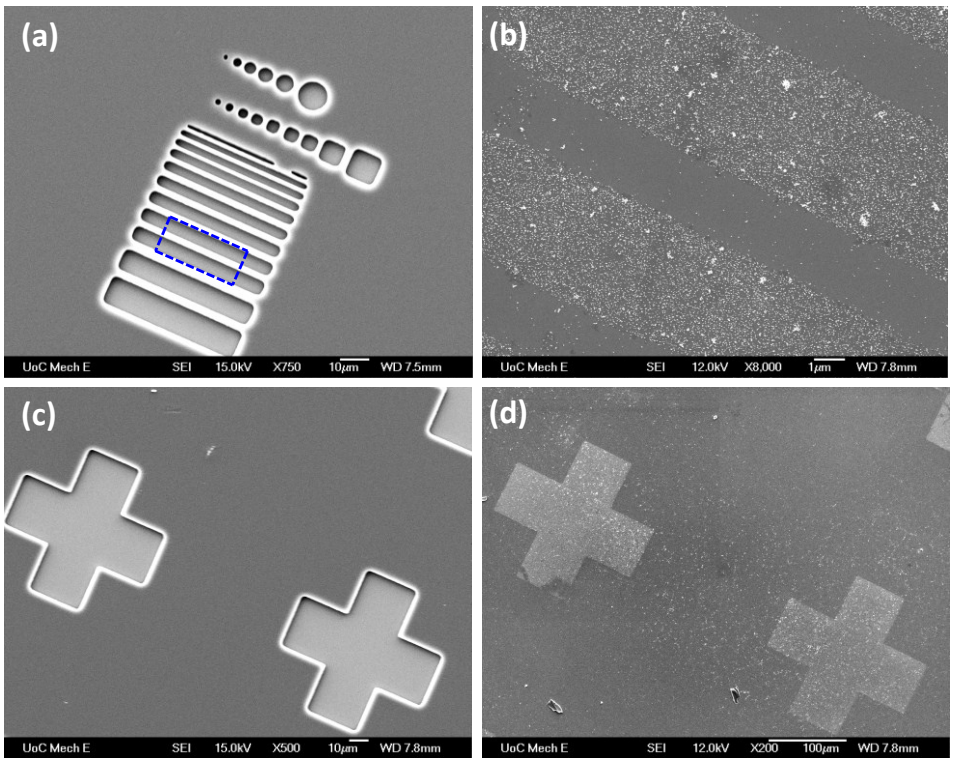

Figure 5.18 SEM micrographs of patterned photoresist on silicon (a, c) and patterned AP films on silicon after removal of photoresist and subsequent immersion in gold nanoparticle solution (b, d). The highlighted section (---) in (a) corresponds to the micrograph shown in (b).

5.7 Conclusion

The use of arylazides for preparing novel two-component films at GC surfaces was investigated in this work. Two principal methods were explored: a method for photografting mixtures of arylazides at GC, and a method for photografting arylazides to preformed electrografted films prepared by electrografting. Both methods proved to be successful for preparing two-component films incorporating a range of desirable organic functionalities.

The preparation of two-component films by mixed grafting is the simplest approach to multifunctional surfaces as only one grafting step is necessary. For mixed NP-AP films, both components were found to be accessible and showed their usual reactivity. Lower surface concentrations of NP and AP were observed compared to single component films, consistent with the lower grafting concentrations and competition for surface sites during grafting. These results demonstrate that grafting from a mixture of arylazides is well-suited to the formation of two component films and could be used for the preparation of multifunctional surfaces. However, the main limitation of grafting using this approach is that no control over the spatial distribution of each component is achieved.

The step-wise strategy, developed in earlier work by Yu, was expanded in this Chapter for preparing new two-component systems; namely, PEG-ITC^{AZ}, TEG-NP^{AZ}, CP-AP^{AZ}, NP-AP^{AZ}, and TEG-AP following electrochemical reduction of TEG-NP. A major advantage of the step-wise strategy compared to the mixed grafting strategy is that the first film component can be grafted to the GC surface by any convenient method, giving very wide possibilities for the incorporation of different functional groups. This versatility was exploited for grafting both alkyl and aryl films as the first component, by electrochemical grafting methods. The electrochemical oxidation of amines was investigated as a route to film components containing aliphatic chains of poly(ethylene glycol) units. PEG and TEG films grafted at GC minimise non-specific adsorption of BSA, and hence represent an

important addition to the suite of two-component films that can be prepared. Furthermore, patterned two-component films; namely PEG-ITC^{AZ}, TEG-NP^{AZ}, were prepared by photolysis of spin-coated arylazides through a photomask. These surfaces demonstrate the preparation of films with spatially addressable tether groups on a non-reactive background. Due to time constrains, the antifouling properties of the background layer were not demonstrated for the two-component films.

Combined electrochemical and SEM studies of two-component films revealed that these surfaces contain functional groups that are accessible and reactive. Films containing amine groups were used as tether layers for coupling nitrophenyl derivatives such as *p*-nitrobenzoic acid or *p*-nitrobenzoyl chloride, or for immobilising gold nanoparticles. In the case of NP^{AZ}-TEG films, the NP groups were converted to AP groups by electrochemical reduction, and the AP groups used as a tether layer for coupling *p*-nitrobenzoic acid.

Tethering reactions were demonstrated successfully by reacting *p*-nitrobenzoic hydrazide with surface-bound isothiocyanate groups, and *p*-nitrobenzoic chloride and *p*-nitrobenzoyl chloride with surface bound amine groups. Very small amounts of the *p*-nitrophenyl derivatives were observed on GC surfaces in the absence of films containing isothiocyanate or amine groups, consistent with these reactions having high selectivity. Surface concentrations of electroactive NP groups are always lower for tethered molecules compared to the underlying grafted film, consistent with the coupling reaction occurring only at the outermost layer of the films, due to poor diffusion of solvated molecules through the film.

In the third section of this chapter, a simple and convenient photolithographic method for patterning silicon substrates with AP^{AZ} films was demonstrated. An important advancement is the demonstration of thermal and photochemical grafting of arylazides at silicon surfaces without the need for removal of the native oxide layer prior to grafting. The development of this reaction therefore expands the range of materials and modification

methods available using arylazides. Thermal and photochemical grafting methods are two very different experimental methods, yet gave films with similar film thickness, surface topography, and chemical reactivity. The films formed after reaction for 30 min are multilayered and have a disordered structure, presumably due to significant cross-linking during film growth, and the inhomogeneity of the native surface oxide layer.

Patterned films with lateral features down to 5 μm were achieved, which is smaller than the minimum feature sizes resolved by directly photografting spin-coated arylazides through a photomask. SEM micrographs of patterned AP films after immobilisation of gold nanoparticles confirmed the site-selective immobilisation of gold nanoparticles on film-modified regions.

Modification and patterning of carbon surfaces using aryltriazenes with microfluidic channels

6.1 Introduction

This chapter describes the formation of patterned thin films on PPF using a general strategy that combines microfluidics with aryldiazonium salt chemistry. This research is motivated by the limitations of existing diazonium-based methods for producing high-resolution (< 10 μm feature sizes) film patterns.

Over the past two decades there has been a growing interest in micro and nanoscale patterned molecular films for construction of chemical[375-376] and biosensors,[377-378] and molecular electronics devices[145, 379]. Patterning surfaces with molecular layers is most commonly achieved using alkanethiols and organosilanes on gold and silicon surfaces, respectively[380]. In recent years, many of the procedures used for patterning SAMs have been adapted for patterning using aryldiazonium salt chemistry[144]. The recent surge in interest for patterning diazonium-derived films is due to the stability of the film-substrate attachment and the range of composite surfaces that can be prepared. Methods of patterning using aryldiazonium salt chemistry have been reviewed in Chapter 1.5.

Of the available aryldiazonium salt patterning techniques, soft lithography[67] and photolithography[381] are the most promising candidates for parallel patterning of films with microscale features. Parallel patterning techniques are desirable as they permit rapid patterning of high-density microscale features over large areas ($\geq$ cm^2). Soft lithography is particularly attractive as it is a low cost and versatile approach to patterning; it tolerates a wide variety of materials and solution chemistries. To date, microscale patterning of aryldiazonium salt solutions by soft lithography has been achieved by μCP[67], electro-printing[176], and moulding techniques[177]. Soft lithography has yet to be exploited for

nanoscale patterning of aryldiazonium salts, despite the availability of technologies such as nanocontact printing[382] or edge printing[383]. In addition, much of the research on parallel patterning methods has failed to establish a general strategy that is capable of patterning diazonium salts from both aqueous and non-aqueous conditions, using spontaneous as well as electrografting techniques. For example, the standard photolithographic patterning method developed in Section 5.6 is not amenable to non-aqueous solutions[381].

Microfluidic patterning using laminar flow solutions represents a form of soft lithography yet to be exploited for assembling films at surfaces using diazonium salt solutions[384-385]. This patterning method relies on manipulation of liquid flow streams in a network of microchannels also known as microfluidic networks (μFNs). In recent years, several reactant solutions have been exploited for depositing patterned structures such as SAMs[386], proteins[384], cells[387], polymer fibres[388], ceramics[388], inorganic salts[388], and single-walled CNTs[389]. Careful manipulation of the chemistry of flow streams provides access to a broad range of surface structures, usually having lateral dimensions between 1-200 μm.

In situ generated aryldiazonium salt solutions are excellent candidates for high-resolution patterning, as has recently been demonstrated by Cougnon and co-workers[390]. The main benefit of the *in situ* approach is the ability to form aryldiazonium ions locally by chemical conversion. In recent work by Cougnon and co-workers, aryldiazonium ions were generated locally, using an SECM tip, by diazotisation of an electrogenerated amine in $NaNO_2$ from a nitrophenyl precursor[390]. In contrast, conversion of aryltriazene precursors using acid (HF[391] or HBF_4[392], for example) provides a cleaner and simpler grafting approach; no strong diazotising agents such as $NaNO_2$ or $NOBF_4$ are required during grafting. The main advantage of the aryltriazene approach is that it is well-suited for deposition of films containing diazotization-sensitive functional groups, such as aromatic and aliphatic amines, or ferrocene groups[172].

The aim of this work is to develop an inexpensive parallel patterning strategy for preparing chemically well-defined molecular films at carbon surfaces. The strategy should be compatible with all aryldiazonium salt solutions and permit both spontaneous and electrografting reactions. There are three major objectives of this study: (i) to synthesise and use aryltriazenes as precursors for aryldiazonium salt grafting; (ii) to characterise the physical and chemical properties of the resulting diazonium-derived films; and (iii) to develop laminar flow stream patterning methods.

Section 6.3 describes electrografting and spontaneous grafting methods for preparing tether layers at carbon surfaces by *in situ* generated aryldiazonium solutions via aryltriazenes. In Section 6.4, the formation of patterned films on PPF by electrografting and spontaneous grafting using single flow stream microfluidics is described. Section 6.5 explores the formation of patterned films by spontaneous grafting at PPF using multistream laminar flow patterning.

6.2 Experimental

6.2.1 Surface preparation

GC rod, GC plate, and PPF electrodes were prepared as described in Chapter 2 with the exception that larger PPF surfaces (≈ 23 × 23 mm) were fabricated. Larger PPF surfaces were fabricated to fit the PDMS moulds (≈ 20 × 20 mm). Prior to use, all carbon surfaces were rinsed for 10 s in IPA then dried with a stream of N_2.

6.2.2 Electrochemistry

The geometric working area of GC rod electrodes was 0.07 cm^2 for electrografting and electrochemical characterisation. The geometric working area of GC plate and PPF was 0.29 cm^2 for electrografting and 0.11 cm^2 for electrochemical characterisation, except for microfluidic experiments. For microfluidic patterning, the working electrode area was defined by solution confined within the capillaries of PDMS microchannels.

For standard electrochemical experiments using a pear-shaped or spring-loaded cell (Figure 2.3) SCE reference electrodes were used. A Ag wire reference was used for electrochemical experiments using microfluidic cells (Figure 6.1b). The ferrocene/ferrocenium couple (Fc/Fc^+ in $TBABF_4$-ACN) appeared at $E_{1/2}$ = 0.42 V vs. SCE (3 M LiCl).

6.2.3 Electrochemical and spontaneous modification using standard cells

Aqueous electrografting in a standard pear-shaped or spring-loaded cell was performed using AMP_D prepared *in situ* from AMP_{DMT} in Milli-Q water. To prepare AMP_D solutions, HBF_4 (0.1 M final solution concentration) was added to 2 mM AMP_{DMT} in Milli-Q water and the reaction allowed to proceed for 2 min with stirring. Sonication was used to aid solubilisation of AMP_{DMT} (5 min at 40 ºC) prior to addition of acid. Electrografting was achieved by recording five consecutive CVs from 0.5 to -1.4 V vs. SCE (sat. KCl).

Non-aqueous electrografting in a standard pear-shaped cell was performed using AMP_D or CP_D prepared *in situ* in acidic ACN (0.1 M HBF_4). To prepare AMP_D or CP_D solutions, HBF_4 (0.1 M final solution concentration) was added to 4 mM AMP_{DMT} or CP_{DMT} in ACN and the reaction allowed to proceed for 2 min with stirring. Note that sonication was used to aid solubilisation of AMP_{DMT} (5 min at 25 ºC) prior to addition of acid. Electrografting was achieved by recording five consecutive CVs from 0.5 to -1.1 V (AMP_D solution) or 0.5 to -1.2 V (CP_D solution) vs. SCE (LiCl).

Spontaneous grafting was performed at room temperature for 30 min in a solution of AMP_D, prepared *in situ* from AMP_{DMT} in Milli-Q water as described above.

After modification, all surfaces were rinsed copiously with Milli-Q water and ACN, sonicated for 60 s in ACN, rinsed with IPA, and dried under a stream of N_2.

6.2.4 Electrochemical modification using a microfluidic cell

Aqueous and non-aqueous electrografting using a microfluidic cell was performed using AMP_D solutions prepared as described in Section 6.2.3. After filling of the microfluidic channels with AMP_D solution, two consecutive CVs from 0.4 to -2.1 V (aqueous grafting) or 0.4 to -2.0 V (non-aqueous electrografting) vs. Ag wire were performed, followed by constant potential grafting for 300 s at -2.0 V. To minimise spontaneous grafting, electrochemical modification was conducted immediately (within 5 s) after submerging the electrodes in aryldiazonium salt solution.

After electrochemical modification, all surfaces were rinsed copiously with Milli-Q water and ACN, sonicated for 60 s in ACN (unless stated otherwise), rinsed with IPA, and dried under a stream of N_2.

6.2.5 Spontaneous modification using a microfluidic cell

Unless stated otherwise, surface modification by spontaneous grafting was performed at room temperature in a solution of AMP_D, prepared *in situ* in Milli-Q water as described in Section 6.2.3. The grafting time was 30 min for single flow experiments and ranged from 2 to 60 min for multistream flow experiments. After modification, all surfaces were rinsed copiously with Milli-Q water and ACN, sonicated for 60 s in ACN (unless stated otherwise), rinsed with IPA, and dried under a stream of N_2.

6.2.6 Microfluidic device fabrication and surface patterning

The procedure for preparation of the microfluidic patterning device, and subsequent grafting of a patterned molecular film at PPF, is shown in Scheme 6.1. The microchannels were fabricated using photolithography and replica moulding in PDMS[393]. First, the photomask and 4" silicon wafers were rinsed with IPA and dried with N_2. Any remaining surface contamination was removed using an Emitech K1050X plasma asher for 10 min at 100W RF. Immediately after cleaning, patterns were transferred into SU-8 by UV exposure and subsequent development. After rinsing with IPA and drying with N_2, the patterned moulds were treated with TMCS to facilitate removal of cured PDMS. Next, the PDMS monomer mixture was treated with the cross-linker in a weight ratio of 10:1 (base/curing agent). The resulting polymer mix was thoroughly degassed, then cast onto the patterned photoresist / silicon wafer. The PDMS was cured at 80 ºC for 3 h on a hotplate. After curing, the PDMS microchannels were cut into ≈ 23 × 23 × 6-7 mm slabs. Prior to use, microchannels were cored to give inlet and outlet holes using a biopsy punch (Stiefel). Dr V. Nock provided assistance with the preparation of PDMS microchannels.

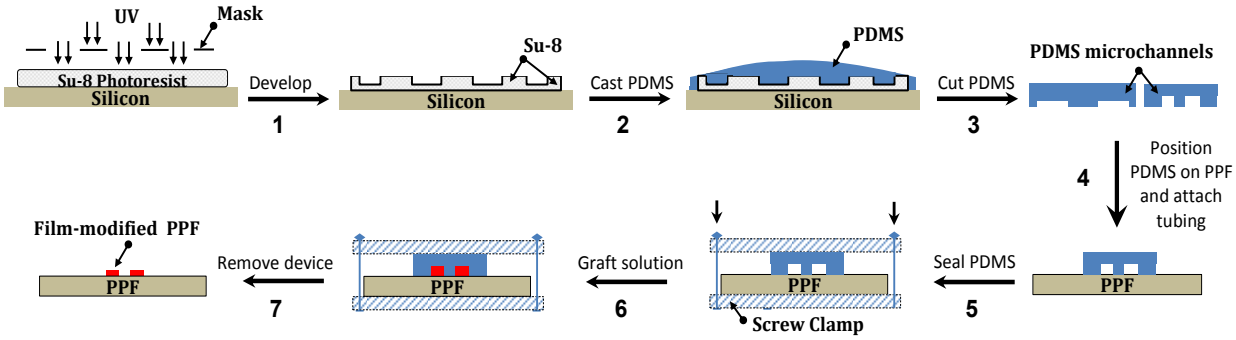

Scheme 6.1 Procedure for microfluidic device fabrication and subsequent patterning of molecular films at PPF.

Patterned films were prepared by positioning and clamping the PDMS microchannels onto a PPF substrate and introducing solution streams into the capillaries by controlled flow. Flow control was achieved using a Sage M362 syringe pump (Thermo Orion) with either one or two 5 mL syringes attached.

The microfluidic device configurations used for grafting are shown in Figure 6.1. Spontaneous grafting was achieved using a single stream flow device (Figure 6.1a) or a multistream flow device (Figure 6.1c). For electrografting, the single stream flow device (Figure 6.1b) was used. This consisted of a three-electrode cell, a plastic base plate (to prevent shorting), home-made copper crimps (to prevent leaking), and ACN-compatible materials for non-aqueous experiments. The latter included fluorinated ethylene propylene-lined tubing (Tygon SE-200, Cole Parmer), polyvinylidene fluoride fittings (PVDF and Kynar®), and glass syringes with a polytetrafluoroethylene (PTFE) luer lock.

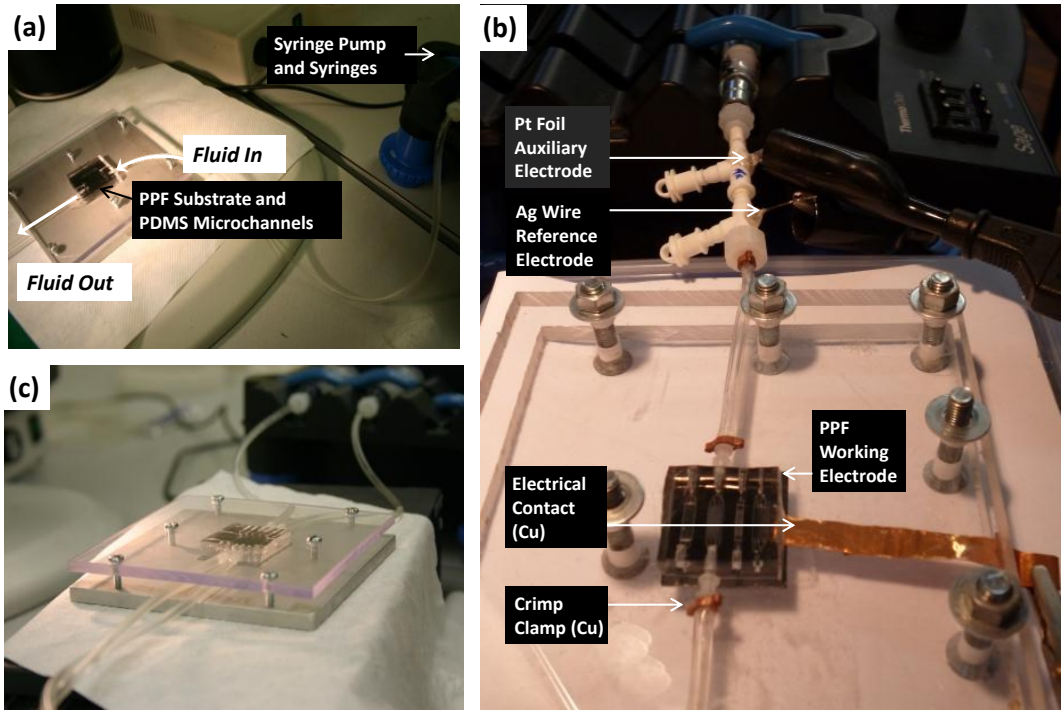

Figure 6.1 Microfluidic patterning devices: (a) single stream spontaneous grafting; (b) single stream electrografting; and (c) multistream spontaneous grafting.

6.2.7 Immobilisation of gold nanoparticles and electroless gold plating

Gold nanoparticles with an average diameter of ≈ 25 nm[198] were assembled on modified surfaces by immersion in the as-prepared nanoparticle solution, with gentle stirring. Immersion times were 180 min and 90 min for GC and PPF, respectively. After preparation, surfaces were rinsed thoroughly with Milli-Q water then dried with a stream of N_2, unless otherwise stated.

Electroless gold plating was achieved using the method of Hu and co-workers[394]. After immobilisation of gold nanoparticles at *p*-(aminomethyl)phenyl (AMP) modified GC, samples were immersed in an aqueous solution containing 10 mL of $HAuCl_4$ (0.01%) and 500 µL of H_2O_2 (30%) for 8 min, with stirring. After plating, surfaces were rinsed with water and dried with N_2 before imaging by optical microscopy.

6.3 Modification of GC and PPF using aryltriazenes in a standard electrochemical cell

Surface modification of GC and PPF surfaces with AMP and CP functionalities was explored using aryltriazenes as precursors for aryldiazonium salts. The dimethyltriazene moiety was employed specifically as a selective protecting group for the aryldiazonium functionality. The target *para*-substituted phenyl derivatives, containing a diazonium salt on one end, and either a carboxy or a methylamine functionality on the other end, are illustrated in Figure 6.2. The diazonium functionality permits direct surface attachment and the *para* substituents were selected as useful tethering groups. The modification strategy used in this chapter is represented in Scheme 6.2.

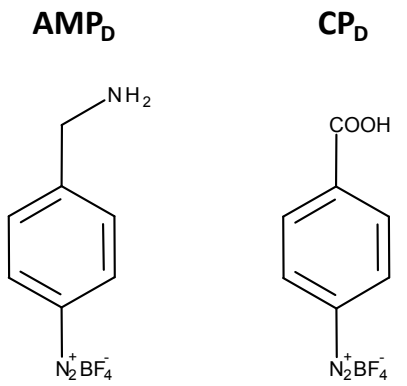

Figure 6.2 *Para*-substituted aryldiazonium salts, AMP_D and CP_D, used to graft AMP and CP films at carbon surfaces.

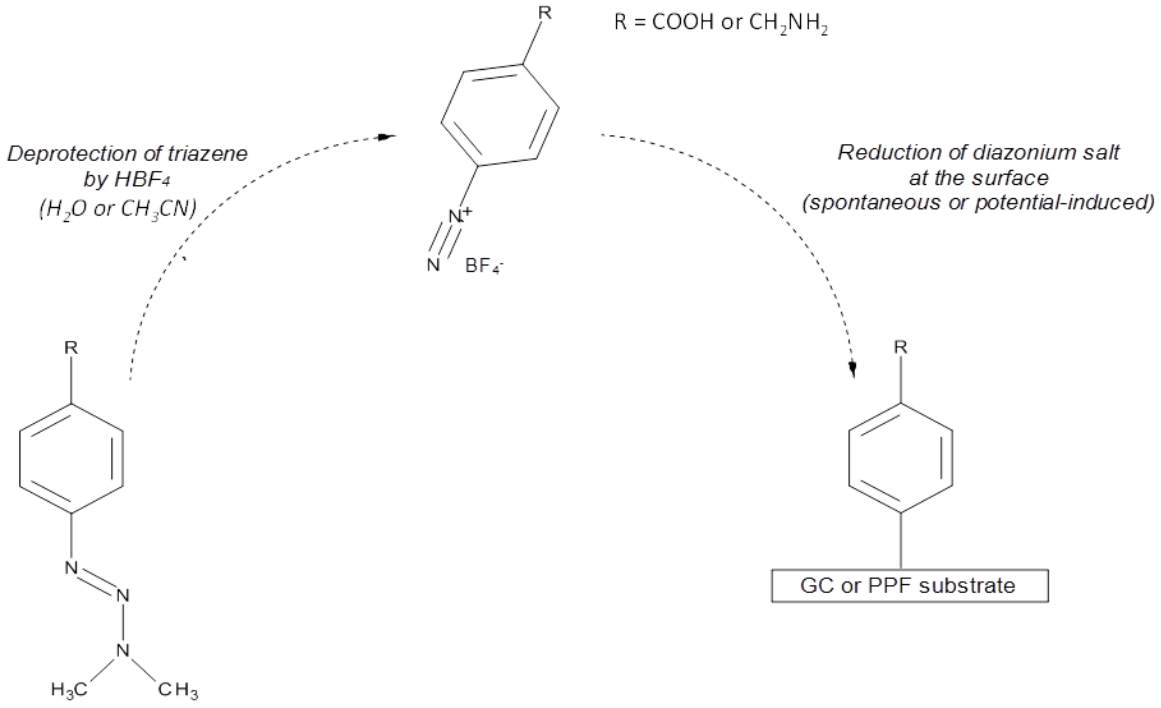

Scheme 6.2 Stepwise reaction scheme for modification of carbon surfaces via *in situ* generated aryldiazonium salts prepared via deprotection of aryltriazenes.

In this section of work, aryldiazonium ions were generated in the bulk solution by addition of HBF_4 to the aryltriazene precursor solution. Grafting of the *in situ* generated aryldiazonium salt solutions, and the characteristics of the resulting films, are described below.

6.3.1 Electroreduction of AMP_D and CP_D at GC and PPF in ACN solution

The electrochemical reduction of *in situ* generated aryldiazonium salts, AMP_D and CP_D, was investigated at GC and PPF surfaces. In preliminary experiments, the conditions necessary for generation of aryldiazonium salt solutions via deprotection of aryltriazenes (AMP_{DMT} or CP_{DMT}) were established. Deprotection of aryltriazenes was achieved with HBF_4 (Section 6.2.3), using a similar approach to that reported by Tour and co-workers[275].

Electrochemical modification of carbon surfaces using *in situ* generated aryldiazonium salt (4 mM) was investigated in acidic ACN (ACN containing 0.1 M HBF_4) with 0.1 M $TBABF_4$ added as an additional supporting electrolyte. The grafting solutions were prepared by deprotection of the aryltriazene precursor using the method described in Section 6.2.3. Figure 6.3a and Figure 6.3b show the electrochemical reduction of AMP_D at GC and PPF, respectively. Figure 6.3c shows the electrochemical reduction of CP_D at PPF. The blank experiment corresponding to electrochemical reduction of AMP_{DMT} at GC, in the absence of HBF_4, is shown in Figure 6.3d. The cyclic voltammetry of AMP_D and CP_D in acidic ACN is typical of that observed for *para*-substituted aryldiazonium ions in ACN solutions, prepared either *in situ* from the amine precursor[212, 244, 358, 395-396], or from the isolated salt [66, 397]. On the first cycle in the cathodic direction, a broad and irreversible reduction peak is observed, which disappears on the second or third, and subsequent scans, due to the formation of a strongly passivating film. Five consecutive CVs were recorded for grafting. Figure 6.3d provides compelling evidence that addition of HBF_4 is necessary for *in situ* generation of aryldiazonium salt from aryltriazene solutions; no reduction peak is observed at GC when cycling AMP_{DMT} in acidic ACN with supporting electrolyte. The mechanism and details associated with the formation of diazonium-derived films at carbon surfaces has been described in detail in Chapter 1.

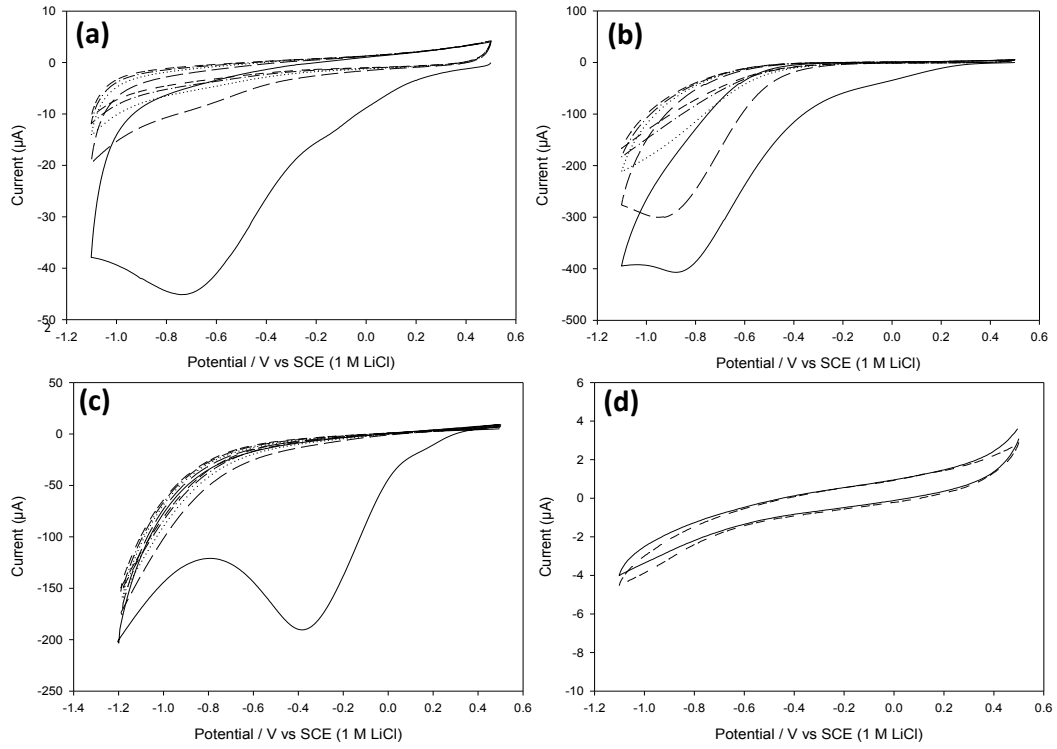

Figure 6.3 Consecutive CVs of (a, b) AMP_D and (c) CP_D at carbon surfaces in acidic ACN (0.1 M HBF_4) with 0.1 M $TBABF_4$: (a) AMP_D at GC rod; (b) AMP_D at PPF; (c) CP_D at PPF. (d) First two CVs at GC rod of 4 mM AMP_{DMT} in ACN with 0.1 M $TBABF_4$.

It is widely accepted that the chemical reactivity of GC and PPF surfaces towards modification by diazonium salts in ACN is similar. Consequently, PPF is often used as a model GC surface for diazonium-derived film studies[65, 107, 136]. The variation observed between GC and PPF in this work is consistent with the variation reported by others[358], nevertheless, some differences between GC and PPF are observed and deserve further comment. Firstly, the peak potential corresponding to diazonium ion reduction shifts to more negative potentials at PPF surfaces relative to GC: E_{pc} of AMP_D ≈ -0.75 V and ≈ -0.85 V at GC and PPF surfaces, respectively. Secondly, the rate at which the reduction current decreased on the second and third scans for grafting of AMP_D was slower at PPF compared to GC. This observation suggests that film growth is more gradual at PPF, or alternatively, that the films formed at PPF have different blocking properties to those

formed at GC[398]. The observed peak potential shift towards a more negative potential, and the apparent slower rate of grafting, is consistent with slower electron transfer kinetics at these PPF surfaces compared to GC surfaces[64].

6.3.2 Electroreduction of AMP_D at GC and PPF in aqueous solution

Electrochemical modification of GC and PPF surfaces using aryltriazene precursors was also explored under aqueous conditions. The development of grafting methods in aqueous media expands the range of films that can be prepared. Additionally, aqueous solutions are easier to handle and more chemically compatible with standard PDMS microfluidics apparatus compared to ACN or DMF. To demonstrate grafting in aqueous media the AMP_{DMT} precursor was employed. The aqueous electrografting method was adapted from the general procedure used for ACN grafting. Lower concentrations of aryltriazene solutions were prepared due to the lower solubility of AMP_{DMT} in Milli-Q water, a wider scan range was employed, and the standard aqueous SCE (sat. KCl) was used as the reference electrode.

Figure 6.4 shows the electrochemical reduction of 2 mM AMP_D in aqueous solution at GC and PPF surfaces using five CV scans. For both types of electrode, the first CV exhibits a broad reduction peak, which disappears on the second or third, and subsequent cycles. The cyclic voltammetry observed here is consistent with the grafting CVs observed in ACN (Figure 6.3) and is typical of the aqueous grafting behaviour reported by others for *para*-substituted aryldiazonium salts[212, 399]. On this evidence, it is assumed that molecular films have been successfully deposited via the potential-induced mechanism of film formation shown in Scheme 6.2.

A comparison of the first scan CVs obtained for AMP_D grafting in aqueous and acidic ACN solutions reveals that the onset of diazonium reduction is medium dependent, occurring at more negative potentials in aqueous acidic solution. The peak potential

differences were ≈ 150 mV and ≈ 250 mV at GC and PPF surfaces, respectively (using SCE and non-aqueous SCE reference electrodes having the same potential). The observed peak shifts are attributed to differences in solvent and/or electrolyte reorganisation around the reactant. This explanation is consistent with stabilisation of the aryldiazonium ion by hydration, which is expected to give a more negative reduction potential in aqueous medium. It is noted that solvent dependant shifts in peak potential have been reported previously for grafting CP_D in aqueous and non-aqueous solutions[244].

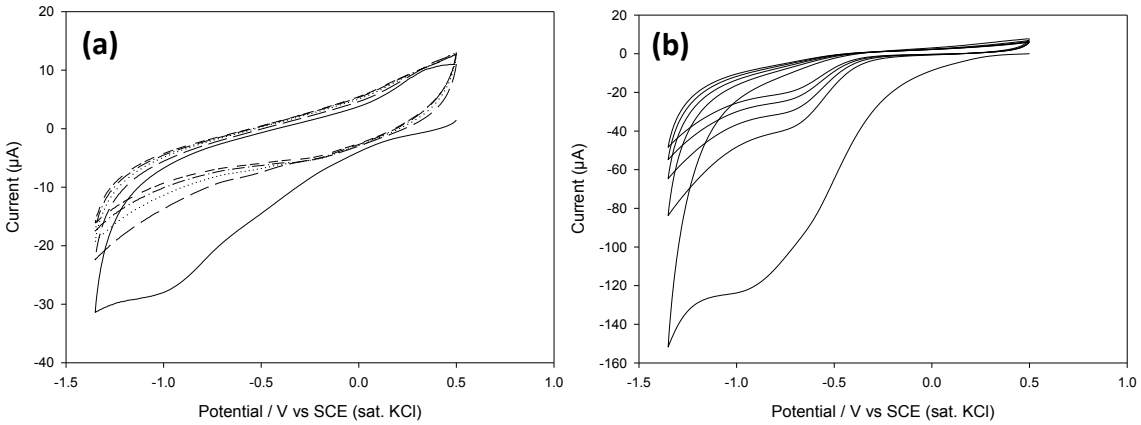

Figure 6.4 Consecutive CVs of AMP_D at (a) GC rod and (b) PPF in aqueous solution with 0.1 M HBF_4.

6.3.3 Electrooxidation of AMP films at GC

The electroactivity of AMP films at GC surfaces was examined using cyclic voltammetry. The main goal of these studies was to confirm the successful attachment of AMP groups following electrografting via AMP_{DMT}. Aliphatic amine groups are electroactive in solution and hence it was assumed that surface-attached amines could be electroactive.

Electrochemical oxidation of AMP modified GC was investigated in ACN with 0.1 M $TBABF_4$ (Figure 6.5a and Figure 6.5b), or 0.1 M H_2SO_4 (Figure 6.5c). On the first scan in ACN solution a broad and irreversible peak at $E_{pc} \approx 1.2$ V is observed, which disappears on

the second scan. This oxidation process was observed for AMP films prepared by electrografting in either aqueous or ACN solutions. The oxidation peak at $E_{pa} \approx 1.2$ V is consistent with that observed for oxidation of primary alkyl amines in DMF at GC (E_{pa} = 1.36 V to 1.51 V vs. SCE for alkyl amines and nitrobenzylamines[110]). The shift in peak potential is attributed to the different solvents and to differences between surface-bound amines and amines in solution. The irreversible oxidation peak can be explained on the basis of the mechanistic studies by Mann and others[110, 400-401]. According to the proposed mechanisms, the primary amine loses one electron to produce a radical cation. After formation, the radical cation either splits into a carbonium ion and amidogen radical, or undergoes deprotonation and further electron transfer to yield an iminium cation. Several electrochemical and chemical steps are therefore possible, giving rise to a variety of reaction products, including thin films as well as solution species[95, 400, 402].

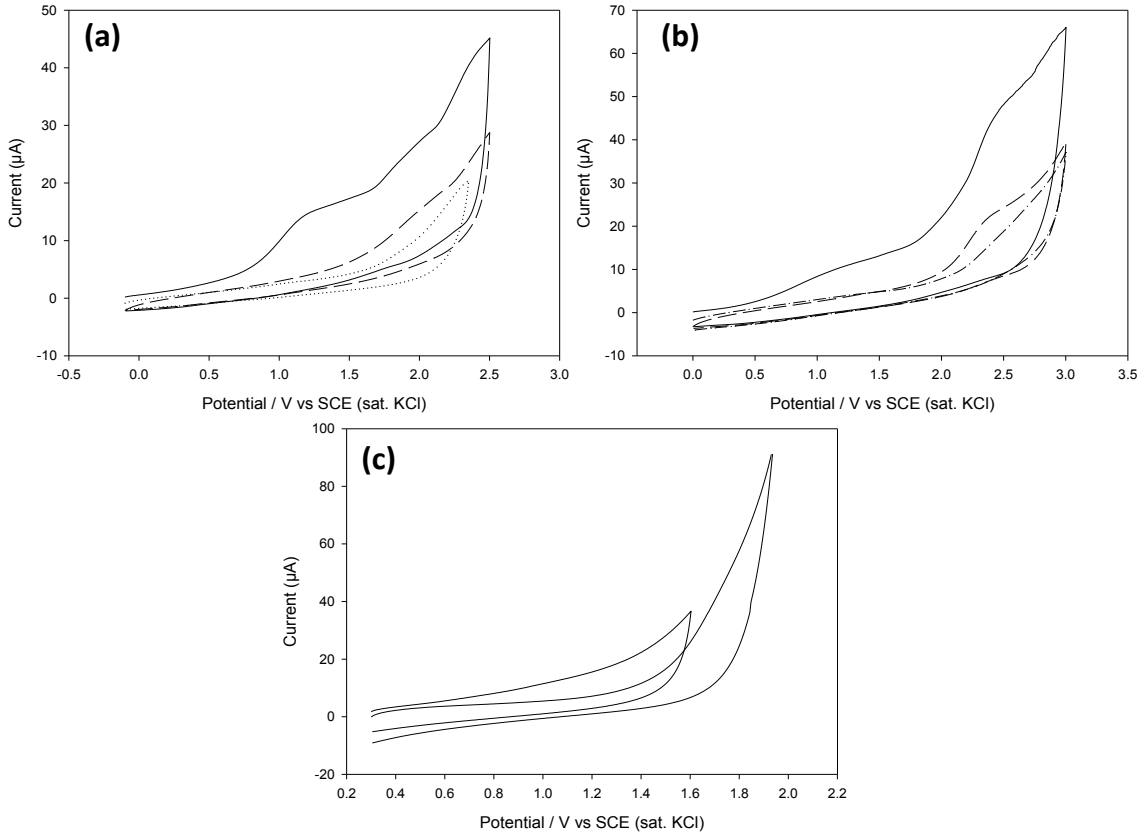

Figure 6.5 Consecutive CVs of AMP-modified GC rod in (a, b) ACN with 0.1 M $TBABF_4$ and (c) 0.1 M H_2SO_4. Films were prepared by (a, c) ACN and (b) aqueous electrografting.

The origin of the oxidation waves at potentials more positive than 1.75 V was not investigated. However, the peaks are attributed, at least in part, to by-products from reactions of radical cations formed during the first oxidation step. Further analysis of the electrochemical oxidation behaviour of AMP films reveals that the oxidation peak at $E_{pa} \approx$ 1.2 V is broader for films grafted in aqueous media than those grafted in ACN media. Diazonium-derived films prepared in aqueous conditions are known to be more compact and less-permeable to solvent than those prepared in ACN[65]. Hence the broader oxidation peaks are attributed to slower diffusion of solvent and ions through the films prepared by aqueous grafting. It is also possible that films grafted from aqueous solutions are more disordered and contain electroactive AMP groups in a wider range of environments, compared to thin films grafted from ACN solutions.

Figure 6.5c shows consecutive voltammograms of an AMP modified GC surface in 0.1 M H_2SO_4. The absence of oxidation waves confirms that the modified surface has a negligible concentration of electroactive groups in this medium. The absence of electroactivity is due to protonation of the alkyl amine groups; protonated amine groups, without the lone pair, cannot be oxidised[110, 403]. The AMP film should be fully protonated in 0.1 M H_2SO_4 (pK_a = 10 for AMP films[212]). It is important to point out that contrasting behaviour is observed for diazonium-derived films containing arylamine groups. For AP films, the arylamine groups were found to be electroactive in 0.1 M H_2SO_4 at GC surfaces[404-405]. The electroactivity observed in that work is presumably due to the presence of unprotonated aromatic amine groups at the surface.

The electrochemical investigations into AMP films at GC confirm the successful deposition of (aminomethyl)phenyl groups at GC via electrografting of AMP_D. Surface-bound primary amine groups are chemically well-defined and are accessible for further reactions, based on their ability to be oxidised or protonated, in ACN or acidic solution, respectively. On this evidence, functional and chemically well-defined films can be

prepared from either aqueous or ACN solutions using potential-induced grafting via aryltriazenes.

6.3.4 Atomic force microscopy of AMP films at PPF

AFM in tapping-mode was used to examine the effect of film deposition on the topography of PPF surfaces before and after modification with an AMP film. For this investigation, films were prepared by electrografting and spontaneous grafting of AMP_D using standard procedures as described in Section 6.2.3. AFM depth-profiling investigations were also performed on AMP Films at PPF surfaces and are reported and discussed in section 6.4.3.

Figure 6.6 shows 2.5 × 2.5 μm AFM images of three PPF surfaces before and after grafting. The topographical images reveal that films formed by electrografting and spontaneous grafting of AMP_D are clean and closely follow the topography of the smooth underlying PPF substrate[64]. The images illustrate that PPF surfaces underwent very small changes on grafting, similar to those previously reported for electrografted diazonium-derived films on PPF[406].

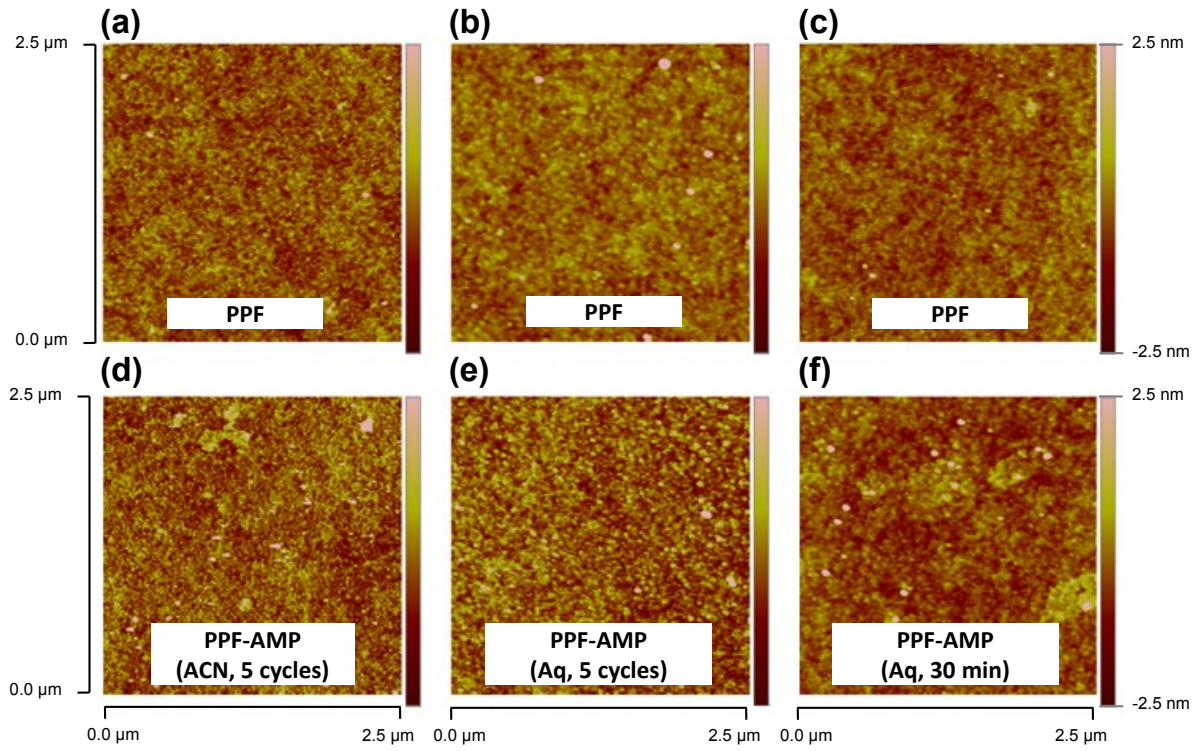

Figure 6.6 Tapping-mode AFM images of three PPF surfaces: (a-c) before and (d-f) after grafting AMP_D. Film-modified surfaces: (d) film electrografted in ACN solution; (e) electrografted in aqueous solution; and (f) spontaneously grafted in aqueous solution. Paired AFM images were taken from near identical regions: (a) and (d); (b) and (e); and (c) and (f).

To further characterise surface modification, and to gain new insight into the nanoscale structuring of AMP films, surface roughness measurements corresponding to the AFM images in Figure 6.6 were calculated using Nanoscope Analysis software. Both the arithmetic (R_a) and geometric (R_q) average roughness measurements were considered. The data in Table 6.1 highlights a common trend: an increase in average roughness following grafting. The significance of the trend was validated by testing the null hypothesis that surface modification does not change the surface roughness of PPF. The mean and pooled standard deviations were calculated from the R_a values for the two conditions: before and after grafting. Since three measurements for each condition were used (4 df in total), the critical value t = 2.78 (P = 0.05)[407]. The experimental value calculated for the statistic |t| was 3.42, hence the difference between the two means tested is significant at the 5% level.

Thus the null hypothesis is rejected. In other words, the deposition of AMP films at PPF leads to a statistically significant increase in surface roughness. Together, the qualitative image analysis and the quantitative surface roughness analysis confirm changes upon modification, consistent with grafting of smooth and homogeneous molecular films at PPF.

Table 6.1 Surface roughness values for PPF surfaces before and after modification with AMP films.

Grafting method	Surface roughness calculation method	Surface roughness (nm) before graft[a]	Surface roughness (nm) after graft[a]
Electrograft (non-aqueous)	R_a	0.34	0.52
	R_q	0.27	0.34
Electrograft (aqueous)	R_a	0.50	0.61
	R_q	0.28	0.47
Spontaneous (aqueous)	R_a	0.44	0.64
	R_q	0.34	0.46

[a] Surface roughness measurements were calculated from 2.5 × 2.5 μm regions.

6.3.5 Immobilisation of gold nanoparticles on AMP films at GC

An important goal of this work is the development of methods for deposition of molecular films with well-defined physical and chemical properties. Using a similar approach to that reported in Section 5.4.1 for films containing AP groups, the reactivity of AMP films towards citrate-capped gold nanoparticles was investigated. For AMP films, the immobilisation is assumed to occur through the electrostatic interaction of negatively charged gold nanoparticles with protonated aliphatic amine groups present at the film-modified surface. To improve visualisation, and to demonstrate the ability to form bulk gold electrodes, an electroless gold plating method was also implemented. Gold plated electrodes act as highly efficient contrast agents for optical microscopy, which facilitates imaging of selectively modified regions of surfaces.

After electrografting AMP_D from ACN media using standard procedures, modified surfaces were immersed in a solution of citrate-capped gold nanoparticles (pH ≈ 5) for 180

min. After immersion, the samples were sonicated for 15 s in Milli-Q water and dried with a stream of N_2. Figure 6.7a shows an optical micrograph of a boundary region of the film-modified GC plate after reaction with gold nanoparticle solution, and subsequent electroless plating. Figure 6.7b shows a graphic illustrating the reaction scheme, highlighting the regions of the surface that were modified then imaged. The optical micrograph reveals the presence of a high loading of gold, which indirectly confirms that a high density of gold nanoparticles were immobilised in the film-modified region. In contrast, little or no gold was observed in the unmodified region that was exposed to gold nanoparticle and subjected to electroless plating. Therefore, the AMP films provide excellent selectivity towards citrate-capped gold nanoparticles, which is consistent with the specific interaction of negatively charged nanoparticles with protonated aliphatic amine groups.

In this study, film-modified GC surfaces with citrate-capped gold nanoparticles assembled surfaces were not used for sensor applications. However, the work by Cruickshank and Downard demonstrates how the system developed here could be used for chemical sensing of hydrogen peroxide by electrochemical oxidation[108].

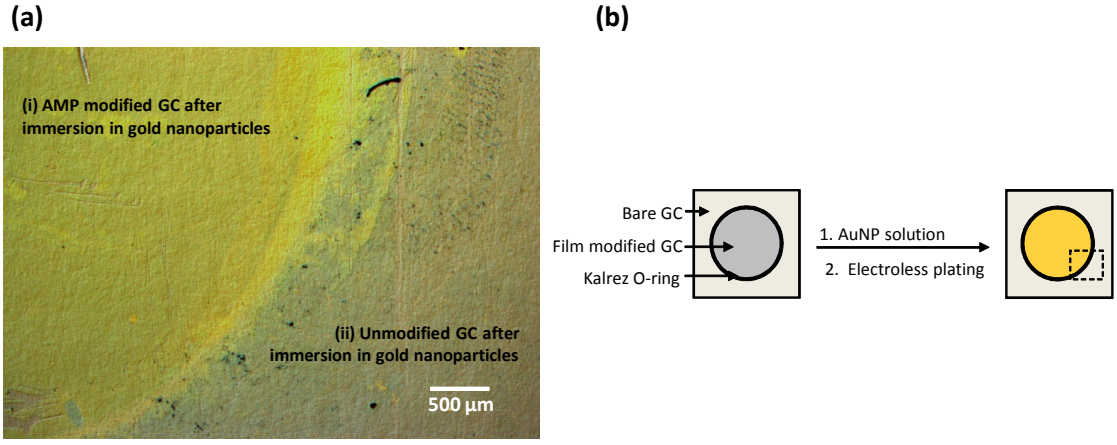

Figure 6.7 (a) Optical micrograph of an AMP modified GC surface after immobilisation of citrate-capped gold nanoparticles and electroless plating of gold: (i) film-modified region and (ii) unmodified region. (b) Graphic illustrating the reaction scheme and the region of the surface that was imaged.

6.4 Single flow patterning of AMP films at PPF

Use of microfluidic systems with aryldiazonium salt solutions permits parallel patterning of films on surfaces with micro and nanoscale resolution. The introduction of a single stream of AMP_D solution into PDMS microchannels enables localised grafting in pre-defined patterns. The work described here represents a comprehensive extension to the PDMS microchannels patterning method reported by Tan and co-workers[177]. Here, PDMS microchannels were integrated with microfluidics and thus laminar flow streams were exploited.

PPF was chosen as the carbon substrate for investigating microfluidic patterning for a number of reasons: PPF surfaces form a reversible seal with PDMS surfaces; PPF can be custom-sized to fit PDMS channel moulds, and PPF is an excellent substrate for high-resolution micro and nanoscale imaging. Modification of PPF surfaces using PDMS microchannels was performed via aqueous or ACN solutions of AMP_{DMT}. Both spontaneous and electrografting methods were investigated. In all of the experiments described in Section 6.4, the aryldiazonium salt solution was generated in the bulk solution by mixing aryltriazene with HBF_4. The AMP_D solution was then introduced into the PDMS microchannels.

6.4.1 Spontaneous grafting of AMP_D at PPF in aqueous solution

Microfluidic patterning of PPF surfaces with diazonium-derived films was investigated by spontaneous grafting in aqueous solution. Patterning was achieved by sealing the PDMS microchannels against a PPF surface, then filling the capillaries with diazonium grafting solution under laminar flow. After the capillaries were completely and homogeneously filled, the grafting solution was allowed to react at the surface of the substrate. The grafting solutions were prepared using the HBF_4 method described in Section 6.2.3. For single flow patterning, grafting was performed either under continuous flow, or in the absence of flow

(under static conditions). Filling of the channels was achieved within a few seconds and thus fresh grafting solution was introduced at the PPF surface. After modification, the elastomeric μFN was peeled away from the PPF substrate under the flow of Milli-Q water, to dilute and rinse away the grafting solution; this procedure minimised undesired grafting reactions. The set-up used for single stream microfluidic patterning, with spontaneous reaction of AMP_D in aqueous solution, is shown in Figure 6.1a.

Deposition of patterned AMP films was typically achieved by introducing freshly-prepared AMP_D solution across a PPF surface and grafting under continuous flow conditions for 30 min (flow rate ≈ 0.5 mL/min). Blank samples were prepared in an identical manner, with the exception that AMP_{DMT} solution (2 mM) was introduced into the channels in place of AMP_D solution. After modification, rinsing, and drying as described in Section 6.2.5, patterned samples and blanks were visualised by SEM (Figure 6.8). The contrast observed in the SEM micrograph (Figure 6.8a) is consistent with the deposition of a film in the region exposed to AMP_D solution. In comparison, no contrast was observed for the blank surfaces that had been exposed to aryltriazene solution for the same length of time (Figure 6.8b), except for the faint lines observed around the edge of the pattern. The faint line is attributed to an accumulation of PDMS residues and insoluble particulates at the wall of the PDMS microchannels during grafting. Similar, but considerably more pronounced residues, were observed by others when printing μCP using PDMS inked with aqueous acidic aryldiazonium salt solutions[175]. The excellent pattern contrast in Figure 6.8a compared to Figure 6.8b confirms that aryldiazonium ions are responsible for surface modification. Furthermore, the observed contrast in the patterned region is continuous across the length of the pattern, consistent with complete wetting of the surface, and deposition of a homogeneous thin-film coating.

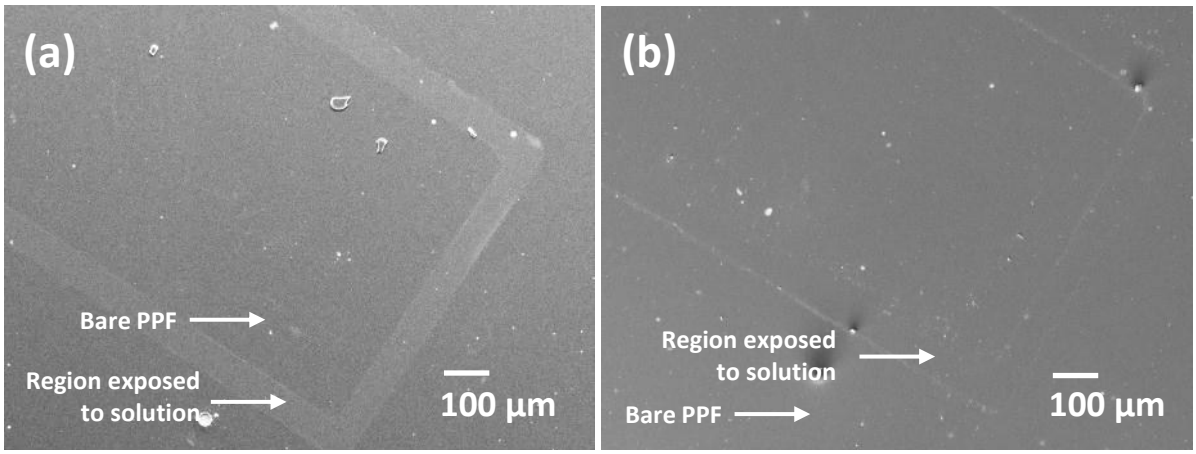

Figure 6.8 SEM micrographs of PPF surfaces patterned by reaction of AMP_D (a) and AMP_{DMT} (b) solutions under flow inside PDMS microchannels. Reaction time = 30 min.

Patterning of AMP films at PPF using the single stream flow device was also demonstrated by spontaneous grafting under static condition. For this approach, PDMS microchannels sealed to PPF were filled with AMP_D solution under laminar flow. After filling was complete, the flow was stopped, and the grafting solution was allowed to react for 30 min under static conditions. Figure 6.9 shows water condensation figures (optical micrographs) of PPF samples patterned by static grafting of AMP_D. High pattern contrast is observed arising from differences in the water droplets formed on the unmodified and modified regions. The observed difference in wettability is consistent with surface modification giving a different surface free energy than that of unmodified PPF.

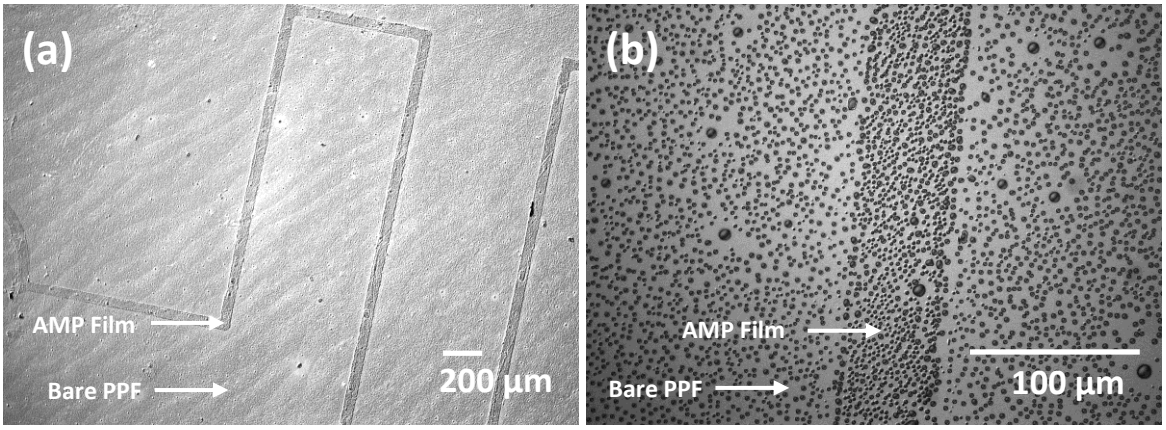

Figure 6.9 Condensation figures of PPF surfaces patterned by reaction of AMP_D under static conditions inside PDMS microchannels. Images were recorded at 5× (a) and 20× (b) magnification. Reaction time = 30 min.

For both static and flow patterned surfaces, line widths with feature sizes between 60 µm and a few centimetres were easily achieved. "Complete" and homogeneous pattern transfers were obtained for all of the samples prepared using this approach. Furthermore, a number of patterned surfaces were generated (at least five separate samples) to confirm reproducibility of the single flow stream patterning approach. The ability to form complete and homogeneous pattern transfers is a notable advantage of this patterning technique compared to other techniques such as µCP and electro-printing. For the printing techniques, problems associated with inking and applied pressure during stamping limit the homogeneity of a complete pattern transfer.

6.4.2 Electroreduction of AMP_D at PPF in ACN solution within microchannels

The single flow stream patterning approach was expanded to enable grafting from non-aqueous solutions. In this work, a three-electrode microfluidic cell was developed (Figure 6.1b) for electrografting patterned films. Spontaneous grafting of AMP_D was not explored, on the basis of reports by Lehr and co-workers, who demonstrated that spontaneous

grafting of even "easy-to-reduce" aryldiazonium salts does not occur to an appreciable extent in ACN at PPF[67, 408].

The viability of the microfluidic cell set-up was evaluated by recording consecutive CVs of 5 mM $K_3Fe(CN)_6$ and comparing the CVs to those obtained using the standard three-electrode cell set-up (Figure 2.3a). CVs of $Fe(CN)_6^{3-}$ at PPF surfaces using the different electrochemical set-ups are illustrated in Figure 6.10a. The suitability of the microfluidic cell set-up was confirmed through observation of the chemically reversible $Fe(CN)_6^{3-/4-}$ redox couple. The ΔE_p of ≈ 3000 mV (Figure 6.10a, i) was very large relative to that routinely observed using a standard experimental design (Figure 6.10a, ii). The high ΔE_p value reveals that the solution resistance, and hence the uncompensated potential drop between the working and reference electrode, was large. This is attributed to non-optimised experimental design giving a large distance (≈ 10 cm) between the working and reference electrodes. Consequently, use of the microfluidic cell set-up incurs significant potential control errors. Nevertheless, the electrochemical cell was used for exploration of aryldiazonium salt electrografting reactions inside PDMS microchannels.

The standard modification procedure described in Section 6.2.4 was used for patterned electrografting of AMP_D at PPF in PDMS microchannels. In brief, three consecutive CVs were recorded between 0.4 V and -2.0 V, followed by fixed potential electrolysis at -2.0 V (vs. Ag wire) for 300 s. Grafting was performed under static solution conditions, after the PDMS capillaries were completely and homogeneously filled with aryldiazonium salt solution. Figure 6.10b shows consecutive grafting CVs corresponding to electrochemical reduction of AMP_D, obtained using the three-electrode microfluidic cell. The broad and irreversible reduction peak at E_{pc} ≈ - 1.5 V (vs. Ag wire) on the first scan is consistent with grafting of AMP_D in ACN solution (Figure 6.3b). The differences in the apparent diazonium reduction potential between Figure 6.3b and Figure 6.10b were anticipated and are the consequence of uncompensated solution resistance. Due to the possibility that

insufficient potential was applied to induce electrografting, fixed potential electrolysis at high cathodic potential (-2.0 V vs. Ag wire) was applied for 300 s.

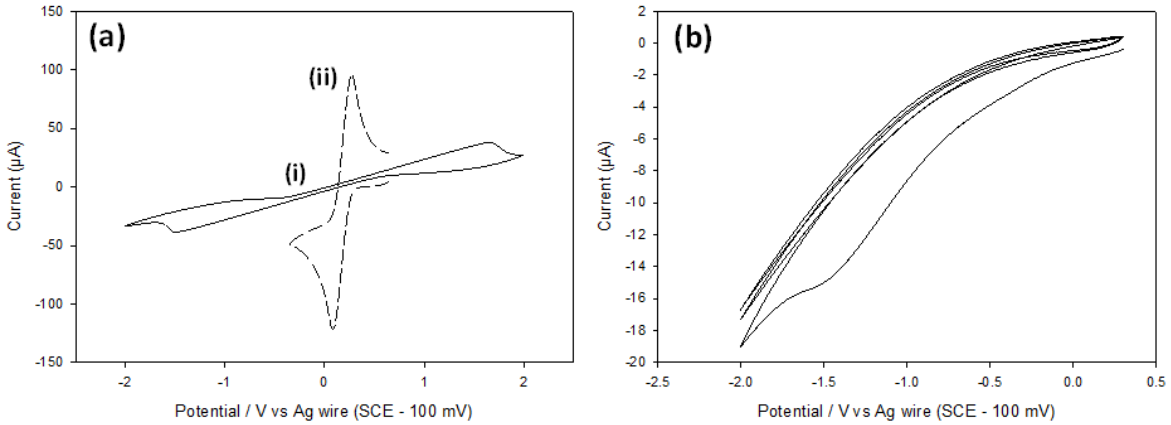

Figure 6.10 (a) Example CVs of $K_3Fe(CN)_6$ at pristine PPF recorded using (i) microfluidic three-electrode cell and (ii) conventional three-electrode cell. (b) First three grafting CVs of *in situ* generated AMP_D in acidic ACN at PPF inside PDMS microchannels.

After removal of the elastomeric microchannels, and subsequent rinsing and sonication cleaning using standard conditions (6.2.4), film-modified surfaces were dried and analysed using condensation figures. Figure 6.11 shows a digital image (a) and optical micrographs (b, c) of patterned AMP films on a PPF surface, after water droplets were condensed onto the surface. Patterning was successful using the ACN-based electrografting method, as illustrated by the significant differences in wettability between the modified (AMP film) and unmodified (bare PPF) regions. The digital image and optical micrographs confirm that large areas of the surface can be patterned (up to 1-2 cm) with isolated features, and that multiple line arrays can be generated in short reaction times (the total reaction time was less than 10 min). The simplicity and speed of patterning illustrated here confirms the potential for high-throughput patterning using this approach.

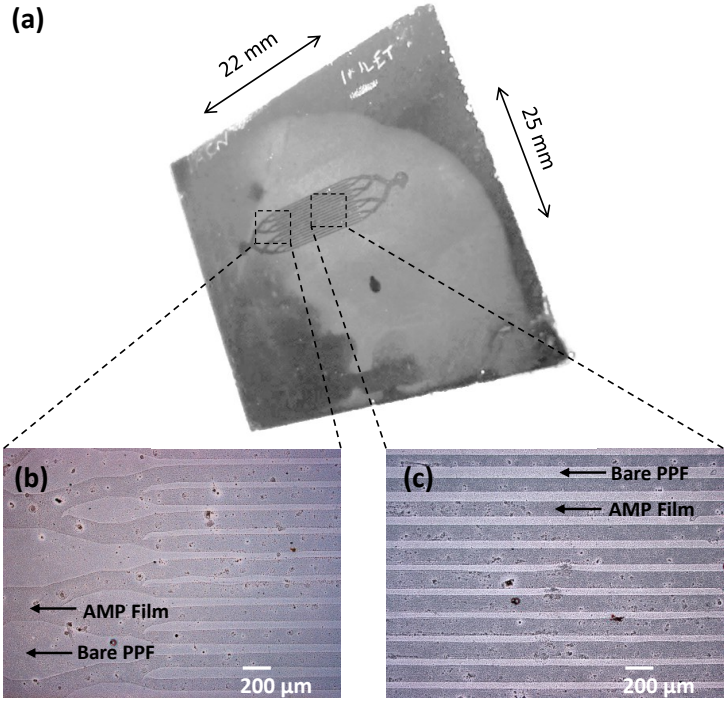

Figure 6.11 Condensation figures of a PPF surface patterned by electrografting AMP_D in ACN under static conditions inside PDMS microchannels. (a) Digital camera image and (b, c) optical micrographs recorded at 5× magnification.

6.4.3 Atomic force microscopy of patterned AMP films at PPF

AFM depth-profiling experiments were performed on patterned PPF surfaces to investigate changes in film thickness and topography. Thicknesses of patterned AMP films, prepared by grafting under different conditions, were measured to investigate whether monolayer or multilayer films were formed. It has been shown that diazonium-derived films prepared via aryltriazenes range from sub-monolayers to 4-5 multilayers[172].

6.4.3.1 Film-thickness and topography of patterned AMP films

Three types of patterned AMP films were prepared for AFM depth-profiling: (i) spontaneously grafted films prepared under flow; (ii) spontaneously grafted films prepared without flow (static grafting); and (iii) electrografted films prepared in aqueous conditions without flow. Aqueous electrografting was performed within microchannels via three

potential cycles between 0.6 V and -2.10 V (vs. Ag wire), followed by fixed potential electrolysis at -2.0 V for 300 s. Surfaces were subsequently cleaned using standard conditions. The diazonium reduction peak potential of $E_{pc} \approx$ -1.7 V was comparable to that observed in ACN. Likewise, the grafting CVs in aqueous solution (not shown) were similar to those observed for ACN grafting (Figure 6.10b).

Figure 6.12 shows AFM images of spontaneously grafted with flow (Figure 6.12a) and electrochemically grafted (Figure 6.12b) AMP films at PPF after a section of the film (1 × 10 μm) was removed by AFM scratching. The corresponding average cross sectional profiles are shown in Figure 6.12c and Figure 6.12d, respectively. Films prepared by spontaneous grafting under flow had a smooth and homogeneous topography with a low surface roughness. Similar topography was found for films spontaneously grafted under static conditions. In comparison, electrografted AMP films also had a low surface roughness, but unlike the spontaneously grafted films, had a high density of nanoscale pores 50-200 nm in diameter (Figure 6.12b). The presence of pores of this magnitude is unusual, given that diazonium-derived films are well-known for their densely-packed and pinhole-free film structures. For example, the comprehensive AFM study by Anariba and co-workers surveyed five different diazonium-derived films and found no observable pinholes for monolayer and multilayer films[406]. However, at least one example of observable pores in diazonium-derived films has been reported[65]. In that work, the nanoscale pores were observed for a two-component diazonium film prepared by step-wise electrografting of two different diazonium modifiers in ACN. It was though that the second electrografting step might be responsible for the formation of pores. The formation of pores in this work was not thoroughly investigated; however, the pores are tentatively attributed to acidic etching at the surface during grafting. The etching occurs due to the presence of fluoroboric acid, or other breakdown products present in solution (HF, for example), or both.

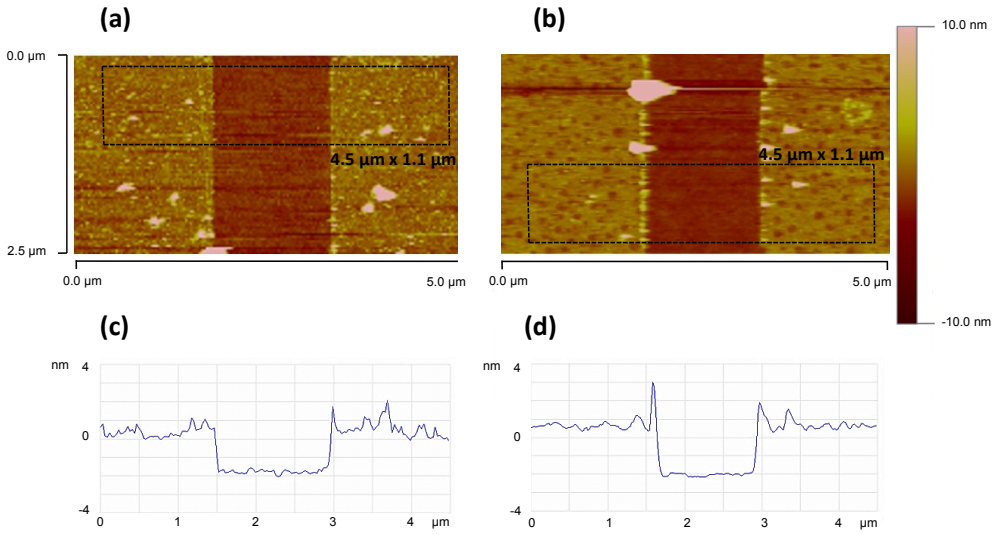

Figure 6.12 (a, b) Tapping-mode AFM images and (c, d) corresponding line profiles of scratched AMP films at PPF: (a, c) spontaneously grafted (aqueous) film prepared under flow and (b, d) electrografted (aqueous) film prepared under static conditions.

The average film thicknesses determined for patterned AMP films, prepared by grafting within microchannels, are shown in Table 6.2. Thicknesses ranged from 1.1 to 3.0 nm for dry films at PPF. The estimated length of the AMP modifier is 0.8 nm (calculated using Spartan software), hence multilayer films were formed. The formation of multilayers by either spontaneous or electrografting of aryldiazonium salts is consistent with other reports[66, 172, 406]. The maximum film thickness of 3.0 ± 0.2 nm corresponds to approximately 4 multilayers. For the films grafted spontaneously under static conditions, it is assumed that depletion of aryldiazonium ions at the surface is responsible for the low film thicknesses (1.1 ± 0.2 nm).

Table 6.2 Film thicknesses determined by AFM depth-profiling for films prepared by spontaneous and electrografting of AMP_D in aqueous solution using standard conditions.

Sample type	Grafting method	Film thickness (nm)
PPF-AMP	Spontaneous (static)	1.1 ± 0.2
PPF-AMP	Spontaneous (flow)	2.4 ± 0.3
PPF-AMP	Electrograft (static)	3.0 ± 0.2

An important feature of the microfluidic patterning approach is the ability to pattern under continuous flow. An average film thickness of 2.4 ± 0.2 nm was determined for AMP films prepared under flow grafting conditions. This compares with the thicknesses of 1.1 ± 0.2 for films grafted without flow. A greater film thickness for the films prepared with flow is consistent with the continual introduction of fresh grafting solution over the PPF surface, which maximises the concentration of AMP_D at the surface during grafting. At the same time, continuous flow ensures that spent grafting solution and by-products are removed from the surface-solution interface throughout the reaction. A major implication of this result is that the limiting thickness of the spontaneously grafted film, prepared under static grafting conditions in the microchannels, is limited by the amount of fresh aryldiazonium ions present at the surface.

6.4.3.2 Film-thickness homogeneity of AMP films prepared with and without flow

An important consideration when patterning films is the extent at which the film remains uniform over the length of the pattern. Ideally, the pattern transfer should be reproducible, with high edgeline resolution and homogeneous thickness. AFM depth-profiling experiments were undertaken to examine film grafted in the region near the inlet, where fresh solution was introduced, and in the region near the outlet, ≈ 10 mm downstream from the inlet.

Figure 6.13a is a schematic representation of the PDMS microchannels pattern that was used for preparation of AMP films. Figure 6.13b represents the patterned surfaces, and the regions of the surface, (i) and (ii), where AFM scratches were made. The microfluidic design consists of two inlet branches, which merge to form the main microchannel, and two outlets. For single stream patterning, only one of the inlets was used for introduction of solution, whereas both outlets were left open.

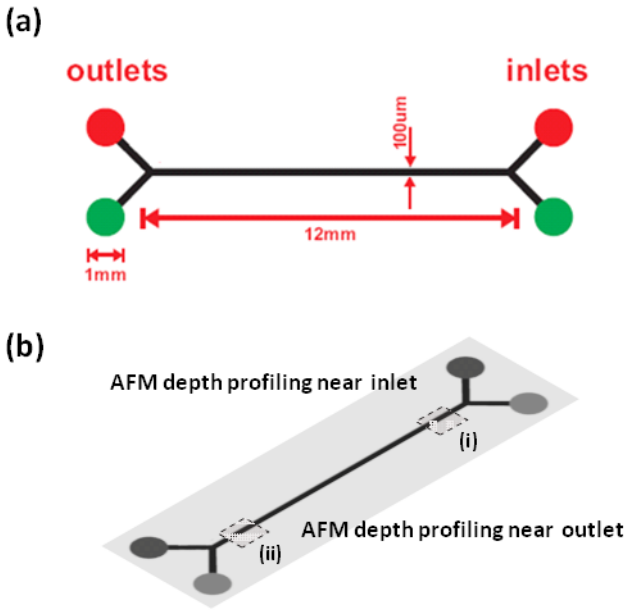

Figure 6.13 (a) Diagram illustrating the PDMS microchannels pattern routinely used for patterning. (b) Diagram of the transferred surface pattern at PPF; regions (i) and (ii) correspond to the areas where film thicknesses were measured.

Several depth profiles were obtained at both ends of the main channel (regions (i) and (ii)) of the film-modified surfaces (Figure 6.13b). The average film thickness data are shown in Table 6.3. No significant differences in average film thickness were observed between region (i) and region (ii). Therefore, spontaneous grafting is amenable to the formation of films with uniform heights across the length of several millimetres.

Table 6.3 Film thicknesses obtained near inlet and outlet regions of a patterned AMP film on PPF. Thicknesses were determined by AFM depth-profiling films prepared by spontaneous grafting of AMP_D in aqueous solution.

Sample type	Grafting method	Sampling region	Film thickness (nm)
PPF-AMP	Spontaneous (static)	(i) Inlet region	1.0 ± 0.2
	Spontaneous (static)	(ii) Outlet region	1.1 ± 0.2
PPF-AMP	Spontaneous (flow)	(i) Inlet region	2.5 ± 0.2
	Spontaneous (flow)	(ii) Outlet region	2.3 ± 0.2

6.4.4 Immobilisation of gold nanoparticles on patterned AMP films at PPF

The chemical functionality of AMP films, prepared by flow grafting inside microfluidic channels, was evaluated by reaction of modified surfaces with gold nanoparticle solution. The method used for gold nanoparticle immobilisation is described in Section 6.2.7.

Figure 6.14 shows an optical micrograph and SEM micrographs of different regions of an AMP modified surface after immersion in gold nanoparticle solution. Figure 6.14a and Figure 6.14b show high pattern contrast between the film-modified and unmodified regions of the surface. High densities of gold nanoparticles were observed in the film modified regions but not in the unmodified regions, confirming that the patterned AMP films exhibit the same reactivity as non-patterned AMP films (Figure 6.7).

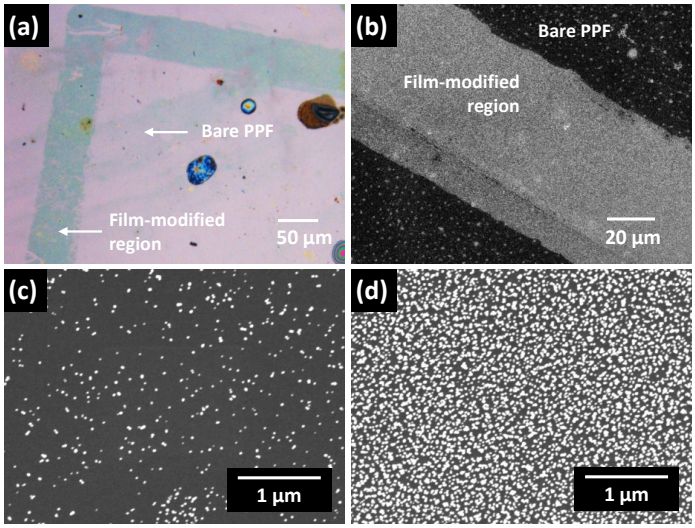

Figure 6.14 Optical and SEM micrographs of patterned AMP films after immobilisation in citrate-capped gold nanoparticles: (a) low magnification (5×) optical micrograph; (b) low magnification SEM micrograph; (c) high magnification micrograph of bare PPF; (d) high magnification micrograph of AMP-modified region.

6.5 Multistream laminar flow patterning of AMP films at PPF

Multistream laminar flow patterning, more commonly known as laminar flow patterning, is a technique that can be applied to pattern surfaces with a wide variety of microstructures[384,

[386, 409]. This method of patterning is based on the introduction of two or more liquid streams inside microchannels, which flow side-by-side without any mixing other than by diffusion at the interface of the two solutions. Surface patterning occurs as a consequence of chemical reactions occurring within confined laminar flow streams or at the boundary between them. For example, Whitesides and co-workers have exploited multistream laminar flow to deposit a range of materials, including metals, polymers and crystals[388, 409]. Zhao, Beebe and co-workers have combined multistream laminar flow and self-assembled monolayer chemistry for patterning different modifiers at glass[386]. Multistream laminar flow patterning has also been used for patterning biological species onto surfaces; Delamarche and co-workers, and others, have applied μFNs for the attachment of protein or cells arrays at a variety of substrates[384-385, 387, 410-411].

The multistream laminar flow system studied in this work is represented by the scheme in Figure 6.15. For the experiments described in this section, patterned surface modification is based on the formation of aryldiazonium ions *in situ* at the diffusive interface between an acid stream and an aryltriazene stream, by the mechanism shown in Scheme 6.2. Once formed, the aryldiazonium ions generated in solution are grafted at the surface by spontaneous or electrografting methods under continuous flow.

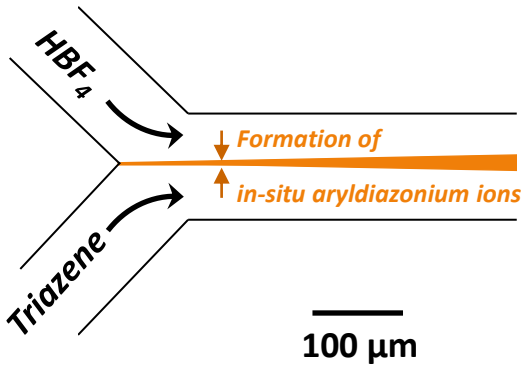

Figure 6.15 Diagram of the Y-junction laminar flow system used for generation and patterning of diazonium ion solutions. The region of diffusive mixing is indicated at the boundary of the HBF_4 and aryltriazene streams.

An essential feature of the multistream microfluidic patterning technique is that liquid streams are continually introduced into microchannels under pressure driven laminar flow. In laminar flow, the fluid has distinct streamlines, or laminae, which are all parallel to the direction of flow. The fluid flow normally assumes a parabolic flow profile; each of the streamlines flow at slightly different velocities. The highest velocities are in the centre of the stream and the lower velocities are towards the capillary wall. In this regime the flow properties of the solution, including velocity and pressure, are well defined. This form of flow is in contrast to turbulent flow in which the fluid undergoes irregular fluctuations and mixing. In order to generate well-defined patterns using laminar flow patterning it is therefore crucial to carefully control the flow streams. For example, if the flow is too fast, or if any debris or artefacts are present within the capillary, then the laminar flow stream breaks down into turbulent flow.

The methods developed herein rely on the phenomena that two or more liquid flow streams in the same microchannel have a low Reynolds number. The Reynolds number is a parameter that represents the ratio of the importance of inertial to viscous forces in the flow; it is a measure of the tendency of a liquid flow to develop turbulence. In the absence of turbulence, the only remaining mechanism of fluid mixing in a laminar flow system is slow diffusion across two streams transverse to the direction flow. It is this mixing that forms the basis of multistream laminar flow patterning. The width of the diffusion boundary depends on the molecular weight of the molecule, the solution viscosity, the velocity of the liquid flow, and the distance from the channel junction[412]. Through careful manipulation of these parameters, a wide variety of structures can be patterned at surfaces with feature sizes of < 10 μm using capillary diameters between 50-400 μm[387, 409].

6.5.1 Spontaneous grafting of patterned AMP films at PPF using multistream laminar flow

The formation of patterned surfaces using multistream laminar flow was explored using spontaneous grafting in aqueous solution. For this approach an aryltriazene solution and an HBF_4 solution were introduced into a Y-junction microfluidic channel (Figure 6.15) sealed onto a PPF substrate. The two separate solution streams were introduced into the Y-junction at similar times (within a few seconds of each other) via controlled infusion using a dual syringe pump. Ideally, the solutions streams are introduced at identical times, however, this is difficult in the present set-up due to factors such as dead-volumes, air bubbles, different solution and channel wetting properties, and pumping mechanics. The experimental set-up used for spontaneous grafting via multistream laminar flow is shown in Figure 6.1c.

6.5.1.1 Formation and characterisation of patterned AMP films after grafting at low flow rate

For these experiments, a 2 mM solution of AMP_{DMT} in 0.1 M KCl and a 0.2 M solution of HBF_4 were introduced into the microchannels sealed onto a PPF substrate. A standard flow rate of ≈ 0.2 mL/min and a reaction time of either 30 min or 60 min were used. After modification and subsequent removal of the elastomeric microchannels, surfaces were sonicated for 5 min in DMF and ACN to remove any physisorbed material, and then dried with a stream of N_2.

Figure 6.16 shows an optical micrograph of a line of AMP grafted to PPF from the interface of an aryltriazene stream and an acid stream. By this method, defined lines were patterned on PPF surfaces, with line-widths significantly narrower than the channel. Widths down to ≈ 15 μm were generated using microchannels ≈ 110 μm in diameter. The grafted film was apparent only in the region corresponding to the interface between the two

solutions. This result provides strong evidence that grafting is a result of mixing of the two streams. The surface patterns are typical of those expected using LFP with Y-junction microchannels: a single spatially well-defined line is formed in the centre of the main microfluidic channel, which tapers slowly over a distance of hundreds of micron.

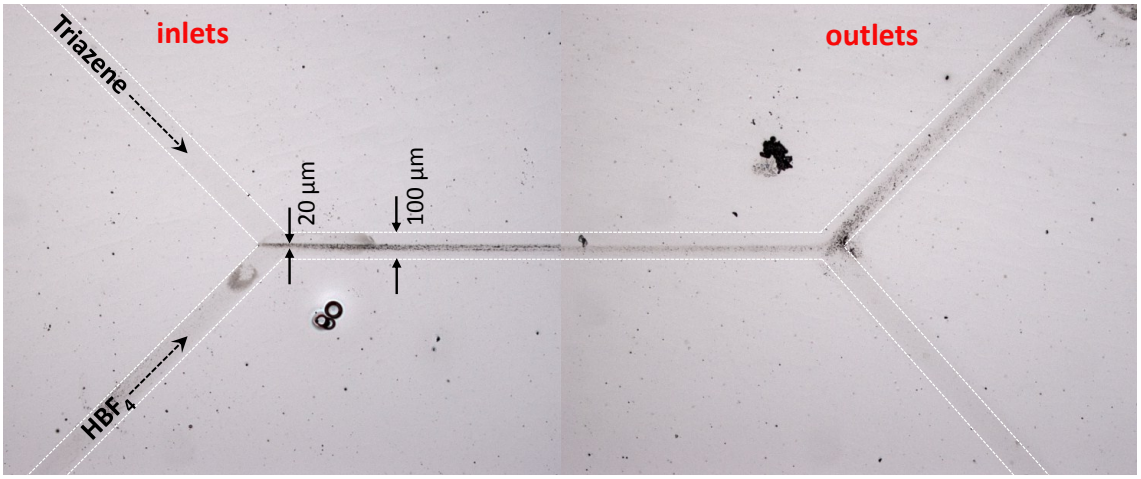

Figure 6.16 Optical micrograph (5× magnification) of a multistream laminar flow patterned AMP surface prepared at low flow rate (≈ 0.2 mL/min). Patterning was achieved by combining HBF_4 and aryltriazene solutions together inside a Y-junction in a PDMS microchannels device.

Figure 6.16 shows that the patterned layer deposited at the surface is non-uniform in contrast to that typically observed for diazonium-derived films, hence a patterned surface was further characterised using AFM in tapping-mode. A 50 × 50 µm region of a patterned PPF surface ≈ 100 µm downstream from the point near the inlet where the two solutions met, at a region where diffusional broadening was minimised, was examined. Figure 6.17 shows 2D (a) and 3D (b) projections of the patterned surface, and a corresponding single line profile (c). The AFM images reveal that a distinct modified line, 15 µm in width, has been grafted at the surface. The surface morphology of the patterned line is consistent with a disordered granular structure consisting of "peaks" with heights of between 5-300 nm. This confirms that the film has not grown uniformly at the diffusion boundary in the multistream laminar flow system.

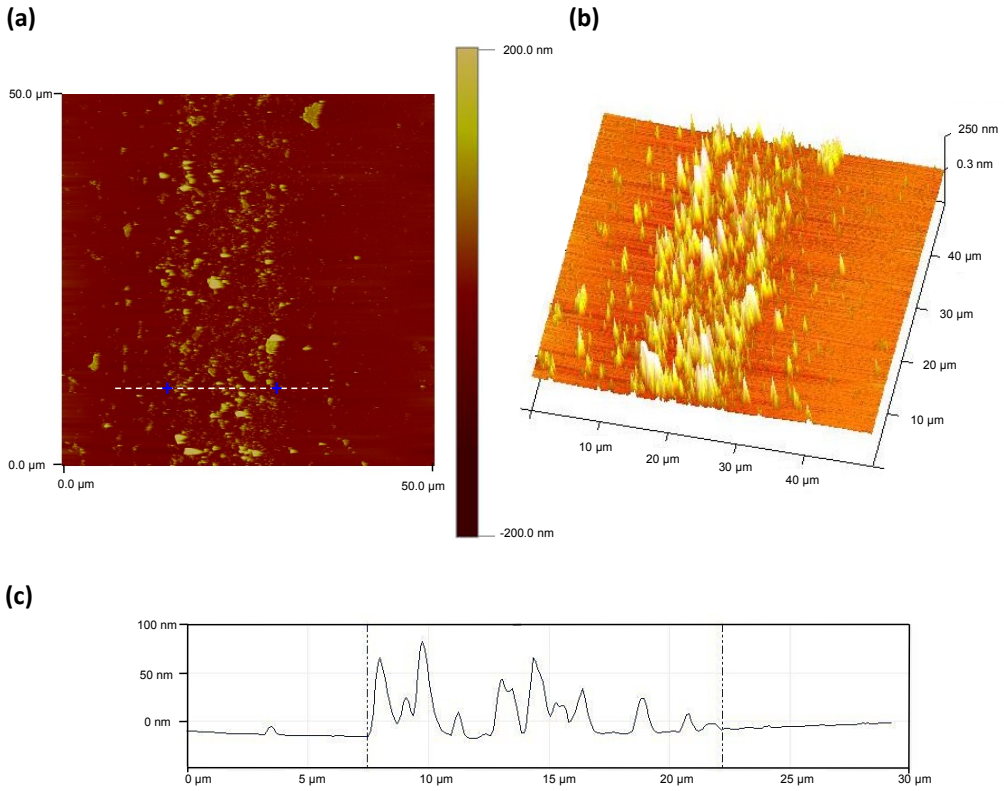

Figure 6.17 AFM images of a multistream laminar flow patterned AMP surface prepared at a low flow rate (≈ 0.2 mL/min): (a) 2D projection; (b) 3D projection; (c) single line profile.

The optical micrographs in Figure 6.18 show patterned AMP-modified PPF (a) before and (b) after sonication in DMF for 30 min. Identical regions of the surface were imaged and no loss of the patterned deposit was observed. After imaging at various magnifications, the surface was further rinsed in ACN and Milli-Q water, and re-analysed; again, the film was unchanged. The stability of the patterned layer to extended sonication periods in DMF, and rinsing in different solvents, strongly support the formation of a strongly attached film to the surface, consistent with covalent attachment.

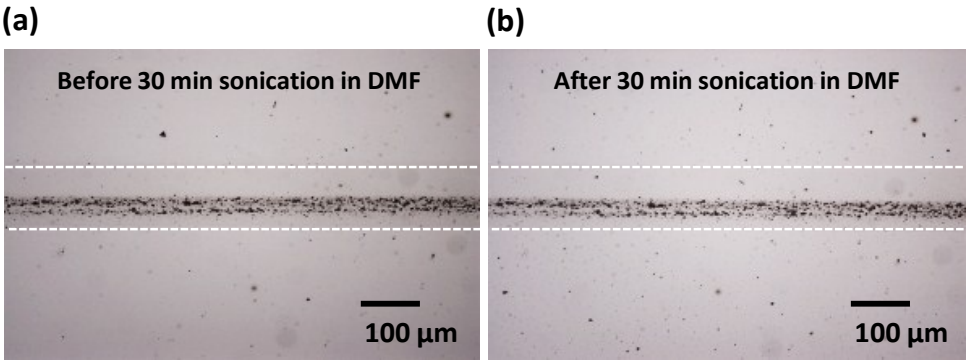

Figure 6.18 Optical micrographs (5× magnification) of a region of a multistream laminar flow patterned AMP surface (a) before and (b) after sonication in DMF for 30 min. Identical regions of the PPF surface were imaged.

6.5.1.2 Formation and characterisation of patterned AMP films after grafting at high flow rate

The ability to pattern surfaces with line widths < 15 µm was investigated by increasing the flow rate during multistream laminar flow. The type and width of the pattern that can be formed by the delivery of solutions using the laminar flow patterning technique is determined by flow dynamics; hence the width of surface patterns can be manipulated by adjusting the relative flow rates of the flow streams[388, 409].

To pattern PPF surfaces, a 2 mM solution of AMP_{DMT} in 0.1 M KCl and a 0.2 M solution of HBF_4 were introduced into the Y-junction PDMS microchannels sealed onto a PPF substrate, using a flow rate of ≈ 2 mL/min. The solutions flowed over the surface for ≤ 2 min. A lower concentration of aryltriazene and a lower grafting time were used than with the low flow rate experiments, with the aim of improving the homogeneity of the surface pattern. After sonication cleaning for 5 min in DMF and ACN, surfaces were dried with a stream of N_2 and analysed by SEM.

Figure 6.19 shows SEM micrographs of a surface pattern at PPF prepared by the multistream laminar flow technique. The images illustrate the formation of a well-defined

line in the centre of the main channel. No line pattern is observed in the regions of the channel where solution mixing did not occur. Near the Y-junction where the two solutions streams were combined, line widths of ≈ 10 μm were produced (Figure 6.19a). The surface film has a granular appearance, similar to that observed at slower flow rates, but more continuous. Further downstream, the flow became focussed and line patterns with significantly reduced feature sizes were produced (Figure 6.19b). The patterned line is straight and represents a continuous thin film. Over a distance of ≈ 5 mm the patterned film had a line width of 1 μm ± 0.5 μm. At high magnification (Figure 6.19c), the pattern is reasonably well-defined but not as homogeneous as films prepared by the single stream flow patterning approach (Figure 6.8).

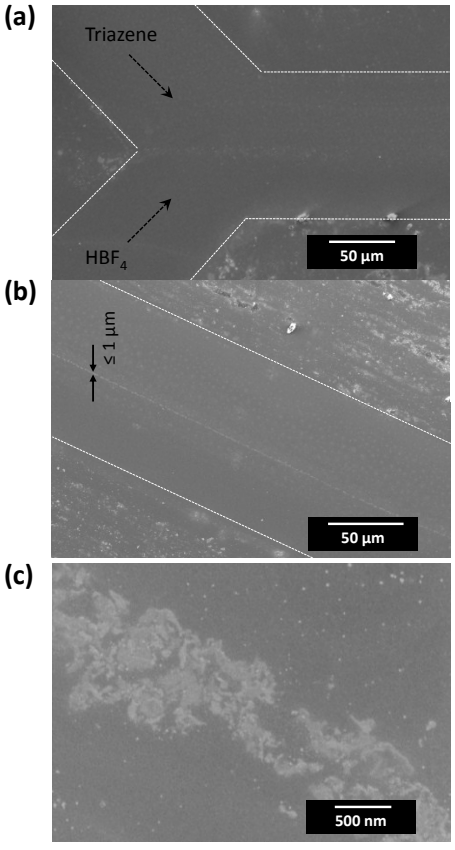

Figure 6.19 SEM micrographs of a multistream laminar flow patterned AMP surface prepared at a high flow rate (≈ 2 mL/min): (a) Y-junction near inlet; (b) main channel downstream; (c) high magnification of patterned film. The dotted lines are added to show the edges corresponding to the edges of the PDMS microchannels.

A multistream laminar flow patterned surface prepared at high flow rates was further characterised using AFM in tapping-mode. The raw AFM image was recorded downstream from the inlet at a region corresponding closely to the region imaged by SEM in Figure 6.19b and Figure 6.19c. Figure 6.20 shows 2D (a) and 3D (b) projections of a 2 × 15 µm area of the patterned surface, and a corresponding single line profile (c). The AFM images show that a distinct straight line of ≈ 1 µm in diameter has been grafted on the surface. As was observed by SEM imaging (Figure 6.19c), the patterned line is rough but spatially well-defined. The average height of the coating is 2.4 nm, based on an average cross section of a 1.2 × 1.8 µm area. The average film thickness is consistent with the thicknesses obtained for AMP films prepared by spontaneous grafting using the single stream flow patterning approach (2.4 ± 0.3 nm). The AFM results therefore confirm that the multistream approach is suitable for patterning *in situ* generated aryldiazonium salt solutions.

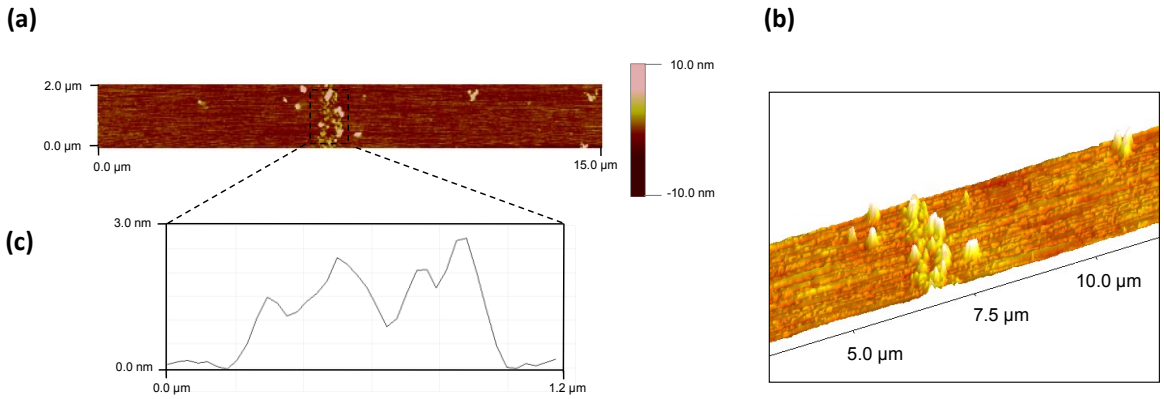

Figure 6.20 AFM images of a multistream laminar flow patterned AMP surface prepared at a high flow rate (≈ 2 mL/min): (a) 2D projection; (b) 3D projection; (c) average line profile of a 1.2 × 1.8 µm region.

6.5.2 Immobilisation of gold nanoparticles on patterned AMP films

The chemical functionality of patterned AMP surfaces was demonstrated by testing the reactivity of multistream laminar flow patterned PPF samples for gold nanoparticles

immobilisation. Figure 6.21 shows an SEM micrograph of a PPF sample prepared using a low flow rate after immobilisation in gold nanoparticles using the standard procedure. Substantial assembly of gold nanoparticles is seen in the region where aryldiazonium ions were generated *in situ*. In the regions where only aryltriazene or acid solutions were exposed to the surface, very low amounts of gold nanoparticles are observed. The high density of gold nanoparticles in the region where aryldiazonium salt grafting occurs is consistent with successful modification of the surface with AMP groups. Thus it can be confirmed that PPF was successfully modified and patterned using the multistream laminar flow approach.

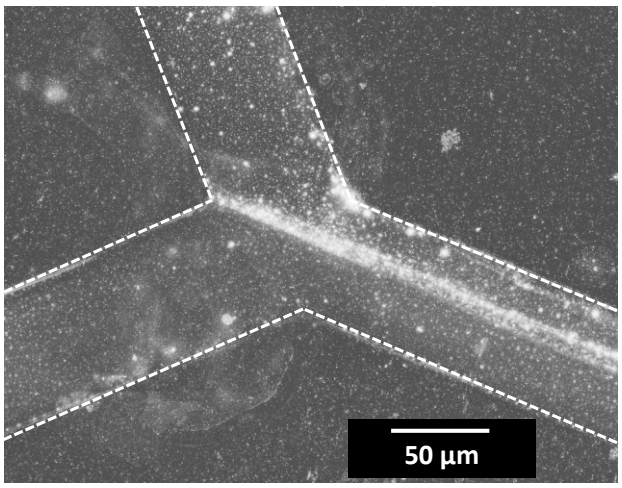

Figure 6.21 SEM micrograph of a multistream laminar flow patterned AMP surface after immobilisation of citrate-capped gold nanoparticles. Surface pattern was obtained using the low flow rate method.

6.6 Conclusion

Aryltriazene precursors have been used for the preparation of diazonium-derived films with aliphatic amine and carboxylic acid functionalities at carbon surfaces, thus expanding the range of surface functionalities that can be deposited from aryltriazene solutions. Cyclic voltammetric experiments performed in aqueous and non-aqueous solutions show clear evidence for the in situ formation of aryldiazonium ions, via deprotection of aryltriazenes with 0.1 M HBF_4, and subsequent film grafting. AMP films prepared from aqueous and non-aqueous electrografting showed similar grafting behaviour and similar electroactivity. The observed electroactivity in ACN-$TBABF_4$ for these films provided direct evidence for the presence of surface-bound alkylamine groups. The AMP films on PPF also show excellent selectivity for the immobilisation of citrate-capped gold nanoparticles on the surface. Spontaneous grafting reactions were also explored and yielded film-modified surfaces.

For the first time, PDMS microfluidics devices were used to prepare patterned diazonium-derived films via laminar flow. The ability to pattern films with microscale features was demonstrated using both single stream and multistream approaches. Multiple lines and networks of films can be patterned in a short sequence of steps in short times (2-60 min) using both methods. Line widths of ≤ 100 μm were easily and conveniently achieved using single stream approaches. Films prepared by single stream patterning under both static and flow conditions also gave "complete" and homogeneous film patterns. Multistream approaches can be used to prepare functional, patterned films with smaller feature sizes ($\leq$ 15 μm), but the resulting films are less homogenous and continuous. The chemical functionality of AMP films prepared by multistream flow was demonstrated by the successful immobilisation of gold nanoparticles on patterned regions.

In addition to surface patterning, the microfluidics approach can also be used to spontaneously graft films under continuous flow. It was found that grafting under flow

resulted in significantly thicker AMP films, consistent with continual renewal of aryldiazonium salt ions at the surface during grafting.

AFM measurements confirmed that electrografted and spontaneously grafted AMP films were smooth (average roughness values between 0.3-0.7 nm) and continuous multilayers (≤ 3 nm thick films) under the conditions explored. A statistically significant increase in roughness was observed at PPF following electrografting and spontaneous grafting of AMP films. The formation of pores in patterned electrografted films was observed for a small number of samples. This is not well-understood and could be addressed in future work. AFM depth-profiling experiments also confirmed that homogeneous thicknesses of flow-patterned films were obtained over millimetre distances (≈ 12 mm).

General conclusion and future work

This thesis shows that there are many ways to modify surfaces with molecular layers using aryldiazonium salts, arylazides, alkylamines, and aryltriazenes. A number of modification and patterning strategies have been developed which enable controlled deposition of organic and inorganic films, in particular on carbon, but also on metal and semiconductor surfaces. In addition to surface modification and patterning strategies, two technical methods were developed for preparing carbon electrodes.

In initial work, exploration of the effect of heat treatment on film-modified and deactivated pyrolysed photoresist film surfaces led to the finding that heating in argon at 545 ± 25 °C removes covalently attached organic films, attached via electrografting aryldiazonium salt solutions. Heat treatment of surfaces deactivated by exposure to air or adsorbates at ≥ 385 ± 25 °C consistently yields small improvements in the electrochemical response of $K_3FeCN_6^{3-/4-}$, hence heat-treatment is a useful method for activating pyrolysed photoresist film surfaces for electroanalysis. Re-use of pyrolysed photoresist film is time and cost-saving and should expand its applications as an electrode material. Future studies should confirm the use of the regeneration method for removing other types of grafted thin films.

An alternative method for preparing thin-film carbon electrodes using electron-beam evaporation was also developed in this thesis. Amorphous carbon films (100 nm) are stable on gold providing that an intermediate nickel or platinum layer is used. The resulting carbon surfaces exhibit comparable electrochemical activity to previously reported evaporated carbon films, but exhibit sluggish electron transfer kinetics for $K_3FeCN_6^{3-/4-}$ compared to glassy carbon and pyrolysed photoresist film electrodes.

The low surface roughness of amorphous carbon films (0.85 ± 0.15 nm) should enable depth-profiling investigations to be performed on films grafted to these surfaces but this was not studied. The grafting behaviour of *p*-nitrophenyl diazonium salt at amorphous carbon film electrodes is similar to that observed at pyrolysed photoresist film, hence amorphous carbon films are suitable as alternative substrates. Future work should investigate the preparation of carbon-coated quartz crystals simply by evaporating the carbon films onto gold-coated quartz crystals. Such electrodes would provide new opportunities for studying molecular layers and for developing carbon-based sensors.

Free-base and nickel (II) tetraphenylporphyrin films can be readily grafted at carbon, gold, and indium tin oxide surfaces from the corresponding mono-aryldiazonium salts. Films prepared by electrochemical reduction under non-aqueous conditions exhibit the expected UV-visible absorption spectra and have well-defined and reversible redox chemistry, characteristic of free-base and nickel (II) tetraphenylporphyrin complexes. Diazonium-derived porphyrin films withstand potential cycling and extensive sonication (≤ 45 min in DMF) in non-aqueous solution. Films formed at glassy carbon exhibit greater stability than films at gold and indium tin oxide, highlighting an important advantage of carbon surface modification. Cycling stability studies show that the films are not ideally suited to multiple electrochemical experiments at commonly employed scan rate (100 mV/s) but are well-suited to such experiments at high scan rates (1 V/s). Under the conditions explored, the film growth of nickel porphyrin films is self-limiting after 20 cycles whereas the film growth of free-base porphyrin films is approximately linear with increasing cycles. The limiting surface concentration of electroactive groups and film thickness of nickel porphyrin films (1.4 ± 0.2 nm) shows that the films formed are approximate monolayers. For free-base porphyrin films, monolayer or multilayer films are formed with estimated thicknesses up to 10 nm. Future applications should explore the use of these films for applications in sensing, electrocatalysis, and in energy conversion.

Grafting organic films by reaction of arylazides at glassy carbon and film-modified surfaces is a simple and versatile route to functional molecular layers. Several two-component films were developed in this work by photografting an arylazide modifier onto a preformed film. In some cases, patterned films were obtained using a photomask via a previously reported procedure. Using these strategies, various organic films containing mixtures of *p*-amino, *p*-nitro, *p*-isothiocyanate, and poly(ethylene glycol) groups can be prepared. Photografting from mixtures of arylazides was developed and is a simple one-step approach to two-component films. For all grafted surfaces, the reactivity of tether or electroactive species was confirmed by coupling electroactive targets to the surface. In general, the coupling reactions are selective with only a small amount of non-specific attachment evident at the unmodified carbon surface. The poly(ethylene glycol) films exhibit anti-protein fouling properties, although this behaviour was not tested for two-component films.

After several failed attempts to couple biomolecules to azide modified carbon surfaces, a different strategy was explored for preparing films from arylazides. In this work, a simple and convenient photolithographic method was developed for patterning silicon with photografted or thermally grafted *p*-aminophenyl films. The method expands the use of arylazides to silicon surfaces and has the attractive feature that removal of the native oxide layer is not necessary prior to grafting. The grafted multilayer films (2.5 to 2.7 ± 0.3 nm) were not explored for coupling molecules but show good selectivity for the electrostatic immobilisation of gold nanoparticles. The photolithographic patterning strategy developed in this work enables the preparation of parallel patterns with a minimum feature size of 5 μm. Parallel "checkerboard" patterns used in this work are conveniently sized and enable preparation of surface patterns that can be depth profiled by AFM without the need for "scratching". Future work should focus on the use of the standard photolithographic

method for preparing two-component films on silicon and carbon surfaces. All of the films developed in this work show promise for future development of biosensors.

Modification of carbon surfaces with *p*-aminomethylphenyl and *p*-carboxyphenyl films via aryltriazene compounds can be achieved using simple, one-step spontaneous and electrografting reactions. The use of new modifiers and the use of fluoroboric acid as opposed to an electrogenerated acid expands the scope of aryltriazene grafting reactions. The grafted multilayer films (1.1 to 3.0 ± 0.3 nm) were not explored for coupling molecules but show excellent selectivity for the immobilisation of gold nanoparticles. A major result of this thesis is that parallel patterned films with microscale feature sizes can be obtained at surfaces by combining aryltriazenes with microfluidics. Feature sizes typically range from ≤ 15 to 200 μm. The ability to generate patterned films using short reactions times (typically ≤ 30 min), aqueous and non-aqueous solutions, and either spontaneous and electrografting methods, makes this patterning strategy one of the most versatile and convenient aryldiazonium salt patterning methods available in the literature. In addition to patterning, grafting in microfluidic channels under flow provides access to thicker films than those prepared in the absence of flow, consistent with continual renewal of reactant at the surface. Single stream flow is experimentally simpler than multistream flow but is limited to minimum feature sizes defined by the width of the microchannels. In contrast, multistream laminar flow provides access to smaller feature sizes than the width of the microchannels, but at the expense of a more difficult experimental set-up. Patterned aminophenyl films are highly desirable tether layers and are used in applications across sensing, hence future studies should build on the patterned films prepared here. Future work should also focus on improving the potential control and flow control of the microfluidic patterning methods to increase the reproducibility of the films.

The attraction of all of the surface modification methods explored in this work is that stably-attached films with well-defined chemical and physical properties are deposited at

desirable electrode surfaces. The electrochemical, photochemical, thermal, and spontaneous grafting reactions used in this thesis are reproducible. In addition, they are all experimentally simple, except for those reactions performed in combination with patterning techniques. The simplest method of grafting involves the spontaneous reaction of aryldiazonium salt solutions, generated *in situ* from aryltriazenes, at carbon surfaces. Electrografting methods are comparatively rapid and facile as reaction times are typically ≤ 15 min and multilayer films up to 10 nm can be formed with modifier concentrations of between 0.5 mM to 5 mM. The findings in this work show that is possible to form approximate monolayers, as well as multilayers, depending on the modifier solution concentration, substrate, and applied potential. The greater film stability for diazonium-derived films observed at carbon surfaces compared to gold and indium tin oxide highlights that modification of carbon surfaces offers practical advantages.

In general, the patterning methods used are straightforward to apply with the exception of multistream laminar flow patterning. Microscale patterns with similarly low microscale features are readily obtained using the two general patterning methods in this thesis; namely, standard photolithography and microfluidics. Patterning films using standard photolithography is the more promising method and represents an important addition to thin film patterning methods. The main limitation is that the method is currently only applicable to aqueous grafting solutions and is unlikely to be compatible with non-aqueous solutions. On the other hand, microfluidics has arguably greater potential for preparing a wider range of surface, but suffers from the need for several additional processing steps compared to the more simple photolithographic method. Overall, both methods are important developments in the broad field of microscale patterning of molecular layers at surfaces.

Appendix

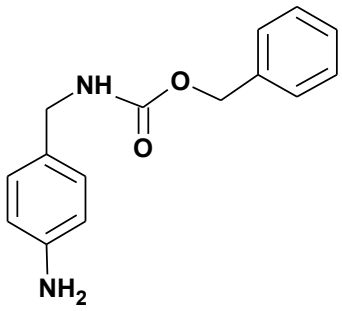

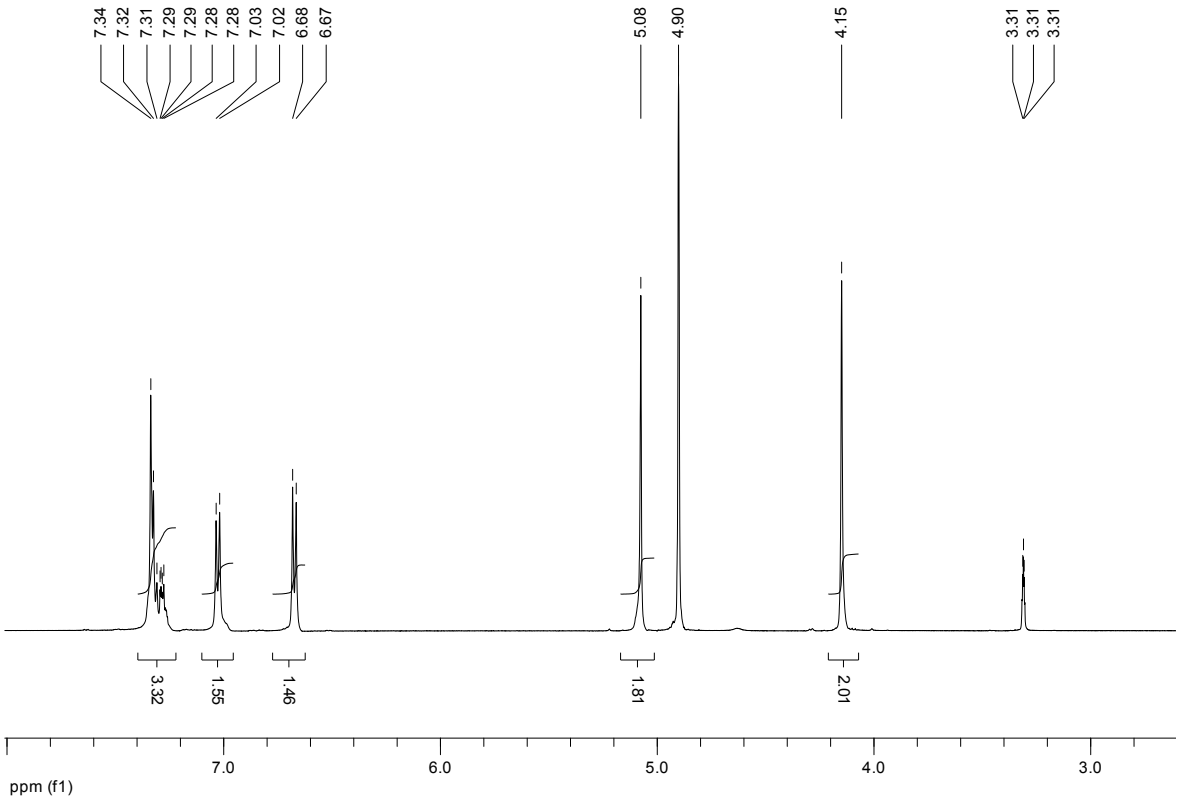

Appendix S-1 ^{1}H NMR ($CDCl_3$, 500 MHz) of benzyl (4-aminobenzyl)carbamate.

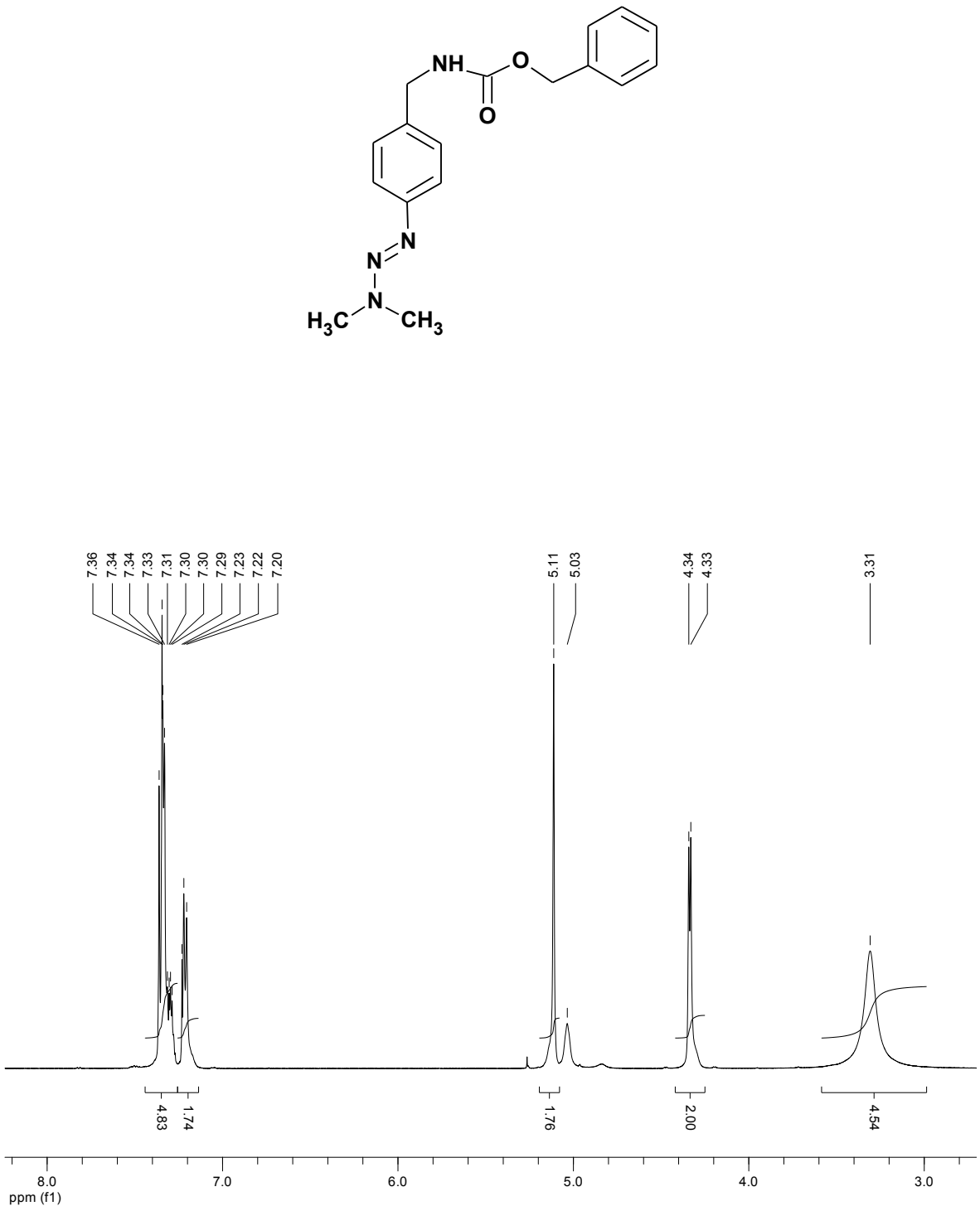

Appendix S-2 ^{1}H NMR ($CDCl_3$, 500 MHz) of benzyl [4-((1E)-3,3-dimethyl-1-triazen-1-yl)benzyl]carbamate

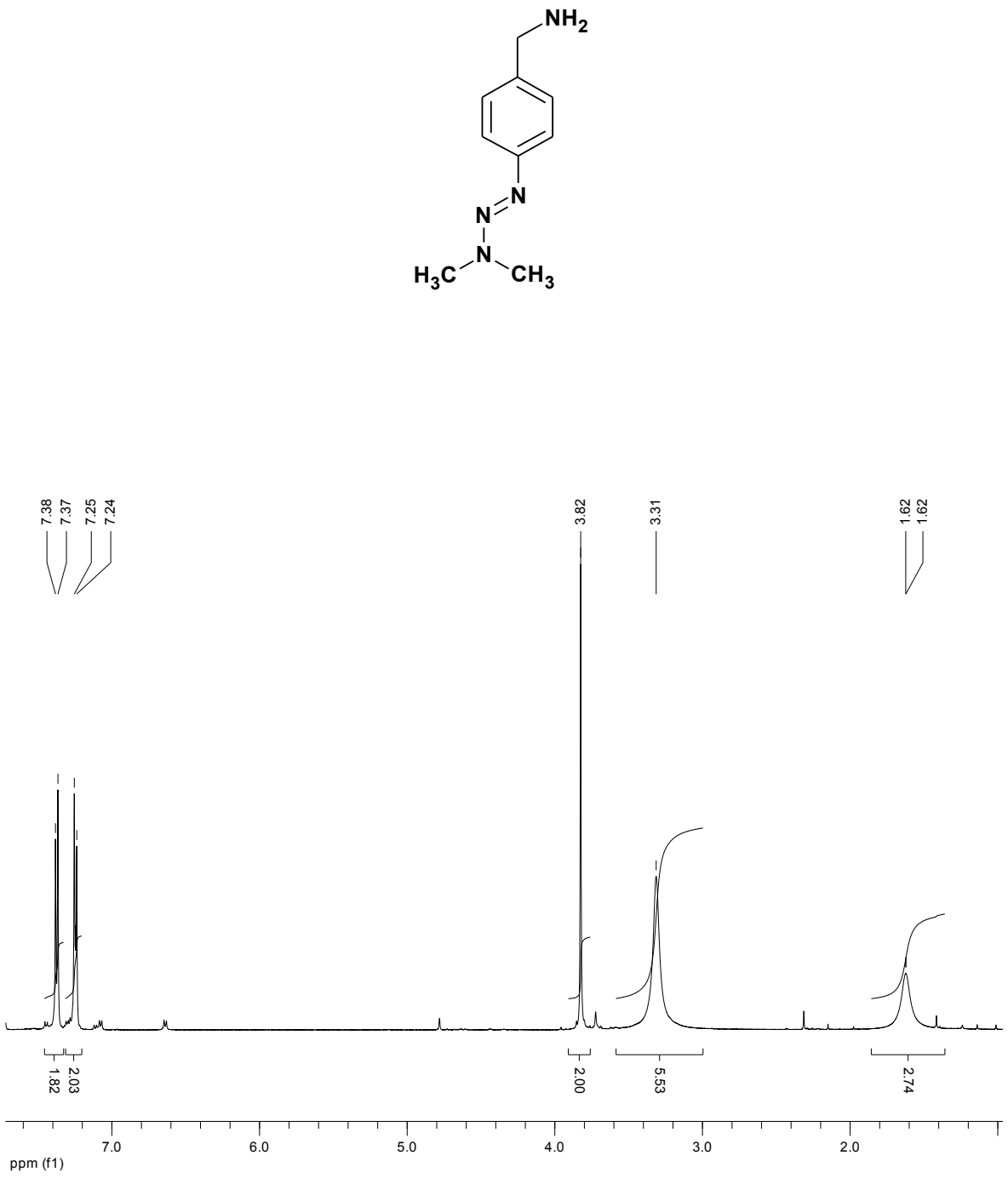

Appendix S-3 ^{1}H NMR ($CDCl_3$, 500 MHz) of [p-(dimethyltriaz-1-en-1-yl)phenyl]methylamine

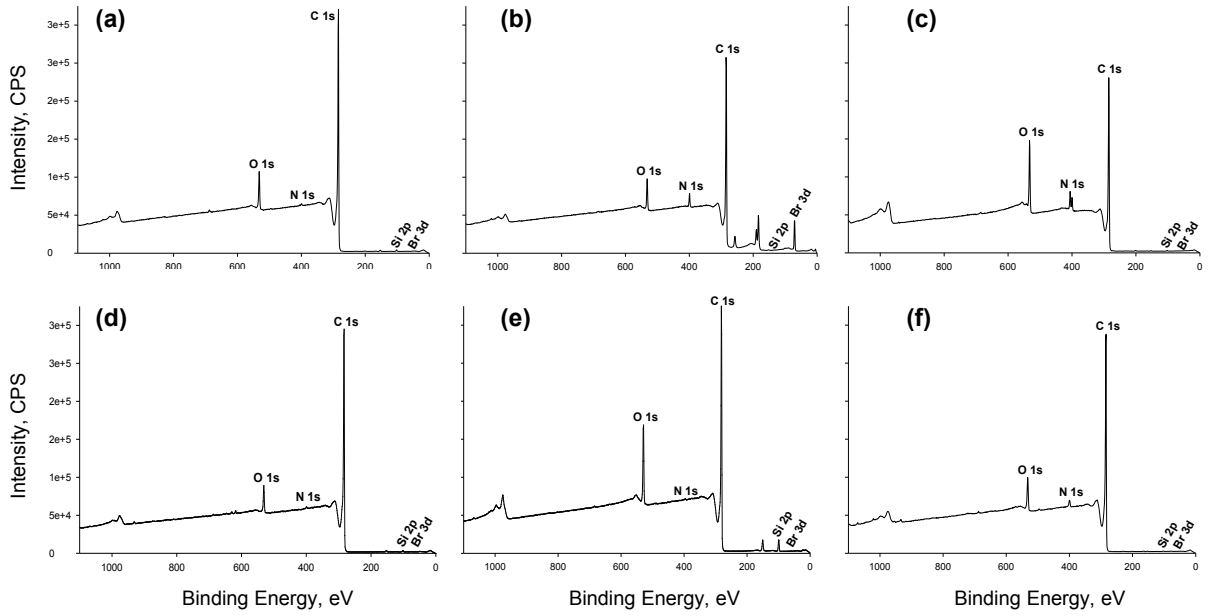

Appendix S-4 XPS survey scan spectra for (a) as-prepared PPF, (b) PPF modified with BrP groups, (c) PPF modified with NP groups, (d) as-prepared PPF (heat-treated), (e) PPF modified with BrP groups (heat-treated) and (f) PPF modified with NP groups and subsequently heat-treated. Heat treatment was performed using standard conditions (545 ˚C for 30 min under Ar).

References

1. Forbes, P., Self-cleaning materials. *Sci. Am.* **2008**, *299* (2), 88.
2. Lyon, S., Materials science: A natural solution to corrosion? *Nature* **2004**, *427* (6973), 406.
3. Messersmith, P. B.; Textor, M., Nanomaterials: Enzymes on nanotubes thwart fouling. *Nat. Nano* **2007**, *2* (3), 138.
4. *The world market for nanocoatings*. Future Markets **2011**.
5. Bard, A. J., Chemical modification of electrodes. *J. Chem. Educ.* **1983**, *60* (4), 302.
6. Murray, R. W.; Ewing, A. G.; Durst, R. A., Chemically modified electrodes. Molecular design for electroanalysis. *Anal. Chem.* **1987**, *59* (5), 379A.
7. Swalen, J. D.; Allara, D. L.; Andrade, J. D.; Chandross, E. A.; Garoff, S.; Israelachvili, J.; McCarthy, T. J.; Murray, R.; Pease, R. F.; Rabolt, J. F.; Wynne, K. J.; Yu, H., Molecular monolayers and films. *Langmuir* **1987**, *3* (6), 932.
8. Love, J. C.; Estroff, L. A.; Kriebel, J. K.; Nuzzo, R. G.; Whitesides, G. M., Self-assembled monolayers of thiolates on metals as a form of nanotechnology. *Chem. Rev.* **2005**, *105* (4), 1103.
9. Gooding, J. J.; Ciampi, S., The molecular level modification of surfaces: From self-assembled monolayers to complex molecular assemblies. *Chem. Soc. Rev.* **2011**, *40* (5), 2704.
10. Lane, R. F.; Hubbard, A. T., Electrochemistry of chemisorbed molecules. I. Reactants connected to electrodes through olefinic substituents. *J. Phys. Chem.* **1973**, *77* (11), 1401.
11. Lane, R. F.; Hubbard, A. T., Electrochemistry of chemisorbed molecules. II. Influence of charged chemisorbed molecules on the electrode reactions of platinum complexes. *J. Phys. Chem.* **1973**, *77* (11), 1411.
12. Murray, R. W., Chemically modified electrodes. *Acc. Chem. Res.* **1980**, *13* (5), 135.
13. Jonkheijm, P.; Weinrich, D.; Schroder, H.; Niemeyer, C. M.; Waldmann, H., Chemical strategies for generating protein biochips. *Angew. Chem. Int. Ed. Engl.* **2008**, *47* (50), 9618.
14. Förch, R.; Schönherr, H.; Jenkins, A. T. A., *Surface design: Applications in bioscience and nanotechnology*. Wiley: **2009**.
15. Collman, J. P.; Devaraj, N. K.; Chidsey, C. E. D., "Clicking" functionality onto electrode surfaces. *Langmuir* **2004**, *20* (4), 1051.
16. Kwon, Y.; Mrksich, M., Dependence of the rate of an interfacial Diels-Alder reaction on the steric environment of the immobilized dienophile: An example of enthalpy-entropy compensation. *J. Am. Chem. Soc.* **2002**, *124* (5), 806.
17. McNaught, A. D.; Wilkinson, A., *IUPAC: Compendium of chemical terminology - the gold book second edition*. Blackwell Scientific **1997**.
18. Bain, C. D.; Troughton, E. B.; Tao, Y. T.; Evall, J.; Whitesides, G. M.; Nuzzo, R. G., Formation of monolayer films by the spontaneous assembly of organic thiols from solution onto gold. *J. Am. Chem. Soc.* **1989**, *111* (1), 321.
19. Sagiv, J., Organized monolayers by adsorption. 1. Formation and structure of oleophobic mixed monolayers on solid surfaces. *J. Am. Chem. Soc.* **1980**, *102* (1), 92.
20. Ulman, A., Formation and structure of self-assembled monolayers. *Chem. Rev.* **1996**, *96* (4), 1533.
21. Pinson, J., Attachment of organic layers to materials surfaces by reduction of diazonium salts. In *Aryl diazonium salts*, Wiley: **2012**; p 1.

22. Gong, Y.; Wang, M. C. P.; Zhang, X.; Ng, H. W.; Gates, B. D., Optimizing the quality of monoreactive perfluoroalkylsilane-based self-assembled monolayers. *Langmuir* **2012**, *28* (32), 11790.
23. Merz, A.; Bard, A. J., A stable surface modified platinum electrode prepared by coating with electroactive polymer. *J. Am. Chem. Soc.* **1978**, *100* (10), 3222.
24. Miller, L. L.; Van de Mark, M. R., Electrode surface modification via polymer adsorption. *J. Am. Chem. Soc.* **1978**, *100* (2), 639.
25. Murray, R. W., Polymer modification of electrodes. *Annu. Rev. Mater. Sci.* **1984**, *14* (1), 145.
26. Nuzzo, R. G.; Allara, D. L., Adsorption of bifunctional organic disulfides on gold surfaces. *J. Am. Chem. Soc.* **1983**, *105* (13), 4481.
27. Bain, C. D.; Whitesides, G. M., Molecular-level control over surface order in self-assembled monolayer films of thiols on gold. *Science* **1988**, *240* (4848), 62.
28. Hirsch, A., The era of carbon allotropes. *Nat. Mater.* **2010**, *9* (11), 868.
29. Kinoshita, K., *Carbon: Electrochemical and physicochemical properties*. Wiley: **1988**.
30. McCreery, R. L., Advanced carbon electrode materials for molecular electrochemistry. *Chem. Rev.* **2008**, *108* (7), 2646.
31. Harris, P. J. F., Structure of non-graphitising carbons. *Int. Mater. Rev.* **1997**, *42* (5), 206.
32. Schueller, O. J. A.; Brittain, S. T.; Whitesides, G. M., Fabrication of glassy carbon microstructures by soft lithography. *Sens. Actuators, A* **1999**, *72* (2), 125.
33. Schueller, O. J. A.; Brittain, S. T.; Marzolin, C.; Whitesides, G. M., Fabrication and characterization of glassy carbon MEMS. *Chem. Mat.* **1997**, *9* (6), 1399.
34. Fitzer, E.; Schaefer, W.; Yamada, S., The formation of glasslike carbon by pyrolysis of polyfurfuryl alcohol and phenolic resin. *Carbon* **1969**, *7* (6), 643.
35. Rautavuori, J.; Törmälä, P., Preparation of bulky glassy carbon bodies from phenolformaldehyde resin. *J. Mater. Sci.* **1979**, *14* (8), 2020.
36. Martinez-Duarte, R.; Teixidor, G. T.; Mukherjee, P. P.; Kang, Q.; Madou, M. J., Perspectives of micro and nanofabrication of carbon for electrochemical and microfluidic applications. In *Microfluidics and microfabrication*, Chakraborty, S., Ed. Springer US: **2010**; p 181.
37. Mildner, D. F. R.; Carpenter, J. M., On the short range atomic structure of non-crystalline carbon. *J. Non-Cryst. Solids* **1982**, *47* (3), 391.
38. Jenkins, G. M.; Kawamura, K., Structure of glassy carbon. *Nature* **1971**, *231* (5299), 175.
39. Harris, P. J. F., Fullerene-related structure of commercial glassy carbons. *Philos. Mag.* **2004**, *84* (29), 3159.
40. Yoshida, A.; Kaburagi, Y.; Hishiyama, Y., Microtexture and magnetoresistance of glass-like carbons. *Carbon* **1991**, *29* (8), 1107.
41. McCreery, R. L.; McDermott, M. T., Comment on electrochemical kinetics at ordered graphite electrodes. *Anal. Chem.* **2012**, *84* (5), 2602.
42. Bowling, R.; Packard, R. T.; McCreery, R. L., Mechanism of electrochemical activation of carbon electrodes: Role of graphite lattice defects. *Langmuir* **1989**, *5* (3), 683.
43. McCreery, R. L.; Cline, K. K.; McDermott, C. A.; McDermott, M. T., Control of reactivity at carbon electrode surfaces. *Colloids Surf., A* **1994**, *93* (0), 211.
44. Cline, K. K.; McDermott, M. T.; McCreery, R. L., Anomalously slow-electron transfer at ordered graphite-electrodes - influence of electronic factors and reactive sites. *J. Phys. Chem.* **1994**, *98* (20), 5314.

45. Kneten, K. R.; McCreery, R. L., Effects of redox system structure on electron-transfer kinetics at ordered graphite and glassy carbon electrodes. *Anal. Chem.* **1992**, *64* (21), 2518.
46. Lai, S. C. S.; Patel, A. N.; McKelvey, K.; Unwin, P. R., Definitive evidence for fast electron transfer at pristine basal plane graphite from high-resolution electrochemical imaging. *Angew. Chem. Int. Ed. Engl.* **2012**, *51* (22), 5405.
47. Chen, P.; McCreery, R. L., Control of electron transfer kinetics at glassy carbon electrodes by specific surface modification. *Anal. Chem.* **1996**, *68* (22), 3958.
48. Kuo, T. C.; McCreery, R. L., Surface chemistry and electron-transfer kinetics of hydrogen-modified glassy carbon electrodes. *Anal. Chem.* **1999**, *71* (8), 1553.
49. Collier, W. G.; Tougas, T. P., Determination of surface hydroxyl groups on glassy carbon with X-ray photoelectron spectroscopy preceded by chemical derivatization. *Anal. Chem.* **1987**, *59* (3), 396.
50. Fryling, M. A.; Zhao, J.; McCreery, R. L., Resonance raman observation of surface carbonyl groups on carbon electrodes following dinitrophenylhydrazine derivatization. *Anal. Chem.* **1995**, *67* (5), 967.
51. McDermott, M. T.; McCreery, R. L., Scanning tunneling microscopy of ordered graphite and glassy carbon surfaces: Electronic control of quinone adsorption. *Langmuir* **1994**, *10* (11), 4307.
52. Hu, I.-F.; Karweik, D. H.; Kuwana, T., Activation and deactivation of glassy carbon electrodes. *J. Electroanal. Chem. Interfac. Electrochem.* **1985**, *188* (1–2), 59.
53. Fagan, D. T.; Hu, I. F.; Kuwana, T., Vacuum heat-treatment for activation of glassy carbon electrodes. *Anal. Chem.* **1985**, *57* (14), 2759.
54. Ranganathan, S.; Kuo, T. C.; McCreery, R. L., Facile preparation of active glassy carbon electrodes with activated carbon and organic solvents. *Anal. Chem.* **1999**, *71* (16), 3574.
55. Chen, P.; Fryling, M. A.; McCreery, R. L., Electron transfer kinetics at modified carbon electrode surfaces: The role of specific surface sites. *Anal. Chem.* **1995**, *67* (18), 3115.
56. Lee, C.-W.; Bard, A. J., Comparative electrochemical studies of N-methyl-N'-hexadecyl viologen monomolecular films formed by irreversible adsorption and the langmuir-blodgett method. *J. Electroanal. Chem. Interfac. Electrochem.* **1988**, *239* (1–2), 441.
57. Ye, H.; Crooks, R. M., Effect of elemental composition of PtPd bimetallic nanoparticles containing an average of 180 atoms on the kinetics of the electrochemical oxygen reduction reaction. *J. Am. Chem. Soc.* **2007**, *129* (12), 3627.
58. Youn, S. W.; Takahashi, M.; Goto, H.; Maeda, R., A study on focused ion beam milling of glassy carbon molds for the thermal imprinting of quartz and borosilicate glasses. *J. Micromech. Microeng.* **2006**, *16* (12), 2576.
59. Ito, T.; Kaneko, S.; Kunimatsu, M.; Hirabayashi, Y.; Soga, M.; Suzuki, K., Electrochemical response of platinum ultrathin layer formed by pulsed laser deposition. *International Journal of Electrochemistry* **2011**.
60. Pontikos, N. M.; McCreery, R. L., Microstructural and morphological changes induced in glassy carbon electrodes by laser irradiation. *J. Electroanal. Chem.* **1992**, *324* (1–2), 229.
61. Kostecki, R.; Schnyder, B.; Alliata, D.; Song, X.; Kinoshita, K.; Kötz, R., Surface studies of carbon films from pyrolyzed photoresist. *Thin Solid Films* **2001**, *396* (1-2), 36.
62. Ranganathan, S.; McCreery, R.; Majji, S. M.; Madou, M., Photoresist-derived carbon for microelectromechanical systems and electrochemical applications. *J. Electrochem. Soc.* **2000**, *147* (1), 277.

63. Kim, J.; Song, X.; Kinoshita, K.; Madou, M.; White, R., Electrochemical studies of carbon films from pyrolyzed photoresist. *J. Electrochem. Soc.* **1998**, *145* (7), 2314.
64. Ranganathan, S.; McCreery, R. L., Electroanalytical performance of carbon films with near-atomic flatness. *Anal. Chem.* **2001**, *73* (5), 893.
65. Brooksby, P. A.; Downard, A. J., Multilayer nitroazobenzene films covalently attached to carbon. An AFM and electrochemical study. *J. Phys. Chem. B* **2005**, *109* (18), 8791.
66. Brooksby, P. A.; Downard, A. J., Electrochemical and atomic force microscopy study of carbon surface modification via diazonium reduction in aqueous and acetonitrile solutions. *Langmuir* **2004**, *20* (12), 5038.
67. Garrett, D. J.; Lehr, J.; Miskelly, G. M.; Downard, A. J., Microcontact printing using the spontaneous reduction of aryldiazonium salts. *J. Am. Chem. Soc.* **2007**, *129* (50), 15456.
68. Anariba, F.; DuVall, S. H.; McCreery, R. L., Mono-and multilayer formation by diazonium reduction on carbon surfaces monitored with atomic force microscopy "scratching". *Anal. Chem.* **2003**, *75* (15), 3837.
69. Zachek, M. K.; Takmakov, P.; Moody, B.; Wightman, R. M.; McCarty, G. S., Simultaneous decoupled detection of dopamine and oxygen using pyrolyzed carbon microarrays and fast-scan cyclic voltammetry. *Anal. Chem.* **2009**, *81* (15), 6258.
70. Hebert, N. E.; Snyder, B.; McCreery, R. L.; Kuhr, W. G.; Brazill, S. A., Performance of pyrolyzed photoresist carbon films in a microchip capillary electrophoresis device with sinusoidal voltammetric detection. *Anal. Chem.* **2003**, *75* (16), 4265.
71. Wang, C.; Taherabadi, L.; Jia, G.; Madou, M.; Yeh, Y.; Dunn, B., C-MEMS for the manufacture of 3D microbatteries. *Electrochem. Solid-State Lett.* **2004**, *7* (11), A435.
72. Lyons, A. M.; Wilkins, C. W.; Robbins, M., Thin pinhole-free carbon films. *Thin Solid Films* **1983**, *103* (1–3), 333.
73. Lyons, A. M., Photodefinable carbon films: Electrical properties. *J. Non-Cryst. Solids* **1985**, *70* (1), 99.
74. McCreery, R. L.; Wu, J.; Prasad Kalakodimi, R., Electron transport and redox reactions in carbon-based molecular electronic junctions. *Phys. Chem. Chem. Phys.* **2006**, *8* (22), 2572.
75. Yan, H.; Bergren, A. J.; McCreery, R. L., All-carbon molecular tunnel junctions. *J. Am. Chem. Soc.* **2011**, *133* (47), 19168.
76. Fairman, C.; Yu, S. S. C.; Liu, G.; Downard, A. J.; Hibbert, D. B.; Gooding, J. J., Exploration of variables in the fabrication of pyrolysed photoresist. *J. Solid State Electrochem.* **2008**, *12* (10), 1357.
77. Del Campo, F. J.; Godignon, P.; Aldous, L.; Pausas, E.; Sarrión, M.; Zabala, M.; Prehn, R.; Compton, R. G., Fabrication of PPF electrodes by a rapid thermal process. *J. Electrochem. Soc.* **2011**, *158* (1), H63.
78. Delamar, M.; Hitmi, R.; Pinson, J.; Savéant, J. M., Covalent modification of carbon surfaces by grafting of functionalized aryl radicals produced from electrochemical reduction of diazonium salts. *J. Am. Chem. Soc.* **1992**, *114* (14), 5883.
79. Malmos, K.; Iruthayaraj, J.; Ogaki, R.; Kingshott, P.; Besenbacher, F.; Pedersen, S. U.; Daasbjerg, K., Grafting of thin organic films by electrooxidation of arylhydrazines. *J. Phys. Chem. C* **2011**, *115* (27), 13343.
80. Gallardo, I.; Pinson, J.; Vilà, N., Spontaneous attachment of amines to carbon and metallic surfaces. *J. Phys. Chem. B* **2006**, *110* (39), 19521.

81. Tanaka, M.; Sawaguchi, T.; Sato, Y.; Yoshioka, K.; Niwa, O., Surface modification of GC and HOPG with diazonium, amine, azide, and olefin derivatives. *Langmuir* **2010**, *27* (1), 170.
82. Lawrence, E. J.; Wildgoose, G. G.; Aldous, L.; Wu, Y. A.; Warner, J. H.; Compton, R. G.; McNaughter, P. D., 3-aryl-3-(trifluoromethyl)diazirines as versatile photoactivated "linker" molecules for the improved covalent modification of graphitic and carbon nanotube surfaces. *Chem. Mat.* **2011**, *23* (16), 3740.
83. Bonifas, A. P.; McCreery, R. L., Assembling molecular electronic junctions one molecule at a time. *Nano Lett.* **2011**, *11* (11), 4725.
84. Bergren, A. J.; McCreery, R. L., Analytical chemistry in molecular electronics. *Annu. Rev. Anal. Chem.* **2011**, *4*, 173.
85. Weissmann, M.; Crosnier, O.; Brousse, T.; Bélanger, D., Electrochemical study of anthraquinone groups, grafted by the diazonium chemistry, in different aqueous media-relevance for the development of aqueous hybrid electrochemical capacitor. *Electrochim. Acta* **2012**.
86. Rengaraj, S.; Kavanagh, P.; Leech, D., A comparison of redox polymer and enzyme co-immobilization on carbon electrodes to provide membrane-less glucose/O_2 enzymatic fuel cells with improved power output and stability. *Biosens. Bioelectron.* **2011**, *30* (1), 294.
87. Jürmann, G.; Schiffrin, D. J.; Tammeveski, K., The pH-dependence of oxygen reduction on quinone-modified glassy carbon electrodes. *Electrochim. Acta* **2007**, *53* (2), 390.
88. Liu, G.; Wang, S.; Liu, J.; Song, D., An electrochemical immunosensor based on chemical assembly of vertically aligned carbon nanotubes on carbon substrates for direct detection of the pesticide endosulfan in environmental water. *Anal. Chem.* **2012**, *84* (9), 3921.
89. Kullapere, M.; Seinberg, J.-M.; Mäeorg, U.; Maia, G.; Schiffrin, D. J.; Tammeveski, K., Electroreduction of oxygen on glassy carbon electrodes modified with in situ generated anthraquinone diazonium cations. *Electrochim. Acta* **2009**, *54* (7), 1961.
90. Chung, D. J.; Kim, K. C.; Choi, S. H., Electrochemical DNA biosensor based on avidin-biotin conjugation for influenza virus (type A) detection. *Appl. Surf. Sci.* **2011**, *257* (22), 9390.
91. Kowalczyk, A.; Nowicka, A.; Jurczakowski, R.; Fau, M.; Krolikowska, A.; Stojek, Z., Construction of DNA biosensor at glassy carbon surface modified with 4-aminoethylbenzenediazonium salt. *Biosens. Bioelectron.* **2011**, *26* (5), 2506.
92. Bélanger, D.; Pinson, J., Electrografting: A powerful method for surface modification. *Chem. Soc. Rev.* **2011**, *40* (7), 3995.
93. Barrière, F.; Downard, A., Covalent modification of graphitic carbon substrates by non-electrochemical methods. *J. Solid State Electrochem.* **2008**, *12* (10), 1231.
94. Barbier, B.; Pinson, J.; Desarmot, G.; Sanchez, M., Electrochemical bonding of amines to carbon fiber surfaces toward improved carbon-epoxy composites. *J. Electrochem. Soc.* **1990**, *137* (6), 1757.
95. Deinhammer, R. S.; Ho, M.; Anderegg, J. W.; Porter, M. D., Electrochemical oxidation of amine-containing compounds: A route to the surface modification of glassy carbon electrodes. *Langmuir* **1994**, *10* (4), 1306.
96. Nasraoui, R.; Bergamini, J. F.; Ababou-Girard, S.; Geneste, F., Sequential anodic oxidations of aliphatic amines in aqueous medium on pyrolyzed photoresist film surfaces for the covalent immobilization of cyclam derivatives. *J. Solid State Electrochem.* **2011**, *15* (1), 139.

97. Pchelintsev, N. A.; Vakurov, A.; Hays, H. H.; Millner, P. A., Thiols deposition onto the surface of glassy carbon electrodes mediated by electrical potential. *Electrochim. Acta* **2011**, *56* (6), 2696.
98. Maeda, H.; Yamauchi, Y.; Hosoe, M.; Li, T. X.; Yamaguchi, E.; Kasamatsu, M.; Ohmori, H., Direct covalent modification of glassy carbon surfaces with 1-alkanols by electrochemical oxidation. *Chem. Pharm. Bull.* **1994**, *42* (9), 1870.
99. Andrieux, C. P.; Gonzalez, F.; Savéant, J. M., Derivatization of carbon surfaces by anodic oxidation of arylacetates. Electrochemical manipulation of the grafted films. *J. Am. Chem. Soc.* **1997**, *119* (18), 4292.
100. Malmos, K.; Iruthayaraj, J.; Pedersen, S. U.; Daasbjerg, K., General approach for monolayer formation of covalently attached aryl groups through electrografting of arylhydrazines. *J. Am. Chem. Soc.* **2009**, *131* (39), 13926.
101. Vase, K. H.; Holm, A. H.; Norrman, K.; Pedersen, S. U.; Daasbjerg, K., Electrochemical surface derivatization of glassy carbon by the reduction of triaryl- and alkyldiphenylsulfonium salts. *Langmuir* **2008**, *24* (1), 182.
102. Vase, K. H.; Holm, A. H.; Norrman, K.; Pedersen, S. U.; Daasbjerg, K., Covalent grafting of glassy carbon electrodes with diaryliodonium salts: New aspects. *Langmuir* **2007**, *23* (7), 3786.
103. Weissmann, M.; Baranton, S.; Coutanceau, C., Modification of carbon substrates by aryl and alkynyl iodonium salt reduction. *Langmuir* **2010**, *26* (18), 15002.
104. Jouikov, V.; Simonet, J., Novel method for grafting alkyl chains onto glassy carbon. Application to the easy immobilization of ferrocene used as redox probe. *Langmuir* **2011**, *28* (1), 931.
105. Chehimi, M. M.; Hallais, G.; Matrab, T.; Pinson, J.; Podvorica, F. I., Electro- and photografting of carbon or metal surfaces by alkyl groups. *J. Phys. Chem. C* **2008**, *112* (47), 18559.
106. Adenier, A.; Barré, N.; Cabet-Deliry, E.; Chaussé, A.; Griveau, S.; Mercier, F.; Pinson, J.; Vautrin-Ul, C., Study of the spontaneous formation of organic layers on carbon and metal surfaces from diazonium salts. *Surf. Sci.* **2006**, *600* (21), 4801.
107. Yu, S. S. C.; Downard, A. J., Photochemical grafting and activation of organic layers on glassy carbon and pyrolyzed photoresist films. *Langmuir* **2007**, *23* (8), 4662.
108. Cruickshank, A. C.; Downard, A. J., Electrochemical stability of citrate-capped gold nanoparticles electrostatically assembled on amine-modified glassy carbon. *Electrochim. Acta* **2009**, *54* (23), 5566.
109. Yang, L.; Chen, J.; Wei, X.; Liu, B.; Kuang, Y., Ethylene diamine-grafted carbon nanotubes: A promising catalyst support for methanol electro-oxidation. *Electrochim. Acta* **2007**, *53* (2), 777.
110. Adenier, A.; Chehimi, M. M.; Gallardo, I.; Pinson, J.; Vilà, N., Electrochemical oxidation of aliphatic amines and their attachment to carbon and metal surfaces. *Langmuir* **2004**, *20* (19), 8243.
111. Ghilane, J.; Martin, P.; Randriamahazaka, H.; Lacroix, J.-C., Electrochemical oxidation of primary amine in ionic liquid media: Formation of organic layer attached to electrode surface. *Electrochem. Commun.* **2010**, *12* (2), 246.
112. Buriez, O.; Labbé, E.; Pigeon, P.; Jaouen, G.; Amatore, C., Electrochemical attachment of a conjugated amino–ferrocifen complex onto carbon and metal surfaces. *J. Electroanal. Chem.* **2008**, *619–620* (0), 169.

113. Cruickshank, A. C.; Tan, E. S. Q.; Brooksby, P. A.; Downard, A. J., Are redox probes a useful indicator of film stability? An electrochemical, AFM and XPS study of electrografted amine films on carbon. *Electrochem. Commun.* **2007**, *9* (7), 1456.
114. Garrett, D. J.; Flavel, B. S.; Shapter, J. G.; Baronian, K. H. R.; Downard, A. J., Robust forests of vertically aligned carbon nanotubes chemically assembled on carbon substrates. *Langmuir* **2009**, *26* (3), 1848.
115. Aramata, A.; Takahashi, S.; Yin, G.; Gao, Y.; Inose, Y.; Mihara, H.; Tadjeddine, A.; Zheng, W. Q.; Pluchery, O.; Bittner, A.; Yamagishi, A., Ligand grafting method for immobilization of metal complexes on a carbon electrode. *Thin Solid Films* **2003**, *424* (2), 239.
116. Rawson, F. J.; Garrett, D. J.; Leech, D.; Downard, A. J.; Baronian, K. H. R., Electron transfer from proteus vulgaris to a covalently assembled, single walled carbon nanotube electrode functionalised with osmium bipyridine complex: Application to a whole cell biosensor. *Biosens. Bioelectron.* **2011**, *26* (5), 2383.
117. Rawson, F. J.; Yeung, C. L.; Jackson, S. K.; Mendes, P. M., Tailoring 3D single-walled carbon nanotubes anchored to indium tin oxide for natural cellular uptake and intracellular sensing. *Nano Lett.* **2012**.
118. Pinson, J.; Podvorica, F., Attachment of organic layers to conductive or semiconductive surfaces by reduction of diazonium salts. *Chem. Soc. Rev.* **2005**, *34* (5), 429.
119. Mahouche-Chergui, S.; Gam-Derouich, S.; Mangeney, C.; Chehimi, M. M., Aryl diazonium salts: A new class of coupling agents for bonding polymers, biomacromolecules and nanoparticles to surfaces. *Chem. Soc. Rev.* **2011**, *40* (7), 4143.
120. Chehimi, M. M., *Aryl diazonium salts: New coupling agents in polymer and surface science*. Wiley: **2012**.
121. Pinson, J., Attachment of organic layers to materials surfaces by reduction of diazonium salts. In *Aryl diazonium salts: New coupling agents in polymer and surface science*, Chehimi, M. M., Ed. Wiley: **2012**; pp 1.
122. Allongue, P.; Delamar, M.; Desbat, B.; Fagebaume, O.; Hitmi, R.; Pinson, J.; Savéant, J.-M., Covalent modification of carbon surfaces by aryl radicals generated from the electrochemical reduction of diazonium salts. *J. Am. Chem. Soc.* **1997**, *119* (1), 201.
123. Andrieux, C. P.; Pinson, J., The standard redox potential of the phenyl radical/anion couple. *J. Am. Chem. Soc.* **2003**, *125* (48), 14801.
124. Toupin, M.; Bélanger, D., Thermal stability study of aryl modified carbon black by in situ generated diazonium salt. *J. Phys. Chem. C* **2007**, *111* (14), 5394.
125. Combellas, C.; Kanoufi, F.; Pinson, J.; Podvorica, F. I., Time-of-flight secondary ion mass spectroscopy characterization of the covalent bonding between a carbon surface and aryl groups. *Langmuir* **2004**, *21* (1), 280.
126. Doppelt, P.; Hallais, G.; Pinson, J.; Podvorica, F.; Verneyre, S., Surface modification of conducting substrates. Existence of azo bonds in the structure of organic layers obtained from diazonium salts. *Chem. Mat.* **2007**, *19* (18), 4570.
127. Anariba, F.; Viswanathan, U.; Bocian, D. F.; McCreery, R. L., Determination of the structure and orientation of organic molecules tethered to flat graphitic carbon by ATR-FT-IR and Raman spectroscopy. *Anal. Chem.* **2006**, *78* (9), 3104.
128. Koehler, F. M.; Jacobsen, A.; Ensslin, K.; Stampfer, C.; Stark, W. J., Selective chemical modification of graphene surfaces: Distinction between single- and bilayer graphene. *Small* **2010**, *6* (10), 1125.

129. Jiang, D.-e.; Sumpter, B. G.; Dai, S., How do aryl groups attach to a graphene sheet? *J. Phys. Chem. B* **2006**, *110* (47), 23628.
130. Anariba, F.; DuVall, S. H.; McCreery, R. L., Mono- and multilayer formation by diazonium reduction on carbon surfaces monitored with atomic force microscopy "scratching". *Analytical Chemistry* **2003**, *75* (15), 3837.
131. Haccoun, J.; Vautrin-Ul, C.; Chaussé, A.; Adenier, A., Electrochemical grafting of organic coating onto gold surfaces: Influence of the electrochemical conditions on the grafting of nitrobenzene diazonium salt. *Prog. Org. Coat.* **2008**, *63* (1), 18.
132. Combellas, C.; Kanoufi, F.; Pinson, J.; Podvorica, F. I., Sterically hindered diazonium salts for the grafting of a monolayer on metals. *J. Am. Chem. Soc.* **2008**, *130* (27), 8576.
133. Ceccato, M.; Bousquet, A.; Hinge, M.; Pedersen, S. U.; Daasbjerg, K., Using a mediating effect in the electroreduction of aryldiazonium salts to prepare conducting organic films of high thickness. *Chem. Mat.* **2011**, *23* (6), 1551.
134. Nielsen, L. T.; Vase, K. H.; Dong, M.; Besenbacher, F.; Pedersen, S. U.; Daasbjerg, K., Electrochemical approach for constructing a monolayer of thiophenolates from grafted multilayers of diaryl disulfides. *J. Am. Chem. Soc.* **2007**, *129* (7), 1888.
135. Malmos, K.; Dong, M.; Pillai, S.; Kingshott, P.; Besenbacher, F.; Pedersen, S. U.; Daasbjerg, K., Using a hydrazone-protected benzenediazonium salt to introduce a near-monolayer of benzaldehyde on glassy carbon surfaces. *J. Am. Chem. Soc.* **2009**, *131* (13), 4928.
136. Leroux, Y. R.; Fei, H.; Noël, J.-M.; Roux, C.; Hapiot, P., Efficient covalent modification of a carbon surface: Use of a silyl protecting group to form an active monolayer. *J. Am. Chem. Soc.* **2010**, *132* (40), 14039.
137. Ortiz, B.; Saby, C.; Champagne, G. Y.; Bélanger, D., Electrochemical modification of a carbon electrode using aromatic diazonium salts. 2. Electrochemistry of 4-nitrophenyl modified glassy carbon electrodes in aqueous media. *J. Electroanal. Chem.* **1998**, *455* (1–2), 75.
138. Yu, S. S. C.; Tan, E. S. Q.; Jane, R. T.; Downard, A. J., An electrochemical and XPS study of reduction of nitrophenyl films covalently grafted to planar carbon surfaces. *Langmuir* **2007**, *23* (22), 11074.
139. Hurley, B. L.; McCreery, R. L., Covalent bonding of organic molecules to Cu and Al alloy 2024 T3 surfaces via diazonium ion reduction. *J. Electrochem. Soc.* **2004**, *151* (5), B252.
140. Gooding, J. J., Advances in interfacial design for electrochemical biosensors and sensors: Aryl diazonium salts for modifying carbon and metal electrodes. *Electroanalysis* **2008**, *20* (6), 573.
141. Polsky, R.; Harper, J. C.; Wheeler, D. R.; Brozik, S. M., Multifunctional electrode arrays: Towards a universal detection platform. *Electroanalysis* **2008**, *20* (6), 671.
142. Berthelot, T.; Garcia, A.; Le, X. T.; El Morsli, J.; Jégou, P.; Palacin, S.; Viel, P., "Versatile toolset" for DNA or protein immobilization: Toward a single-step chemistry. *Appl. Surf. Sci.* **2011**, *257* (8), 3538.
143. Yuan, R.; Chai, Y.-Q.; Shen, G.-L.; Yu, R.-Q., Chemically modified electrode based on poly[tetra(4-aminophenyl)porphyrin] as a pH sensor. *Talanta* **1993**, *40* (8), 1255.
144. Downard, A. J.; Gross, A. J.; Simons, B. S., Patterned molecular layers on surfaces. In *Aryl diazonium salts: New coupling agents in polymer and surface science*, Chehimi, M. M., Ed. Wiley: **2012**; p 53.

145. McCreery, R. L., The merger of electrochemistry and molecular electronics. *The Chemical Record* **2012**, *12* (1), 149.
146. Keana, J. F. W.; Cai, S. X., New reagents for photoaffinity labeling: Synthesis and photolysis of functionalized perfluorophenyl azides. *J. Org. Chem.* **1990**, *55* (11), 3640.
147. Katritzky, A.; Scriven, E., Organic azides: Syntheses and applications. *J. Am. Chem. Soc.* **2010**, *132* (34), 12156.
148. Lutz, J.-F., 1,3-dipolar cycloadditions of azides and alkynes: A universal ligation tool in polymer and materials science. *Angew. Chem. Int. Ed. Eng.* **2007**, *46* (7), 1018.
149. Takumi, U.; Robert, A., Chemistry of photoresist materials. In *Microlithography*, CRC Press: **2007**; p 503.
150. Liu, L.-H.; Yan, M., Perfluorophenyl azides: New applications in surface functionalization and nanomaterial synthesis. *Acc. Chem. Res.* **2010**, *43* (11), 1434.
151. Pastine, S. J.; Okawa, D.; Kessler, B.; Rolandi, M.; Llorente, M.; Zettl, A.; Fréchet, J. M. J., A facile and patternable method for the surface modification of carbon nanotube forests using perfluoroarylazides. *J. Am. Chem. Soc.* **2008**, *130* (13), 4238.
152. Liu, L.-H.; Yan, M., Functionalization of pristine graphene with perfluorophenyl azides. *J. Mater. Chem.* **2011**, *21* (10), 3273.
153. Tanaka, M.; Sawaguchi, T.; Sato, Y.; Yoshioka, K.; Niwa, O., Surface modification of GC and HOPG with diazonium, amine, azide, and olefin derivatives. *Langmuir* **2011**, *27* (1), 170.
154. Yu, S. S. C. Covalent attachment of nanoscale organic films to carbon surfaces. University of Canterbury, Christchurch, **2008**.
155. Hengsakul, M.; Cass, A. E. G., Protein patterning with a photoactivatable derivative of biotin. *Bioconjugate Chem.* **1996**, *7* (2), 249.
156. Wilde, L. M.; Farace, G.; Roberts, C. J.; Davies, M. C.; Sanders, G. H. W.; Tendler, S. J. B.; Williams, P. M., Molecular patterning on carbon based surfaces through photobiotin activation. *Analyst* **2001**, *126* (2), 195.
157. Liu, L.-H.; Lerner, M. M.; Yan, M., Derivitization of pristine graphene with well-defined chemical functionalities. *Nano Lett.* **2010**, *10* (9), 3754.
158. Liu, L.-H.; Zorn, G.; Castner, D. G.; Solanki, R.; Lerner, M. M.; Yan, M., A simple and scalable route to wafer-size patterned graphene. *J. Mater. Chem.* **2010**, *20* (24), 5041.
159. Lwowski, W., *Nitrenes*. Interscience Publishers: **1970**.
160. Yan, M. D.; Cai, S. X.; Keana, J. F. W., Photochemical and thermal-reactions of C-60 with n-succinimidyl 4-azido-2,3,5,6-tetrafluorobenzoate - a new method for functionalization of C-60. *J. Org. Chem.* **1994**, *59* (20), 5951.
161. Dontha, N.; Nowall, W. B.; Kuhr, W. G., Generation of biotin/avidin/enzyme nanostructures with maskless photolithography. *Anal. Chem.* **1997**, *69* (14), 2619.
162. Holzinger, M.; Steinmetz, J.; Samaille, D.; Glerup, M.; Paillet, M.; Bernier, P.; Ley, L.; Graupner, R., [2+1] cycloaddition for cross-linking swcnts. *Carbon* **2004**, *42* (5–6), 941.
163. Liu, L.-H.; Yan, M., Simple method for the covalent immobilization of graphene. *Nano Lett.* **2009**, *9* (9), 3375.
164. Nowall, W. B.; Dontha, N.; Kuhr, W. G., Electron transfer kinetics at a biotin/avidin patterned glassy carbon electrode. *Biosens. Bioelectron.* **1998**, *13* (11), 1237.
165. Brooks, S. A.; Ambrose, W. P.; Kuhr, W. G., Micrometer dimension derivatization of biosensor surfaces using confocal dynamic patterning. *Anal. Chem.* **1999**, *71* (13), 2558.

166. Dontha, N.; Nowall, W. B.; Kuhr, W. G., Development of sub-micron patterned carbon electrodes for immunoassays. *J. Pharm. Biomed. Anal.* **1999**, *19* (1–2), 83.
167. Brooks, S. A.; Dontha, N.; Davis, C. B.; Stuart, J. K.; O'Neil, G.; Kuhr, W. G., Segregation of micrometer-dimension biosensor elements on a variety of substrate surfaces. *Anal. Chem.* **2000**, *72* (14), 3253.
168. Gates, B. D.; Xu, Q.; Stewart, M.; Ryan, D.; Willson, C. G.; Whitesides, G. M., New approaches to nanofabrication: Molding, printing, and other techniques. *Chem. Rev.* **2005**, *105* (4), 1171.
169. Champness, N. R., Surface patterning: SAMs are better by design. *Nat. Nano* **2008**, *3* (6), 324.
170. Xia, Y.; Rogers, J. A.; Paul, K. E.; Whitesides, G. M., Unconventional methods for fabricating and patterning nanostructures. *Chem. Rev.* **1999**, *99* (7), 1823.
171. Brooksby, P. A.; Downard, A. J., Nanoscale patterning of flat carbon surfaces by scanning probe lithography and electrochemistry. *Langmuir* **2005**, *21* (5), 1672.
172. Kongsfelt, M.; Vinther, J.; Malmos, K.; Ceccato, M.; Torbensen, K.; Knudsen, C. S.; Gothelf, K. V.; Pedersen, S. U.; Daasbjerg, K., Combining aryltriazenes and electrogenerated acids to create well-defined aryl-tethered films and patterns on surfaces. *J. Am. Chem. Soc.* **2011**, *133* (11), 3788.
173. Ghorbal, A.; Grisotto, F.; Charlier, J.; Palacin, S.; Goyer, C.; Demaille, C., Localized electrografting of vinylic monomers on a conducting substrate by means of an integrated electrochemical AFM probe. *ChemPhysChem* **2009**, *10* (7), 1053.
174. Mandon, C. A.; Blum, L. J.; Marquette, C. A., Aryl diazonium for biomolecules immobilization onto SPRi chips. *ChemPhysChem* **2009**, *10* (18), 3273.
175. Lehr, J.; Garrett, D. J.; Paulik, M. G.; Flavel, B. S.; Brooksby, P. A.; Williamson, B. E.; Downard, A. J., Patterning of metal, carbon, and semiconductor substrates with thin organic films by microcontact printing with aryldiazonium salt inks. *Anal. Chem.* **2010**, *82* (16), 7027.
176. Mouanda, B.; Eyeffa, V.; Palacin, S., Agarose-based hydrogel as an electrografting cell. *J. Appl. Electrochem.* **2009**, *39* (3), 313.
177. Downard, A. J.; Garrett, D. J.; Tan, E. S. Q., Microscale patterning of organic films on carbon surfaces using electrochemistry and soft lithography. *Langmuir* **2006**, *22* (25), 10739.
178. Corgier, B. P.; Bélanger, D., Electrochemical surface nanopatterning using microspheres and aryldiazonium. *Langmuir* **2010**, *26* (8), 5991.
179. Mesnage, A.; Deniau, G.; Tessier, L.; Mévellec, V.; Palacin, S., Localized grafting through chemical lift-off. *Appl. Surf. Sci.* **2011**, *257* (17), 7805.
180. Charlier, J.; Palacin, S.; Leroy, J.; Frari, D. D.; Zagonel, L.; Barrett, N.; Renault, O.; Bailly, A.; Mariolle, D., Local silicon doping as a promoter of patterned electrografting of diazonium for directed surface functionalization. *J. Mater. Chem.* **2008**, *18* (26), 3136.
181. Lee, C. S.; Baker, S. E.; Marcus, M. S.; Yang, W.; Eriksson, M. A.; Hamers, R. J., Electrically addressable biomolecular functionalization of carbon nanotube and carbon nanofiber electrodes. *Nano Lett.* **2004**, *4* (9), 1713.
182. Krämer, S.; Fuierer, R. R.; Gorman, C. B., Scanning probe lithography using self-assembled monolayers. *Chem. Rev.* **2003**, *103* (11), 4367.
183. Liu, G. Y.; Xu, S.; Qian, Y., Nanofabrication of self-assembled monolayers using scanning probe lithography. *Acc. Chem. Res.* **2000**, *33* (7), 457.

184. Xia, Y.; Whitesides, G. M., Soft lithography. *Annu. Rev. Mater. Sci.* **1998**, *28* (1), 153.
185. Qin, D.; Xia, Y.; Whitesides, G. M., Soft lithography for micro- and nanoscale patterning. *Nat. Protocols* **2010**, *5* (3), 491.
186. Harper, J. C.; Polsky, R.; Wheeler, D. R.; Lopez, D. M.; Arango, D. C.; Brozik, S. M., A multifunctional thin film Au electrode surface formed by consecutive electrochemical reduction of aryl diazonium salts. *Langmuir* **2009**, *25* (5), 3282.
187. Harper, J. C.; Polsky, R.; Wheeler, D. R.; Dirk, S. M.; Brozik, S. M., Selective immobilization of DNA and antibody probes on electrode arrays: Simultaneous electrochemical detection of DNA and protein on a single platform. *Langmuir* **2007**, *23* (16), 8285.
188. Corgier, B. P.; Marquette, C. A.; Blum, L. J., Diazonium−protein adducts for graphite electrode microarrays modification: Direct and addressed electrochemical immobilization. *J. Am. Chem. Soc.* **2005**, *127* (51), 18328.
189. Downard, A. J.; Prince, M. J., Barrier properties of organic monolayers on glassy carbon electrodes. *Langmuir* **2001**, *17* (18), 5581.
190. Kruper Jr, W. J.; Chamberlin, T. A.; Kochanny, M., Regiospecific aryl nitration of meso-substituted tetraarylporphyrins: A simple route to bifunctional porphyrins. *J. Org. Chem.* **1989**, *54* (11), 2753.
191. Hayvali, M.; Gündüz, H.; Gündüz, N.; Kiliç, Z.; Hökelek, T., Synthesis and characterization of unsymmetrically tetrasubstituted porphyrin and their nickel (II) complexes with the crystal structure of 5,15- bis(4-aminophenyl)- 10, 20-diphenylporphyrinatonickel(II). *J. Mol. Struct.* **2000**, *525* (1-3), 215.
192. Kosynkin, D.; Bockman, T. M.; Kochi, J. K., Fluorinated biphenyls from aromatic arylations with pentafluorobenzenediazonium and related cations. Competition between arylation and azo coupling. *J. Chem. Soc., Perkin Trans. 2* **1997**, (10), 2003.
193. Kosynkin, D. V.; Tour, J. M., Phenylene ethynylene diazonium salts as potential self-assembling molecular devices. *Org. Lett.* **2001**, *3* (7), 993.
194. Audette, R. C. S.; Connors, T. A.; Mandel, H. G.; Merai, K.; Ross, W. C. J., Studies on the mechanism of action of the tumour inhibitory triazenes. *Biochem. Pharmacol.* **1973**, *22* (15), 1855.
195. Hansen, M. N.; Farjami, E.; Kristiansen, M.; Clima, L.; Pedersen, S. U.; Daasbjerg, K.; Ferapontova, E. E.; Gothelf, K. V., Synthesis and application of a triazene−ferrocene modifier for immobilization and characterization of oligonucleotides at electrodes. *J. Org. Chem.* **2010**, *75* (8), 2474.
196. Leyva, E.; Munoz, D.; Platz, M. S., Photochemistry of fluorinated aryl azides in toluene solution and in frozen polycrystals. *J. Org. Chem.* **1989**, *54* (25), 5938.
197. Grabar, K. C.; Freeman, R. G.; Hommer, M. B.; Natan, M. J., Preparation and characterization of au colloid monolayers. *Anal. Chem.* **1995**, *67* (4), 735.
198. Frens, G., Controlled nucleation for regulation of particle-size in monodisperse gold suspensions. *Nature Physical Science* **1973**, *241* (105), 20.
199. Loring, J. S. University of California, Davis, **2000**.
200. Marinkovic, Z.; Roy, R., Preparation and properties of sputtered “glassy” carbon films. *Carbon* **1976**, *14* (6), 329.
201. Robertson, J., Amorphous carbon. *Adv Phys* **1986**, *35* (4), 317.
202. Schelz, S.; Richmond, T.; Kania, P.; Oelhafen, P.; Güntherodt, H. J., Electronic and atomic structure of evaporated carbon films. *Surf. Sci.* **1996**, *359* (1-3), 227.

203. Besold, J.; Thielsch, R.; Matz, N.; Frenzel, C.; Born, R.; Mobius, A., Surface and bulk properties of electron-beam evaporated carbon-films. *Thin Solid Films* **1997**, *293* (1-2), 96.
204. Blackstock, J. J.; Rostami, A. A.; Nowak, A. M.; McCreery, R. L.; Freeman, M. R.; McDermott, M. T., Ultraflat carbon film electrodes prepared by electron beam evaporation. *Anal. Chem.* **2004**, *76* (9), 2544.
205. Sun, B.; Colavita, P. E.; Kim, H.; Lockett, M.; Marcus, M. S.; Smith, L. M.; Hamers, R. J., Covalent photochemical functionalization of amorphous carbon thin films for integrated real-time biosensing. *Langmuir* **2006**, *22* (23), 9598.
206. Mattson, J. S.; Smith, C. A., Optically transparent carbon film electrodes for infrared spectroelectrochemistry. *Anal. Chem.* **1975**, *47* (7), 1122.
207. Donner, S.; Li, H.-W.; Yeung, E. S.; Porter, M. D., Fabrication of optically transparent carbon electrodes by the pyrolysis of photoresist films: Approach to single-molecule spectroelectrochemistry. *Anal. Chem.* **2006**, *78* (8), 2816.
208. DeAngelis, T. P.; Hurst, R. W.; Yacynych, A. M.; Mark, H. B.; Heineman, W. R.; Mattson, J. S., Carbon and mercury-carbon optically transparent electrodes. *Anal. Chem.* **1977**, *49* (9), 1395.
209. Bonifas, A. P.; McCreery, R. L., In-situ optical absorbance spectroscopy of molecular layers in carbon based molecular electronic devices. *Chem. Mater.* **2008**, *20* (12), 3849.
210. Pinto, E. M.; Gouveia-Caridade, C.; Soares, D. M.; Brett, C. M. A., Electrochemical and surface characterisation of carbon-film-coated piezoelectric quartz crystals. *Appl. Surf. Sci.* **2009**, *255* (18), 8084.
211. Tadigadapa, S.; Mateti, K., Piezoelectric mems sensors: State-of-the-art and perspectives. *Meas. Sci. Technol.* **2009**, *20* (9), 092001.
212. Breton, T.; Bélanger, D., Modification of carbon electrode with aryl groups having an aliphatic amine by electrochemical reduction of in situ generated diazonium cations. *Langmuir* **2008**, *24* (16), 8711.
213. Ghodbane, O.; Roué, L.; Bélanger, D., Copper electrodeposition on pyrolytic graphite electrodes: Effect of the copper salt on the electrodeposition process. *Electrochim. Acta* **2007**, *52* (19), 5843.
214. Kargl, R.; Kahn, M.; Köstler, S.; Reischl, M.; Doliška, A.; Stana-Kleinschek, K.; Waldhauser, W.; Ribitsch, V., Deposition of silicon doped and pure hydrogenated amorphous carbon coatings on quartz crystal microbalance sensors for protein adsorption studies. *Thin Solid Films* **2011**, *520* (1), 83.
215. Colavita, P. E.; Sun, B.; Wang, X.; Hamers, R. J., Influence of surface termination and electronic structure on the photochemical grafting of alkenes to carbon surfaces. *J. Phys. Chem. C* **2009**, *113* (4), 1526.
216. Kissinger, P. T.; Heineman, W. R., *Laboratory techniques in electroanalytical chemistry*. Marcel Dekker: **1996**.
217. Zhang, H.; Coury, L. A., Effects of high-intensity ultrasound on glassy carbon electrodes. *Anal. Chem.* **1993**, *65* (11), 1552.
218. Stutts, K. J.; Kovach, P. M.; Kuhr, W. G.; Wightman, R. M., Enhanced electrochemical reversibility at heat-treated glassy-carbon electrodes. *Anal. Chem.* **1983**, *55* (9), 1632.
219. Takmakov, P.; Zachek, M. K.; Keithley, R. B.; Walsh, P. L.; Donley, C.; McCarty, G. S.; Wightman, R. M., Carbon microelectrodes with a renewable surface. *Anal. Chem.* **2010**, *82* (5), 2020.

220. Lehr, J.; Williamson, B. E.; Flavel, B. S.; Downard, A. J., Reaction of gold substrates with diazonium salts in acidic solution at open-circuit potential. *Langmuir* **2009**, *25* (23), 13503.
221. Saby, C.; Ortiz, B.; Champagne, G. Y.; Bélanger, D., Electrochemical modification of glassy carbon electrode using aromatic diazonium salts. 1. Blocking effect of 4-nitrophenyl and 4-carboxyphenyl groups. *Langmuir* **1997**, *13* (25), 6805.
222. Hinge, M.; Gonçalves, E. S.; Pedersen, S. U.; Daasbjerg, K., On the electrografting of stainless steel from para-substituted aryldiazonium salts and the thermal stability of the grafted layer. *Surf. Coat. Technol.* **2010**, *205* (3), 820.
223. Suzuki, T.; Kyotani, T.; Tomita, A., Study on the carbon-nitric oxide reaction in the presence of oxygen. *Ind. Eng. Chem. Res.* **1994**, *33* (11), 2840.
224. Agarwal, N. K.; Haubold, A. D., Vacuum-deposited carbon coatings. *Thin Solid Films* **1977**, *40* (0), 299.
225. Franssila, S., *Introduction to microfabrication*. Wiley: **2010**.
226. Larson, D. M.; Downing, K. H.; Glaeser, R. M., The surface of evaporated carbon films is an insulating, high-bandgap material. *J. Struct. Biol.* **2011**, *174* (2), 420.
227. Cullen, R. J.; Jayasundara, D. R.; Soldi, L.; Cheng, J. J.; Dufaure, G.; Colavita, P. E., Spontaneous grafting of nitrophenyl groups on amorphous carbon thin films: A structure–reactivity investigation. *Chem. Mat.* **2012**, *24* (6), 1031.
228. Jia, J.; Kato, D.; Kurita, R.; Sato, Y.; Maruyama, K.; Suzuki, K.; Hirono, S.; Ando, T.; Niwa, O., Structure and electrochemical properties of carbon films prepared by a electron cyclotron resonance sputtering method. *Anal. Chem.* **2006**, *79* (1), 98.
229. Fu, Y.; Du, H.; Sun, C. Q., Interfacial structure, residual stress and adhesion of diamond coatings deposited on titanium. *Thin Solid Films* **2003**, *424* (1), 107.
230. Yoshino, N.; Shibuya, Y.; Naoi, K.; Nanya, T., Deposition of a diamond-like carbon film on a stainless steel substrate: Studies of intermediate layers. *Surf. Coat. Technol.* **1991**, *47* (1–3), 84.
231. Ensinger, W.; Lensch, O.; Matsutani, T.; Kiuchi, M., Corrosion performance of thin amorphous carbon films on aluminum formed by ion beam-based coating techniques. *Surf. Coat. Technol.* **2005**, *196* (1–3), 231.
232. Chen, C.-C.; Hong, F. C.-N., Interfacial studies for improving the adhesion of diamond-like carbon films on steel. *Appl. Surf. Sci.* **2005**, *243* (1–4), 296.
233. Frankel, G. S., Pitting corrosion of metals: A review of the critical factors. *J. Electrochem. Soc.* **1998**, *145* (6), 2186.
234. Bard, A. J.; Faulkner, L. R., *Electrochemical methods: Fundamentals and applications*. Wiley: **2001**.
235. Nicholson, R. S., Theory and application of cyclic voltammetry for measurement of electrode reaction kinetics. *Anal. Chem.* **1965**, *37* (11), 1351.
236. Konopka, S. J.; McDuffie, B., Diffusion coefficients of ferri- and ferrocyanide ions in aqueous media, using twin-electrode thin-layer electrochemistry. *Anal. Chem.* **1970**, *42* (14), 1741.
237. McCreery, R. L., Advanced carbon electrode materials for molecular electrochemistry. *Chem. Rev. (Washington, DC, U. S.)* **2008**, *108* (7), 2646.
238. Rice, R. J.; Pontikos, N. M.; McCreery, R. L., Quantitative correlations of heterogeneous electron-transfer kinetics with surface properties of glassy carbon electrodes. *J. Am. Chem. Soc.* **1990**, *112* (12), 4617.

239. Seghiouer, A.; Chevalet, J.; Barhoun, A.; Lantelme, F., Electrochemical oxidation of nickel in alkaline solutions: A voltammetric study and modelling. *J. Electroanal. Chem.* **1998**, *442* (1–2), 113.
240. Niwa, O.; Jia, J.; Sato, Y.; Kato, D.; Kurita, R.; Maruyama, K.; Suzuki, K.; Hirono, S., Electrochemical performance of angstrom level flat sputtered carbon film consisting of sp^2 and sp^3 mixed bonds. *J. Am. Chem. Soc.* **2006**, *128* (22), 7144.
241. Chen, Q.; Gruen, D. M.; Krauss, A. R.; Corrigan, T. D.; Witek, M.; Swain, G. M., The structure and electrochemical behavior of nitrogen-containing nanocrystalline diamond films deposited from Ch_4/N_2/Ar mixtures *J. Electrochem. Soc.* **2001**, *148* (1), E44.
242. Wang, J.; Anik Kirgöz, Ü.; Mo, J.-W.; Lu, J.; Nasser Kawde, A.; Muck, A., Glassy carbon paste electrodes. *Electrochem. Commun.* **2001**, *3* (4), 203.
243. Xu, J.; Chen, Q.; Swain, G. M., Anthraquinonedisulfonate electrochemistry: A comparison of glassy carbon, hydrogenated glassy carbon, highly oriented pyrolytic graphite, and diamond electrodes. *Anal. Chem.* **1998**, *70* (15), 3146.
244. Baranton, S.; Bélanger, D., Electrochemical derivatization of carbon surface by reduction of in situ generated diazonium cations. *J. Phys. Chem. B* **2005**, *109* (51), 24401.
245. Azarko, I. I.; Goncharov, V. K.; Gusakov, G. A.; Ismailov, D. R.; Puzyrev, M. V., Effect of the structure of a graphite target on the parameters of carbon films obtained by the laser plasma method *J. Appl. Spectrosc.* **2008**, *75* (4), 560.
246. Wiltner, A.; Linsmeier, C.; Jacob, T., Carbon reaction and diffusion on Ni(111), Ni(100), and Fe(110): Kinetic parameters from X-ray photoelectron spectroscopy and density functional theory analysis. *J. Chem. Phys.* **2008**, *129* (8), 084704.
247. Walter, M. G.; Rudine, A. B.; Wamser, C. C., Porphyrins and phthalocyanines in solar photovoltaic cells. *J. Porphyrins Phthalocyanines* **2010**, (14), 759.
248. Campbell, W. M.; Jolley, K. W.; Wagner, P.; Wagner, K.; Walsh, P. J.; Gordon, K. C.; Schmidt-Mende, L.; Nazeeruddin, M. K.; Wang, Q.; Grätzel, M.; Officer, D. L., Highly efficient porphyrin sensitizers for dye-sensitized solar cells. *J. Phys. Chem. C* **2007**, *111* (32), 11760.
249. Bessho, T.; Zakeeruddin, S. M.; Yeh, C.-Y.; Diau, E. W.-G.; Grätzel, M., Highly efficient mesoscopic dye-sensitized solar cells based on donor–acceptor-substituted porphyrins. *Angew. Chem. Int. Ed. Eng.* **2010**, *49* (37), 6646.
250. Yamada, H.; Imahori, H.; Nishimura, Y.; Yamazaki, I.; Ahn, T. K.; Kim, S. K.; Kim, D.; Fukuzumi, S., Photovoltaic properties of self-assembled monolayers of porphyrins and porphyrin−fullerene dyads on ITO and gold surfaces. *J. Am. Chem. Soc.* **2003**, *125* (30), 9129.
251. Jiao, J.; Schmidt, I.; Taniguchi, M.; Lindsey, J. S.; Bocian, D. F., Comparison of electron-transfer rates for metal- versus ring-centered redox processes of porphyrins in monolayers on Au(111). *Langmuir* **2008**, *24* (20), 12047.
252. Lindsey, J. S.; Bocian, D. F., Molecules for charge-based information storage. *Acc. Chem. Res.* **2011**, *44* (8), 638.
253. Zak, J.; Yuan, H.; Ho, M.; Woo, L. K.; Porter, M. D., Thiol-derivatized metalloporphyrins: Monomolecular films for the electrocatalytic reduction of dioxygen at gold electrodes. *Langmuir* **1993**, *9* (11), 2772.
254. Mezour, M. A.; Cornut, R.; Hussien, E. M.; Morin, M.; Mauzeroll, J., Detection of hydrogen peroxide produced during the oxygen reduction reaction at self-assembled

thiol−porphyrin monolayers on gold using secm and nanoelectrodes. *Langmuir* **2010**, *26* (15), 13000.

255. Hutchison, J. E.; Postlethwaite, T. A.; Murray, R. W., Molecular films of thiol-derivatized tetraphenylporphyrins on gold: Film formation and electrocatalytic dioxygen reduction. *Langmuir* **1993**, *9* (11), 3277.
256. Nishimura, N.; Ooi, M.; Shimazu, K.; Fujii, H.; Uosaki, K., Post-assembly insertion of metal ions into thiol-derivatized porphyrin monolayers on gold. *J. Electroanal. Chem.* **1999**, *473* (1–2), 75.
257. Malinski, T.; Taha, Z., Nitric oxide release from a single cell measured in situ by a porphyrinic-based microsensor. *Nature* **1992**, *358* (6388), 676.
258. Ciszewski, A.; Milczarek, G., Electrocatalytic oxidation of alcohols on glassy carbon electrodes electrochemically modified by conductive polymeric nickel(II) tetrakis(3-methoxy-4-hydroxyphenyl) porphyrin film. *J. Electroanal. Chem.* **1996**, *413* (1–2), 137.
259. Trevin, S.; Bedioui, F.; Guadalupe Gomez Villegas, M.; Bied-Charreton, C., Electropolymerized nickel macrocyclic complex-based films: Design and electrocatalytic application. *J. Mater. Chem.* **1997**, *7* (6), 923.
260. Nagashree, K. L.; Ahmed, M. F., Electrocatalytic oxidation of methanol on ni modified polyaniline electrode in alkaline medium. *J. Solid State Electrochem.* **2010**, *14* (12), 2307.
261. Kruper, W. J.; Chamberlin, T. A.; Kochanny, M., Regiospecific aryl nitration of meso-substituted tetraarylporphyrins: A simple route to bifunctional porphyrins. *J. Org. Chem.* **1989**, *54* (11), 2753.
262. Brittle, S. A.; Richardson, T. H.; Dunbar, A. D. F.; Turega, S. M.; Hunter, C. A., Tuning free base tetraphenylporphyrins as optical sensing elements for volatile organic analytes. *J. Mater. Chem.* **2011**, *21* (13), 4882.
263. Dolci, L. S.; Marzocchi, E.; Montalti, M.; Prodi, L.; Monti, D.; Di Natale, C.; D'Amico, A.; Paolesse, R., Amphiphilic porphyrin film on glass as a simple and selective solid-state chemosensor for aqueous Hg^{2+}. *Biosens. Bioelectron.* **2006**, *22* (3), 399.
264. Vlascici, D.; Fagadar-Cosma, E.; Pica, E.; Cosma, V.; Bizerea, O.; Mihailescu, G.; Olenic, L., Free base porphyrins as ionophores for heavy metal sensors. *Sensors* **2008**, *8* (8), 4995.
265. Buntem, R.; Intasiri, A.; Lueangchaichaweng, W., Facile synthesis of silica monolith doped with meso-tetra(p-carboxyphenyl)porphyrin as a novel metal ion sensor. *J. Colloid Interface Sci.* **2010**, *347* (1), 8.
266. Macor, K. A.; Spiro, T. G., Porphyrin electrode films prepared by electrooxidation of metalloprotoporphyrins. *J. Am. Chem. Soc.* **1983**, *105* (17), 5601.
267. Walter, M. G.; Wamser, C. C., Synthesis and characterization of electropolymerized nanostructured aminophenylporphyrin films. *J. Phys. Chem. C* **2010**, *114* (17), 7563.
268. Bedioui, F.; Devynck, J.; Bied-Charreton, C., Immobilization of metalloporphyrins in electropolymerized films: Design and applications. *Acc. Chem. Res.* **1995**, *28* (1), 30.
269. Paul-Roth, C.; Rault-Berthelot, J.; Simonneaux, G.; Poriel, C.; Abdalilah, M.; Letessier, J., Electroactive films of poly(tetraphenylporphyrins) with reduced bandgap. *J. Electroanal. Chem.* **2006**, *597* (1), 19.
270. Boeckl, M. S.; Bramblett, A. L.; Hauch, K. D.; Sasaki, T.; Ratner, B. D.; Rogers, J. W., Self-assembly of tetraphenylporphyrin monolayers on gold substrates. *Langmuir* **2000**, *16* (13), 5644.

271. Yasseri, A. A.; Syomin, D.; Malinovskii, V. L.; Loewe, R. S.; Lindsey, J. S.; Zaera, F.; Bocian, D. F., Characterization of self-assembled monolayers of porphyrins bearing multiple thiol-derivatized rigid-rod tethers. *J. Am. Chem. Soc.* **2004**, *126* (38), 11944.
272. Liu, Z.; Yasseri, A. A.; Loewe, R. S.; Lysenko, A. B.; Malinovskii, V. L.; Zhao, Q.; Surthi, S.; Li, Q.; Misra, V.; Lindsey, J. S.; Bocian, D. F., Synthesis of porphyrins bearing hydrocarbon tethers and facile covalent attachment to Si(100). *J. Org. Chem.* **2004**, *69* (17), 5568.
273. Ssenyange, S.; Anariba, F.; Bocian, D. F.; McCreery, R. L., Covalent bonding of alkene and alkyne reagents to graphitic carbon surfaces. *Langmuir* **2005**, *21* (24), 11105.
274. Kim, S. K.; Jeon, S., Improved electrocatalytic effect of carbon nanomaterials by covalently anchoring with CoTAPP via diazonium salt reactions. *Electrochem. Commun.* **2012**, *22*, 141.
275. Lu, M.; Chen, B.; He, T.; Li, Y.; Tour, J. M., Synthesis, grafting, and film formation of porphyrins on silicon surfaces using triazenes. *Chem. Mat.* **2007**, *19* (18), 4447.
276. Picot, M.; Nicolas, I.; Poriel, C.; Rault-Berthelot, J.; Barrière, F., On the nature of the electrode surface modification by cathodic reduction of tetraarylporphyrin diazonium salts in aqueous media. *Electrochem. Commun.* **2012**, *20*, 167.
277. Guo, Z.; Ren, D.-M.; Ouyang, Q.; Shi, X.-Y.; Du, F.; Chen, Y.-S.; Zheng, J.-Y., A novel light harvesting system: Synthesis, characterization, and photophysical properties of covalently porphyrin-modified single-walled carbon nanotubes. *Synth. React. Inorg., Met.-Org., Nano-Met. Chem.* **2008**, *38* (6), 553.
278. Guo, Z.; Du, F.; Ren, D.; Chen, Y.; Zheng, J.; Liu, Z.; Tian, J., Covalently porphyrin-functionalized single-walled carbon nanotubes: A novel photoactive and optical limiting donor-acceptor nanohybrid. *J. Mater. Chem.* **2006**, *16* (29), 3021.
279. Jousselme, B.; Bidan, G.; Billon, M.; Goyer, C.; Kervella, Y.; Guillerez, S.; Hamad, E. A.; Goze-Bac, C.; Mévellec, J.-Y.; Lefrant, S., One-step electrochemical modification of carbon nanotubes by ruthenium complexes via new diazonium salts. *J. Electroanal. Chem.* **2008**, *621* (2), 277.
280. Gervaldo, M.; Liddell, P. A.; Kodis, G.; Brennan, B. J.; Johnson, C. R.; Bridgewater, J. W.; Moore, A. L.; Moore, T. A.; Gust, D., A photo- and electrochemically-active porphyrin-fullerene dyad electropolymer. *Photochem. Photobiol. Sci.* **2010**, *9* (7), 890.
281. Semenikhin, O. A.; Ovsyannikova, E. V.; Ehrenburg, M. R.; Alpatova, N. M.; Kazarinov, V. E., Electrochemical and photoelectrochemical behaviour of polythiophenes in non-aqueous solutions: Part 2. The effect of charge trapping. *J. Electroanal. Chem.* **2000**, *494* (1), 1.
282. Zakavi, S.; Najafi Ragheb, M.; Rafiee, M., Electrochemical study of the dication of porphyrins with carboxylic acids: Shift of the absorption bands compared to that of the redox potentials. *Inorg. Chem. Commun.* **2012**, *22*, 48.
283. Chernyy, S.; Bousquet, A.; Torbensen, K.; Iruthayaraj, J.; Ceccato, M.; Pedersen, S. U.; Daasbjerg, K., Elucidation of the mechanism of redox grafting of diazotated anthraquinone. *Langmuir* **2012**, *28* (25), 9573.
284. Bousquet, A.; Ceccato, M.; Hinge, M.; Pedersen, S. U.; Daasbjerg, K., Redox grafting of diazotated anthraquinone as a means of forming thick conducting organic films. *Langmuir* **2011**, *28* (2), 1267.

285. White, B.; Murray, R. W., Electroactive porphyrin films from electropolymerized metallotetra (o-aminophenyl) porphyrins. *J. Electroanal. Chem. Interfac. Electrochem.* **1985**, *189* (2), 345.
286. Bettelheim, A.; White, B. A.; Raybuck, S. A.; Murray, R. W., Electrochemical polymerization of amino-, pyrrole-, and hydroxy-substituted tetraphenylporphyrins. *Inorg. Chem.* **1987**, *26* (7), 1009.
287. Wilson, G. S.; Peychal-Heiling, G., Electrochemical studies of tetraphenylporphin, tetraphenylchlorin, and tetraphenylbacteriochlorin. *Anal. Chem.* **1971**, *43* (4), 550.
288. Kadish, K. M.; Morrison, M. M., Solvent and substituent effects on the redox reactions of para-substituted tetraphenylporphyrin. *J. Am. Chem. Soc.* **1976**, *98* (11), 3326.
289. Hayvalı, M.; Gündüz, H.; Gündüz, N.; Kılıç, Z.; Hökelek, T., Synthesis and characterization of unsymmetrically tetrasubstituted porphyrin and their nickel (II) complexes with the crystal structure of 5,15-bis(4-aminophenyl)-10, 20-diphenylporphyrinatonickel(II). *J. Mol. Struct.* **2000**, *525* (1-3), 215.
290. Zhuang, Q.; Gao, X., Electrochemical studies of tetraphenylporphyrin and vanadyl porphyrin. *Sci. China, Ser. B: Chem.* **1997**, *40* (2), 215.
291. Kadish, K. M.; Camelbecke, E. V.; Royal, G., Electrochemistry of metalloporphyrins in nonaqueous media. In *The porphyrin handbook: Electron transfer, volume 8*, **2000**.
292. Liu, G.; Liu, J.; Böcking, T.; Eggers, P. K.; Gooding, J. J., The modification of glassy carbon and gold electrodes with aryl diazonium salt: The impact of the electrode materials on the rate of heterogeneous electron transfer. *Chem. Phys.* **2005**, *319* (1–3), 136.
293. Liu, G.; Chockalingham, M.; Khor, S. M.; Gui, A. L.; Gooding, J. J., A comparative study of the modification of gold and glassy carbon surfaces with mixed layers of in situ generated aryl diazonium compounds. *Electroanalysis* **2010**, *22* (9), 918.
294. Erbacher, M.; Viana, A. S.; Abrantes, L. M.; Montforts, F. P., Metal insertion into phosphonic acid terminated porphyrins immobilized on TiO_2 electrodes. *J. Porphyrins Phthalocyanines* **2012**, *16* (4), 351.
295. Nishimura, N.; Ooi, M.; Shimazu, K.; Fujii, H.; Uosaki, K., Post-assembly insertion of metal ions into thiol-derivatized porphyrin monolayers on gold. *Journal of Electroanalytical Chemistry* **1999**, *473* (1), 75.
296. Nann, T.; Kielmann, U.; Dietrich, C., Electrochemical metallization of self-assembled porphyrin monolayers. *Anal. Bioanal. Chem.* **2002**, *373* (8), 749.
297. Wolberg, A.; Manassen, J., Electrochemical and electron paramagnetic resonance studies of metalloporphyrins and their electrochemical oxidation products. *J. Am. Chem. Soc.* **1970**, *92* (10), 2982.
298. Yamaguchi, H.; Soeta, A.; Toeda, H.; Itoh, K., Raman scattering study on electrochemical reduction products of magnesium, zinc and copper tetraphenylporphines. *J. Electroanal. Chem. Interfac. Electrochem.* **1983**, *159* (2), 347.
299. Felton, R. H.; Linschitz, H., Polarographic reduction of porphyrins and electron spin resonance of porphyrin anions. *J. Am. Chem. Soc.* **1966**, *88* (6), 1113.
300. Giraudeau, A.; Callot, H. J.; Jordan, J.; Ezhar, I.; Gross, M., Substituent effects in the electroreduction of porphyrins and metalloporphyrins. *J. Am. Chem. Soc.* **1979**, *101* (14), 3857.
301. Maji, S.; Sarkar, S., Homo based two electrons and one-electron oxidation in planar and nonplanar methoxy-substituted nickel tetraphenylporphyrins. *Inorg. Chim. Acta* **2010**, *363* (12), 2778.

302. Chang, D.; Malinski, T.; Ulman, A.; Kadish, K. M., Electrochemistry of nickel(II) porphyrins and chlorins. *Inorg. Chem.* **1984**, *23* (7), 817.
303. Renner, M.; Fajer, J., Oxidative chemistry of nickel porphyrins. *J. Biol. Inorg. Chem.* **2001**, *6* (8), 823.
304. Kadish, K. M.; Morrison, M. M., Substituent effects on the oxidation-reduction reactions of nickel para-substituted tetraphenylporphyrin in nonaqueous media. *Inorg. Chem.* **1976**, *15* (4), 980.
305. Johnson, E. C.; Niem, T.; Doolphin, D., Electron transport via metalloporphyrins. *Can. J. Chem.* **1978**, *56* (10), 1381.
306. Kadish, K. M.; Lin, M.; Caemelbecke, E. V.; De Stefano, G.; Medforth, C. J.; Nurco, D. J.; Nelson, N. Y.; Krattinger, B.; Muzzi, C. M.; Jaquinod, L.; Xu, Y.; Shyr, D. C.; Smith, K. M.; Shelnutt, J. A., Influence of electronic and structural effects on the oxidative behavior of nickel porphyrins. *Inorg. Chem.* **2002**, *41* (25), 6673.
307. Kadish, K. M.; Sazou, D.; Liu, Y. M.; Saoiabi, A.; Ferhat, M.; Guilard, R., Electrochemical and spectroelectrochemical studies of nickel(II) porphyrins in dimethylformamide. *Inorg. Chem.* **1988**, *27* (7), 1198.
308. Huang, S.-S.; Tang, H.; Li, B.-F., Electrochemistry of electropolymerized tetra (p-aminophenyl)porphyrin nickel film electrode and catalytic oxidation of acetaminophen *Microchim. Acta* **1998**, *128* (1), 37.
309. Vuković, M., Voltammetry and anodic stability of a hydrous oxide film on a nickel electrode in alkaline solution. *J. Appl. Electrochem.* **1994**, *24* (9), 878.
310. Yasseri, A. A.; Syomin, D.; Loewe, R. S.; Lindsey, J. S.; Zaera, F.; Bocian, D. F., Structural and electron-transfer characteristics of O-, S-, and Se-tethered porphyrin monolayers on Si(100). *J. Am. Chem. Soc.* **2004**, *126* (47), 15603.
311. Imahori, H.; Norieda, H.; Ozawa, S.; Ushida, K.; Yamada, H.; Azuma, T.; Tamaki, K.; Sakata, Y., Chain length effect on photocurrent from polymethylene-linked porphyrins in self-assembled monolayers. *Langmuir* **1998**, *14* (19), 5335.
312. Imahori, H.; Hosomizu, K.; Mori, Y.; Sato, T.; Ahn, T. K.; Kim, S. K.; Kim, D.; Nishimura, Y.; Yamazaki, I.; Ishii, H.; Hotta, H.; Matano, Y., Substituent effects of porphyrin monolayers on the structure and photoelectrochemical properties of self-assembled monolayers of porphyrin on indium−tin oxide electrode. *J. Phys. Chem. B* **2004**, *108* (16), 5018.
313. Van Galen, D. A.; Majda, M., Irreversible self-assembly of monomolecular layers of a cobalt(II) hexadecyltetrapyridylporphyrin amphiphile at gold electrodes and its catalysis of oxygen reduction. *Anal. Chem.* **1988**, *60* (15), 1549.
314. Ju, H.; Leech, D., Electrochemical study of a metallothionein modified gold disk electrode and its action on Hg^{2+} cations. *J. Electroanal. Chem.* **2000**, *484* (2), 150.
315. Shewchuk, D. M.; McDermott, M. T., Comparison of diazonium salt derived and thiol derived nitrobenzene layers on gold. *Langmuir* **2009**, *25* (8), 4556.
316. Maclean, A.; Foran, G.; Kennedy, B.; Turner, P.; Hambley, T., Structural characterization of nickel(II) tetraphenylporphyrin. *Aust. J. Chem.* **1996**, *49* (12), 1273.
317. Marsh, D.; Mink, L., Microscale synthesis and electronic absorption spectroscopy of tetraphenylporphyrin H_2(TPP) and metalloporphyrins Zn^{II}(TPP) and Ni^{II}(TPP). *J. Chem. Educ.* **1996**, *73* (12), 1188.
318. Gamboa, M.; Campos, M.; Torres, L. A., Experimental determination of enthalpies of solution of tetraphenyl porphyrin (TPP) and some metal derivatives, in chloroform:

Interpretation of the solvation processes at a molecular level. *Inorg. Chem.* **2010**, *49* (2), 659.

319. Seth, J.; Palaniappan, V.; Bocian, D. F., Oxidation of nickel(II) tetraphenylporphyrin revisited. Characterization of stable nickel(III) complexes at room temperature. *Inorg. Chem.* **1995**, *34* (8), 2201.
320. Blawas, A. S.; Reichert, W. M., Protein patterning. *Biomaterials* **1998**, *19* (7–9), 595.
321. Lee, K.-B.; Park, S.-J.; Mirkin, C. A.; Smith, J. C.; Mrksich, M., Protein nanoarrays generated by dip-pen nanolithography. *Science* **2002**, *295* (5560), 1702.
322. Jonkheijm, P.; Weinrich, D.; Köhn, M.; Engelkamp, H.; Christianen, P. C. M.; Kuhlmann, J.; Maan, J. C.; Nüsse, D.; Schroeder, H.; Wacker, R.; Breinbauer, R.; Niemeyer, C. M.; Waldmann, H., Photochemical surface patterning by the thiol-ene reaction. *Angew. Chem. Int. Ed. Eng.* **2008**, *47* (23), 4421.
323. Mooney, J. F.; Hunt, A. J.; McIntosh, J. R.; Liberko, C. A.; Walba, D. M.; Rogers, C. T., Patterning of functional antibodies and other proteins by photolithography of silane monolayers. *Proc. Natl. Acad. Sci. U. S. A.* **1996**, *93* (22), 12287.
324. Uttamchandani, M.; Yao, S. Q., Peptide microarrays: Next generation biochips for detection, diagnostics and high-throughput screening. *Curr. Pharm. Des.* **2008**, *14* (24), 2428.
325. Laurent, N.; Haddoub, R.; Voglmeir, J.; Wong, S. C. C.; Gaskell, S. J.; Flitsch, S. L., Spot synthesis of peptide arrays on self-assembled monolayers and their evaluation as enzyme substrates. *ChemBioChem* **2008**, *9* (16), 2592.
326. Fodor, S. P. A.; Read, J. L.; Pirrung, M. C.; Stryer, L.; Lu, A. T.; Solas, D., Light-directed, spatially addressable parallel chemical synthesis. *Science* **1991**, *251* (4995), 767.
327. Demers, L. M.; Ginger, D. S.; Park, S.-J.; Li, Z.; Chung, S.-W.; Mirkin, C. A., Direct patterning of modified oligonucleotides on metals and insulators by dip-pen nanolithography. *Science* **2002**, *296* (5574), 1836.
328. Sassolas, A.; Leca-Bouvier, B. D.; Blum, L. J., DNA biosensors and microarrays. *Chem. Rev.* **2007**, *108* (1), 109.
329. Ng, J. H.; Ilag, L. L., Biochips beyond DNA: Technologies and applications. *Biotechnol Annu Rev* **2003**, *Volume 9*, 1.
330. Köhn, M., Immobilization strategies for small molecule, peptide and protein microarrays. *J. Pept. Sci.* **2009**, *15* (6), 393.
331. Lahiri, J.; Ostuni, E.; Whitesides, G. M., Patterning ligands on reactive SAMs by microcontact printing. *Langmuir* **1999**, *15* (6), 2055.
332. Mrksich, M.; Dike, L. E.; Tien, J.; Ingber, D. E.; Whitesides, G. M., Using microcontact printing to pattern the attachment of mammalian cells to self-assembled monolayers of alkanethiolates on transparent films of gold and silver. *Exp. Cell Res.* **1997**, *235* (2), 305.
333. Li, N.; Ho, C.-M., Photolithographic patterning of organosilane monolayer for generating large area two-dimensional B lymphocyte arrays. *Lab Chip* **2008**, *8* (12), 2105.
334. Bashir, R.; Gomez, R.; Sarikaya, A.; Ladisch, M. R.; Sturgis, J.; Robinson, J. P., Adsorption of avidin on microfabricated surfaces for protein biochip applications. *Biotechnol. Bioeng.* **2001**, *73* (4), 324.
335. Ni, L.; Chemtob, A.; Croutxé-Barghorn, C.; Brendlé, J.; Vidal, L.; Rigolet, S., Photopatterning of multilayer N-alkylsilane films. *Langmuir* **2012**, *28* (18), 7129.

336. Zhang, G.-J.; Tanii, T.; Zako, T.; Hosaka, T.; Miyake, T.; Kanari, Y.; Funatsu, T.; Ohdomari, I., Nanoscale patterning of protein using electron beam lithography of organosilane self-assembled monolayers. *Small* **2005**, *1* (8-9), 833.
337. Kolodziej, C. M.; Maynard, H. D., Electron-beam lithography for patterning biomolecules at the micron and nanometer scale. *Chem. Mat.* **2011**, *24* (5), 774.
338. Choi, H. J.; Kim, N. H.; Chung, B. H.; Seong, G. H., Micropatterning of biomolecules on glass surfaces modified with various functional groups using photoactivatable biotin. *Anal. Biochem.* **2005**, *347* (1), 60.
339. Mrksich, M.; Whitesides, G. M., Patterning self-assembled monolayers using microcontact printing: A new technology for biosensors? *Trends Biotechnol.* **1995**, *13* (6), 228.
340. Pritchard, D. J.; Morgan, H.; Cooper, J. M., Micron-scale patterning of biological molecules. *Angew. Chem. Int. Ed. Engl.* **1995**, *34* (1), 91.
341. Ryan, M. A.; Spitler, M. T., Light-initiated surface modification of oxide semiconductors with organic dyes. *Langmuir* **1988**, *4* (4), 861.
342. Holzinger, M.; Vostrowsky, O.; Hirsch, A.; Hennrich, F.; Kappes, M.; Weiss, R.; Jellen, F., Sidewall functionalization of carbon nanotubes. *Angew. Chem. Int. Ed. Eng.* **2001**, *40* (21), 4002.
343. Chapman, R. G.; Ostuni, E.; Yan, L.; Whitesides, G. M., Preparation of mixed self-assembled monolayers (SAMs) that resist adsorption of proteins using the reaction of amines with a SAM that presents interchain carboxylic anhydride groups. *Langmuir* **2000**, *16* (17), 6927.
344. Ostuni, E.; Grzybowski, B. A.; Mrksich, M.; Roberts, C. S.; Whitesides, G. M., Adsorption of proteins to hydrophobic sites on mixed self-assembled monolayers. *Langmuir* **2003**, *19* (5), 1861.
345. Bain, C. D.; Whitesides, G. M., Formation of two-component surfaces by the spontaneous assembly of monolayers on gold from solutions containing mixtures of organic thiols. *J. Am. Chem. Soc.* **1988**, *110* (19), 6560.
346. Liu; Gooding, J. J., An interface comprising molecular wires and poly(ethylene glycol) spacer units self-assembled on carbon electrodes for studies of protein electrochemistry. *Langmuir* **2006**, *22* (17), 7421.
347. Brooksby, P. A.; Downard, A. J., Multilayer nitroazobenzene films covalently attached to carbon. An AFM and electrochemical study. *J. Phys. Chem. B* **2005**, *109* (18), 8791.
348. Santos, L.; Ghilane, J.; Lacroix, J. C., Formation of mixed organic layers by stepwise electrochemical reduction of diazonium compounds. *J. Am. Chem. Soc.* **2012**, *134* (12), 5476.
349. Leroux, Y. R.; Hui, F.; Noël, J.-M.; Roux, C.; Downard, A. J.; Hapiot, P., Design of robust binary film onto carbon surface using diazonium electrochemistry. *Langmuir* **2011**, *27* (17), 11222.
350. Sweetman, M. J.; Shearer, C. J.; Shapter, J. G.; Voelcker, N. H., Dual silane surface functionalization for the selective attachment of human neuronal cells to porous silicon. *Langmuir* **2011**, *27* (15), 9497.
351. Hong, S.; Zhu, J.; Mirkin, C. A., Multiple ink nanolithography: Toward a multiple-pen nano-plotter. *Science* **1999**, *286* (5439), 523.
352. Alang Ahmad, S. A.; Wong, L. S.; ul-Haq, E.; Hobbs, J. K.; Leggett, G. J.; Micklefield, J., Protein micro- and nanopatterning using aminosilanes with protein-resistant photolabile protecting groups. *J. Am. Chem. Soc.* **2011**, *133* (8), 2749.

353. Prime, K. L.; Whitesides, G. M., Adsorption of proteins onto surfaces containing end-attached oligo(ethylene oxide): A model system using self-assembled monolayers. *J. Am. Chem. Soc.* **1993**, *115* (23), 10714.
354. Mrksich, M.; Whitesides George, M., Using self-assembled monolayers that present oligo(ethylene glycol) groups to control the interactions of proteins with surfaces. In *Poly(ethylene glycol)*, American Chemical Society: **1997**; Vol. 680, p 361.
355. Liu, Y.-C.; McCreery, R. L., Reactions of organic monolayers on carbon surfaces observed with unenhanced Raman spectroscopy. *J. Am. Chem. Soc.* **1995**, *117* (45), 11254.
356. Ceccato, M.; Nielsen, L. T.; Iruthayaraj, J.; Hinge, M.; Pedersen, S. U.; Daasbjerg, K., Nitrophenyl groups in diazonium-generated multilayered films: Which are electrochemically responsive? *Langmuir* **2010**, *26* (13), 10812.
357. Benedetto, A.; Balog, M.; Viel, P.; Le Derf, F.; Sallé, M.; Palacin, S., Electro-reduction of diazonium salts on gold: Why do we observe multi-peaks? *Electrochim. Acta* **2008**, *53* (24), 7117.
358. Cline, K. K.; Baxter, L.; Lockwood, D.; Saylor, R.; Stalzer, A., Nonaqueous synthesis and reduction of diazonium ions (without isolation) to modify glassy carbon electrodes using mild electrografting conditions. *J. Electroanal. Chem.* **2009**, *633* (2), 283.
359. Downard, A. J.; bin Mohamed, A., Suppression of protein adsorption at glassy carbon electrodes covalently modified with tetraethylene glycol diamine. *Electroanalysis* **1999**, *11* (6), 418.
360. Zhang, J.; Lao, R.; Song, S.; Yan, Z.; Fan, C., Design of an oligonucleotide-incorporated nonfouling surface and its application in electrochemical DNA sensors for highly sensitive and sequence-specific detection of target DNA. *Anal. Chem.* **2008**, *80* (23), 9029.
361. Lopez, G. P.; Biebuyck, H. A.; Whitesides, G. M., Scanning electron microscopy can form images of patterns in self-assembled monolayers. *Langmuir* **1993**, *9* (6), 1513.
362. Hamers, R. J., Formation and characterization of organic monolayers on semiconductor surfaces. *Annu. Rev. Anal. Chem.* **2008**, *1* (1), 707.
363. Wang, X.; Colavita, P. E.; Metz, K. M.; Butler, J. E.; Hamers, R. J., Direct photopatterning and sem imaging of molecular monolayers on diamond surfaces: Mechanistic insights into uv-initiated molecular grafting. *Langmuir* **2007**, *23* (23), 11623.
364. Lopez, G. P.; Biebuyck, H. A.; Frisbie, C. D.; Whitesides, G. M., Imaging of features on surfaces by condensation figures. *Science* **1993**, *260* (5108), 647.
365. Koyano, T.; Saito, M.; Miyamoto, Y.; Kaifu, K.; Kato, M., Development of a technique for microimmobilization of proteins on silicon wafers by a streptavidin−biotin reaction. *Biotechnol. Prog.* **1996**, *12* (1), 141.
366. Herzer, N.; Hoeppener, S.; Schubert, U. S., Fabrication of patterned silane based self-assembled monolayers by photolithography and surface reactions on silicon-oxide substrates. *Chem. Commun.* **2010**, *46* (31), 5634.
367. John, P. M. S.; Craighead, H. G., Microcontact printing and pattern transfer using trichlorosilanes on oxide substrates. *Appl. Phys. Lett.* **1996**, *68* (7), 1022.
368. Charlier, J.; Palacin, S.; Leroy, J.; Del Frari, D.; Zagonel, L.; Barrett, N.; Renault, O.; Bailly, A.; Mariolle, D., Local silicon doping as a promoter of patterned electrografting of diazonium for directed surface functionalization. *J. Mater. Chem.* **2008**, *18* (26), 3136.
369. Le Floch, F.; Matheron, M.; Vinet, F., Electrochemical grafting on SOI substrates using aryl diazonium salts. *J. Electroanal. Chem.* **2011**, *660* (1), 127.

370. Wang, J.; Guo, D. J.; Xia, B.; Chao, J.; Xiao, S. J., Preparation of organic monolayers with azide on porous silicon via Si-N bonds. *Colloids Surf., A* **2007**, *305* (1-3), 66.
371. Orth, R. N.; Clark, T. G.; Craighead, H. G., Avidin-biotin micropatterning methods for biosensor applications. *Biomed Microdevices* **2003**, *5* (1), 29.
372. Leftwich, T. R.; Teplyakov, A. V., Cycloaddition reactions of phenylazide and benzylazide on a Si(100)-2 × 1 surface. *J. Phys. Chem. C* **2008**, *112* (11), 4297.
373. Harmer, M. A., Photomodification of surfaces using heterocyclic azides. *Langmuir* **1991**, *7* (10), 2010.
374. Chin, S.-F.; Pantano, P., Antibody-modified microwell arrays and photobiotin patterning on hydrocarbon-free glass. *Microchem. J.* **2006**, *84* (1–2), 1.
375. Delalande, M.; Clavaguera, S.; Toure, M.; Carella, A.; Lenfant, S.; Deresmes, D.; Vuillaume, D.; Simonato, J.-P., Chemical functionalization of electrodes for detection of gaseous nerve agents with carbon nanotube field-effect transistors. *Chem. Commun.* **2011**, *47* (21).
376. Rickert, J.; Weiss, T.; Göpel, W., Self-assembled monolayers for chemical sensors: Molecular recognition by immobilized supramolecular structure. *Sens. Actuators, B* **1996**, *31* (1–2), 45.
377. Kane, R. S.; Takayama, S.; Ostuni, E.; Ingber, D. E.; Whitesides, G. M., Patterning proteins and cells using soft lithography. *Biomaterials* **1999**, *20* (23-24), 2363.
378. Chaki, N. K.; Vijayamohanan, K., Self-assembled monolayers as a tunable platform for biosensor applications. *Biosens. Bioelectron.* **2002**, *17* (1-2), 1.
379. McCreery, R. L., Molecular electronic junctions. *Chem. Mat.* **2004**, *16* (23), 4477.
380. Smith, R. K.; Lewis, P. A.; Weiss, P. S., Patterning self-assembled monolayers. *Prog. Surf. Sci.* **2004**, *75* (1–2), 1.
381. Flavel, B. S.; Gross, A. J.; Garrett, D. J.; Nock, V.; Downard, A. J., A simple approach to patterned protein immobilization on silicon via electrografting from diazonium salt solutions. *ACS Appl. Mater. Interfaces* **2010**, *2* (4), 1184.
382. Li, H.-W.; Muir, B. V. O.; Fichet, G.; Huck, W. T. S., Nanocontact printing: A route to sub-50-nm-scale chemical and biological patterning. *Langmuir* **2003**, *19* (6), 1963.
383. George, A.; ten Elshof, J. E., Sub-50 nm patterning of functional oxides by soft lithographic edge printing. *J. Mater. Chem.* **2012**.
384. Delamarche, E.; Bernard, A.; Schmid, H.; Michel, B.; Biebuyck, H., Patterned delivery of immunoglobulins to surfaces using microfluidic networks. *Science* **1997**, *276* (5313), 779.
385. Delamarche, E.; Bernard, A.; Schmid, H.; Bietsch, A.; Michel, B.; Biebuyck, H., Microfluidic networks for chemical patterning of substrates: Design and application to bioassays. *J. Am. Chem. Soc.* **1998**, *120* (3), 500.
386. Zhao, B.; Moore, J. S.; Beebe, D. J., Surface-directed liquid flow inside microchannels. *Science* **2001**, *291* (5506), 1023.
387. Takayama, S.; McDonald, J. C.; Ostuni, E.; Liang, M. N.; Kenis, P. J. A.; Ismagilov, R. F.; Whitesides, G. M., Patterning cells and their environments using multiple laminar fluid flows in capillary networks. *Proc. Natl. Acad. Sci. U. S. A.* **1999**, *96* (10), 5545.
388. Kenis, P. J. A.; Ismagilov, R. F.; Whitesides, G. M., Microfabrication inside capillaries using multiphase laminar flow patterning. *Science* **1999**, *285* (5424), 83.
389. Park, J.-U.; Meitl, M. A.; Hur, S.-H.; Usrey, M. L.; Strano, M. S.; Kenis, P. J. A.; Rogers, J. A., In situ deposition and patterning of single-walled carbon nanotubes by laminar flow

and controlled flocculation in microfluidic channels. *Angew. Chem. Int. Ed. Eng.* **2006**, *45* (4), 581.

390. Cougnon, C.; Gohier, F.; Bélanger, D.; Mauzeroll, J., In situ formation of diazonium salts from nitro precursors for scanning electrochemical microscopy patterning of surfaces. *Angew. Chem. Int. Ed. Eng.* **2009**, *48* (22), 4006.
391. Chen, B.; Flatt, A. K.; Jian, H.; Hudson, J. L.; Tour, J. M., Molecular grafting to silicon surfaces in air using organic triazenes as stable diazonium sources and HF as a constant hydride-passivation source. *Chem. Mat.* **2005**, *17* (19), 4832.
392. Chen, B.; Flatt, A. K.; Jian, H. H.; Hudson, J. L.; Tour, J. M., Molecular grafting to silicon surfaces in air using organic triazenes as stable diazonium sources and HF as a constant hydride-passivation source. *Chem. Mat.* **2005**, *17* (19), 4832.
393. Duffy, D. C.; McDonald, J. C.; Schueller, O. J. A.; Whitesides, G. M., Rapid prototyping of microfluidic systems in poly(dimethylsiloxane). *Anal. Chem.* **1998**, *70* (23), 4974.
394. Hu, J.; Li, W.; Chen, J.; Zhang, X.; Zhao, X., Novel plating solution for electroless deposition of gold film onto glass surface. *Surf. Coat. Technol.* **2008**, *202* (13), 2922.
395. Baranton, S.; Bélanger, D., In situ generation of diazonium cations in organic electrolyte for electrochemical modification of electrode surface. *Electrochim. Acta* **2008**, *53* (23), 6961.
396. Radi, A.-E.; Muñoz-Berbel, X.; Lates, V.; Marty, J.-L., Label-free impedimetric immunosensor for sensitive detection of ochratoxin a. *Biosens. Bioelectron.* **2009**, *24* (7), 1888.
397. Fau, M.; Kowalczyk, A.; Olejnik, P.; Nowicka, A. M., Tight and uniform layer of covalently bound aminoethylophenyl groups perpendicular to gold surface for attachment of biomolecules. *Anal. Chem.* **2011**, *83* (24), 9281.
398. Reilson, R.; Kullapere, M.; Tammeveski, K., Blocking behavior of covalently attached anthraquinone towards solution-based redox probes. *Electroanalysis* **2010**, *22* (5), 513.
399. Lyskawa, J.; Bélanger, D., Direct modification of a gold electrode with aminophenyl groups by electrochemical reduction of in situ generated aminophenyl monodiazonium cations. *Chem. Mat.* **2006**, *18* (20), 4755.
400. Barnes, K. K.; Mann, C. K., Electrochemical oxidation of primary aliphatic amines. *J. Org. Chem.* **1967**, *32* (5), 1474.
401. Brennan, M. P. J.; Brown, O. R., Carbon electrodes: Part 2. The anodic oxidation of N-propylamine. *J. Appl. Electrochem.* **1973**, *3* (3), 231.
402. Thirumoorthi, A.; Elango, K. P., Solvent and substituent effects on the electrochemical oxidation of substituted benzylamines in 2-methylpropan-2-ol/water medium. *Int. J. Chem. Kinet.* **2007**, *39* (7), 371.
403. Grimshaw, J., *Electrochemical reactions and mechanisms in organic chemistry*. Elsevier: **2000**.
404. Flavel, B. S.; Garrett, D. J.; Lehr, J.; Shapter, J. G.; Downard, A. J., Chemically immobilised carbon nanotubes on silicon: Stable surfaces for aqueous electrochemistry. *Electrochim. Acta* **2010**, *55* (12), 3995.
405. Lyskawa, J.; Grondein, A.; Bélanger, D., Chemical modifications of carbon powders with aminophenyl and cyanophenyl groups and a study of their reactivity. *Carbon* **2010**, *48* (4), 1271.

406. Anariba, F.; DuVall, S. H.; McCreery, R. L., Mono- and multilayer formation by diazonium reduction on carbon surfaces monitored with atomic force microscopy "scratching". *Anal. Chem.* **2003**, *75* (15), 3837.
407. Miller, J.; Miller, J., *Statistics and chemometrics for analytical chemistry*. Pearson Prentice Hall: **2005**.
408. Lehr, J. Modification of surfaces with thin organic films by reaction with aryldiazonium salts. University of Canterbury, Christchurch, **2010**.
409. Kenis, P. J. A.; Ismagilov, R. F.; Takayama, S.; Whitesides, G. M.; Li, S.; White, H. S., Fabrication inside microchannels using fluid flow. *Acc. Chem. Res.* **2000**, *33* (12), 841.
410. Patel, N.; Sanders, G. H. W.; Shakesheff, K. M.; Cannizzaro, S. M.; Davies, M. C.; Langer, R.; Roberts, C. J.; Tendler, S. J. B.; Williams, P. M., Atomic force microscopic analysis of highly defined protein patterns formed by microfluidic networks. *Langmuir* **1999**, *15* (21), 7252.
411. Berthier, E.; Warrick, J.; Casavant, B.; Beebe, D. J., Pipette-friendly laminar flow patterning for cell-based assays. *Lab Chip* **2011**, *11* (12), 2060.
412. Ismagilov, R. F.; Stroock, A. D.; Kenis, P. J. A.; Whitesides, G.; Stone, H. A., Experimental and theoretical scaling laws for transverse diffusive broadening in two-phase laminar flows in microchannels. *Appl. Phys. Lett.* **2000**, *76* (17), 2376.